Aplicación de imágenes de satélites y datos LiDAR en la modelización e inventario de *Eucalyptus spp* en Uruguay

Andrés Hirigoyen

Doctor en Ciencias Agrarias opción Ciencias Vegetales

Setiembre 2021

Tesis aprobada por el tribunal integrado por Leónidas Carrasco (Presidente), Ricardo Methol (Relator) y Pablo González Barrios (Relator), el 27 de setimebre de 2021.

Autor: Andrés Hirigoyen

Director: (Dr.) Rafael Navarro-Cerrillo
Codirector: (Dr.) Jorge Franco.

AGRADECIMIENTOS

Sin duda debo empezar agradeciendo a Rafael Navarro, Cecilia Rachid y Jorge Franco por el apoyo técnico-profesional y emocional que me brindaron durante todo el proceso.

A FOSA por brindarme los datos y la confianza en este trabajo especialmente a: José Carlos de Mello, Mariano Blanco, Carola Odonne, Nubia Pérez, Santiago Heguarburu, Reiner Borghi, Juan Pablo Galli, Taiana Lleija, María Inés Ibarburu, Pablo Rodríguez y Ricardo Methol.

A INIA por el financiamiento de la beca y por poner a disposición todo lo necesario para realizar este trabajo.

A Roberto Scoz, Zenia Barrios, Gustavo Brito y todo el personal de INIA-Tacuarembó por estar siempre y colaborar conmigo.

A Demian Gómez, Gustavo Balmelli, Sofia Simetto, Fernando Resquin, Leónidas Carrasco, Gonzalo Martínez por el apoyo y ánimo constate.

A María Ángeles Varo, Cristina Acosta, Javier Pérez, Antonio Ariza, Chelo Brigido por el recibimiento y el tiempo compartido.

A Elizabeth Carrega, Elisa Darré, Isabel Sans y a todo el departamento de posgrado (FAgro) por el apoyo en el Doctorado y la Maestría.

TABLA DE CONTENIDO

página

RESUMEN

La integración de información de inventarios de campo, con datos procedentes de sensores remotos y su alta correlación con la estructura de la vegetación, permite ajustar modelos precisos para la estimación de la producción forestal. Esto impacta reduciendo costos, tiempos y sesgos, generando productos que son insumos para procesos como la segmentación y la optimización de la cosecha. En este trabajo se presenta una alternativa a los inventarios forestales y al procesamiento de datos, mediante el uso de sensores LiDAR e imágenes multiespectrales. El objetivo general fue evaluar el uso de LiDAR y datos multiespectrales, en plantaciones de *Eucalyptus grandis* y *Eucalyptus dunnii* en Uruguay; para mejorar la calidad y la cantidad de información brindada para optimizar los procesos de gestión forestal con respecto a los sistemas de inventario tradicionales. Los resultados obtenidos demuestran la mejora en la precisión y en la calidad de los datos frente a los inventarios tradicionales. Se proporcionan herramientas que permiten mejorar la precisión en cuatro aspectos para la cuantificación y el manejo de la producción forestal: i) el uso de modelos compatibles y aditivos; ii) el modelado de las variables del rodal a gran escala empleando datos de teledetección; iii) la delimitación de zonas homogéneas dentro del rodal basada en una evaluación no supervisada; y iv) un método de programación lineal que optimiza los planes de corta basado en la disponibilidad de madera, el secuestro de carbono y el Valor Actual Neto. Se concluye que la aplicación de herramientas de geomática en el sector forestal supone un cambio fundamental en las prácticas de inventarios, desde su planificación, ejecución y resolución, así como de la capacidad para generar modelos predictivos y de algoritmos de segmentación con mayor precisión. Se comprobó que el uso de datos procedentes de sensores activos y pasivos incrementa las posibilidades de automatización de inventarios forestales, aumentando la resolución espacial y la temporal de la cartografía forestal. Esto, junto con el uso de técnicas estadísticas paramétricas y no paramétricas, constituyen un avance en el campo del manejo forestal en Uruguay.

Palabras clave: inventarios, LiDAR, biomasa, segmentación, cosecha forestal

Application of satellite images and LiDAR data for modeling and inventory of *Eucalyptus spp* in Uruguay

SUMMARY

The integration of information from field inventories, with data from remote sensors, and its high correlation with the structure of the vegetation, allows to adjust precise models for the estimation of forest production. This allows for a reduction in costs, time and bias, producing valuable inputs for processes such as segmentation and optimizing the harvest. Here we present an alternative to forest inventories and data processing through the use of LiDAR and multispectral images. The main objective was to evaluate the use of LiDAR information and high-resolution multispectral data in *Eucalyptus* plantations in Uruguay, to improve the quality and quantity of information provided to optimize forest management processes with respect to traditional inventory systems. The results obtained demonstrate the improvement in precision and quality of the data compared to traditional inventories. Tools that improve precision in four fundamental aspects for the quantification and management of forest production are provided: i) the use of compatible and additives models; ii) modeling of stand variables on a large scale using remote sensing data; iii) delimitation of homogeneous areas within the stand based on an unsupervised assessment; and iv) a method for optimizing felling plans based on timber availability, carbon prices, and harvest age. The main conclusion is that the application of geomatic tools in the forestry sector represent a fundamental change in inventory practices, from planning, execution and resolution, as well as the ability to generate predictive models and segmentation algorithms with greater precision than those obtained with field inventories. Throughout the thesis, it is shown that the use of data from different active and passive sensors increases the possibilities for automating forest inventories, increasing the spatial and temporal resolution of forest cartography. This, together with the use of parametric and non-parametric statistical techniques, constitutes an advance in the field of forest management in Uruguay.

Keywords: forest inventories, LiDAR, biomass, segmentation, forest harvest

1. INTRODUCCIÓN

El sector forestal y los bosques tienen cada vez un papel más preponderante en la transición hacia una economía innovadora y eficiente en el consumo de recursos naturales (Wong y Prokofieva, 2014). Si bien la madera sigue siendo la principal fuente de ingresos financieros generados por los bosques, la biomasa forestal, junto con los productos forestales no madereros, brindan fuentes de empleo y una diversificación de la renta en una economía sostenible y con bajas emisiones de carbono. Así, esta economía tiene sus fundamentos en el conocimiento y el manejo de recursos ecológicos y biológicos para proporcionar bienes y servicios de forma sostenible (Carus, 2017). La gestión forestal debe tener una visión orientada a la optimización sostenible y multifuncional de los recursos y servicios ecosistémicos forestales (Wong y Prokofieva, 2014).

1.1. SECTOR FORESTAL EN URUGUAY

En 2018 el sector forestal en Uruguay ocupó el tercer lugar (14%) en el total de las exportaciones de origen agropecuario. El monto exportado por los productos de origen forestal registrado para el 2018 fue de 1.052 millones de dólares, ascendido a 2.160,6 millones de dólares si se incluyen las exportaciones a las zonas francas (MGAP-DIEA, 2019). De acuerdo con Resquin (2019), el crecimiento sostenido del sector forestal ocurre gracias a tres aspectos fundamentales: i) un buen comportamiento productivo de ciertas especies (principalmente algunos eucaliptus y pinos), ii) la promoción de la instalación de plantaciones forestales y su posterior industrialización de acuerdo al marco normativo instrumentado en la década de los años 80 y iii) al contexto político y social tradicionalmente estable. En el año 1987 se promulgó la “Segunda ley forestal” N° 15.939 (Poder Legislativo, 1987), con la cual se aplicaron subsidios y exoneraciones fiscales a las plantaciones forestales, pasando de ocupar 44 mil hectáreas (año 1988) a más de un millón de hectáreas que ocupan en la actualidad (MGAP-DIEA, 2019). Dentro de este proceso, cabe mencionar el establecimiento de dos plantas de celulosa en Uruguay (UPM con un consumo anual de más de 3.500.000 m^3 de pulpa, y Montes del Plata con un consumo anual

estimado de 5.000.000 m^3) así como, la próxima instalación de una tercera planta de UPM. Esto, basado en las proyecciones de demanda, suponen aproximadamente unos 10 millones de m^3 en promedio anuales para próximos 15 años (Dieste, 2012).

Al 2018 en Uruguay, existían 1.034.712 hectáreas de plantaciones forestales comerciales, siendo la superficie efectiva de bosques plantados superior al millón de hectáreas (MGAP-OPYPA, 2019), las cuales representan un 5,9% de la superficie del país. En 2018, se plantaron 74.834 ha, 99 % con especies de *Eucalyptus* sp. (MGAP-DIEA, 2019). Las especies predominantes a nivel nacional son *Eucalyptus grandis*, *E. dunnii*, *Pinus taeda* y *P. elliottii* (MGAP-OPYPA, 2019). Las áreas efectivas de estas especies son para *E. grandis* de 235.620 ha, para *E. dunnii* de 191.035 ha y para *E. globulus* de 149.329 ha (MGAP-DIEA, 2019). En el período 2015-2017 la producción a nivel de viveros forestales se concentró principalmente en *E. dunnii* (58,4%) y *E. grandis* (29,4%) (MGAP-OPYPA 2019). *E. grandis* y *E. dunnii* se destinan a la obtención de madera pulpable y madera maciza, mientras que *E. globulus* sólo se utiliza para producir pulpa.

La madera de las especies de eucaliptus se utiliza principalmente para la producción de pulpa Kraft, constituyendo uno de los productos principales de exportación de Uruguay, segundo después de la carne vacuna (Instituto Uruguay XXI, 2019), con un valor bruto de producción forestal de 462 millones de US$ y una exportación forestal de 1.684.875 miles de US$ (Instituto Uruguay XXI, 2019) para 2018. Las plantaciones de producción usan turnos cortos, de ocho años desde el establecimiento de la plantación hasta las cosechas finales, y presentan diferentes valores de incremento medio anual (IMA) debido al manejo silvícola y a la región en la que se plantan. De acuerdo con MGAP-OPYPA (2018) los rangos esperados de IMA para *E. grandis* varían entre 23 y 37 $m^3\ ha^{-1}$ y para *E. dunnii* de 23 a 34 $m^3\ ha^{-1}$.

1.2. INVENTARIO FORESTAL

La disponibilidad de datos procedentes de inventarios forestales que puedan proyectarse espacialmente, así como la evaluación temporal de los recursos maderables y no maderables, es clave para una gestión forestal sostenible (Tinkham et al., 2018). La caracterización dasométrica de bosques y de los rodales para fines de manejo forestal se realiza tradicionalmente a través del muestreo en campo, partiendo de la teoría general de muestreo que permite dimensionar un inventario forestal considerando un nivel de error y un nivel de incertidumbre aceptables (Cruz-Leyva et al., 2010). Recolectar información de calidad implica tiempo y costos considerables para la obtención de parámetros biofísicos del bosque como son el área basal, el volumen maderable, la biomasa aérea total o la densidad (Hawbaker et al., 2010). Los inventarios forestales representan costos relativamente altos dentro del presupuesto global de una empresa, lo cual puede ocasionar la reducción de la actividad a la medición de unas pocas parcelas, a partir de la cuales se infiere toda la información de la masa forestal. Los inventarios tradicionales se planifican según el presupuesto para el establecimiento de cierto número parcelas de medición (González-Ferreiro et al., 2012), y a través de ellas se generalizan las estimaciones a toda la superficie forestal. La reducción de costos y de tiempo en el proceso de inventario es uno de los principales objetivos de mejora de la gestión forestal (White et al., 2016). Se han propuesto varios medios para optimizar el muestreo y el relevamiento de campo orientados a mejorar el manejo con un nivel de error y de incertidumbre aceptables (Hawbaker et al., 2010), entre los que cabe destacar la modelización y el uso de nuevas tecnologías (Fankhauser et al., 2018).

La modelización forestal es una herramienta que permite simular los efectos de los tratamientos silvícolas, y proyectar las consecuencias de una determinada decisión sobre la producción final. Esta dinámica forestal se representa mediante modelos que explican de manera cuantitativa las tasas de cambio en crecimiento y densidad del rodal a través del tiempo. Un modelo es una abstracción simplificada de la realidad, en la cual se representan algunas de las propiedades, consideradas fundamentales del sistema original, que pasa a ser expresado en términos de

ecuaciones matemáticas que lo describen de forma más sencilla (Vanclay 1994, Sanquetta et al., 2015).

1.3. TELEDETECCIÓN FORESTAL

La teledetección, o el uso de sensores remotos, es el conjunto de técnicas de adquisición y procesamiento de datos de la superficie terrestre sobre diferentes plataformas a distancia del objeto medido. Estos sensores emplean la señal reflejada desde la superficie terrestre en una o más regiones del espectro electromagnético, ya sea por reflexión de la energía solar o de un haz energético artificial o bien por la emisión propia del objeto (Chuvieco-Salinero, 1996). Los sensores remotos suelen clasificarse en activos y pasivos. Los sensores activos se caracterizan por emitir y capturar radiación generando la información (por ejemplo, Radar y LiDAR). Los sensores pasivos, por su parte, registran la energía electromagnética en diferentes longitudes de onda, como resultado de la interacción de la energía proveniente del Sol con un elemento en la Tierra (por ejemplo, sensores multi o hiperespectrales) (Chuvieco-Salinero, 1996). Las técnicas avanzadas de teledetección basadas en sensores activos y pasivos pueden respaldar un inventario forestal tradicional, brindando información que permite diferenciar el tipo de bosque y la distribución de especies a nivel regional y nacional de forma más eficiente, oportuna y económica (Aguirre-Salado et al., 2014). En ese sentido, el sensoramiento remoto permite optimizar los tiempos, los recursos necesarios y abarcar grandes áreas, incluso aquellas de difícil acceso para un inventario tradicional (Stereńczak et al., 2018).

Para el correcto uso de los datos de teledetección, así como para asegurar una buena calibración con las variables del rodal, es necesarios contar con datos de campo. La adquisición y el procesamiento de los datos procedentes de sensores remotos no sustituyen la necesidad de medidas de campo, sino que disminuyen su volumen y el tiempo invertido para su obtención (Stereńczak et al., 2018). Para identificar y manejar las variables estructurales del rodal de forma tridimensional, se emplean combinaciones de datos LiDAR e imágenes de satélite (Kangas et al., 2018). Este uso combinado de datos resulta una técnica complementaria y accesible

para la caracterización espacial y temporal de los rodales forestales, dado que brindan información espacial y temporalmente continua (Blázquez-Casado, 2019). De acuerdo con Parker et al. (1995), se puede definir la estructura del dosel como el arreglo espacio-temporal que incluye la posición, la cantidad, la extensión, el tipo y la conectividad de los elementos vegetales. La estructura del dosel queda definida por las siguientes variables: altura, fracción de cubierta, área basimétrica, índice de área foliar, biomasa, volumen, entre otras. El poder relacionar estas variables medidas en parcelas de campo, con métricas derivadas de sensoramiento remoto, permitirá expandir su estimación y cuantificación, abracando grandes áreas lo cual resulta tedioso y costoso a nivel de inventarios tradicionales.

1.3.1 LiDAR

Existen numerosos estudios que demuestran el potencial de la aplicación de los sistemas LiDAR (*Light Detection and Ranging*) para la cuantificación y la evaluación de los recursos forestales, tanto maderables como no maderables. La tecnología LiDAR se aplica para la estimación de variables forestales, tales como la biomasa, la estructura de copas, el área basimétrica, el volumen y la densidad (Arias-Rodil et al., 2018, Guerra-Hernández et al., 2016, Zhao y Popescu, 2009). Los sensores activos, como LiDAR, ofrecen un panorama mejorado sobre la estructura forestal tridimensional, dando como resultado estimaciones de variables de rodal con mayor precisión. Se ha demostrado que las métricas derivadas de LiDAR son muy sensibles a los atributos estructurales y su aplicación puede mejorar la precisión y la rentabilidad de los inventarios en comparación con las técnicas tradicionales (Deo et al., 2017). Con la incorporación de la tecnología LiDAR se puede reducir el costo de los inventarios, obteniendo información del arbolado en su conjunto y su estructura espacial.

El uso de la tecnología LiDAR integra un conjunto de técnicas que permiten determinar la distancia desde un emisor a un objeto o superficie utilizando un haz laser. Esta distancia se determina midiendo el tiempo de retraso entre la emisión y su detección a través de la señal reflejada. En el arbolado, el pulso laser choca con la

copa de los árboles, y parte de él se refleja y vuelve al sensor, otra parte va atravesando la vegetación hasta llegar al suelo, lo que da lugar a varios retornos que vuelven al emisor. En una superficie sólida dura (edificios, suelo, etc.), el pulso laser se refleja sin ningún problema y vuelve al avión (un único retorno); en cuerpo de agua el pulso es absorbido rápidamente por lo que no se obtiene ninguna información (Sullivan et al., 2017, Silva et al., 2016, Mora et al., 2013). Basado en este principio, el resultado de un vuelo LiDAR es una red irregular de puntos con tres coordenadas que describe la forma de la superficie en un momento determinado.

El sistema LiDAR aerotransportado (*Airborne Laser Scanning*, ALS) consiste en un sensor instalado en una plataforma móvil (avión, helicóptero o dron). El equipo ALS está integrado por un sensor láser, una unidad de medición inercial y un receptor GPS (*Global Positioning System*) sobre una plataforma móvil (Vo et al. 2016). Los datos proporcionados por los sistemas ALS registran las coordenadas (x, y, z), es decir la posición de los puntos donde se refleja el pulso láser emitido. Junto con las coordenadas se registra también la intensidad de cada uno de los retornos, la cual representa la cantidad de energía reflejada y otros atributos relativos al pulso emitido como el ángulo de escaneo, la distancia sensor-objeto y el número de retorno correspondiente. El formato para datos LiDAR aprobado por la American Society for Photogrammetry and Remote Sensing (ASPRS) es el denominado *LAS (Laser File Format Exchange Activities) o su versión comprimida *LAZ. Existen dos formas de adquisición de datos en los sistemas LiDAR; de onda completa (*full-waveform*) y de retornos discretos (Crespo et al., 2015). Estos últimos son los de mayor uso en el ámbito forestal. Los sistemas discretos almacenan las coordenadas tridimensionales de todos los retornos individuales. Los sistemas *full-waveform*, en cambio, almacenan la onda completa (Crespo et al., 2015).

Los datos ALS proporcionan información horizontal y vertical con una alta resolución espacial y una elevada precisión, brindan información sobre atributos como la altura del dosel, la topografía subyacente, la biomasa aérea, el área basimétrica, el diámetro medio del fuste, el volumen de copa y la distribución vertical de la vegetación (Noordermeer et al., 2019). Algunos de estos atributos se

obtienen de manera directa, como por ejemplo la altura de la vegetación; otros de manera indirecta mediante la construcción y calibración de modelos estadísticos o relaciones empíricas entre otros atributos. Partiendo de la distribución de elevaciones e intensidades (una vez calibradas) de los retornos, es posible derivar variables relacionadas con la altura de la vegetación, la estructura del dosel, la distribución de los elementos del dosel en el espacio, la fracción de cabida cubierta, la densidad de copa o la distribución de biomasa entre otras.

1.3.2 Imágenes espectrales

Existe una amplia gama de imágenes de detección remota que brindan información sobre los ecosistemas forestales mediante una variedad de sensores aéreos y satelitales, desde sensores multiespectrales hasta hiperespectrales, con diferentes resoluciones espaciales y temporales (Pettorelli, 2019). La mejora de las plataformas y sensores, en cuanto a resolución espacial, temporal y radiométrica, así como el acceso gratuito a bases de datos satelitales, permitió que la investigación relacionada con la extracción de información biofísica de imágenes se haya incrementado en los últimos años (Woodcock et al., 2008). La relación entre algunas variables de rodal (biomasa, índice de área foliar-IAF-, volumen), y la información brindada por imágenes multi e hiperespectrales (como los índices de vegetación), ha servido de base para el desarrollo de modelos matemáticos de estimación. Con la validación estadística correspondiente, estos modelos son utilizados para estimar variables de rodal extrapolando los valores obtenidos del procesamiento de la imagen a un área o región (White et al., 2016).

El uso de la teledetección ha ganado importancia en la gestión de recursos forestales, ya que emplea menos tiempo que los tradicionales inventarios de campo, reduciendo las incertidumbres asociadas con la inferencia y la estimación en grandes áreas heterogéneas (Franklin, 2001). Los datos satelitales registran la respuesta espectral de la parte superior de las copas y de las fracciones descubiertas del suelo. El manejo de la información contenida en las bandas resulta en los índices espectrales de vegetación (IV) que se emplean en la evaluación de la cobertura

vegetal, la distribución espacial de contenido de clorofila y otros componentes, así como la estructura de la vegetación de manera fiable y rápida. Los IV obtenidos a partir de datos de teledetección son valiosos para la estimación de IAF, los que se utilizan con más frecuencia son el índice de vegetación de diferencia normalizada (normalized difference vegetation index -NDVI-) y el índice simple (simple ratio -SR-), en bosques de coníferas, pastizales y bosques caducifolios (Staben et al., 2018). Sin embargo, estos índices pueden saturar en vegetación densa como los bosques mixtos. Los IV se ven fácilmente afectados por las condiciones atmosféricas y el suelo, por lo que tienden a saturarse, y reduce la precisión de la predicción de los parámetros forestales (Luo et al., 2019), dando lugar a una subestimación del IAF. La reflectancia espectral de la vegetación puede ser similar a la reflectancia del suelo, incluso con el uso de sistemas de teledetección hiperespectrales que cuentan con un espectro alto (Tesfamichael et al., 2018). Los datos de inventario de campo y la información generada en los IV, son la base para el desarrollo y ajuste de modelos de estimación, los cuales una vez validados, son utilizados para estimar las variables forestales extrapolando los valores obtenidos del procesamiento de la imagen a las zonas de interés.

1.4 MODELOS NUMÉRICOS APLICADOS AL INVENTARIO FORESTAL

La modelización es la abstracción o simplificación de fenómenos que se dan en la naturaleza con el objetivo de predecir y/o explicar dicho fenómeno (Vanclay, 1994). Mediante expresiones matemáticas se busca predecir el crecimiento y la producción de sistemas forestales, siendo herramientas útiles para la gestión a cualquier nivel (Sileshi, 2014, García, 1995). La importancia de los modelos forestales reside en la capacidad para predecir el desarrollo de un sistema forestal, facilitando la toma de decisiones a distintos niveles dependiendo del alcance o el nivel de información disponible.

Existen varios métodos de modelización paramétricos y no paramétricos capaces de estimar variables forestales de rodal como la altura dominante, altura media, área basimétrica, volumen y biomasa a partir de datos obtenidos por sensores remotos

(Blázquez-Casado, 2019). Dentro del enfoque paramétrico, los modelos de regresión lineal múltiple, no lineales, lineales generalizados o mixtos son algunos de los más empleados (Blázquez-Casado, 2019). Las técnicas paramétricas tienen las limitaciones derivadas de la sensibilidad de los modelos a las observaciones influyentes, la multicolinealidad de los predictores y los supuestos inherentes sobre la homocedasticidad y la normalidad (Deo et al., 2017). Las relaciones entre las variables predictoras y de respuesta no son siempre lineales, y no tienen una distribución normal, lo cual hace que las técnicas de modelización no paramétricas se presenten como una alternativa más eficiente en la modelización forestal. Los métodos comúnmente utilizados incluyen *K-nearest neighbors* (k-NN), *random forest* (RF), *decision trees* (DT), *artificial neural networks* (ANN) y *support vector machines* (SVM). Si estas técnicas de modelación (paramétricas o no paramétricas) se aplican en datos de teledetección, permiten la estimación de las variables de rodal complementado los inventarios clásicos. Además, posibilitan la extrapolación de las variables de interés a otras partes del territorio, en el que se tengan datos del sensor. Se pueden generar cartografías continuas que proporcionen valores estimados de las variables cubriendo áreas donde no se tienen datos de campo (García, 2010).

1.4.1 Sistemas de ecuaciones de biomasa y volumen

En la estimación de biomasa para distintas fracciones del árbol (fuste, ramas y follaje), se ajustan ecuaciones independientes para cada una de ellas. Estas ecuaciones deben ser coherentes y deben cumplir con la condición de aditividad (Sileshi 2014, Parresol 2001,1999). La aditividad consiste en que la suma de las estimaciones de las fracciones sea igual a la estimación del total. Esto es esencial en los casos de variables aditivas, como el caso de la biomasa total, que pueden ser estimadas por sí solas o como la sumatoria de las fracciones que las integran. Si no se emplean métodos de estimación de parámetros que contemplen esta aditividad, los modelos individuales que se ajustan a las fracciones pueden no tener sentido biológico, ya que su suma puede ser diferentes a la estimación de la biomasa total.

El desarrollo de herramientas que incluyan modelos para la estimación del volumen, permite a los gestores forestales obtener de forma rápida, precisa y confiable, la producción generada por las plantaciones forestales. Si esta herramienta está acompañada de una función de ahusamiento, es posible determinar la forma del fuste, así como, los volúmenes de los productos de aserrío que se necesiten. Estos sistemas de ahusamiento-volumen representan una oportunidad para mejorar las estimaciones de la oferta maderera en la planificación forestal. Una característica esperable de estos sistemas es que presenten compatibilidad en sus predicciones, es decir, que los volúmenes obtenidos por la función de volumen total sean igual a la obtenida por la suma de los volúmenes comerciales parciales y al obtenido por la integral de la función de ahusamiento.

El sistema aditivo de biomasa y el sistema compatible de volumen-ahusamiento, están integrados por un conjunto de ecuaciones interdependientes. La interdependencia es una característica inherente al sistema que debe tenerse en cuenta al momento del ajuste y del uso. En estos sistemas es probable que los residuos de las ecuaciones estén correlacionados por estar asociados a atributos de la misma unidad de medición, existiendo correlaciones contemporáneas en la matriz de varianza y covarianza. El método de estimación de parámetros a emplear, debe considerar todas las interdependencias, así como la existencia de correlación entre las variables involucradas. Gujarati (1996) menciona que el método de mínimos cuadrados ordinarios (OLS) no brinda estimadores eficientes y consistentes para un sistema de ecuaciones, por lo que es necesario emplear un método de estimación multietapa. Autores como Somers y Farrar (1991), han demostrado que algunas técnicas procedentes del campo de la econometría se pueden emplear en la estimación de sistemas de ecuaciones aditivas y compatibles, técnicas como: *seemingly unrelated regression* (SUR) (Zellner y Theil, 1962), *two stage least squares* (2SLS) (Theil, 1953), *three-stage least squares* (3SLS) (Zellner y Theil, 1962) y *full information of maximum likelihood* (FIML) (Hausman, 1975).

1.5. OPTIMIZACIÓN DE LA COSECHA

El costo de oportunidad del recurso suelo ha ido en aumento, lo que hace que la competitividad del sector forestal frente a otros rubros dependa, entre otros factores, de un aumento de la productividad y una mejora en la eficiencia de la cadena de producción forestal. La planificación de la cosecha está estrechamente relacionada con los requisitos de la industria, así como la ubicación y las características de los sitios forestales. El manejo forestal implica una compleja toma de decisiones con consecuencias a corto y largo plazo. La planificación forestal en los niveles estratégico, táctico y operativo involucra sistemas ecológicos, productivos y económicos y su interacción (Broz et al., 2017). Este enfoque de planificación jerárquica busca incrementar la eficiencia en el uso, conservación y protección del recurso forestal, así como asegurar el suministro sostenible y continuo de los productos y beneficios forestales, manteniendo el potencial económico y ambiental de los bosques y sus funciones ecológicas (Kuzminyh et al., 2020). Esta planificación busca optimizar los recursos humanos, económicos, ambientales, de salud y seguridad ocupacional (Viana Céspedes, 2018). Sobre la base del inventario forestal, algunas empresas nacionales planifican la cosecha de árboles con destino celulosa, a una edad promedio de ocho años (Viana Céspedes, 2018). Un posible escenario sería acortar las edades de cosecha para satisfacer la creciente demanda de madera que tendrá el sector en los próximos años.

La asignación de los equipos de cosecha, la reubicación de las bases de operaciones, el traslado de máquinas junto con el personal y la asignación de puntos de extracción son actividades costosas. Esta asignación utiliza sistemas de gestión comercial, que tienen la capacidad de gestionar los activos forestales e indicar dónde, cuándo y qué volúmenes de madera cosechar (Viana Céspedes, 2018). La gestión de los recursos forestales plantea la toma de decisiones en entornos complejos, donde dichas decisiones implican consecuencias tanto a corto como a largo plazo.

Por otro lado, las rotaciones óptimas no se emplean con frecuencia en el manejo de plantaciones de eucaliptus para la industria de la celulosa (Diaz-Balteiro y Rodríguez, 2006). Para determinar la edad óptima de rotación forestal, los beneficios

económicos y la captura de carbono pueden considerarse criterios en el proceso de decisión, teniendo en cuenta las fluctuaciones en los precios de la madera. La consideración de créditos por la captura de carbono implica actividades de cortas menos intensivas, así como edades de rotación más largas. Cuantificar el impacto de los precios del carbono y la madera en la programación de la cosecha y la edad de rotación óptima, es esencial para definir estrategias para el manejo sostenible de las plantaciones de rotación corta, de modo que puedan proporcionar productos maderables y contribuir al secuestro de carbono.

El dióxido de carbono se almacena en diferentes áreas como agua de mar, suelos, atmósfera y bosques (Juntheikki, 2014). Así, el almacenamiento de carbono en los ecosistemas forestales incluye numerosos componentes, principalmente el carbono de la biomasa y el carbono del suelo (Lal, 2005). Este secuestro de carbono en los sistemas forestales es generalmente alto y el balance neto de carbono positivo (Lal, 2005). Esto supone que los créditos del carbono en los mercados internacionales pueden modificar las actividades de cosecha en grandes áreas geográficas y dentro de un horizonte de planificación a largo plazo (Pukkala, 2020). Permitir que la edad de corta varíe en respuesta a la fijación de precios del carbono, da como resultado mayores aumentos en la captura de carbono que en los niveles de recolección predeterminado.

Es evidente la necesidad de modelos matemáticos que permiten la generalización del crecimiento y que produzcan respuestas con resultados financieros para una serie de combinaciones de edades, incluidas aquellas para las que no existen estudios experimentales. Tener en cuenta solo el carbono forestal en los cálculos aumenta las rotaciones óptimas, lo que hace que la planificación de la cosecha sea más desafiante, al requerir soluciones cuantitativas para optimizar las decisiones de cosecha (Pukkala, 2020). El problema de la determinación de las edades óptimas de rotación forestal, considerando tanto la producción de madera como la fijación de carbono, se encuentra ampliamente en la literatura forestal (Diaz-Balteiro y Rodriguez, 2006). La elección de la edad de corta es una decisión fundamental y puede tener un impacto significativo en el almacenamiento de carbono. Los créditos por carbono en los

mercados internacionales pueden modificar las actividades de recolección en vastas áreas geográficas y dentro de un horizonte de planificación muy largo (Pukkala, 2020). Siguiendo a Asante (2011), la maximización del valor actual neto (VAN) para un solo ciclo de cosecha es un criterio común para la determinación de la edad de cosecha forestal. Este criterio asume que maximizará el VAN de la inversión forestal en un ciclo de cosecha, pero no tiene en cuenta los VAN de ciclos repetidos. La duración de la rotación forestal se puede abordar desde el punto de vista económico, cuando la diferencia entre el valor presente de los ingresos y los costos es máxima (maximizando el VAN); o biológico, cuando el IMA es igual al incremento corriente anual (Loza-Balbuena, 2001).

1.6. HIPÓTESIS

La integración de información de inventarios de campo, con datos procedentes de sensores remotos (e.g., imágenes multi e hiperespectrales, y LiDAR), y su alta correlación con la estructura de la vegetación y las variables de gestión forestal, permite ajustar modelos precisos para la estimación de la producción forestal. Esto reducirá los costos, tiempos y errores, generando productos que son insumos para otros procesos como la rodalización y la optimización de la cosecha.

1.7. OBJETIVO GENERAL

Evaluar el uso de información LiDAR y datos multiespectrales de alta resolución, en plantaciones de *Eucalyptus grandis* y *Eucalyptus dunnii* en Uruguay, para mejorar la calidad y la cantidad de información brindada para optimizar los procesos de gestión forestal con respecto a los sistemas de inventario tradicionales.

1.8. PREGUNTAS DE INVESTIGACIÓN

a) ¿Cuál es la ganancia en precisión al emplear modelos de estimación de biomasa total y de sus fracciones que aseguren la aditividad para *E. grandis* y *E. dunnii* en Uruguay?
b) ¿Cuánto mejoran las estimaciones de volumen si se emplean modelos de volumen-ahusamiento compatibles para *E. grandis* y *E. dunnii* en Uruguay?
c) ¿Qué beneficios presentan los modelos empíricos de estimación de volumen, biomasa y altura media dominante ajustados con métricas LiDAR en plantaciones de *E. grandis* y *E. dunnii*?
d) ¿Qué utilidad tiene segmentar rodales de *E. grandis* y *E. dunnii* según su producción de volumen o biomasa y su relación con la altura media dominante, en la construcción de zonas homogéneas?
e) ¿Qué ventajas tiene el uso de métricas LiDAR e imágenes multiespectrales en la estimación del IAF en rodales de *E. grandis* y *E. dunnii*?
f) ¿Cuál es el impacto de emplear un modelo de optimización para planificar los esquemas de cosecha, contemplando los turnos de corta y los ingresos por madera y créditos de carbono en rodales de *E. grandis* y *E. dunnii*?

En la Figura 1 se muestran los principales aportes de este trabajo y sus conexiones.

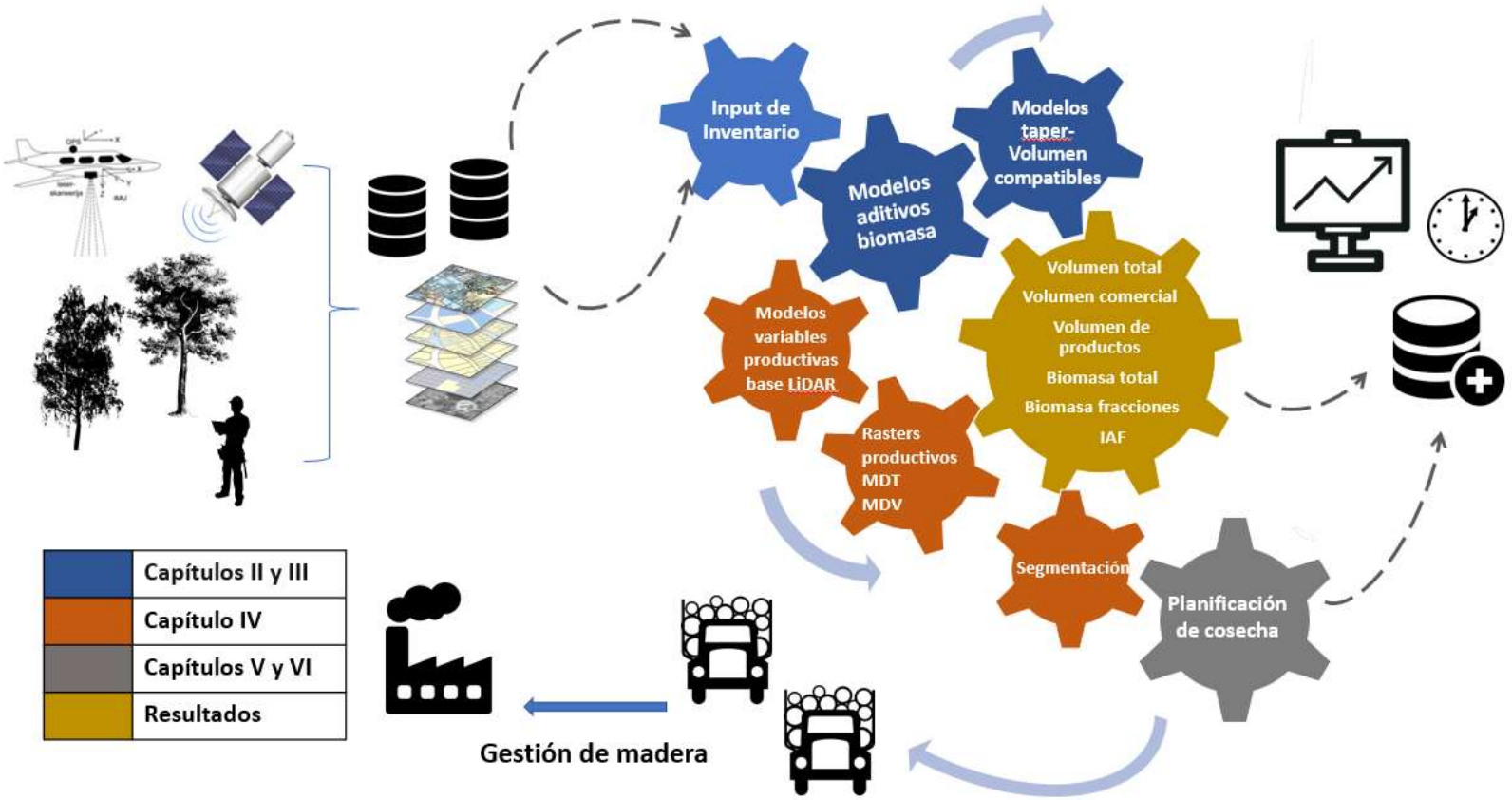
Input de Inventario
Modelos aditivos biomasa
Modelos taper-Volumen compatibles
Modelos variables productivas base LiDAR
Rasters productivos MDT MDV
Volumen total
Volumen comercial
Volumen de productos
Biomasa total
Biomasa fracciones
IAF
Segmentación
Planificación de cosecha
Capítulos II y III
Capítulo IV
Capítulos V y VI
Resultados
Gestión de madera

1.9. ESTRUCTURA DE LA TESIS

En el Capítulo 1 se desarrollan*:* Introducción, Hipótesis, Objetivos, Preguntas de investigación y Esquema general de la tesis. En los siguientes capítulos se busca contestar las preguntas de investigación.

En los Capítulos 2 y 3 se trabaja sobre: ¿cómo se pueden caracterizar productivamente los rodales de eucaliptus? y ¿cómo se puede asegurar la aditividad y la compatibilidad en los resultados de estimaciones de biomasa, volumen y ahusamiento? La falta de modelos aditivos de biomasa aérea total con respecto a las fracciones del árbol (biomasa de fuste, de follaje y de ramas), así como, la falta de modelos compatibles de volumen total, comercial y ahusamiento compatibles fue la motivación para estos Capítulos. Estos sistemas aseguran que las herramientas de gestión que los utilicen brinden resultados compatibles y coherentes (la suma de las estimaciones de las partes es igual a la estimación del todo). Estos Capítulos están integrado por dos artículos aceptados y publicados: Capítulo 2: Hirigoyen A, Resquin F, Franco J, Navarro-Cerrillo RM, Rachid-Casnati C. 2020. Stand biomass estimation methods for *Eucalyptus grandis* and *Eucalyptus dunnii* in Uruguay. Bosque 42(1): 53-66, 2021 DOI: 10.4067/S0717-92002021000100053. Capítulo 3: Hirigoyen A, Navarro-Cerrillo R, Bagnara M, Franco J, Resquin F, Rachid-Casnati C.2021. Modelling taper and stem volume considering stand density in *Eucalyptus grandis* and *Eucalyptus dunnii*. iForest 14:127-136. – doi: 10.3832/ifor3604-014.

En los Capítulos 4 y 5 se aborda: ¿cómo puede mejorar la gestión forestal el uso de sensores remotos? Se investigan el uso de datos LiDAR e imágenes multiespectrales, para ajustar modelos de estimación de las principales variables productivas forestales: Volumen total (VT), Bimasa área total (BMT), altura media dominante (Ho) e índice de área foliar (IAF). En las parcelas de calibración LiDAR se calculó el volumen total y la biomasa empelando los modelos ajustados en el capítulo anterior, para el IAF se contaba con datos medidos en las mismas con un sensor óptico (Ceptómero). Se evaluaron modelos paramétricos y no paramétricos, una vez seleccionados y validados se procedió a construir coberturas ráster para toda el área de estudio y así contar con datos de inventarios derivados de teledetección.

A partir de los archivos ráster de VT, BMT y Ho se realizó una segmentación no supervisada para obtener segmentos homogéneos que ayuden en el manejo forestal. En el caso del IAF se utilizaron algoritmos de *machine learning* para estimar su valor en toda el área de trabajo mediante la integración de métricas LiDAR y datos multiespectrales (imágenes Planet). Estos Capítulos están integrados por un artículo publicado y uno en revisión: Capítulo 4: Hirigoyen A, Varo-Martinez, Mª A, Rachid-Casnati C, Franco J, Navarro-Cerrillo R. 2020. Stand Characterization of *Eucalyptus spp*. plantations in Uruguay Using Airborne Lidar Scanner Technology Remote Sens. 12, 23: 3947. https://doi.org/10.3390/rs12233947. Capítulo 5: Hirigoyen A, Acosta C, Ariza A, Varo-Martínez Mª A, Rachid-Casnati C, Franco J, Navarro-Cerrillo R. A machine learning approach to model leaf area index in Eucalyptus plantations using satellite imagery and airborne laser scanner data (en revision Annals of Forest Research).

El Capítulo 6 se centra en: ¿cuál es la mejora en los planes de cosecha si se contemplan los ingresos por créditos de carbono? Y ¿qué edad resulta óptima para la cosecha forestal sin comprometer los ingresos económicos ni el suministro de madera? Este capítulo propone un modelo de programación lineal para optimizar los planes de cosecha del área de estudio, teniendo en cuenta los ingresos por créditos de carbono y los ingresos por precio de la madera. Se propone también un estudio de las posibles edades de corta que maximicen los ingresos. En este Capítulo se emplean como input los ráster generados en el Capítulo 4, así como las estimaciones de crecimiento interanual empelando los sistemas de los Capítulos 2 y 3. Este Capítulo está integrado un artículo publicado:
Capítulo 6: Hirigoyen A, Acuna M, Rachid-Casnati C, Fracno J, Navarro-Cerrillo R. 2021. Use of optimization modelling to assess the effect of timber and carbon pricing on harvest scheduling, carbon sequestration, and net present value of *Eucalyptus* plantations. Forests, 12(6), 651; https://doi.org/10.3390/f12060651

En el Capítulo 7 se presenta la Discusión general del proyecto finalizando en el Capítulo 8 con las Conclusiones y Perspectivas y en el Capítulo 9 la Bibliografía.

2. STAND BIOMASS ESTIMATION METHODS FOR *EUCALYPTUS GRANDIS* AND *EUCALYPTUS DUNNII* IN URUGUAY

Andrés Hirigoyen [a]*, Fernando Resquin [a], Rafael Navarro-Cerrillo [b], Jorge Franco [c], Cecilia Rachid-Casnati [a]

*Corresponding author: [a] National Institute of Agricultural Research (INIA), Tacuarembó, Ruta 5 km 386, Tacuarembó, Uruguay, +59899268636, andreshirigoyen@gmail.com

[b] University of Cordoba, Department of Forestry Engineering, Laboratory of Silviculture, Dendrochronology and Climate Change, DendrodatLab- ERSAF, Campus de Rabanales, Crta. IV, km. 396, E-14071 Córdoba, Spain.

[c] University of the Republic, Faculty of Agronomy, Paysandú, Ruta 3 km 363, Uruguay.

2.1. RESUMEN

La aditividad es una característica deseable en un sistema de ecuaciones para predecir la biomasa total y sus componentes, ya que las ecuaciones ajustadas de forma independiente generan resultados biológicamente inconsistentes. El objetivo de este estudio fue ajustar y comparar tres métodos para estimar biomasa: (i) regresión individual de la biomasa total, (ii) función de regresión de biomasa total calculada como la suma de los componentes de biomasa por separados, y (iii) ecuaciones simultáneas de componentes de biomasa basados en regresión no lineal aparentemente no relacionada. Un total de 208 árboles de *Eucalyptus dunnii* y *Eucalyptus grandis* fueron cosechados y muestreados de forma destructiva para registrar la biomasa aérea. Los resultados indican que un sistema de ecuaciones ajustadas por ecuaciones simultáneas proporciona estimaciones precisas de biomasa, garantizando la aditividad. Este sistema mostró un buen ajuste y un buen desempeño de predicción, dado que el coeficiente de correlación fue superior al 97% para la biomasa aérea total, para ambas especies, mientras que el error cuadrático medio fue de 23,9 kg y 30,2 kg para *E. grandis*. y *E. dunnii*, respectivamente. Se desarrolló un

sistema de ecuaciones de biomasa para cada especie de eucaliptus, de manera que la suma de las estimaciones de los componentes de la biomasa iguale la estimación de la biomasa aérea. Los resultados mostraron que los sistemas de ecuaciones tienen un gran potencial para mejorar la precisión de las estimaciones de biomasa aérea de árboles individuales para ambas especies.

2.2. SUMMARY

Biomass additivity is a desirable characteristic of a system of equations for predicting components and total biomass, since equations adjusted independently generate biologically inconsistent results. The aim of this study was to fit and compare three methods for modelling biomass: (i) total biomass individual regression, (ii) total biomass regression function calculated as the sum of separate biomass components, and (iii) simultaneous equations of biomass components based on Nonlinear Seemingly Unrelated Regression. A total of 208 trees of *Eucalyptus dunnii and Eucalyptus grandis* were harvested and destructively sampled to record above-ground biomass. The results indicate that a system of equations adjusted by simultaneous equations provides accurate biomass estimations, guaranteeing additivity. This model system showed a good fit and a good prediction performance, given that the correlation coefficient was greater than 97 % for total above-ground biomass, for both species, whereas the root mean square error was 23.9 kg and 30.2 kg for *E. grandis and E. dunnii*, respectively. A system of biomass equations was developed for each eucalyptus species, such that the sum of the estimations of the biomass components equalled the estimate of above-ground biomass. The results showed that the systems of equations have great potential for improving the accuracy of individual tree above-ground biomass estimates for both species.

Key words: Additive biomass equations, biomass partitioning, NSUR, system of equations.

2.3. INTRODUCTION

Estimates of the components of the total biomass of individual trees are of interest for researchers and forest managers, for either scientific or commercial purposes. This information is critical for estimating global carbon storage and assessing ecosystem responses to climate change and anthropogenic disturbances (Ni-Meister et al. 2010). It is also important for commercial uses and national development planning, as well as for scientific studies of ecosystem productivity and energy and nutrient flows. Therefore, information on the above-ground biomass (AGB) is needed for estimation of site productivity, and stand and tree growth and yield (Poudel and Temesgen 2015).

The traditional numerical approaches for estimating tree biomass from inventory data are biomass expansion factors and biomass equations (allometric models); allometric models are common tools for biomass prediction (Lei and Shirong 2016), in particular for individual trees, because biomass measurement in the field is difficult and time consuming. Instead, empirical relationships between biomass and easily measured stand variables, such as tree diameter at breast height (*d*) and total height (*h*), have been developed through regression analysis (Parresol 1999).

In Uruguay, several growth models have been developed for *Eucalyptus globulus* Labill, *Eucalyptus grandis* W. Hill ex Maiden, *Eucalyptus dunnii* Maiden and *Pinus taeda* L., for both solid wood and cellulose production (Rachid-Casnati *et al.* 2014, Hirigoyen *et al.* 2018, Resquin *et al.* 2018). It is necessary to adjust systems for uruguayan plantations, to avoid the use of allometric models from elsewhere or based on unsuitable ranges of predictive variables, which can lead to over- or under-estimation of the AGB. Traditionally, component models and individual AGB are fitted independently using ordinary least squares method (OLS) or the weighted least method (WLS), without considering the inherent relationship between the measured components and total tree biomass. Thus, the estimates are less accurate and do not reflect the additive relationship among the component equations (Bi *et al.* 2004). Usually, the sum of the biomass of the components (in this study: branch, foliage, stem) predicted through individual models does not correspond to the value obtained

by applying AGB equations. However, additivity is a desired and logical feature of equations for estimating biomass components. According to Bi *et al.* (2004), the lack of additivity means that the sum of the predicted values from biomass models of tree components does not match the value obtained from models predicting the total AGB of the trees. A simultaneous adjustment allows to verify if the sum of the equations of each fraction is equal to the AGB equation, guaranteeing the additivity of the biomass fraction and improving the statistical adjustment (Sanquetta *et al.* 2019).

Since Parresol (2001) introduced the use of seemingly unrelated regression (SUR) for simultaneously fitting equations for component and total biomass, SUR and its nonlinear version (NSUR) have been applied by many forest researchers (Poudel and Temesgen 2015). SUR ensures the additivity among the components and total biomass predictions, taking into account the possible correlated errors. This study attempts to identify the best total tree biomass estimation method, for *Eucalyptus* spp. forests of Uruguay; by comparing three methods for modelling the AGB of *Eucalyptus dunnii* and *Eucalyptus grandis* plantations in Uruguay. The compatible biomass models assessed were: i) above-ground biomass individual regression: WLS individual approach; ii) above-ground biomass regression calculated as the sum of separate biomass components: WLS sum approach; iii) simultaneous biomass equations based on nonlinear seemingly unrelated regressions: NSUR approach. Since it is not practical to fell trees to develop equations for each biomass component, and because destructive sampling is tedious and expensive, biomass equations systems that depend on individual tree variables like *d* and *h* could be useful. The NSUR procedure comprises better biological properties and statistics to adjust allometric equations for fraction and total biomass.

2.4. METHODS

Study area. The sampling was located in three different regions prioritised for forest plantations (Lanfranco and Sapriza 2011): northwest (38º05'18´´S–64º27'63´´W, next to Guichon city, Paysandú), centre-east (38º99'28´´S–61º80'18´´W, next to Sarandí del Yi, Durazno) and west-centre (39º42'43´´S–63º12'10´´W, near Trinidad city, Flores). These zones have a temperate subtropical climate, with a mean annual

temperature of 18 °C (12 °C in the coldest month, 24 °C in the warmest month) and a mean annual rainfall between 1,300 and 1,400 mm (Castaño *et al.* 2011).

Field data collection. The AGB data used in this study correspond to the PROBIO project carried out by National Research Institute of Agriculture Research (INIA) in 2015 (PROBIO 2015). The data were collected from 90 trees of *Eucalyptus dunnii* and 118 trees of *Eucalyptus grandis*. All 208 trees were harvested and destructively sampled as follows: stems were cut into 1-m sections and each section was weighed; the total height (H) and diameter at breast height (D, 1.3 m above the ground) were measured. For each tree, two discs (3 cm thick) were cut, at 50 % and 75 % of the commercial height, and weighed. One of the discs was weighed in the field, with and without bark, and oven-dried to constant weight (70±2 ºC) to estimate the dry matter percentage (PROBIO 2015). All the green and dry branches and foliage in each crown were classified and weighed in the field. Samples of 0.5 kg of branches and foliage were taken to the laboratory for moisture content determination. The dry weights of branches and foliage per tree were calculated by multiplying the fresh weights by the dry weight-fresh weight ratios determined in the laboratory through sampling. The dry weight of each stem section with bark was calculated considering the green weight and the average ratio of dry weight to green weight of discs sampled at the large and small end of each section. The dry weights of stem wood and bark were calculated using the average bark to stem wood dry weight ratio obtained from the discs sampled at both ends. The total stem biomass of each tree was calculated by summing the dry weights of all stem sections. Descriptive statistics of the total above-ground biomass, biomass components and other variables are shown in table 1.

Table 1. Allometric and biomass characteristics of *Eucalyptus grandis and Eucalyptus dunnii*. Diameter at breast height (d, cm), total tree height (h, m); stem biomass (SB); foliage biomass (LB); branches biomass (BB); and above-ground biomass (AGB).

Species	Summary	*d*(cm)	*h* (m)	Age (years)	SB (kg)	LB (kg)	BB (kg)	AGB (kg)
E. dunnii (n=90)	Min	9.9	12.6	6.3	6.4	2.8	2.1	11.8
	Mean	18.8	23.9	8.6	344.6	21.3	20.9	389.1
	Max	31.6	33.2	12.0	1133.7	60.8	58.4	1223.3
	Sd	5.2	4.8	2.89	246.7	13.5	14.5	272.0
E. grandis (n=118)	Min	11.1	16.6	6.5	69.8	1.2	2.0	73.3
	Mean	22.3	26.7	10.0	485.7	31.4	47.3	564.5
	Max	36.9	30.8	17.0	1725.7	114.0	177.8	1.914
	Sd	5.6	5.3	3.5	332.4	25.0	33.9	377.3

Model assessment and validation. To evaluate the fit of the models, their accuracy and precision were compared through the graphical and numerical analysis of residuals. The statistical criteria applied were: the adjusted coefficient of determination (R^2-adj), during the model development stages; the correlation coefficient (R^2), which is a simple linear regression between observed and predicted values, employed as a classical method of evaluation of a nonlinear model; and the Akaike information criterion (AIC), to measure the relative quality of each model (Myers 1990). The model performance for the different approaches was assessed based on the estimation errors, using the root-mean-square error (RMSE) to indicate the absolute value of the error (Myers 1990).These expressions are summarised as follows:

$$R^2adj = 1 - \frac{\sum_{i=1}^{n}(y_i - \hat{y}_i)^2}{\sum_{i=1}^{n}(y_i - \bar{y})^2}\left(\frac{n-1}{n-p}\right) \quad [1]$$

$$R^2 = r^2_{y_i\widehat{y_y}} \quad [2]$$

$$RMSE = \sqrt{\frac{\sum_{i=1}^{n}(y_i - \hat{y}_i)^2}{n}} \quad [3]$$

Where y_i and $\hat{y}_i$ are the measured and estimated values of the dependent variable, respectively, n is the total number of observations and p is the number of equation

parameters. $r^2_{y_i\widehat{y_y}}$ is the correlation coefficient for linear regression between the observed and predicted values.

In addition, it is necessary to assess whether the goodness of the fit reflects the quality of the predictions, through validation (Huang 2002). This analysis assists the selection of the best model. To evaluate the prediction quality of the system of simultaneous equations, cross-validation was performed with the fitting dataset (Myers 1990). Cross-validation in forestry is a common practice (Hirigoyen *et al.* 2018) for model selection through consideration of the predictive ability of the assessed model. It consists of the calculation of the residuals of the *i-th* observation using parameters estimated using all the data except the *i-th* observation. This process is named leave-one-out cross-validation (LOOCV) (Kohavi 1995). The residual removed from the *i-th* observation is the difference between the observed value of the modelled variable and the value estimated by a function that has been adjusted to all the data except the *i-th* observation. The sum of squares of the eliminated residual is called PRESS (predicted residual sum of squares) (Picard and Cook 1984) and it is used to calculate the selection criteria or root-mean-square-error for cross-validation (RMSEcv). A close agreement between RMSEcv and RMSE indicates that the model is not over-fitting the data and has a good predictive value. The efficiency of the model represents the proportion of the variability observed in the original data that is explained by the model, and it varies between 0 (without adjustment) and 1 (perfect fit). The statistics of validation were calculated as follows:

$$PRESS = \sum_{i=1}^{n}(y_i - \hat{y}_{i-1})^2 \quad [4]$$

$$RMSE_{cv} = \sqrt{\frac{\sum_{i=1}^{n}(y_i - \hat{y}_{i-i})^2}{n-p}} \quad [5]$$

$$\text{ME}=1 - \frac{\sum_{i=1}^{n}(y_i - \hat{y}_{i-i})^2}{\sum_{i=1}^{n}(y - \bar{y}_{i-1})^2}\left(\frac{n-1}{n-p}\right) \quad [6]$$

Where y_i and $\hat{y}_i$ are the measured and estimated values of the dependent variable, respectively, *n* is the total number of observations and *p* is the number of equation parameters.

The Proc sql program of SAS (SAS Institute 2004) was used to perform the routine. The characteristic heteroscedasticity of the biomass data was evaluated with the White test (SAS Institute 2004), and was corrected with a residual variance power function as the weighting factor.

Individual model selection: OLS individual and WLS sum approaches. Twenty-seven linear and nonlinear regression models available in the literature were tested for each tree biomass component and the total tree biomass (Appendix). *WLS* was applied to homogenise residuals and to improve the statistics of fit (Parresol 2001, Dong *et al.* 2018). For each biomass component, only the models in which all parameters were significant at $P < 0.05$ were considered. The best model was selected considering the following statistics: the lowest values for the AIC and RMSE, and the largest proportion of the variance explained by the model (R^2-adj). The relative error (RE%) of the predicted biomass ($AGB_{predict}$) versus the total measured biomass ($AGB_{measured}$) was calculated to evaluate the general predictive power of the selected models (Chave *et al.* 2005). The mean relative error represents the general bias of the model, whereas the precision was assessed through the standard deviation of the relative error.

$$RE\% = 100 * \left(AGB_{predict} - AGB_{measured}\right)/AGB_{predict} \quad [7]$$

Additive biomass equations: NSUR approach. Individual models selected for each biomass component were fitted simultaneously using NSUR in an additive system of equations (Parresol 2001). NSUR accounts for the contemporaneous correlations among the regression residuals, resulting in a lower variance of the regression coefficients. It also incorporates the additivity property into the equation systems obtained by constraining the parameters (Parresol 2001). The model residuals of biomass data always exhibit heteroscedasticity, and the variance of the error is often functionally related to one or more explanatory variables of the model (Parresol 2001, Riofrío *et al.* 2015). To deal with the heteroscedasticity and achieve minimum variance estimates, a weight function was defined and used for the biomass models for each component. Caillez and Alder (1980), working with compatible taper and

volume functions, proposed a power function of the variable $d_i^2 Hh_i$ (the square of the *d* multiplied by *h*) as weight function:

$$\sigma_2^i = (d_i^2 h_i)^k \quad [8]$$

Where, *d*is tree diameter at breast height, *h* is total height total height and *k* as power.

It was programmed in the model procedure of SAS/ETS (SAS Institute 2004). Statistical analyses and plots were performed using R statistical software (R Core Team 2015), while SAS statistical software (SAS Institute 2004) was used for fitting the weighted nonlinear systems of equations using NSUR.

2.5. RESULTS

Allometric relationships. The stem, branches, foliage and total biomass of the sampled trees and their relationships with *d* and *h* are shown in figure 1. In all cases an exponential relationship was observed. Exponential models with *d* and *h* as independent variables were adjusted and were evaluated using R^2-adj.

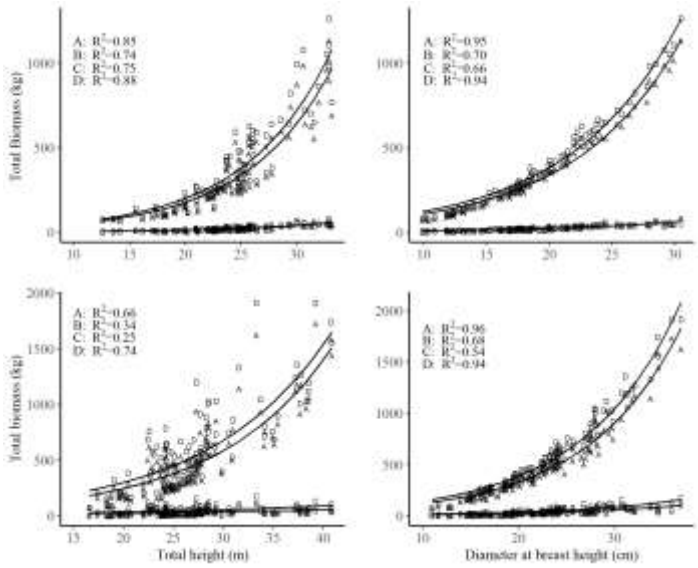

Figure 1. Relationships between total (A), branch (B), foliage (C) and stem (D) biomass and diameter at breast height and total height for *Eucalyptus dunnii* (upper panel) and *Eucalypts grandis* (bottom panel).

For both species, *d* was strongly and significantly correlated with stem biomass and AGB, accounting for 95 % and 94 % of the variation for *E. grandis* and *E. dunnii*, respectively. For *E. dunnii*, the R^2-adj values for the branch and foliage fractions were 70 % and 66 %, respectively, indicating moderate correlation; however, for *E. grandis*, these values were lower (68 and 54 %, respectively). For *h*, all the values were lower in *E. grandis*, 34 %, 25 %, 74 % and 66 % for branches, foliage, stem and AGB, respectively, while *E. dunnii* had values of 85 %, 88 %, 74 % and 71 % for AGB, stem, branches and foliage, respectively.

Individual biomass equations. For the individual biomass components, the same models were selected for the WLS individual and WLS sum approaches. For the WLS sum approach, the total *k* was estimated as the sum of the independent tree components models. The models selected for the biomass components and AGB with their corresponding statistics of fit are given in table 2. For *E. grandis*, the values of the White test were similar. For *E. grandis*, models considering only *d* showed the best fit, whereas for *E. dunnii*, the selected models included *d* and *h* (table 2). The accuracy of the adjusted models was verified by plotting the correlation between the model predictions and the observed biomass fractions (figure 2). All parameters were significant at the 95 % confidence level. All models fitted the total AGB data well, with the model R^2-adj ranging from 0.96 to 0.97. For the foliage and branches components was obtained the minor adjust.

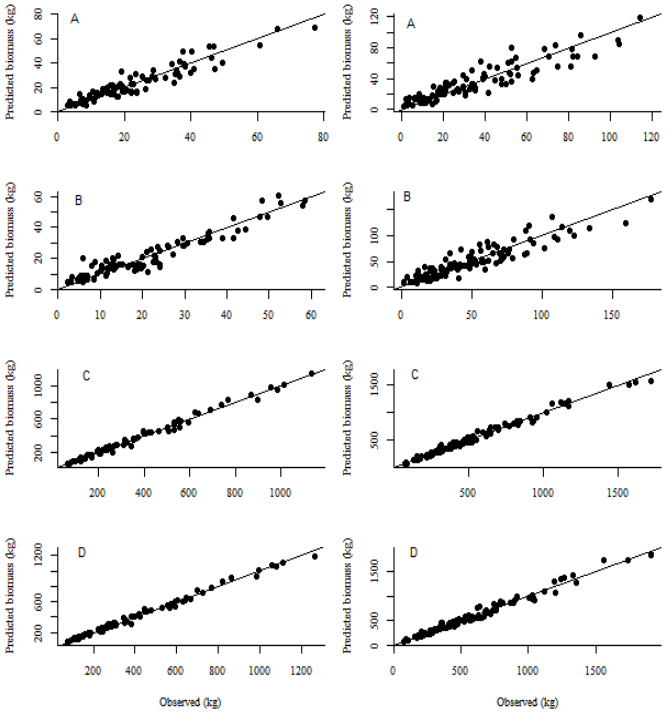

Figure 2. Model predictions against observed data; (A) foliage, (B) branches, (C) stem and (D) total tree biomass for *Eucalyptus dunnii* (right) and *Eucalypts grandis* (left).

Table 2. Allometric equations for tree biomass estimation by fractions (kg) and overall aboveground dry weight biomass (AGB, kg) for *Eucalyptus grandis* and *Eucalyptus dunnii* using WLS regression. Independent variables are total height (h, m) and diameter at breast height (d, cm). Adjusted coefficient of determination (R^2-adj), root mean squared error (RMSE, kg) and White test.

Species	Biomass fractions	Biomass equation	Model number	RMSE (kg)	R^2-adj	Weighting factor	White test
E. grandis	Foliage	$\exp(-2.561+ 3.995\ln(d) - 1.997\ln(h))$	15	11.8	0.77	$1/d^{2.3}$	0.08
	Branches	$\exp(-1.577 + 3.589\ln(d) - 1.776\ln(h))$	15	13.1	0.85	$1/d^{2.46}$	0.09
	Stem	$0.0447d^{2.069}h^{0.835}$	3	24.2	0.98	$1/d^{2.86}$	0.11
	AGB	$d^2(0.656 + 0.0005H)$	22	34.5	0.97	$1/d^{1.87}$	0.60
E. dunnii	Foliage	$\exp(-3.248+ 2.890\ln(d) - 0.712\ln(h))$	15	4.76	0.89	1/d	0.80
	Branches	$\exp(-3.046+2.939\ln(d) - 0.835\ln(h))$	15	4.38	0.90	$1/d^{2.02}$	0.30
	Stem	$0.069d^{2.23}h^{0.566}$	3	23.6	0.97	$1/d^2h^2$	0.08
	AGB	$0.091d^{2.285}h^{0.473}$	3	24.7	0.96	$1/ d^2h^2$	0.75

Incompatibility was observed between AGB and the sum of the fractions estimated independently. Therefore, there was an inconsistency between the AGB estimation and the sum of the estimated values for the biomass fractions, indicating the need to apply simultaneous adjustments to ensure the additivity of biomass fractions.

Additive biomass equations. For the NSUR approach, models for the biomass components (table 3) were fitted simultaneously using joint-generalized least squares and restricting the coefficients of regression, ensuring additivity.

The NSUR method consisted firstly of fitting and selecting the best models for each tree component, since the AGB model was a function of the independent variables used in each tree component model (table 3). The plots of the NSUR residuals against the predicted values and of the predicted values against the observed values, for both species, are presented in figures 3 and 4, respectively.

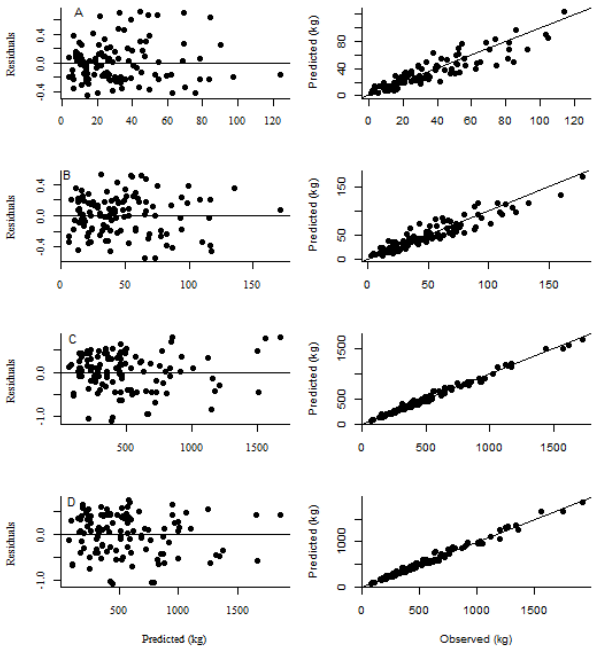

Figure 3. Residuals against predicted biomass (right) and predicted against observed data (left) by NSUR: (A) foliage, (B) branches, (C) stem and (D) total tree biomass, to *E. dunnii.*

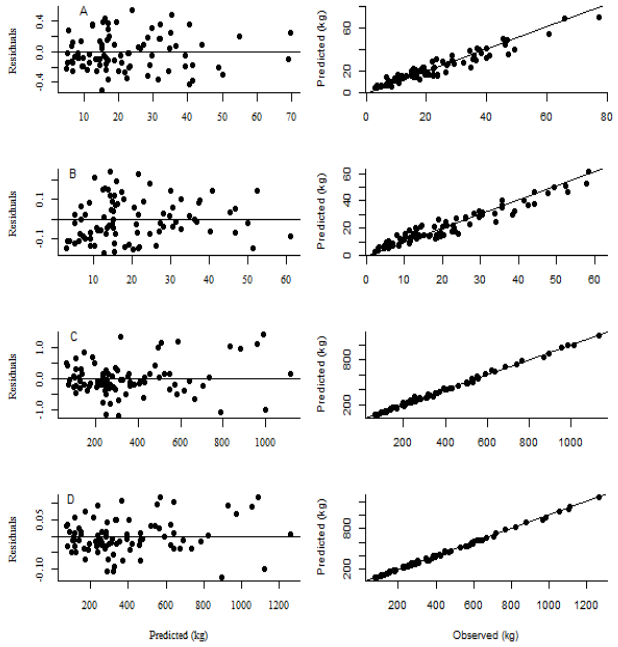

Figure 4. Residuals against predicted biomass (right) and predict model against observed data (left) by NSUR: (A) foliage, (B) branches, (C) stem and (D) total tree biomass, to *E. grandis*.

Table 3. Biomass equation systems simultaneously fitted for tree biomass estimation by fractions (kg) and overall aboveground dry weight biomass (AGB, kg) for *Eucalyptus* using NSUR regression. Independent variables are total height (h, m), diameter at breast height (d, cm), coefficient of correlation (R^2) and root mean squared error (RMSE, kg).

Species	Biomass fractions	Biomass equation	R^2	RMSE
E. grandis	Foliage	$\exp(-2.365+ 4.019\ln(d) - 2.084\ln(h))$	0.78	11.6
	Branches	$\exp(-1.775 + 3.651\ln(d) - 1.783\ln(h))$	0.85	12.9
	Stem	$0.044d^{2.077}h^{0.831}$	0.98	23.1
	AGB	Stem + Foliage+ Branches	0.97	30.2
E. dunnii	Foliage	$\exp(-3.301 +2.928\ln(d) - 0.731\ln(h))$	0.90	4.7
	Branches	$\exp(-3.683 +2.773\ln(d) - 0.488\ln(h))$	0.89	4.5
	Stem	$0.082d^{2.269}h^{0.478}$	0.97	22.5
	AGB	Stem + Foliage + Branches	0.97	23.9

The graphs of the residuals with weighting do not show any trend or heteroscedasticity. All parameters were significant (P <0.001) at the 99 % confidence level. All models fitted the total AGB data properly (R^2 around 0.98). A minor adjust for biomass of foliage was obtained for *E. grandis* (R^2 0.78) than for *E. dunnii* (R^2 0.90). The relative errors (RE%) of the AGB, based on relative stem diameters for individual WLS and adjusted NSUR, were plotted (figure 5) and compared (table 4). For both species, the AGB was estimated with a RE% below 1 % for NSUR. The *WLS* individual approach had a RE% value greater than 1 %.

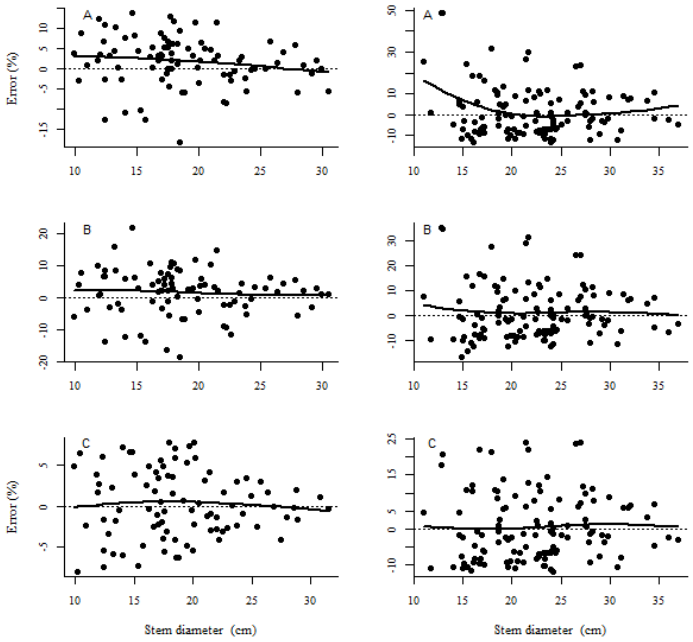

Figure 5. Relative error in AGB predictions: (A) individual equation, (B) components sum, (C) additive equation. For *E. dunnii* (right) and *E. grandis* (left) by stem diameter (cm), solid lines are smoothed errors using a lowess method.

Table 4. Mean and standard deviation (Sd) of relative error (%) to overall aboveground dry weight biomass (AGB. kg) for *Eucalyptus grandis* and *Eucalyptus dunnii* by method adjusted, induvial equation by weighted least squares (WLS indi), total sum of components adjusts by weighted least squares (WLS sum) and adjust by fitted simultaneously (SUR)

.

Species	Approach	Mean	Sd
E. dunnii	WLS indi	1.73	6.14
	WLS sum	1.65	7.23
	SUR	0.25	4.07
E. grandis	WLS indi	1.49	11.83
	WLS sum	1.11	10.67
	SUR	0.42	8.26

The accuracy of the models was assessed by performing a leave-one-out cross-validation of the AGB (table 5). NSUR yielded the best cross-validation results, with the lowest RMSEcv and best ME; similar values were registered for the WLS individual approach.

Table 5. Result for Cross validation to overall aboveground dry weight biomass (AGB, kg) for *Eucalyptus grandis* and *Eucalyptus dunnii* models by method adjusted, induvial equation by weighted least squares (WLS indi), total sum of components adjusts by weighted least squares (WLS sum) and adjust by fitted simultaneously (SUR).

Species	Approach	Model efficienty	Root-mean-square-error for cross-validation (RSMEcv)
E. dunnii	WLS indi	0.98	26.83
	WLS sum	0.95	27.65
	NSUR	0.98	26.48
E. grandis	WLS indi	0.97	34.07
	WLS sum	0.94	39.29
	NSUR	0.97	34.14

2.6. DISCUSSION

In this study, we have developed consistent additive biomass functions for *Eucalyptus dunnii* and *E. grandis* in Uruguay. Models for all components and systems were fitted using the same procedure, which accounted for biological correlation between components. Several growth and yield model systems have been proposed for these species, but few allometric biomass equations are available for eucalypt plantations (see Resquin *et al.* 2018). Most of the equations used for commercial forests of eucalypts and pine species in Uruguay derive from independent fittings. Individual approaches do not satisfy the condition of biological consistency, ensured by the restriction that the biomass estimates for the components must be additive to equal the estimate of the total biomass. Several approaches (Parresol 2001, Li *et al.* 2014, Bi *et al.* 2015) have emphasised the importance of establishing additive equations of biomass. Systems of biomass equations with tree diameter and height as the predictors are tools to provide biomass estimates for field inventories. Estimates for the stem and whole tree are more accurate, whereas branch and foliage biomass estimates are less accurate (Li *et al.* 2014, Bi *et al.* 2015).

Biomass allocation. Variation in biomass allocation among tree components is usually observed when comparing species or trees of different ages. In this study, the stem biomass was the major component of the AGB, constituting of the total tree biomass (88.5 % and 86.1 % for *E. grandis* and *E. dunnii*, respectively), while the branch biomass represented 8.4 % and 5.4 % and the foliage biomass 5.5 % and 6.1 % for *E. grandis* and *E. dunnii*, respectively.

Individual tree component and AGB models. Once the different linear and nonlinear models for each component and the total tree biomass had been adjusted, the best model was selected in each case based on goodness-of-fit statistics and graphical analysis. The predictive variables tested were *d, h* or both, *d* being a key predictor in growth and yield models as well as in biomass models. Models that include only *d* are simple in structure and require only basic forest inventory data (Wang 2006). Our

results show that *d* and *h* had a strong positive relationship with all the biomass components evaluated; they were included as predictor variables in all the allometric models and improved the predictive ability of the biomass equations (Bi *et al.* 2015, Dong *et al.* 2015). Heteroscedasticity problems are inherent in biomass models since trees with greater *d* and *h* have more biomass than small trees. As shown in figure 1 the relationship between biomass and *d* and *h* is exponential. To deal with this issue, logarithmic transformations are commonly applied in the modelling of tree biomass (Wang 2006). To back-transform biomass to its original scale, the use of a correction factor is common to correct for systematic bias introduced by anti-logarithmic transformation. This anti-logarithmic transformation leads to a systematic overestimate of biomass (Dong *et al.* 2015) and also, in a system of additive biomass equations, the additivity property of the system may not be achieved (Dong *et al.* 2015).We used weighted least-squares regression to fit individual models, thus accounting for the inherent heteroscedasticity (Parresol 1999). The foliage and branches biomass models were less accurate and less precise than the biomass models for the stem and AGB, probably due to the variability of the crown structure.

For both species, model [15] was selected to estimate foliage and branches biomass, and model [3] to estimate stem biomass (see Appendix). However, different models were selected for AGB. For the stem biomass, both parameters of model [3] were positive, meaning that the stem biomass was directly and positively related to *d* and *h*. For *E. grandis,* in the AGB model [22] the parameter estimated for *h* was positive, implying that, for the same *d*, taller trees have more above-stump stem biomass than shorter trees. For *E. dunnii,* model [3] shows that the parameters estimated for *h* and *d* were both positive, indicating that the estimate of AGB is superior in thick-stemmed and tall trees.

Additive biomass equations. Biomass additivity is a desirable characteristic of a system of equations for predicting tree component and total tree biomass. Most biomass equations reported in the literature are not additive and were developed separately for each biomass component (Lin *et al.* 2017, Resquin *et al.* 2018). The biomass additivity approach has been used by some researchers in the fitting of

biomass equations (*e.g.* Riofrío *et al.* 2015, Kralicek *et al.* 2017). However, there is no record of the use of NSUR in Uruguay to estimate tree AGB. Equations adjusted independently generate biologically inconsistent results, which implies that models for components biomass and total AGB should be comprised of systems of equations. The biomass components were expressed as an individual model, where each model was selected from a group of candidate models. The AGB model was a function of the biomass components, resulting in additivity; all the equations of the system had their own weighting function to ensure estimates with minimum variance.

Our additive systems of biomass used only one constraint on the total tree biomass. The cross-equation error correlations between the total tree biomass and components biomass were accounted (Carvalho and Parresol 2003, Bi *et al.* 2015). Once each biomass component had been individually adjusted, the selected models were simultaneously fitted using NSUR methodology. The results presented in table 3 show high goodness of fit in all the components equation systems (by species) fitted with NSUR methodology. Comparing the two fitting methods (individual fitting and the NSUR approach), the statistics of fitting were similar (with small gains in RSME and R^2 for the NSUR approach); however, the residuals plots presented different trends (figures 2-4). According to Sanquetta *et al.* (2019), when comparing individual fitting and NSUR, it can be seen that both approaches have similar precision statistics. NSUR models should be used to predict total biomass and its fractions because biological consistency must be considered. For the AGB, NSUR achieved an R^2 value of approximately 98 % and an improvement in the distribution of the residuals. Equations adjusted by means of OLS-WLS do not take into account the contemporaneous correlations, which impairs the efficiency of estimation. The inclusion of the contemporaneous correlations between the biomass of the components and the total biomass in the fitting of the equation systems through NSUR resulted in an efficiency gain, by reduction of the confidence and prediction intervals of the biomass estimates (Parresol 1999).

The classical individual approach to the fitting of biomass equations ignores the inherent correlation among the biomass components measured in the same

sample trees. Taking this correlation into account in the development of a system of additive biomass equations yields greater statistical efficiency (Parresol 2001). Some authors (Parresol 2001, Carvalho and Parresol 2003) have compared different methods of enforcing additivity, concluding that NSUR achieves more efficient estimates and should be the choice for additivity. In the present work, the simultaneous systems tended to slightly bias the AGB estimates, by 0.25 %, 0.42 % for *E. dunnii* and *E. grandis* respectively. According to Chave *et al.* (2005), despite the estimation errors that can derive from the use of specific allometric models fitted using a small number of samples, such models are useful because of their ease of implementation. In our study, for both species, estimation by NSUR had a lower bias than the other methods, ranging from -7.9 to 7.7 and from -11.8 to 24.7 for *E. dunnii* and *E. grandis*, respectively. This represents an improvement over the traditional individual approach, which gave values ranging from -18.3 to 13.7 for *E. dunnii* and from -13.2 to 48.5 for *E. grandis*, and the WLS sum approach, with ranges of -18.3 to 21.9 and -16.7 to 35.2 for *E. dunnii* and *E. grandis*, respectively. The WLS method tended to overestimate the AGB. In general, the higher overestimation yielded by WLS approaches compared to NSUR reflects the gain in prediction quality obtained when applying the latter.

To improve the overall biomass stocks estimation and its components, an additive system was proposed which ensures that the estimation functions of the components was compatible with the total biomass estimated. The model fit and validation statistics indicate that the systems of equations developed in this study will contribute to the accurate estimation of total biomass. The NSUR method is not intended to improve the precision of AGB estimates, but rather to reconcile estimates of total biomass and the sum of biomass fractions (Coutinho *et al.* 2018). With the application of NSUR we have developed full allometric models, which can be used to compute the biomass of components for trees of interest.

2.7. CONCLUSIONS

This study represents a first attempt at quantifying total tree biomass in Uruguay through the use of a simultaneously fitted system of weighted nonlinear equations. Our approach, fitting additive biomass functions, led to a consistent set of additive biomass functions for two of the most relevant *Eucalyptus* species in Uruguay. In this work the aboveground biomass of *E. grandis* and *E. dunnii was* estimated using an NSUR approach; to our knowledge, this represents the first attempt at quantifying total tree biomass with simultaneously fitted system of weighted nonlinear equations for forests in Uruguay. The correlation matrix among the biomass equations shows that strong inherent correlations existed among the biomass components measured in the same sample trees. By taking into account this cross-equation error correlation, methods like NSUR result in more efficient estimation of the system of equations than classical methods. The allometric models adjusted using NSUR methodology provided accurate biomass estimates that guarantee additivity among biomass components for *E. grandis* and *E. dunnii* in Uruguay. Simultaneous fit provided a slight improvement in most goodness-of-fit statistics. This ensures the correct performance of the additive system in new samples. The structural characteristics of the models improve the predictive capacity and extend their range of application, since they include total height and diameter as explanatory variables. These models can be implemented in procedures that require a simple and efficient method for estimation of biomass.

2.8. ACKNOWLEDGEMENTS

The authors thank the Instituto Nacional de Investigación Agropecuaria (INIA-Uruguay) for supporting fieldwork and the INIA Scholarship for PhD studies The authors thank Pablo Nuñez, Federico Rodriguez and Wilfredo Gonzalez and Jorge Basso for helping with data collection. RMNC acknowledges the support of the ESPECTRAMED (CGL2017-86161-R) and ISO-Pine (UCO-1265298) projects.

2.9. REFERENCES

Bi H, S Murphy, L Volkova, C Weston, T Fairman, Y Li, R Law, J Norris, X Lei, G. 2015. Additive biomass equations based on complete weighing of sample trees for open eucalypt forest species in south-eastern Australia. *Forest Ecology and Management* 100(349):106–121. DOI: https://doi. org/10.1016/j.foreco.2015.03.007

Bi H, J Turner, M Lambert. 2004. Additive biomass equations for native eucalypt forest trees of temperate Australia. *Trees* 18(4):467–479. DOI: https://doi.org/10.1007/s00468-004- 0333-z

Caillez F, D Alder. 1980. Estimación del volumen forestal y predicción del rendimiento con referencia especial a los trópicos. Roma, Italy. FAO 92 p.

Carvalho JP, BR Parresol. 2003. Additivity in tree biomass components of Pyrenean oak (*Quercus pyrenaica* Willd.). *Forest Ecology and Management* 179(1-3):269–276. DOI: https://doi.org/10.1016/S0378-1127(02)00549-2

Castaño J, A Ceroni, M Furest, J Aunchayna, R Bidegain. 2011. Caracterización agroclimática del Uruguay 1980-2009, Serie Técnica INIA 193. Montevideo, Uruguay. 33 p.

Chave J, C Andalo, S Brown, MA Cairns, JQ Chambers, D Eamus, H Fölster, F Fromard, N Higuchi, T Kira, JP Lescure, BW Nelson, H Ogawa, H Puig, B Riera, T Yamakura. 2005. Tree allometry and improved estimation of carbon stocks and balance in tropical forests. *Oecologia* 145(1):87–99. DOI: https://doi.org/10.1007/s00442-005-0100-x

Coutinho V, C Sanquetta, P Bittencourt, S Alves, K Henkel, W Macedo, J Moreau. 2018. Simultaneous Equations to Estimate Aboveground Biomass of *Pinus caribaea* var . hondurensis. *Floresta e Ambiente* 25(3): e20160452. DOI: https://doi.org/10.1590/2179-8087.045216

Dong L, L Zhang, F Li. 2018. Additive Biomass Equations Based on Different Dendrometric Variables for Two Dominant Species (*Larix gmelini* Rupr. and *Betula platyphylla* Suk.) in Natural Forests in the Eastern Daxing'an Mountains, Northeast China. *Forests* 9(5):261. DOI: https://doi. org/10.3390/f9050261

Dong L, L Zhang, F Li. 2015. Developing additive systems of biomass equations for nine hardwood species in Northeast China. *Trees - Structure and Function* 29(4):1149–1163. DOI: https://doi.org/10.1007/s00468-015-1196-1

Hirigoyen A, J Franco, U Diéguez. 2018. Modelo dinámico de rodal para *Eucalyptus globulus* (L.) en Uruguay. *Agrociencia Uruguay* 22(1): 63-80. DOI: https://dx.doi.org/10.31285/ agro.22.1.7

Huang S. 2002. Validating and localizing growth and yield models: procedures, problems and prospects. *In* Proceedings of IUFRO Workshop on Reality, models and parameter estimation: the forestry scenario. Sesimbra, Portugal (2-5 de junio de 2002).

Kohavi R. 1995. A Study of Cross-Validation and Bootstrap for Accuracy Estimation and Model Selection. *In* International Joint Conference of Artificial Intelligence. Montreal, Quebec, Canada. Morgan Kaufmann, Los Altos, CA. USA. p. 1137–1143.

Kralicek K, H Bao, KP Poudel, H Temesgen, C Salas. 2017. Simultaneous estimation of above- and below-ground biomass in tropical forests of Viet Nam. *Forest Ecology and Management* 100(390):147–156. DOI: https://doi.org/10.1016/j.foreco.2017.01.030

Lanfranco B, G Sapriza. 2011.El índice CONEAT como medida de productividad y valor de la tierra. Serie Técnica 187 INIA. Montevideo, Uruguay. INIA. 57 p.

Lei S, L Shirong L.2016. Methods of Estimating Forest Biomass: A Review, Biomass Volume Estimation and Valorization for Energy, Jaya Shankar Tumuluru, *IntechOpen* 10:65733. DOI: http://dx.doi.org/10.5772/65733

Li M, J Im, LJ Quackenbush, T Liu. 2014. Forest biomass and carbon stock quantification using airborne LiDAR data: A case study over huntington wildlife forest in the Adirondack park. IEEE Journal of Selected Topics in *Applied Earth Observations and Remote Sensing* 7(7):3143–3156. DOI: https://doi.org/10.1109/JSTARS.2014.2304642

Lin K, M Lyu, M Jiang, Y Chen, Y Li, G Chen, J Xie, Y Yang. 2017. Improved allometric equations for estimating biomass of the three Castanopsis carlesii H.

forest types in subtropical China. *New Forests* 48(1):115–135. DOI: https://doi.org/10.1007/s11056-016-9559-z

Myers, R. 1990. Classical and modern regression with applications. Second ed. Belmont, CA. USA. Duxbury Press. 488 p.

Ni-Meister W, S Lee, AH Strahler, CE Woodcock, C Schaaf, T Yao, KJ Ranson, G Sun, JB Blair. 2010. Assessing general relationships between aboveground biomass and vegetation structure parameters for improved carbon estimate from lidar remote sensing. Journal of *Geophysical Research: Biogeosciences* 115(G2):1-12. DOI: https://doi. org/10.1029/2009JG000936

Parresol BR. 1999. Assessing tree and stand biomass: a review with examples and critical comparisons. *Forest Science* 45(4):573–593.

Parresol BR. 2001. Additivity of nonlinear biomass equations. *Canadian Journal of Forest Research* 31(5):865–878. DOI: https://doi.org/10.1139/x00-202

Picard RR, Cook RD. 1984. Cross-validation of regression models. *Journal of the American Statistical Association* 79(387):575–583.

Poudel KP, H Temesgen H. 2015. Methods for estimating aboveground biomass and its components for Douglas-fir and lodgepole pine trees. *Canadian Journal of Forest Research* 46(1):77–87. DPOI: https://doi.org/10.1139/cjfr-2015-0256

PROBIO (Producción de Electricidad a partir de Biomasa, UY). 2015. Mejoramiento en la calidad de la información vinculada con la utilización de la biomasa forestal. Tacuarembó, Uruguay. 157 p.

R Core Team 2015.R: A Language and Environment for Statistical Computing, 3.2.1 ed. R Foundation for Statistical Computing, Vienna, Austria.

Rachid-Casnati C, M Euan, W Richard, F Resquin. 2014. Volume and Taper Equations for *P. taeda* (L.) and *E. grandis* (Hill ex. Maiden). *Agrociencia* 18(2):47–60. DOI: https://doi. org/10.2477/vol18iss2pp47-60

Resquin F, RM Navarro-Cerrillo, C Rachid-Casnati, A Hirigoyen, L Carrasco-Letelier, J Duque-Lazo. 2018. Allometry, growth and survival of three eucalyptus species (*Eucalyptus benthamii* Maiden and Cambage, *E. dunnii* Maiden and *E. grandis* Hill ex Maiden) in high-density plantations in Uruguay. *Forests* 9(12):745. DOI: https://doi.org/10.3390/f9120745

Riofrío J, C Herrero, J Grijalva, F Bravo. 2015. Aboveground tree additive biomass models in Ecuadorian highland agroforestry systems. *Biomass and Bioenergy* 100(80):252–59. DOI: https://doi.org/10.1016/j.biombioe.2015.05.026

Sanquetta CR, M Minatti, SC Junior, JW Trautenmuller, AP Dalla Corte. 2019. Independent and simultaneous modeling of biomass and carbon of Guinean Elaeis. *Floresta* 49(3):421– 430. DOI: https://doi.org/10.5380/rf.v49i3.58897

SAS Institute Inc. 2004. SAS/ETS 9.1 User's Guide. SAS Institute Inc., Cary, NC, USA.

Wang C. 2006. Biomass allometric equations for 10 co-occurring tree species in Chinese temperate forests. *Forest Ecology and Management* 222(1-3):9–16. DOI: https://doi. org/10.1016/j.foreco.2005.10.074

West PW. 2017. Simulation studies to examine bias and precision of some estimators that use auxiliary information in design-based sampling in forest inventory. *New Zealand Journal of Forestry Science* 47(1):22. DOI: https://doi.org/10.1186/ s40490-017-0101-7 65

3. MODELLING TAPER AND STEM VOLUME CONSIDERING STAND DENSITY IN *EUCALYPTUS GRANDIS* AND *EUCALYPTUS DUNNII*.

Hirigoyen Andrés[1*], Navarro-Cerrillo Rafael[2], Bagnara Maurizio[3], Franco Jorge[4], Rachid-Casnati Cecilia[1],

[1]National Institute of Agricultural Research (INIA) Tacuarembó. Ruta 5 km 386, Tacuarembó, Uruguay

[2]Department of Forestry Engineering, Laboratory of Silviculture, dendrochronology and climate change. DendrodatLab- ERSAF, University of Cordoba, Campus de Rabanales, Crta. IV, km. 396, E-14071 Córdoba. Spain.

[3]Senckenberg Biodiversity and Climate Research Centre (SBiK-F), Senckenberganlage 25, 60325 Frankfurt am Main, Germany

[4]University of the Republic, Faculty of Agronomy, Paysandú, Uruguay

3.1. RESUMEN

Eucalyptus grandis y *Eucalyptus dunnii* son las especies arbóreas más plantadas en Uruguay. Anticipar la información sobre la cantidad y calidad de la madera es importante para el manejo de las plantaciones forestales intensivas. La estimación del volumen total y comercial de madera es una herramienta esencial en la planificación y gestión forestal. El objetivo de este estudio fue evaluar sistemas de ahusamiento y volumen comercial que comprenden: una función de ahusamiento, una ecuación de volumen comercial y una ecuación de volumen total. Una estructura de error autorregresiva continua de segundo orden corrigió la autocorrelación inherente a observaciones repetidas en un mismo árbol. La función de ahusamiento y las ecuaciones de volumen se ajustaron simultáneamente después de la corrección de autocorrelación mediante el método de máxima verosimilitud de información completa. El sistema segmentado propuesto por Fang et al. (2000) produjo el mejor ajuste, ya que explicó más del 98% de la variación del ahusamiento, volumen comercial y volumen total para ambas especies. Además, se comparó la precisión de modelado y predicción del sistema segmentado con y sin incorporar la densidad del rodal como variable. Los resultados de este análisis mostraron que para *Eucalyptus*

grandis, la precisión predictiva del modelo mejoró al incluir la variable de densidad del rodal, mientras que no hubo diferencias significativas para *Eucalyptus dunnii*. Este marco de modelado proporciona una mejora en las predicciones de la conicidad y el volumen de árboles para *Eucalyptus dunnii* y *Eucalyptus grandis* en Uruguay. Las posibilidades que ofrece esta metodología podrían ser de interés para su aplicación en países donde se manejan plantaciones de rápido crecimiento y especialmente países donde se cultivan las especies estudiadas.

3.2. ABSTRACT

Eucalyptus grandis and *Eucalyptus dunnii* are the most planted tree species in Uruguay. Anticipating information about the quantity and quality of wood is important for managing intensive forest plantation. The estimate of merchantable and total wood volume is an essential tool in forest planning and management. The aim of this study was to evaluate four systems of taper and merchantable volume that consisted in a taper function, a merchantable volume equation and a total tree volume equation. A modified second-order continuous autoregressive error structure corrected the inherent serial autocorrelation of different observations in one tree. The taper function and volume equations were fitted simultaneously after autocorrelation correction by full information maximum likelihood method. The segmented system proposed by Fang et al. (2000) produced the best fit as it explained more than 98 % of the taper, merchantable volume and total volume variability for both species. In addition, the modelling and prediction precision of the segmented system were compared with and without incorporating stand density as a variable. Results of this analysis showed that for *Eucalyptus grandis*, the predictive accuracy of the model was improved by including the stand density variable, while there was no significant difference for *Eucalyptus dunnii*. This modelling framework provides an improvement in taper and tree volume predictions for *Eucalyptus dunnii* and *Eucalyptus grandis* in Uruguay. The possibilities offered by this methodology could be of interest for its application in countries where fast growth plantations are managed, and specially countries growing the studied species.

Key words: compatible systems, taper, simultaneous estimation, intensive silviculture, *Eucalyptus*

3.3. INTRODUCTION

The total volume of individual trees is commonly estimated using models that take into account the tree diameter and total height, but this method does not allow to estimate the distribution of products according to their final commercial destiny. To solve this problem, stem taper function have been developed in the past (Kozak 1988, Bi 2000). The use of taper functions ensures an accurate description of the diametric profile of the stem and facilitates the estimation of merchantable logs´ distribution at any arbitrary diameter or length (Teshome 2011).

Taper functions are equations that describe the diameter narrowing rate along the stem (Gray 1956), which can be expressed as a function of the total height of the tree (*H*), and the diameter at the breast height (*D*) (Clutter 1980). Taper equations utilize three basic characteristics of the trees: *i)* the diameter (with or without bark) at any point of the stem; *ii)* the height at a certain diameter, and *iii)* the commercial volume (with or without bark) at a given commercial height or minimum diameter from any stump height (Kozak 2004). According to Prodan et al. (1997), the use of those functions allows to assess the combination of wood products that can be obtained from a stand, and they are usually applied along with simulations of different silvicultural regimes. One of the most applied methods for estimating the volume at any height is to fit an equation that describes the stem taper (Kozak 1988, Bi 2000). The integration of the taper function from ground level to any height will provide an estimate of the merchantable volume at that height.

These functions can also be compatible with volume equations that are used to estimate individual tree volumes: ideally, the volume computed by integration of the taper equation from the ground to the top of the tree should be equal to that calculated by the total volume equation (Clutter 1980). Following Diéguez-Aranda et al. (2006), in the development of a compatible volume system, the most common approach has been to express the α coefficient of a simplified Spurr's volume equation (Spurr 1954) in terms of the taper equation coefficients, or vice versa, by

using a compatibility relationship. This ensures that the taper function and the volume equation are analytically consistent (Sharma & Oderwald 2001). Another approach involves the development of a system that ensures compatibility between the taper function and a pre-established volume equation, by including this function in the mathematical expression of the taper function (Fang et al. 2000). Examples of volume equations used for this purpose are those proposed by Schumacher & Hall (1933) and Spurr (1954). Compatible systems have been usually fitted using two different approaches: ordinary least squares (OLS) and simultaneously, using seemingly unrelated regression (SUR) or full information maximum likelihood (FIML-Diéguez-Aranda et al. 2006, Rachid-Casnati et al. 2014). In classic OLS adjust, it must be decided whether the error is minimized in the taper equations or in the merchantable volume. Then, the selected equation is fitted and the specific compatibility relationship is used to obtain the parameters of the non-fitted equation; while the simultaneous fitting of the complete systems using FIML or SUR presents consistent estimators for all the equations of the system (Fang et al. 2000).

Data for adjusting taper models include multiple height and diameter measurements from each of the individuals in the sample, which determines a longitudinal data structure (Lindstrom & Bates 1990). Simultaneously, the variability of records within each tree is lower than the variability between trees; therefore, the assumption of independence is not fulfilled. Problems associated to the use of longitudinal data to adjust taper functions include multicollinearity, autocorrelation, and heteroscedasticity. In the presence of autocorrelation, the estimated parameters are not those of minimum variance since the mean square error of the model underestimates the variance of the error term, thus invalidating the significance contrasts. Although the estimators obtained in the regression adjustment remain unbiased, they are not the most efficient (Kozak 1988). For a correct analysis of longitudinal data, numerous works propose to assume a particular error structure, expressing this autocorrelation among the errors as a stationary autoregressive model CAR(x) of order x (Garber & Maguire 2003). The advantages of this methodology are: (i) greater efficiency in obtaining the estimators of the parameters of the model; (ii) adequate estimators for the standard errors of parameters´ estimators; (iii) the

problems of lack of data or different number of measurements between individuals is solved; and (iv) it can be used even when the number of measurements is very large compared to the number of individuals (Zimmerman & Núñez-Antón 2001). According to Teshome (2011) these system should be designed to be simple, flexible and easy to handle so that they can accurately estimate merchantable volume of any log length or to a specific diameter, based solely on easily measurable individual parameters such as diameter at breast height and tree height.

Tree growth follows biological limitations, stem growth depends on complex multifactorial and site-specific factor combinations. Thus the shape of a tree is influenced by stand conditions, it is important to include stand density information in taper equations, as it potentially improves model performance (Sharma & Zhang 2004, Sharma & Parton 2009). Sharma and Zhang (2004) included stand density in modelling the taper of black spruce trees and reported improved fit statistics and predictive accuracy. Calama & Montero (2006) pointed out that the high level of random variability with respect to stem form indicated the presence of factors that acted both at plot (silvicultural treatment) and tree levels (competition). They showed that pines trees growing free of competition were less tapered than trees growing in large stocking densities. Jacobs et al. (2020) determined that when decreasing stand density, the lower part of the stem is conic instead of cylindrical. Diameter increment at the bottom part of the stem is due to the reduction in density stress, for the lowering of stand density can cause a decrease in form factors, an increase in taper rates, and a decline in the slenderness. Social status also affected stem shape: dominant trees increased in stem taper, while dominated trees in closed stands produced smaller crowns with less stem taper (Jacobs et al. 2020).

To this day, compatible taper and volume equation systems do not have widespread use in Uruguay. The development of more accurate taper and volume models for intensive Eucalyptus plantations will significantly contribute to improve forest yield and planning. Therefore, the aim of the present study was to simultaneously fit a system of equations for predicting taper, merchantable volume and total tree volume, for *Eucalyptus grandis* (Hill ex. Maiden) and *Eucalyptus dunnii* (Maiden) growing in different zones of Uruguay. Specific objectives were: i) to adjust four widely used

stem taper profile models for predicting merchantable volume; ii) to select and validate the best system; iii) to assess the effect of stand density on stem taper and volume predictions. The present study involved simultaneous fitting, while addressing the autocorrelation, multicollinearity among independent variables, and heteroscedasticity.

3.4. MATERIALS AND METHODS

3.4.1. Study site

Data was collected in the trials of the National Institute of Agricultural Research (INIA) in 2015 (PROBIO 2015), located in three different zones in Uruguay: northwest (32° 18′ 18″ S, 57° 44′ 06″ W, next to Guichon city, Paysandú); central east (33° 01′ 43″ S, 55° 31′ 08″ W, next to Sarandí del Yi, Durazno) and central west (33° 21′ 06″ S, 56° 41′ 17″ W, near Trinidad city, Flores) (Fig. 1).

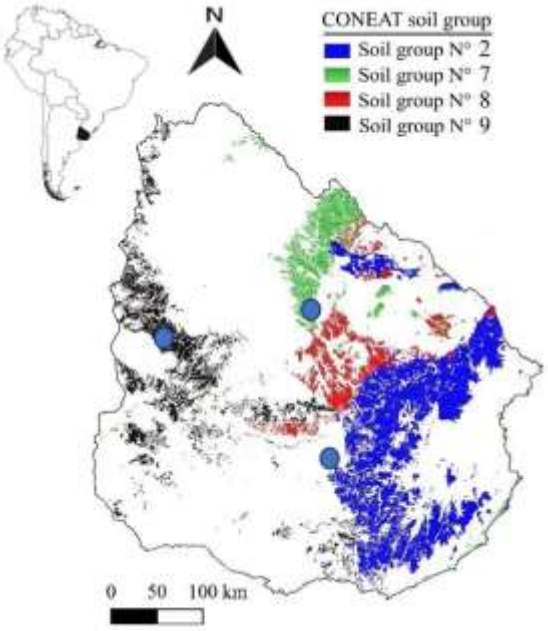

Figure 1. Location of the study area (blue points) and soils forest classification sites in Uruguay.

The study zones have a temperate subtropical climate, with a mean annual temperature of 18 °C (12 °C in the coldest month, 24 °C in the warmest month) and

mean annual rainfall between 1300 and 1400 mm (Castaño et al. 2011). According to the National Commission for Agroeconomic Studies of the Land classification (CONEAT), the Guichon predominant soil is planosols, with low fertility, horizon A 40-50 cm depth, weak structure, low level of organic matter, slopes of 1%–3%, sandy texture, medium to low risk of drought, imperfect drainage, moderately-slow to slow permeability and good rooting ability. Trinidad soils are Vertisols, with medium fertility, horizon A 50-60 cm depth, weak structure, medium level of organic matter, slopes of 2%–5%, loam franc structure, low risk of drought, moderate drainage, moderately permeability and good rooting ability. Sarandí del Yi presented soils corresponding vertisols ruptic and Brunosols with a horizon A 50–60 cm depth, sandy-loam, loam franc texture, low fertility, low risk of erosion, moderate slopes (1%–3%), weak structure, low organic matter, imperfect drainage and good rooting capacity.

3.4.2. Data and data collection

A total of 60 trees of *Eucalyptus dunnii* and 113 trees of *E. grandis* were felled and diameters at breast height (*D*), total height (*H*), and diameters (d_i) at the corresponding heights (h_i) (0.2; 0.7; 1.3 m; and beyond this point, every 1.0 m up to total height) were measured (Tab. 1). The stump height was fixed at approx. 20 cm from the ground. Partial and total volumes of the stem (with and without bark), used for fitting the system, were estimated by Smalian method (Prodan et al. 1997). The top section volume was estimated using the volume formula for a cone. Plots of relative height (*hi/H*) against relative diameter (*di/D*) for each species were carefully examined to detect possible anomalies: knots, bark defects, etc. (Fig. 2).

Table 1. Summary statistics of the data for taper and volume of *Eucalyptus grandis* and *Eucalyptus dunnii* in Uruguay. Variables and abbreviations: diameter over bark (*dob*, cm); diameter under bark (*dubi*, cm); diameter at breast height (D, cm); total height (*H*, m); total tree volume over bark (*Vob*, m^3) and total tree volume under bark (*Vub*, m^3). N= number of trees, Sd=standard deviation, Min= minimum, Max= maximum

Species	Variable	N	Mean	Sd	Max	Min
	D(cm)	60	18.21	3.55	24.40	9.90
	H(m)	60	23.72	3.21	30.75	15.72
	$V_{ob}(m^3)$	60	0.28	0.13	0.65	0.05
E. dunnii	$V_{ub}(m^3)$	60	0.24	0.11	0.55	0.04
	d_{obi}(cm)	1285	12.33	5.78	33.10	0.00
	d_{ubi}(cm)	1285	11.32	5.31	31.83	0.00
	D (cm)	113	22.71	5.82	36.90	10.95
	H(m)	113	27.56	5.72	40.90	16.60
	$V_{ob}(cm^3)$	113	0.56	0.39	1.83	0.06
E. grandis	$V_{ub}(cm^3)$	113	0.51	0.36	1.69	0.06
	d_{obi}(cm)	2667	15.64	7.23	38.45	0.00
	d_{ubi}(cm)	2667	14.80	6.95	33.50	0.00

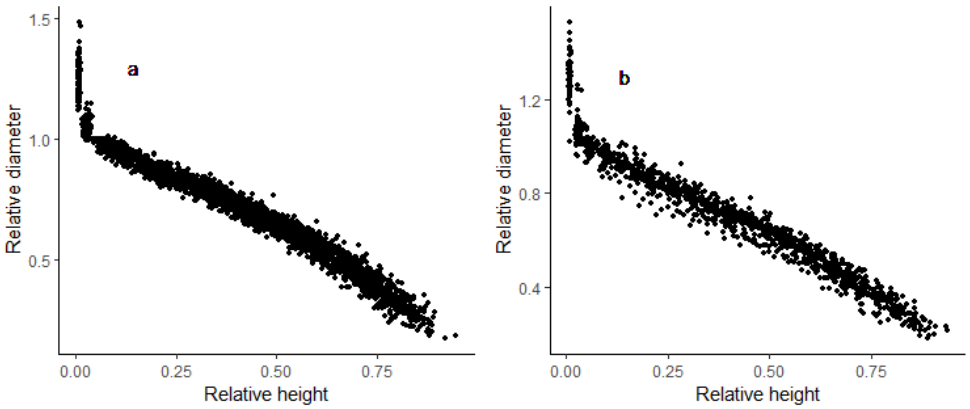

Figure 2. Relative diameter (quotient between an objective diameter and the diameter at breast height) against relative height (quotient between height to an objective diameter and total tree height) for *Eucalyptus grandis* (a) and *Eucalyptus dunnii* (b) in Uruguay.

3.4.3. Compatible System Fitting

Four compatible volume systems widely used in forestry were selected from literature (Martin 1981, Diéguez-Aranda et al. 2006, Tang et al. 2016), to test and to evaluate the taper and stem volume of both species (supplementary materials Tab. S1) . It is possible to adjust simultaneously compatible taper and volume systems if the volume and taper equations use the same parameters, and share a common geometric and mathematical structure (Tamarit Urías et al. 2014). The compatible systems analysed had two components, a taper function and a total volume equation. In addition, the system proposed by Fang et al. (2000) includes also a merchantable volume equation to or above any specified height or diameter limit.

3.4.4. Model Fitting

Compatible taper and volume equations were fitted using a simultaneous method, where all parameter must be expanded through a compatibility relationship. This method reduces the total system squared error (SAS Institute 2004), minimizing prediction errors in diameter at different heights and volume (Diéguez-Aranda et al.

2006). Parameter estimation was carried out using the Proc model of SAS/ETS® (SAS Institute 2004). The compatible system requires adequate parameter estimation methods: if the error terms of the taper model and the merchantable volume model were independent and homogeneous, ordinary least squares estimation (OLS) was applied. Generalized least squares (GLS) methods, such as full information maximum likelihood estimation method (FIML), generalized method of moments (GMM), and seemingly unrelated regression (SUR), are valid options to fit simultaneous equations (Fang et al. 2000). The FIML method homogenizes and minimizes the standard error of the parameters and allows total compatibility between taper and merchantable volume (Fang et al. 2000). Systems were simultaneously fitted using the FIML method , that properly accounts for cross-equation correlation and is appropriate for systems of simultaneous equations, (SAS Institute 2004). We considered the full information of maximum likelihood estimation in the proc model procedure. Simultaneous fitting of the systems applied requires an equal number of observations for all the equations. However, the number of observations in each equation was not equal, as there was more than one diameter observation for each tree but only one observation for total stem volume. Therefore, we applied the following structure of the data (Diéguez-Aranda et al. 2006, Tang et al. 2016): the total volume of each tree was assigned to each diameter observation of the same tree, and the inverse of the number of observations in each tree ($1/n_i$) was used as a weight of the total volume observation in the fitting process.

3.4.5. Multicollinearity, autocorrelation and heteroscedasticity

There are several problems associated with stem taper and volume equation analysis, due to the violation of the fundamental least squares assumption of independence and equal distribution of errors with zero mean and constant variance. The most important issues are multicollinearity, autocorrelation and heteroscedasticity. These problems affect the efficiency of the regression coefficients, although the least-squares estimates remain unbiased and consistent. The existence of multicollinearity does not seriously affect the predictive ability of the model (Kozak 1988). To

evaluate the presence of multicollinearity between variables in the models analysed, the condition number (CN) was used. According to (Belsley 1991), if 5≤CN≤10, multicollinearity is not a serious issue. If 30≤CN≤100 problems associated with multicollinearity may arise, and if CN>100 severe problems of multicollinearity exist. Thus, for CN values greater than 30, corrections must be made. The data used in the study includes hierarchical relationships, with multiple observations for each tree; thus, autocorrelation within the residuals for each individual might be expected**.** To demonstrate the autocorrelation, the residuals were analysed graphically and the Durbin-Watson statistic (*Dw*) was calculated (Hernández-Ramos et al. 2017). *Dw* values close to 2 allow the non-rejection of the null hypothesis (of non-existence of autocorrelation); a value of *Dw* lower than 2 was indicative of positive autocorrelation of order one, while values between 2 and 4 indicated negative autocorrelation of order one (Dufour & Dagenais 1985).

One of the general methods proposed to deal with continuous, unbalanced, multilevel longitudinal data is to model the correlation structure directly. In the present study a second-order continuous autoregressive error structure CAR (2), where *h* accounted for the distance between measurements, and their relative position on the stem was used to overcome the inherent autocorrelation of the longitudinal data. This structure is applied to data from the same sample unit measured at intervals that are not constant in time or space and with a different number of measurements in each sample unit, which is characteristic of the taper functions. The CAR(x) error structure was programmed to enable dynamic updating of the residuals. To account for second-order autocorrelation, a CAR(2) model form that expands the error terms in the following way was used (Zimmerman & Núñez-Antón 2001):

$$e_{ij} = d_1 \rho_1^{h_{ij}-h_{ij-1}} e_{1j-1} + d_2 \rho_2^{h_{ij}-h_{ij-2}} e_{ij-2} + \varepsilon_{ij} \qquad [1]$$

Where e_{ij} is the *j*th ordinary residual on the *i*th individual (i.e., the difference between the observed and the estimated diameters of the *i* tree at *j* height measurement), d_1=1 for $j > k$,k=1, 2 and it is zero for $j \leq k$, ρ_k are the autoregressive

parameters to be estimated, $h_{ij} - h_{ij-k}$ are the distances separating the *j*th from the *j*th-*k* observations within each tree, $h_{ij} > h_{ij-k}$

When data from different sample units with different characteristics are used, it is expected that the variance of the errors (σ_i^2) is not constant, resulting in heteroscedasticity problems. To detect the deviation of the homoscedasticity of the residuals, the Breusch-Pagan test was applied. To remove the restriction of the variance heterogeneity of errors, since variances are unknown, an alternative is to graphically identify those independent variables (or combinations thereof) that cause such variation. (Neter et al. 1996) suggest using a:

$$\sigma_i^2 = (X_i)^k \quad [2]$$

Researchers like Prodan et al. (1997), working with compatible taper and volume functions, proposed a power function of the variable $D_i^2 Ht_i$, (the square of the tree diameter multiplied by the total height tree) as a candidate for:

$$\sigma_i^2 = (D_i^2 Ht_i)^k \quad [3]$$

To estimate the *k* value (power term), we used the method suggested by Harvey (1976, in Parresol 1993), which consists of using the errors obtained with the unweighted model as a dependent variable in the power model of error variance.

The *k* parameter of eq. 3 was estimated through linear regression using Proc Reg (SAS Institute 2012) following the methodology described above. According to Diéguez-Aranda et al. (2006), the weighting factor for heteroscedasticity $1/(D_i^2 Ht_i)^k$ along with the correction for the special structure of the data, was multiplied and programmed in the model procedure of SAS/ETS® (SAS Institute 2012) by specifying:

$$resid.V = resid.V/sqrt(n_i (D_i^2 Ht_i)^k) \quad [4]$$

where n_i is the number of observations in each tree.

The use of models with random effects parameters can handle autocorrelation and heteroskedasticity, but increases operating costs (Liu et al. 2020). This methodology involve additional measurements to estimate random effects parameters, as upper

stem diameter-height measurements (calibration) for improving diameter prediction. (Liu et al. 2020).

3.4.6. Model comparison and validation

The accuracy and precision of each model were compared through graphical and numerical analysis of their residuals. The statistical criteria applied were: the root of the mean squared error (RMSE), adjusted coefficient of determination (R^2-adj), coefficient of determination for nonlinear regression (R^2), and mean absolute bias (MAB) (Prodan et al. 1997). These expressions are summarized as follows:

$$R^2adj = 1 - \frac{\sum_{i=1}^{n}(y_i - \hat{y}_i)^2}{\sum_{i=1}^{n}(y_i - \bar{y})^2} \quad [5]$$

$$R^2 = r^2_{y\hat{y}_i} \quad [6]$$

$$RMSE = \sqrt{\frac{\sum_{i=1}^{n}(y_i - \hat{y}_i)^2}{n-p}} \quad [7]$$

$$MAB = \frac{\Sigma(|y_i - \hat{y}_i|)}{n} \quad [8]$$

Where $r^2_{y_i\hat{y}_i}$ is the correlation coefficient between the measured and estimated values ($y, \hat{y}_i$ respectively) of the dependent variable, *n* is the total number of observations and *p* is the number of equation parameters.

The validation process was used to collaborate whether the goodness-fit also reflects in the quality of the predictions (Myers 1990), which influences the selection of the best model. The use of cross validation in forestry is a common practice (Hirigoyen et al. 2018), and it is a method for model selection considering the predictive ability of the model. This is performed using the same data used for fitting (Myers 1990), and consists of the calculation of the residuals of the *i*-th observation using parameters estimated by fitting the equation with all data except the *i*-th observation. This process is known as leave-one-out cross-validation, LOOCV (Kirschen et al. 2000).

The sum of squares of the eliminated residues is called PRESS (Predicted Residual Sum of Squares (Picard & Cook 1984), and it is used to calculate the selection criteria or RMSE for cross-validation (RMSEcv).

$$PRESS = \sum_{i=1}^{n}(y_i - \hat{y}_{i-1})^2 \quad [9]$$

$$RMSE_{cv} = \sqrt{\frac{\sum_{i=1}^{n}(y_i - \hat{y}_{i-1})^2}{n-p}} \quad [10]$$

A close agreement between RMSEcv and RMSE indicates that the model is not overfitting the data and has good predictive value (Anderson-Sprecher 1994). The Model Efficiency (ME) represents the proportion of variability observed in the original data that is explained by the model, and it varies between 0 (without adjustment) and 1 (perfect fit) (Vanclay & Skovsgaard 1997).

$$\text{ME}=1 - \frac{\sum_{i=1}^{n}(y_i - \hat{y}_{i-i})^2}{\sum_{i=1}^{n}(y - \bar{y}_{i-1})^2}\left(\frac{n-1}{n-p}\right) \quad [11]$$

Plots of residuals versus predicted values, as well as versus dependent and independent variables, were examined for detecting bias. Statistics and the graphical analysis of residuals are essential to describe the goodness of fit of a model to understand which of the systems better represents observations, and therefore as a criterion for recommending a model.

3.4.7. Model ranking

A classical procedure of ranking *m* models is to assign numbers (1, 2, 3, …, *m*) for model comparison. In this respective model order the exact place of a model with reference to other models is not known (Poudel & Cao 2013). Poudel & Cao (2013) proposed a method where relative ranks were developed to display the relative positions of the methods. This method was used to get the specific and relative position of each model, relative rank of method *i* is defined as:

$$R_i = 1 + \frac{(m-1)(S_i - S_{min})}{S_{max} - S_{min}} \quad [12]$$

where R_i is the relative rank of model i (i =1,2, 3…, m), S_i is the goodness-of-fit statistics produced by model i, S_{min} is the minimum value of Si, and S_{max} is the maximum value of S_i. Assigned numbers by respective order of the model show the best and the worst methods have relative ranks of 1 and *m*. Because the magnitude, and not only the order, of the Si's are taken into consideration, this ranking method

provides more information than the common ordinal ranks. In our study the ranking system was applied to R^2, RMSE and MAB statistics for diameter, merchantable and total volume to calculate mean rank. The overall rank was determined by taking the mean of the ranks (MR) for these variables.

3.4.8. Stand density effects

The stand density variable was tested into the selected system taper equations to improve the fitting. (Liu et al. 2020) work with *Larix gmelinii* showed the viability of including ecologically parameters (as stocking degree) and improving accuracy of taper equations by random effects. Stand density was introduced through mathematical relationship between the resulting coefficients of volume equation and the density classes. For example Schumacher (1933) volume model included in Fang et al. (2000) or its modification version in Sharma & Oderwald (2001) in compatible system ($v=a_0 dbh^{a_1} H^{a_2}$) have three parameters. Parameter a_0 represents the estimated asymptotic volume at a dbh and H determined. Selecting parameter a_0 as expanded parameter in the model can improve the estimation and indicates that the stand density has a significant effect on dbh and H-individual volume relationship. The suitable taper system with stand density variable was fitted and evaluated by the whole fit data set and cross validation. We adjusted model compatible system taper and volume for *E. grandis* and *E. dunnii* with stand density into parameters used in the volume compatible equations (see Tab. 2). The resultant parameter prediction equation for predicting a_0 can be given by:

$$a_{0=a_{01}*\log(N)^{a_{02}}} \quad [13]$$

$$a_{0=a_{01}+\log(N)^{a_{02}}} \quad [14]$$

$$a_{0=a_{01}*N^{a_{02}}} \quad [15]$$

$$a_{0=a_{01}+N^{a_{02}}} \quad [16]$$

where N refers to stand density, a_{01}, a_{02} parameters to be estimated. Equations (13 to 16) were substituted into selected model system to examine the effect of stand density on tree taper and volume. We named this modified version of the

model as “Modified system”, to differentiate it from the original “Original system”.

3.5. RESULTS

3.5.1. Model Fitting and selection

To obtain consistent parameter estimation the taper and merchantable volume equations were fitted simultaneously through the FIML method. Parameter shared by both the taper and volume equations estimates and their approximated standard errors for each compatible volume system are listed in Tab. 2. The goodness-of-fit statistics for both species are shown in Tab. 3. All systems were initially fitted without expanding the error term to account for autocorrelation. As expected, because of the hierarchical nature of the data, the values of the Durbin-Watson (*Dw*) test for all functions of both species indicated that the residual trend could be described as a function of lag1- and lag2-residuals within the same tree. The error term was, therefore, expanded as a first order and a second order autoregressive structure. The correlation trend disappears with a first-order autoregressive error structure which was sufficient to eliminate the autocorrelation in the system for both species (Tab. 3). For both species, the best systems taking into account the goodness-of-fit statistics and MR were Max & Burkhart (1976) and Fang et al. (2000) models. These equations exhibited the lowest values of RMSE (<0.8 cm), MAB (<0.62 cm), and the highest R^2-adj (98.8%) for *E. grandis* and *E. dunnii*. Concerning the total volume, the MR suggests that the models fall into two groups separated by a large gap. Fang et al. (2000), Max & Burkhart (1976) and Kozak et al. (1969) models were included into a group with lower MR for *E. grandis* (MR=1.1) and *E. dunnii* (MR=1.8). On the other hand, Sharma and Oderwald (2001) model appeared to be an inadequate model for both species (MR=4). R^2-adj, RMSE and MAB statistics show the same trend: all models except Sharma and Oderwald (2001) were competitive and small differences were found. The total volume variance was similar for all the models for both species. However, Fang et al. (2000) had the best MR for both species and was selected as the best. Based on the best fit, 99% of the total variation in predicting

upper stem diameters and total volume was explained; and RMSE was lower than 1 cm and 0.035 m^3 in predicting stem diameter and total volume for both species. The model had an average absolute bias less than 0.0025 m^3 for volume over bark and 0.61 cm for diameters.

Table 2. Values of the estimated parameters for simultaneous fitting for *Eucalyptus grandis* and *Eucalyptus dunnii*. Approximated standard errors are in brackets.

	Volume system	a_0	a_1	a_2	b_1	b_2	b_3	b_4	p_1	p_2
E. grandis	Fang et al. (2000)	0.00005 (3.34E-7)	2.136 (0.0014)	0.761 (0.0014)	3.88E-6 (3.69E-8)	0.00003 (1.03E-7)	-0,0004 (0.0002)		0.027 (0.0002)	0.946 (0.0054)
	Kozak et al. (1969)				-2.9181 (0.008)	1.0254 (0.004)				
	Max and Burkhart (1976)		0.694 (0.026)	0.038 (0.0006)	-2.667 (0.111)	1.213 (0.062)	-0.887 (0.073)	524.4 (15.31)		
	Sharma and Oderwald (2001)	0.00003 (7.58E-9)	2.207 (0.0003)							
	Fang et al. (2000)	0.00002 (8.64E-7)	1.860 (0.0063)	1.194 (0.0095)	4.20E-6 (4.91E-8)	0.00003 (1.55E-7)	0.00006 (8.44E-6)		0.034 (0.0004)	0.851 (0.006)
E. dunnii	Kozak et al. (1969)				-2.431 (0.023)	0.789 (0.012)				
	Max and Burkhart (1976)		0.701 (0.104)	0.0413 (0.001)	-2.261 (0.236)	1.002 (0.133)	-0.410 (0.146)	503.38 (25.86)		
	Sharma and Oderwald (2001)		2.243 (0.0004)	0.00003 (4.67E-8)						

Note: All parameters significant at p-value < 0.0001.

Table 3. Goodness of fit statistics for compatible volume systems for *Eucalyptus grandis* and *Eucalyptus dunnii* in Uruguay. Variables and abbreviations: R^2-adj= adjusted coefficient of determination, RMSE=root mean squared error, MAB= mean absolute bias, DW= Durbin-Watson statistic and MR= Mean Rank. Selected models are shown in bold.

		Taper equation					Volume equation				
	Compatible volume systems tested	RMSE (cm)	R^2-adj	MAB (cm)	Dw	MR	RMSE (m3)	R^2-adj	MAB (m3)	Dw	MR
E. grandis	**Fang et al. (2000)**	**0.790**	**0.99**	**0.610**	**2.2**	**1.000**	**0.035**	**0.99**	**0.024**	**1.99**	**1.000**
	Kozak et al. (1969)	1.789	0.93	1.255	2.08	2.000	0.035	0.99	0.024	1.98	1.100
	Max and Burkhart (1976)	0.840	0.98	0.620	2.2	1.002	0.035	0.99	0.024	1.98	1.075
	Sharma and Oderwald (2001)	1.146	0.97	0.816	1.9	1.382	0.036	0.99	0.025	1.96	4.000
E. dunnii	**Fang et al. (2000)**	**0.787**	**0.99**	**0.612**	**2.0**	**1.000**	**0.021**	**0.98**	**0.015**	**1.9**	**1.000**
	Kozak et al. (1969)	1.802	0.88	1.352	2.0	2.000	0.022	0.97	0.015	2.09	1.789
	Max and Burkhart (1976)	0.898	0.97	0.624	2.2	1.001	0.023	0.97	0.015	2.0	1.711
	Sharma and Oderwald (2001)	1.042	0.96	0.800	1.9	1.253	0.024	0.97	0.018	2.1	4.000

In addition, the Fang et al. (2000) model allowed including a function to estimate the merchantable volume; thereby, we readjusted a system with three equations: taper, merchantable volume, (integration of taper equation to any height limit) and total stem volume (integration of taper equation to total tree height). The coefficient estimates for complete system after correction for autocorrelation, their approximated standard errors, and the goodness-of-fit statistics of the taper function, merchantable stem volume and total stem volume are given in Tab. 4.

Table 4. Values of the estimated parameters for simultaneous fitting of Fang et al. (2000) approximated standard errors are in brackets, and goodness of fit statistics for taper, total volume and merchantable volume for *Eucalyptus grandis* and *Eucalyptus dunnii* in Uruguay. Variables and abbreviations: R^2-adj= adjusted coefficient of determination, RMSE=root mean squared error.

	Eucalyptus grandis	*Eucalyptus dunnii*
Parameters	Estimate	Estimate
a0	0.00004(2.4E-7)	0.00002 (5.4E-7)
a1	2.09(0.001)	1.87 (0.005)
a2	0.862(0.001)	1.233 (0.007)
b1	4.2E-06(3.3E-5)	4.3E-6 (4.5E-8)
b2	0.00003(5.2E-5)	0.00003 (1.3E-7)
b3	0.0002(0.00008)	0.00018 (0.00002)
p1	0.031(0.0002)	0.037 (0.0004)
p2	0.941(0.011)	0.868 (0.0033)
Taper function		
RMSE (cm)	0.712	0.867
R^2-adj	0.98	0.98
Total Volume equation		
RMSE (m^3)	0.042	0.021
R^2-adj	0.99	0.98
Merchantable Volume equation		
RMSE (m^3)	0.039	0.025
R^2-adj	0.98	0.97

For Fang et al. (2000) with three equation, mean average bias (MAB) were 0.610 and 0.659 cm for taper equation; 0.003 m^3 and 0.016 m^3 for total volume and 0.031m^3 and 0.022 m^3 for merchantable volume for *E. grandis* and *E. dunnii* respectively. Scatter plots of studentized residuals against predicted and observed values against predicted values for d_{ub}, merchantable volume and total volume are shown in Fig. 3. The residuals did not show a trend of increasing error variances, and the zero-studentized residuals cross the centre of the data points. This suggests that the taper and volume function were appropriately identified, and the error structure of the model is associated with the equal error variance. The multicollinearity was inferred by CN, 46 for *E. grandis* and 56 for *E. dunnii*.

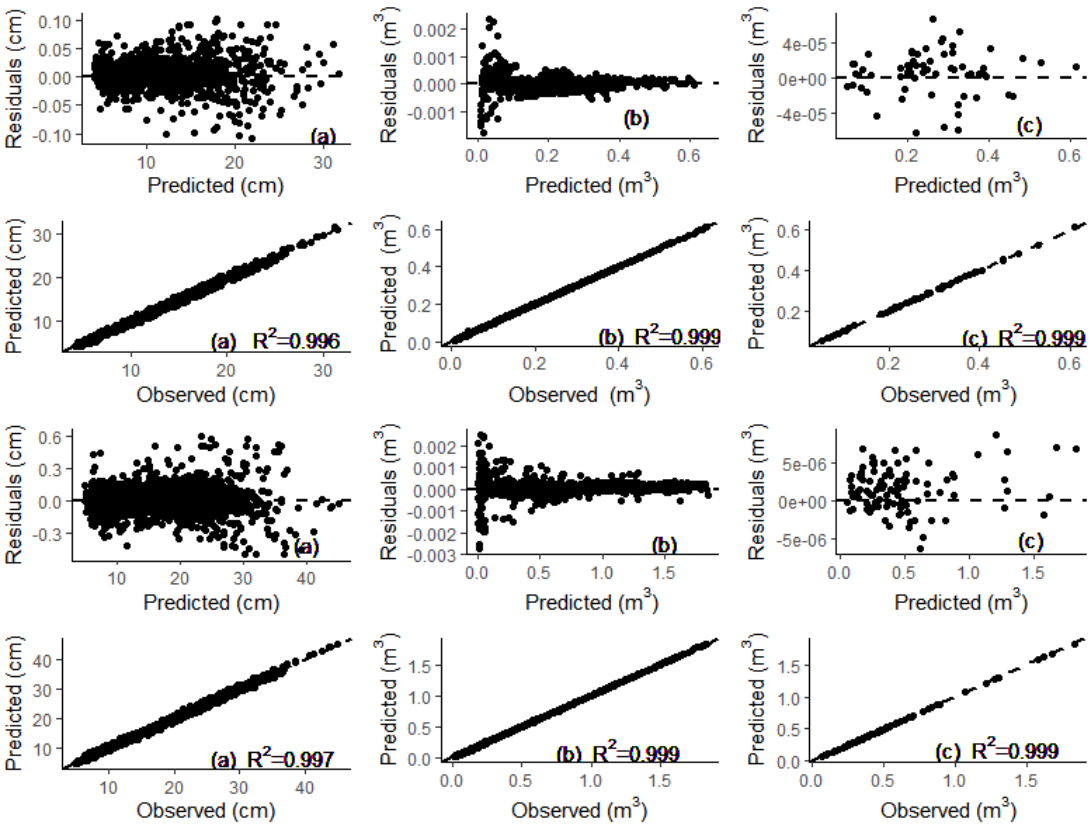

Figure 3. Studentized residuals and observed values against predicted values against predicted values for a: diameters under bark (d_{ub}. cm); b: merchantable volume (m^3) and c: total volume (m_3). obtained with (Fang et al. 2000) model for *Eucalyptus dunnii* (firsts row) and *Eucalyptus grandis* (seconds row) in Uruguay. R^2 = Coefficient of determination.

The prediction precision (through LOOCV) of Fang et al. (2000) was evaluated in terms of model efficiency (ME) and root mean square error ($RMSE_{cv}$) of estimated diameters, merchantable volume and total stem volume. For *E. grandis* ME=0.98, 0.98 and 0.87; $RMSE_{cv}$=0.803 cm, 0.037 m^3 ,0.024 m^3 for taper, total volume and merchantable volume respectively. For *E. dunnii* ME=0.95, 0.98 and 0.87; $RMSE_{cv}$=1.03 cm, 0.028 m^3 ,0.03 m^3 for taper, total volume and merchantable volume respectively. Mean average bias (MAB) values were 0.708 and 0.877 cm for

taper equation, 0.02 6m^3 and 0.025 m^3 for total volume and 0.014 $m^3$and 0.019 $m^3$for merchantable volume for *E. grandis* and *E. dunnii* respectively.

3.5.2. Model development and evaluation with density variable

When comparing the quotient between RMSEcv and RMSE of the selected model, we expected values lower o close to 1, indicating a good predictive value of fitted models. For *E. dunnii* this was confirmed, since the RMSE ratio was always lower than 1 (ranged 0.8-0.88) for taper, total and merchantable volume. However, we found quotient values of 1.14 for total volume and 1.7 for merchantable volume for *E. grandis*, which indicated a possible overfitting.

The stand density range significantly affected the compatible system for *E. grandis*. The stand density in this study was 390, 453, 535, 850, 930 and 1090 tree ha^{-1}. However, for *E. dunnii* there were not significantly effects, probably due to the fact that the study only covered a limited range of stand densities (930, 990, 1010 and 1100 tree ha^{-1}).

Equations (13 to 16) were fitted and evaluated to the entire data set composed of different stand density by MR (calculated on R^2-adj, RMSE and MAB values). Equation 13 obtained the first place into mean ranking (R^2-adj=0.98; 0.99; 0.99; RMSE 0.895 cm; 0.034 m^3; 0.031 m^3; MAB= 0.668 cm, 0.024 m^3; 0.025 m^3 for taper, total and merchantable volume), followed by Equation 14. In bias term Equation 13 had the lowest values: 0.18 cm 0.0025 m^3 and 0.021 m^3.

In reference to Original system, Modified system improves in terms of R^2-adj, RMSE and MAB for total and merchantable volume, while for the taper equation the goodness-of-fit was almost invariant (Tab. 5). The effect of stand density was analysed visually by generating tree profiles, total and merchantable volume using

Original and Modified systems for an average tree with d=22.7 cm and H =26.6 m at different stand densities (Fig. 4).

Table 5. Values of the estimated parameters for Modified model (Fang et al. 2000) approximated standard errors (Estd), and goodness of fit statistics for taper, total volume and merchantable volume for *Eucalyptus grandis* in Uruguay. Variables and abbreviations: R^2-adj= adjusted coefficient of determination, RMSE=root mean squared error, MAB=mean absolute bias.

Parameters	Estimate	Estd	p value
p1	0.032	0.00026	<.0001
p2	0.942	0.00959	<.0001
a01	0.000023	3E-7	<.0001
a02	0.162	0.0045	<.0001
a1	2.079	0.0015	<.0001
a2	0.953	0.0019	<.0001
b1	4.26E-06	3.4E-8	<.0001
b2	0.000032	8E-8	<.0001
b3	0.000401	1.5E-4	0.0086
Taper equation			
RMSE (cm)		0.795	
R^2-adj		0.98	
MAB (cm)		0.668	
Total Volume equation			
RMSE (m^3)		0.034	
R^2-adj		0.99	
MAB (cm)		0.024	
Merchantable Volume equation			
RMSE (m^3)		0.031	
R^2-adj		0.99	
MAB (cm)		0.025	

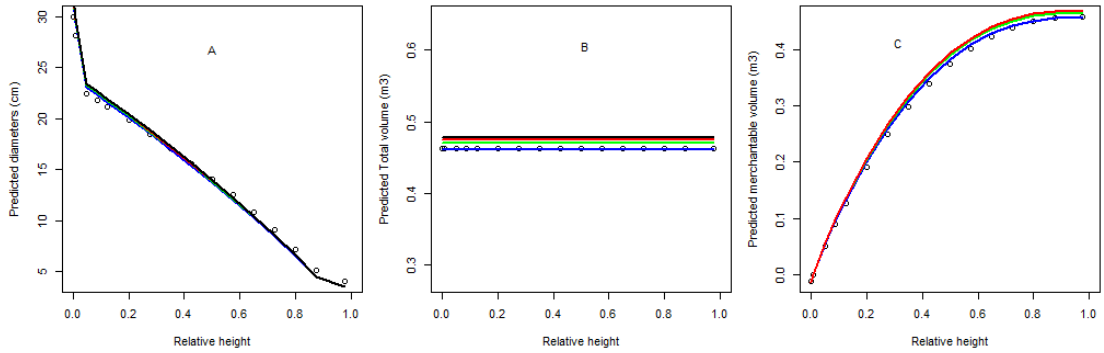

Figure 4: Profiles (A), total volume (B) and merchantable volume (C) generated by Original (points) and Modified system, for the average tree (d =22.7 cm and H = 26.6 m) at different stand densities (400: blue line; 850: green line; 1200: red line and 1600: black line, trees ha^{-1}) for *Eucalyptus grandis* in Uruguay.

Box plots of residuals for both systems, Modified and Original, for total volume and diameter against relative height class and relative diameters class are in Fig. 5.

Data for total volume was grouped into four diameters classes (20-25-30-35 cm). Original system has an overestimation trend while Modified system improved results for all classes, particularly for high diameter ones. For diameters data, height classes were 18, 25, 35 and 45 m, both Original and Modified system showed an overestimation for diameters in all classes. However Modified system residuals have a homogeneous distribution around zero.

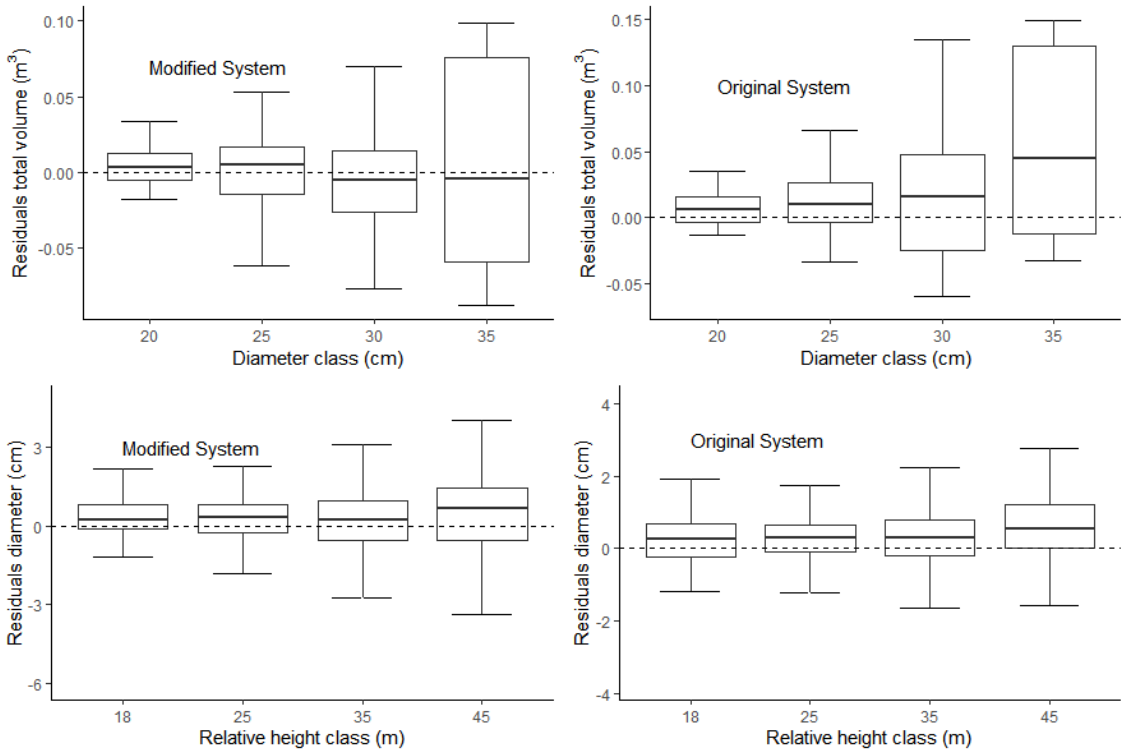

Figure 5. Residuals boxplot of estimated total volume and estimated diameters by relative diameters classes of the Fang et al. (2000) Original and Modified systems. The boxes represent the interquartile ranges. The maximum and minimum total volume and diameters prediction errors are represented respectively by the upper and lower whiskers.

3.6. DISCUSSION

3.6.1. Original system model

After estimating the fit and cross-validation statistics of the four models fitted, Fang et al. (2000) model was selected as the best one and used in subsequent analysis. To ensure numeric consistency, a simultaneous fitting procedure based on the FIML estimation method was used this method has been used successfully in several

studies because it optimizes the parameters of taper and commercial volume, while minimizes and homogenizes standard deviation. Results for the taper and volume equations fitted for both species indicated that Fang et al. (2000) model is the most precise and least biased. This model had the first place in ranking of models. Previous research found that the modification of the Muhairwe variable exponent model was the best model to describe stem shape to *E. grandis* (Gomat et al. 2011). On the other hand, Methol (2008) adjusted the segmented model of Max & Burkhart (1976) for both species this model has second place in our study.

The system of Fang et al. (2000) is widely used for the description of stems form and estimated volume, and its implementation has been reported in biometric systems for a wide range of species and countries (Diéguez-Aranda et al. 2006, Tamarit Urías et al. 2014, Tang et al. 2016, Hernández-Ramos et al. 2017). This model has the merits of being a flexible and analytically integrable into a system providing high accurate estimates of stem volume for any stem segment. (Rachid-Casnati et al. 2014) adjusted for *E. grandis* the explicit model for total volume of Schumacher-Hall, and this model is integrated to the adjusted model in this study. The quality of fit in terms of ME was similar in both studies, the RSME was slightly lower in (Rachid-Casnati et al. 2014), and the parameters values were similar, with small differences attributable to the simultaneous adjustment of the models.

The Fang et al. (2000) segmented model, presents two inflection points on the relative height of the stem: *p1* and *p2* are relative heights from ground level where the points are assumed by the model to occur, dividing the stem in three sections. The first inflexion point, where the neiloid changes to a paraboloid (as percentage of the total height), and the second inflexion point, at which the change from the paraboloid to a cone occurs. The inflection points for the selecting system occur at 3.1% and 94% for *E. grandis* and 3.7% and 86% for *E. dunnii*. The first inflection

points for *E. grandis* and *E. dunnii* were the very short as a percentage of total height, these results are similar to those of previous studies; 3.6% (Özçelik & Göçeri 2015) for *E. grandis;* however, p2 was less (45%). The presence of multicollinearity (correlations among variables) in the model has been examined by CN, its value for both species was in range of 30–100. This values are tolerated when models contain polynomial and cross-product terms (Belsley 1991).The equation systems of Fang et al. (2000) showed weak multicollinearity for both *Eucalyptus* species, and Mora et al. (2013) stated that multicollinearity does not seriously affect the predictive ability of the model. Through the comparison of the RSMEcv through LOOCV, and RMSE of the simultaneous adjustment, it was evidenced that the values were very close (Tables 5 and 6), this indicates that the model is not overfitting the data and has a good predictive value.

3.6.2. Modified system model

Sharma and Parton (2009) and improved fit statistics and predictive accuracy by including stand density information into a variable taper equation. These studies identified competition as a relevant stand property responsible for volume miscalculation. (Liu et al. 2020) work with taper models included both fixed-effects parameters showed that age and stocking degree had significant effects on tree stem and improved the predictive taper equations. Traditional and simple volume functions do not consider the dependency of volume on competition or stem form. They generally involve *dbh* and *H* as predict variable (Spurr 1954).

Including age and density of trees, part of the site variability that affects the growing conditions of each individual tree is taken into account. This achieves an improvement in predictions of the stem taper is achieved (Liu et al. 2020).

In our study the stand density had a statistically significant influence in volume estimation for *E. grandis*, while for *E. dunnii* the limited range of stand density compared with *E. grandis* could be too narrow to properly explore effects on volume. Jacobs et al. (2020) pointed out that the effect of the competition was significant on both stem volume and stem taper in *Picea abies*. Sharma & Parton (2009) reported that the difference in bole diameter between trees at lower and higher stand densities diminished as stand density increased, the density treatments only significantly affected the stem form of the smallest trees. According with Jacobs et al. (2020), there is a lack of knowledge on how the stem form of trees with the same *dbh* and *H* is affected by the individual competition situation inside the stand. However, for the average tree no differences in profile were observed, while for merchantable and total volume the differences were appreciable.

Original Fang et al. (2000) results for merchantable volume showed an underestimation for densities greater than 400 tree h^{-1}. The effect is stronger in the tree top section (0.8 to 1 relative height). For the total volume the trend in underestimation for all relative height classes is more evident. This means that the Original (Fang et al. 2000) model tends to underestimate the total volume regardless of the total height of the tree, while the underestimation of the merchantable volume is limited to the upper part of the tree.

Our results did not show difference in stem form by density range. Similar results were found by (Ahnlund et al. 2014) with *Pinus sylvestris*, where there were no significant differences in stem form for trees with dbh > 5 cm between density treatment . In a study on *Eucalyptus* in Congo with density range of 500-1300 tree h^{-1}, Gomat et al. (2011) reports that planting density had no significant influence on the stem profile. Unlike what was reported by (Jacobs et al. 2020), who reports density effects in stem form, the butt logs of trees of the same size decreased in taper given

increasing competition, stem taper of the top log decreased with increasing competition. While the stem taper of the mid log increased with competition.

The inflection points for Modified system do not vary significantly compared to the Original system. These results show that a segmented model with two inflection points is appropriate to describe the stems of *Eucalyptus* species, and that stand density has no effects. Gomat et al. (2011) studied factors affecting stem taper variation in *Eucalyptus*, they report the tree shape changes markedly between 1 and 2 years and then is roughly stabilised afterwards. The plantations in this research had range between 7 -17 years, therefore pronounced changes are not expected in inflection point. The overall form of the trees remains the same irrespective of the stand age and density, although slight volume differences can be observed (Fig. 5).

Results showed that stand density had an effect on volume parameters. Based on the fitting, validation statistics, and graphical analysis Fang et al. (2000) system with stand density information is recommended for *E. grandis*. Thus, a system including stand density, results in more accurate estimates for *E. grandis*, considering that stand density affects volume and shape of stems. However, for *E. dunnii*, the inclusion of stand density was not significant and the variable was not included in compatible volume and taper systems.

3.7. CONCLUSIONS

The compatible volume system of Fang et al. (2000) is proposed as the most adequate for describing the stem profile and predicting stem volume of *E. dunnii* and *E. grandis*. A modified second order continuous autoregressive error structure corrected the inherent serial autocorrelation of different observations within tree. In *E. grandis*, the model fit, and prediction performance of the taper and volume

compatible systems were greatly improved by including stand density within the volume equation. For *E. dunnii* no improvement was observed probably due to a narrow population range in the dataset. Adding the stand density variable improved the evaluation efficacy of the system taper equations for *E. grandis*, while for *E. dunnii* no significant effects of stand density were found. Including stand density in taper and volume equations has practical implications, since for the same diameter and height a range of values are obtained depending on the population of the stand. This improves charterization of stands associated to different management practices and subsequently assortment of products.

3.8. ACKNOWLEDGMENTS

The authors thank the Instituto Nacional de Investigaciones Agropecuarias (INIA-Uruguay) for supporting fieldwork and the INIA Scholarship for PhD studies. We are particularly grateful for the support of Leonidas Carrasco Letelier, Roberto Scoz, Demian Gomez, Gonzalo Martinez, Jorge Basso (INIA), Mariano Blanco and José Carlos de Mello (FOSA). We acknowledge the institutional support of the University of Cordoba-Campus de Excelencia CEIA3. We also thank the ERSAF group. We thank Dr. David Walker for his revisions of the different versions of this manuscript, and the anonymous referees for their comments and corrections

3.9. REFERENCES

Ahnlund K, Ulvcrona T, Nilsson U, Lundmark T (2014). Stand density and fertilization effects on aboveground allocation patterns and stem form of Pinus sylvestris in young stands. 29: 197–209.

Anderson-Sprecher R (1994). Model comparisons and r2. American Statistician. 48: 113–117. - doi: 10.1080/00031305.1994.10476036

Belsley DA (1991). Conditioning diagnostics: collinearity and weak data in regression. Wiley, New York, pp. 396.

Bi H (2000). Trigonometric variable-form taper equations for Australian eucalypts. Forest Science. 46: 397–409.

Calama R, Montero G (2006). Stand and tree-level variability on stem form and tree volume in Pinus pinea L .: A multilevel random components approach. i: 24–41.

Castaño JP, Giménez A, Ceroni M, Furest J, Aunchayna R, Bidegain M (2011). Caracterización agroclimática del Uruguay 1980-2009. Montevideo, Serie Técnica INIA. 193: 33.

Clutter J (1980). Development of Taper Functions from Variable-Top Merchantable Volume Equations. Forest Science. 26: 117–120. - doi: 10.1093/forestscience/26.1.117

Diéguez-Aranda U, Castedo-Dorado F, Álvarez-González JG, Rojo A (2006). Compatible taper function for Scots pine plantations in northwestern Spain. Canadian Journal of Forest Research. 36: 1190–1205. - doi: 10.1139/x06-008

Dufour JM, Dagenais MG (1985). Durbin-Watson tests for serial correlation in regressions with missing observations. Journal of Econometrics. 27: 371–381. - doi: 10.1016/0304-4076(85)90012-0

Fang Z, Borders BE, Bailey RL (2000). Compatible volume-taper models for loblolly and slash pine based on a system with segmented-stem form factors. Forest Science. 46: 1–12. - doi: 10.1093/forestscience/46.1.1

Garber SM, Maguire DA (2003). Modeling stem taper of three central Oregon species using nonlinear mixed effects models and autoregressive error structures. Forest Ecology and Management. 179: 507–522. - doi: 10.1016/S0378-1127(02)00528-5

Gomat HY, Deleporte P, Moukini R, Mialounguila G, Ognouabi N, Saya AR, Vigneron P, Saint-Andre L (2011). What factors influence the stem taper of Eucalyptus: Growth, environmental conditions, or genetics? In: Annals of Forest Science, Vol. 68. - doi: 10.1007/s13595-011-0012-3

Gray HR (1956). the Form and Taper of Forest-Tree Stems. Imperial Forestry Institute - University of Oxford - Institute Paper. 79. - doi: 10.1016/S0261-3050(00)00005-X

Hernández-Ramos J, Hernández-Ramos A, García-Magaña JDJ, García-Cuevas X, García-Espinoza GG, Muñoz Flores HJ, Olvera-Delgadillo EH (2017). Sistema compatible de ahusamiento-volumen comercial para plantaciones de Pinus greggii Engelm. en Hidalgo, México. Revista Mexicana de Ciencias Forestales. 8: 59–70. - doi: 10.29298/rmcf.v8i39.43

Hirigoyen A, Franco J, Diéguez-Aranda U (2018). Modelo dinámico de rodal para Eucalyptus globulus (L.) en Uruguay. Agrociencia Uruguay. 22: 63–80. - doi: 10.31285/agro.22.1.7

Jacobs M, Rais A, Pretzsch H (2020). Analysis of stand density effects on the stem form of Norway spruce trees and volume miscalculation by traditional form factor equations using terrestrial laser scanning (TLS). mi: 51–64.

Kirschen RH, O'Higgins EA, Lee RT (2000). The Royal London space planning: An integration of space analysis and treatment planning. American Journal of Orthodontics and Dentofacial Orthopedics. 118: 456–461. - doi: 10.1067/mod.2000.109032

Kozak A (2004). My last words on taper equations. Forestry Chronicle. 80: 507–515. - doi: 10.5558/tfc80507-4

Kozak A (1988). A variable-exponent taper equation. Canadian Journal of Forest Research. 18: 1363–1368. - doi: 10.1017/CBO9781107415324.004

Kozak A, Munro DD, Smith JHG (1969). Taper Functions and their Application in Forest Inventory. The Forestry Chronicle. 45: 278–283. - doi: 10.5558/tfc45278-4

Lindstrom MJ, Bates DM (1990). Nonlinear Mixed Effects Models for Repeated Measures Data. Biometrics. 46: 673. - doi: 10.2307/2532087

Liu Y, Yue C, Wei X, Blanco JA, Trancoso R (2020). Tree profile equations are significantly improved when adding tree age and stocking degree: an example for Larix gmelinii in the Greater Khingan Mountains of Inner Mongolia, northeast China. European Journal of Forest Research. 139: 443–458. - doi: 10.1007/s10342-020-01261-z

Martin AJ (1981). Taper and volume equations for selected Appalachian hardwood species.Northeastern Forest Experiment Station, USDA Forest Service. 1981, No. NE-490..

Max T, Burkhart HE (1976). Segmented polynomial regression applied to taper equations. Forest Science. 22: 283–289.

Methol R (2008). SAG Eucalyptus : Sistema de apoyo a la gestión de Eucalyptus orientadas a la producción de celulosa en Uruguay.Montevideo, INIA. Serie Técnia 173.

Mora B, Wulder MA, White JC, Hobart G (2013). Modeling stand height, volume, and biomass from very high spatial resolution satellite imagery and samples of airborne LIDAR. Remote Sensing. 5: 2308–2326. - doi: 10.3390/rs5052308

Myers RH (1990). Classical and modern regression with applications. Duxbury press Belmont, CA, Vol. 2.

Neter J, Kutner MH, Nachtsheim CJ, Wasserman W (1996). Applied linear statistical models. Irwin Chicago, Vol. 4.

Özçelik R, Göçeri MF (2015). Compatible merchantable stem volume and taper equations for eucalyptus plantations in the eastern mediterranean region of Turkey. Turkish Journal of Agriculture and Forestry. 39: 851–863. - doi: 10.3906/tar-1501-27

Parresol BR (1993). Modeling multiplicative error variance - An example predicting tree diameter from stump dimensions in baldcypress. Forest Science. 39: 670–679. - doi: 10.1093/forestscience/39.4.670

Picard RR, Cook RD (1984). Cross-validation of regression models. Journal of the American Statistical Association. 79: 10. - doi: 10.1080/01621459.1984.10478083

Poudel KP, Cao QV (2013). Evaluation of Methods to Predict Weibull Parameters for Characterizing Diameter Distributions. Forest Science. 59: 243–252. - doi: 10.5849/forsci.12-001

Prodan M, Peters R, Cox F, Real P (1997). Mensura Forestal. GTZ/IICA. Serie Investigación y Educación en Desarrollo …. Agroamerica, pp. 563.

Rachid-Casnati, Euan M, Richard W, Fernando R (2014). Volume and Taper Equations for P. taeda (L.) and *E. grandis* (Hill ex. Maiden). Agrociencia Uruguay. 18: 47–60. - doi: 10.2477/vol18iss2pp47-60

SAS Institute (2004). SAS/ETS 9.1 User's Guide. SAS Institute. SAS Institute Inc., Cary, NC, USA

SAS Institute (2012). SAS/STAT Software, Version 9.1. SAS Institute Inc., Cary, NC, USA

Schumacher, F. Hall F (1933). Logaritmic expression of timber-tree volume. Journal of Agricultural Research. 47: 719–734.

Shao J (1993). Linear Model Selection by Cross-Validation. Source: Journal of the American Statistical Association. 88: 46.

Sharma M, Oderwald RG (2001). Dimensionally compatible volume and taper equations. Canadian Journal of Forest Research. 31: 797–803. - doi: 10.1139/x01-005

Sharma M, Parton J (2009). Modeling stand density effects on taper for jack pine and black spruce plantations using dimensional analysis. Forest Science. 55: 268–282.

Sharma M, Zhang SY (2004). Variable-exponent taper equations for jack pine , black spruce , and balsam fir in eastern Canada. 198: 39–53. - doi: 10.1016/j.foreco.2004.03.035

Spurr S (1954). Simplified Computation of Volume and Growth. Journal of Forestry. 52: 914–922. - doi: 10.1093/jof/52.12.914

Tamarit Urías JC, De los Santos Posadas HM, Aldrete A, Valdez Lazalde JR, Ramírez Maldonado H, Guerra De la Cruz V (2014). Sistema de cubicación para árboles individuales de Tectona grandis L. f. mediante funciones compatibles de ahusamiento-volumen. Revista Mexicana de Ciencias Forestales. 5: 58–74.

Tang X, Pérez-Cruzado C, Fehrmann L, Álvarez-González JG, Lu Y, Kleinn C (2016). Development of a compatible taper function and stand-level merchantable volume model for Chinese fir plantations. PLoS ONE. 11: 147610. - doi: 10.1371/journal.pone.0147610

Teshome T (2011). Compatible volume-taper equations for predicting merchantable volume to variable merchantable limits for Cupressus lusitanica, Ethiopia. SINET: Ethiopian Journal of Science. 28: 15–22. - doi: 10.4314/sinet.v28i1.18227

Vanclay JK, Skovsgaard P (1997). E(OIJ61(AIL mODELUli6 Evaluating forest growth models. Ecological Modelling. 98: 1–12.

Zimmerman DL, Núñez-Antón V (2001). Parametric modelling of growth curve data: An overview. Test. - doi: 10.1007/BF02595823

Table S1: Compatible taper and volume systems tested for *Eucalyptus grandis* and *Eucalyptus dunnii* plantations in Uruguay**.**

Reference	Systems
(Kozak et al. 1969)	Taper function: $d_i^2=D^2(b_1(q-1)+b_2(q^2-1))$ Volume equation: $V=\beta D^2 H$ Compatibility relationship (Martin 1981): $\beta=-k\left(\frac{b_1}{2}+\frac{2b_2}{2}\right)$
(Max & Burkhart 1976)	Taper function: $d_i^2=D^2(b_1(q-1)+b_2(q^2-1)+b_3(a_1-q)^2I_1+b_4(a_2-q)^2I_2)$ where $\begin{cases} I_1=1 \text{ if} q\leq a_1;0 \text{ otherwise} \\ I_2=1 \text{ if} q\leq a_2;0 \text{ otherwise} \end{cases}$ Volume equation: $V=\beta D^2 H$ Compatibility relationship (Martin 1981): $\beta=k\left(\frac{b_1}{2}+\frac{b_2}{3}-(b_1+b_2)+\frac{b_3}{3}a_1^3+\frac{b_4}{3}a_2^3\right)$
(Fang et al. 2000)	Taper function: $d_i=c_1\sqrt{H^{(k-b_1)/b_1}(1-q)^{(k-\beta)/\beta}\alpha_1^{I_1+I_2}\alpha_2^{I_2}}$ where $\begin{cases} I_1=1 \text{ if} p_1\leq q\leq p_2;0 \text{ otherwise} \\ I_2=1 \text{ if} p_2\leq q\leq 1;0 \text{ otherwise} \end{cases}$ p_1 and p_1 are relative heights from ground level where the two inflection points are assumed by the model to occur, dividing the stem in three sections.$\beta=b_1^{1-(I_1+I_2)}b_2^{I_1}b_3^{I_2}\alpha_1=(1-p_1)^{\frac{(b_2-b_1)k}{b_1b_2}}$; $\alpha_2=(1-p_2)^{\frac{(b_3-b_2)k}{b_2b_3}}$; $r_0=(1-\frac{h_{st}}{H})^{k/b_1}$; $r_1=(1-p_1)^{k/b_1}$; $r_2=(1-p_2)^{k/b_2}$ $c_1=\sqrt{\frac{a_0D^{a_1}H^{a_2-k/b_1}}{b_1(r_0-r_1)+b_2(r_1-\alpha_1r_2)+b_3\alpha_1r_2}}$ Merchantable volume equation: $v=c_1^2H^{k/b_1}[b_1r_0+(I_1+I_2)(b_2-b_1)r_1+I_2(b_3-b_2)\alpha_1r_2-\beta(1-q)^{k/\beta}\alpha_1^{I_1+I_2}\alpha_2^{I_2}]$ Volume equation: $V=a_0D^{a_1}H^{a_2}$
(Sharma & Oderwald 2001)	Taper function: $d_i^2=D^2\left(\frac{h_i}{1.3}\right)^{2-a_1}\left(\frac{H-h_i}{H-1.3}\right)$ Volume equation: $V=a_0D^{a_1}H^{3-a_1}$ Compatibility relationship: $a_0=\frac{k(D/1.3)^{2-a_1}}{\left(1-\frac{1.3}{H}\right)(3-a_1)(4-a_1)}$

where k is π/40,000, a metric constant; b_i is the form factor of tree section i; D is the diameter at breast height over bark (1.3 m above ground, cm); d_i (cm) is the diameter over bark at height h_i (m); H is the total tree height (m); q is h_i/H; h_{st} is the stump height (m) and a_0, a_1, a_2, b_1, b_2, b_3, p_1 and p_2 are parameters to be estimated.

4. STAND CHARACTERIZATION OF *EUCALYPTUS* SPP. PLANTATIONS IN URUGUAY USING AIRBORNE LIDAR SCANNER TECHNOLOGY

Andrés Hirigoyen [1,*], Mª Angeles Varo-Martinez [2], Cecilia Rachid-Casnati [1], Jorge Franco [3] and Rafael Mª Navarro-Cerrillo [2]

[1] National Institute of Agricultural Research (Instituto Nacional de Investigación Agropecuaria—INIA Uruguay) Tacuarembó. Ruta 5 km 386, Tacuarembó PC 45000, Uruguay; crachid@inia.org.uy (C.R.-C)

[2] Department of Forestry Engineering, Laboratory of Silviculture, Dendrochronology and Climate Change, DendrodatLab- ERSAF, University of Cordoba, Campus de Rabanales, Crta. IV, km. 396, E-14071 Córdoba, Spain; g72vamam@uco.es (M.A.V.-M.); rmnavarro@uco.es (R.M.N.-C.)

[3] Faculty of Agronomy, University of the Republic, Paysandú, Uruguay; jfranco@fagro.edu.uy

***** Correspondence: ahirigoyen@inia.org.uy or andreshirigoyen@gmail.com (A.H)

Received: 16 October 2020; Accepted: 21 November 2020; Published: date

4.1. RESUMEN

La tecnología de escáner lidar aerotransportado (ALS) se utiliza en una variedad de aplicaciones, incluida la forestal. ALS tiene un enorme potencial para la estimación de parámetros biométricos relevantes en plantaciones forestales. Este estudio investiga el uso de un algoritmo de segmentación semiautomático orientado a objetos para la delimitación de rodales, basado en datos de modelos de ALS, en plantaciones *de Eucalyptus grandis* y *E. dunnii* en Uruguay. Los resultados muestran que los métodos no paramétricos arrojaron resultados más precisos y menos sesgados para el volumen total (TV) con R^2 0.93, RMSE 20.04 m^3h^{-1} para *E. grandis* y R^2 0.93, RMSE 18.43 m^3 h^{-1} para *E. dunnii*; y biomasa aérea (AGB) con R^2 0.95, RMSE 70.2 kg h^{-1} para *E. grandis* y R^2 0.96, RMSE: 71.2 Kg h^{-1} para *E. dunnii*. Los métodos paramétricos se desempeñaron mejor para la altura

dominante (Ho) con R^2 0.98, RMSE 0.67 my R2: 0.96, RMSE: 0.8 m para *E. grandis* y *E. dunnii*, respectivamente. Las métricas de ALS más informativas para la estimación de AGB y TV fueron las métricas relacionadas con la elevación en modelos paramétricos (Elev.70 y Elev.75), mientras que para los modelos no paramétricos (k-NN) fueron Elev.75 y *canopy density*. Para Ho, las métricas de ALS seleccionadas también se relacionaron con la elevación tanto en los modelos paramétricos (Elev.90 y Elev.99) como en modelo de *random forest* (Elev.max y Elev.75). La metodología de segmentación propuesta aquí coincidió estrechamente con los segmentos delineados por operadores humanos, y proporciona un modelo de bajo costo, rentable, fácil de aplicar y actualizar destinado a generar mapas de AGB o TV para tareas de cosecha, basados en rásteres derivados de métricas ALS. La presente investigación muestra la capacidad de las métricas ALS para mejorar inventarios estratégicos; validando y promoviendo la adopción de tecnología ALS para inventarios de masas forestales de Eucalyptus spp. en Uruguay

4.2. ABSTRACT

Airborne lidar scanner (ALS) technology is used in a variety of applications, including forestry. ALS has enormous potential for the estimation of relevant biometric parameters in forest plantations. This study investigates the use of an object-oriented semi-automated segmentation algorithm for stands delineation, based on modeling ALS data, in plantations of *Eucalyptus grandis* and *E. dunnii* in Uruguay. The results show that non-parametric methods delivered more accurate and less biased results for total volume (TV) with R^2 0.93, RMSE 20.04 m^3h^{-1} for *E. grandis* and R^2 0.93, RMSE 18.43 $m^3\ h^{-1}$ for *E. dunnii;* and above ground biomass (AGB) with R^2 0.95, RMSE 70.2 kg h^{-1} for *E. grandis* and R^2 0.96, RMSE: 71.2 Kg h^{-1} for *E. dunnii*. Parametric methods performed better for dominant height (Ho) with R^2 0.98, RMSE 0.67 m and R^2: 0.96, RMSE: 0.8 m for *E. grandis* and *E. dunnii*, respectively. The most informative ALS metrics for the estimation of AGB and TV were metrics related to the elevation in parametric models (Elev.70 and Elev.75), while for the non-parametric models (k-NN) they were Elev.75 and canopy density. For Ho, the ALS metrics selected were also related to elevation both in the

parametric (Elev.90 and Elev.99) and random forest models (Elev.max and Elev.75). The segmentation methodology proposed here matched closely the segments delineated by human operators, and provides a low-cost, cost-effective, easy to apply and update model aimed at generating AGB or TV maps for harvest tasks, based on rasters derived from ALS metrics. The present research shows the capacity of ALS metrics to improve extensive strategic inventories; validating and promoting the adoption of ALS technology for inventory forest stands of *Eucalyptus* spp. in Uruguay.

Keywords: intensive silviculture; parametric and non-parametric methods; dominant height; volume; above ground biomass; stand segmentation

4.3. INTRODUCTION

The quantification of forest stock is of key importance to forest management operations, such as habitat assessment, timber harvest, timber extraction, replanting, ecosystem modeling and stand delineation. Field inventory methods depend on the number of sampling plots measured, being time-consuming and expensive [1,2]. The most important variables affecting forest planning are: tree basal area, tree height, and stand-level volume [3].

Airborne lidar scanner (ALS) can support traditional forest inventories by providing precise measurements of forest attributes (e.g., stand density, mean basal area and dominant height) [4]. ALS has great potential to estimate and describe structural parameters in forest plantations [5]. Discrete ALS data has been employed to describe stands forest structure, through two approaches according to the scale of analysis; single tree identification and data aggregation [1]. Aggregation is known as the area-based approach (ABA) and is more efficient. This is because, by reducing the volume of discrete ALS returns to manageable grids, the data can be summarized within fixed-area units such as pixels, irregularly shaped segments, or forest stands [1]. In the ABA approach, stand attribute estimations are calculated from the statistical relationships between plot-level metrics from LIDAR data and plot-stand attributes [6].

There are numerous statistical techniques, including parametric and non-parametric approaches, for the estimation of forest attributes with LIDAR [7]. Common prediction methods are ordinary least square regression (OLS), weight least square regression (WLS), support vector machines (SVM), nearest neighbor approaches (k-NN), and random forest (RF). OLS and WLS with stepwise variable selection are the methods that have been used most frequently for building models involving field measurements and statistical metrics from ALS data. Both are parametric techniques that depend on the distribution of residuals, and require normality, homoscedasticity and independence of the raw data [8]. Non-parametric approaches, including k-NN and RF, are considered as alternatives to OLS, since they do not rely on any distributional assumptions of the data and deal with non-linear and possibly diverse relationships between independent and dependent variables [8]

In forest management, stands are the basic units for statistical forest inventory and management. A stand is a surface covered by a distinguishable group of homogeneous trees with characteristics that are different from those of the adjacent areas [9]. Stands can be defined in terms of attributes like tree species, age, structural arrangement, and forest condition. Forest stand delineation is critical to the management of forested areas and it is expected to yield ecological and economic management benefits [10]. Traditionally, these stands are manually delineated and interpreted by human operators based on field surveys and very-high-resolution geospatial images [11]. Manual delineation is time consuming, and its requirement for professional foresters may result in partially subjective delineation results because this procedure is subjective and its results usually vary between analysts [9]. According to Haara and Haarala [12], from a remote sensing perspective, stands delineation is a segmentation problem. Optimal segmentation should maximize intra-segment homogeneity and inter-segment heterogeneity [13]. Most unsupervised evaluation methods involve the calculation of intra-segment and inter-segment uniformity and dissimilarity for each segment, and the subsequent aggregation of these values into a unique comprehensive value [14].

In Uruguay, the commercial use of ALS is relatively new with no studies on its application in forest inventories. The objective of this study was to propose and validate an object-oriented semi-automated segmentation methodology for forest stand delineation based on LIDAR data in plantations of *E. grandis* and *E. dunnii* in Uruguay. The specific objectives were i) to develop an empirical model to estimate total volume (TV) and above ground biomass (AGB) using LIDAR metrics; ii) to compare parametric and non-parametric methods for estimating TV and AGB, and iii) to assess and optimize the object-oriented segmentation for stand delineation based on variables derived from LIDAR metrics: the Assmann´s dominant height (Ho), total volume and above ground biomass of *E. grandis* and *E. dunnii* stands. The methodology developed on this research provides accurate estimates and mapping of TV, AGB and Ho at stand scale based on LIDAR data, and implemented a stand delineation method in plantations of *Eucalyptus* using Orpheo ToolBox (OTB).

4.4. MATERIALS AND METHODS

4.4.1 Study Area

This study was conducted in Uruguay across plantations owned by Forestal Oriental SA company, representing a total area of 2468 ha (Figure 1). Three zones were established (Figure 1): sites B1A and B1B, covering 861 ha (43°13´97" S–64°24´78" W, hereafter Guichon); sites B2A and B2B, covering 870.1 ha (63°07´44" S–52°22´64"W, hereafter Trinidad); and site B3, covering 716.9 ha (63°44´33.05" S–63°95´58" W, hereafter Sarandí del Yi).

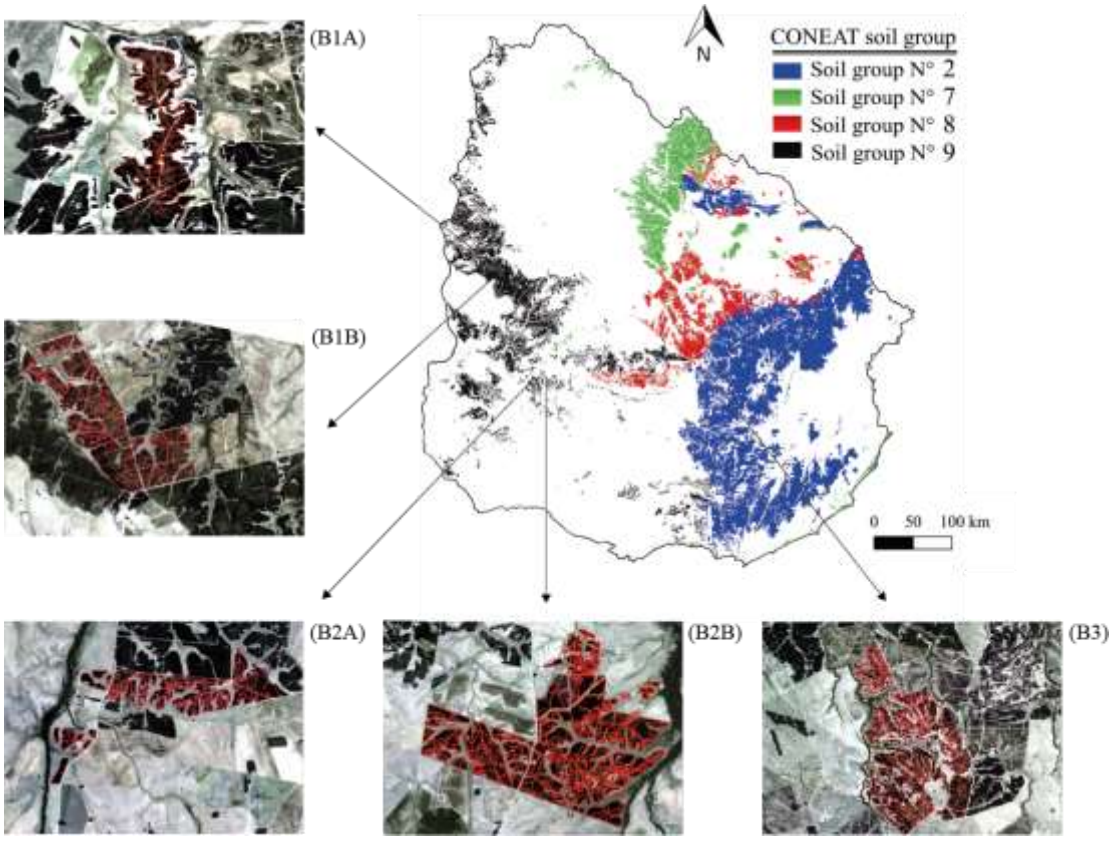

Figure 1. Location of the study sites in Uruguay soils prioritized for forestry (soil groups: 2, 7, 8, 9) and Planet satellite images (March 2018) of study sites: B1A and B1B (Guichon); B2A and B2B (Trinidad) and site B3 (Sarandí del Yi).

The study zones have a temperate subtropical climate, with a mean annual temperature of 18 °C and a mean annual rainfall ranges between 1300 and 1400 mm [15]. According to the National Commission for Agroeconomic Studies of the Land (CONEAT) classification, the predominant soil**s** at three locations were characterized by low and middle fertility, an A horizon 40–60 cm in depth, weak structure, a low to medium level of organic matter, slopes between 1%–5%, sandy to loam-silt texture, and moderately-slow to slow permeability.

4.4.2. Field Data

In May–June 2018, 151 plots with a radius of 10 m (314.16 m^2), were established using a systematic sampling design according to traditional inventory procedures within the *E. grandis* and *E. dunnii* mono-species plantations selected. In each plot, the diameter at breast height (1.3 m above ground level, cm) (dbh), stand density (N, trees ha^{-1}), basal area (G, m^2 ha^{-1}) and total height (H, m) of all trees with a dbh greater than or equal to 7 cm were measured using a caliper (Haglöf Mantax, Långsele, Sweden) and Vertex III hypsometer. The silvicultural conditions together with the state of structure of the forest were defined using the following stand parameters: basal area per hectare (G), number of trees per hectare (N), quadratic mean diameter (dg), mean arithmetic diameter (dm), Assmann dominant height (Ho) and mean arithmetic height (Hm). For above ground biomass (AGB) and total volume (TV) estimations, equations developed by Hirigoyen [16] based on dbh and total height (Hm), were used at the tree level. These equations are as follows:

For *Eucalyptus dunnii*:

$$AGB = 0.091 dbh^{2.285} Hm^{0.473} \quad (1)$$

$$TV = 0.00004 dbh^{2.089} Hm^{0.862} \quad (2)$$

For *Eucalyptus grandis*:

$$AGB = dbh^2(0.656 + 0.0005 Hm) \quad (3)$$

$$TV = 0.00002 dbh^{1.871} Hm^{1.233} \quad (4)$$

The AGB and TV of the plots were computed by aggregating the individual values; a summary of the measurements made in the sample plots is presented in Table 1. The location of the center of each plot was mapped with sub-meter accuracy using post-processed, differentially corrected GPS data collected with a Trimble geo Explorer 3000 unit (Trimble Navigation Ltd., Sunnyvale, CA, USA).

Table 1. Silvicultural and biomass variables of *Eucalyptus grandis* and *Eucalyptus dunnii* in Uruguay: number of plot(n), stem density (N, trees ha^{-1}); diameter at breast height (dbh, cm); basal area (G, m^2 ha^{-1}), above ground biomass (AGB, Mg ha^{-1}), total height (TH, m), total volume (TV, m^3 ha^{-1}), and age (years). stdev: standard deviation, min: minimum, max: maximum.

	Field Attributes	Min	Mean	Max	stdev
E. grandis (n=76)	Dbh (cm)	10.65	15.49	19.33	1.81
	TH (m)	12.57	21.69	33.30	4.46
	G (m^2 ha^{-1})	8.97	20.28	29.79	4.52
	AGB (Mg ha^{-1})	215.2	653.3	1175	213.2
	TV (m^3 ha^{-1})	45.01	185.37	342.12	67.71
	Age	4.5	6.8	9.5	1.5
	N (tree ha^{-1})	634	1041	1336	144
E. dunnii (n=75)	Dbh (cm)	10.83	15.27	19.38	1.53
	TH (m)	9.52	19.55	29.22	4.23
	G (m2 ha^{-1})	0.76	20.51	33.79	5.41
	AGB (Mg ha^{-1})	153.3	686.7	1296	218.2
	TV (m^3 ha-^{1})	18.81	154.73	300.60	64.49
	Age	4.5	6.3	8.4	1.2
	N (tree ha^{-1})	669	1070	1432	159

4.4.3. Airborne LiDAR Data Acquisition and Processing

ALS data was collected in March 2018, covering a total of 2468 hectares using a Riegl VUX-1 laser scanner installed on an autogyro helicopter, at a flight altitude of 110 m above ground level, a pulse repetition rate of 550 kHz, an angular step width of 0.0687º and a FOV of 55º. The resulting point density was 40 pulses m^2 (Table

S1, Supplementary Material). The plots were geo-referenced in the WGS84 UTM 21 coordinate system. The planimetric x and y coordinates as well as ellipsoidal height values were recorded for all echoes.

All LiDAR point clouds were checked and processed with the software FUSION [17], and this generated four products: digital terrain model (DTM), digital surface model (DSM), canopy height model (CHM) and the LIDAR metrics used in this research. The Catalog tool was used to ensure the quality of the products created from the point clouds, evaluating various characteristics of the LIDAR data, as well as the continuity of coverage and the correct pulse return density. Areas without coverage were excluded from the study. The GroundFilter algorithm was applied to identify and remove the returns that hit the ground surface. Afterwards, a DTM with a pixel size of 1 m^2 was created using these filtered points, through the GridSurfaceCreate function. The Clipdata tool was used to normalize the heights and ensure that the z coordinate corresponds to the height above ground. The Polyclipdata tool was applied to select the LIDAR points falling within the field sample plots [18]. Cloudmetrics and Grid metrics tools were used to build LIDAR metrics within the sample plots and to produce the same metrics over the LIDAR tiles at 17.7 m resolution (equivalent to a plot of ~314 m^2), respectively. The LIDAR height distributional parameters (Table S2, Supplementary Material) were treated as independent variables.

4.4.4. Variable Selection and Statistical Analysis of the Parametric Methods

A Pearson correlation test was used to recognize highly correlated predictor variables; variables with a *p*-value > 0.05 were removed. Furthermore, before discarding them, we looked for correlations between the excluded variables with the target variables (Ho, TV and AGB), to fit simple linear regressions. To determine the best combinations of predictive variables, the regsubsets function (leaps package [19]) in R [20] was used. We used the Mallows Cp statistic to determine the best subsets. This compares the sum of squares error (SSE) for a reduced model with *p* parameters, with the mean square error of the full model (MSEfull) for a N number of samples. Models with low Cp values are generally similar to those with higher

adjusted R-squared values. This criterion was selected to determine the optimal model, since it favors parsimonious models [21]. By default, regsubsets reports the best eight-variable model [22], and we used the *nvmax* to compare the maximum number of predictor variables that optimized Cp and the adjusted coefficients of determination.

After selecting the best set of variables, predictive models were built using forest inventory variables and LIDAR metrics. Simple and multiple linear regressions were fitted, as well as exponential, logarithmic and power transformations, considering all possible combinations. The nlsLM function from the package *minpack.lm* [23], a modified version of nonlinear least-squares incorporating the Levenberg-Marquardt algorithm, was used. For linear models, we used the *lm* function to define the prospective models, and weighted regression (using weighted least squares) was applied if heteroscedasticity was detected by *ncvTest* (a score test for non-constant error variance) from the car package.

4.4.5. Variable Selection and k-NN Models

Before the implementation of the k-NN algorithm, a multicollinearity analysis was carried out to reduce data redundancy. It was performed using the Variance Inflation Factor (VIF). Collinear variables were deleted and independent variables were selected considering a VIF >10 as the critical threshold [24], using the varSelection function from *yaImpute* [25] in the R package. The varSelection function keeps only those variables that strengthen the imputation process [25]. VarSelection calculates the generalized root mean square distance (grmsd) each time variables are added to an imputation algorithm. Based on several studies that have shown that the RF approach achieves better results compared to other imputation methods [26]; in this study, the k-NN models were implemented employing the RF distance metric.

After the selection of the variables, raw data were divided into training (70% of the input data) and validation (30% of the input data) sets. With the selected variables, model fitting was computed by the *yai* and *impute.yai* functions from *yaimpute* package [25], applied to the training set. The *k-NN* value (*k*) varied for each

imputation, calculating the root-mean-square error value for each one. The k value that minimized the RMSE within the validation dataset was selected. The *k*-value varied for each imputation, and the one minimizing RMSE value was selected. Then, the k-NN imputations were adjusted and compared with the best selected parametric model, using reliability measures obtained in cross-validation [8].

4.4.6. Model Assessment and Validation

To determine the goodness of fit, the R^2 adj was used during the model development stages. Simple linear regressions relating the observed and predicted values were assessed using the determination coefficient (R^2) to evaluate non-linear models[26]. To analyze the relative quality of each model, the Akaike information criterion (AIC) was calculated. Model performance for the distinct approaches was evaluated based on the estimation errors, using the root-mean-square error (RMSE) and the RMSE normalized by the observed mean of the dependent variables (nRMSE, %) [26]. Thus, RMSE represents the absolute value of the error and nRMSE indicates the relative value of the error with respect to the average at the stand level.

We used R^2, RMSE, and nRMSE to compare non-parametric and parametric models since, when reporting model performance the correlation between predictions and observations, should be provided along with the RMSE [26].

Cross-validation was carried out using the same data as in the fitting calculating the residuals of the i-th observation [27,28]. The sum of squares of the eliminated residues (PRESS, predicted residual error sum of squares) was used to calculate the root-mean-square-error for cross-validation (RMSEcv). The close values of RMSEcv and RMSE indicate that the model does not overfit the data and has a good predictive behavior [29].

4.4.7. Segmentation Method

Stand segmentation was developed, using an algorithm based in a non-parametric estimator: Mean Shift (MS), with Orpheo ToolBox (OTB) software for QGIS [30]. The MS was applied to segment the image and it can automatically detect

the number of segments. In OTB three parameters were specified: spatial radius, to define the neighborhood; range radius, to define the interval in spectral space; and the minimum size of the regions that will remain after the grouping to cover all segmentation possibilities [31]. Based on the forest production (biomass and pulpwood), we used two combinations of stand silvicultural variables to define and group the LIDAR data within a single segment: i) AGB and Ho; and ii) TV and Ho. With this data, a two-band raster was created for both combinations (AGB and Ho; TV and Ho)

OTB segmentation was compared to that performed by a trained human operator considering the differences between species, tree ages, and values of ABG and TV. The objective was to define homogeneous areas with an optimal area of 3 hectares and a minimum of 1 hectare for: i) TV and Ho; ii) AGB and Ho. These silvicultural variables were selected to identify and group LiDAR data in a single support, since forest harvest takes into account wood production (volume or biomass), and Ho is used as an indicator of the quality of the forest site.

4.4.8. Unsupervised Evaluation of the Segmentation Method

Unsupervised evaluation (UE) was used for segmentation evaluation, based on expert knowledge. This procedure allows the results to be more efficient and less subjective compared to supervised methods [32,33]. In UE methods, each segment should be internally homogeneous and should be distinguishable from other segments [33]. UE involves calculation of intersegment homogeneity and heterogeneity measures and the aggregation of these values into a global value, thus, UE with the minimum global value is selected as the optimal segmentation [34,35]. We considered the global intra-segment homogeneity and inter-segment heterogeneity based on the variance weighted and Moran's Index (MI) combined in a global score (GS) for measuring the quality of resulting segmentation [14]. GS is defined as the sum of the normalized weighted variance (wVar) and the normalized MI, according to [33], and has been widely used due to its simplicity of calculation, understandability, and effectiveness [36]. As there was more than one layer in each

image, GS values were averaged according to the number of bands [14]. Weighted variance was calculated for each segment as follows:

$$wVar = \frac{\sum_{i=1}^{n} a_i * v_i}{\sum_{i=1}^{n} a_i} \quad (5)$$

where n is the total number of segmentations, vi is the variance and ai is the area of segment i.

Moran's index was calculated as follows:

$$MI = \frac{n \sum_{i=1}^{n} \sum_{j=1}^{n} w_{ij}(y_i - \bar{y})(y_j - \bar{y})}{\sum_{i=1}^{n} (y_i - \bar{y})^2 \left(\sum_{i \neq j} \sum w_{ij}\right)} \quad (6)$$

where n is the total number of segmentations, w_{ij} is a measure of the spatial proximity, y_i is the mean spectral value of segment i and $\bar{y}$ is the mean spectral value of the image. Each weighted w_{ij} is a measure of the spatial adjacent regions [37]. MI and wVar were both normalized by rescaling to a similar range (0–1). The optimal segmentation has low variance and low spatial autocorrelation; this means that a lower average GS indicates better results [14]. GS ranges between 0 and 2; where a value close to zero shows a low weighted variance and a low MI value [14,36]. GS was calculated as follows:

$$GS = wVar_{norm} + MI_{norm} \quad (7)$$

where $wVar_{norm}$ is the normalized weighted variance and MI_{norm} is the normalized Moran's index.

4.5. RESULTS

4.5.1. Parametric and Non-Parametric Models for Ho, TV and AGB

For *E. dunnii*, eight candidates' LIDAR metrics were selected after performing multicollinearity and Pearson's correlation tests, while for *E. grandis* nine LiDAR metrics were selected (Figures S1 and S2 in supplementary material show the selected metrics and their correlations with Ho, TV and AGB). Allometric simple linear or non-linear equations (applying the chosen metrics) were tested, using weighted least squares (WLS) to balance correlated regressor variables in multiple

regression. The optimal weights that homogenized the residues and improved ncvTest were used as weight functions. Only simple linear models yielded significant parameters ($p < 0.05$) (candidate models, ordered by goodness of fit, are displayed in Table S3, Supplementary Material).

Models selected for *E. grandis* included Height percentile 99th (Elev.P99) for predicting Ho, and Height percentile 70th (Elev.P70) for predicting TV and AGB; they had determination coefficient (R^2) values of 0.98, 0.96, and 0.92, respectively. For *E. dunnii*, models including the variables Height percentile 90th (Elev.P90) for Ho and Height percentile 75th (Elev.P75) for TV and AGB models, R^2 values were 0.98, 0.96 and 0.93, respectively. In all cases, predicted values were in near-perfect agreement with the observed measurements (with R^2 values higher than 0.92). The Shapiro–Wilk test and *ncvTest* showed that both normality and homogeneity of the residues were achieved. Scatter plots of the predicted values of Ho, TV and AGB versus the real data are shown in Figure 2.

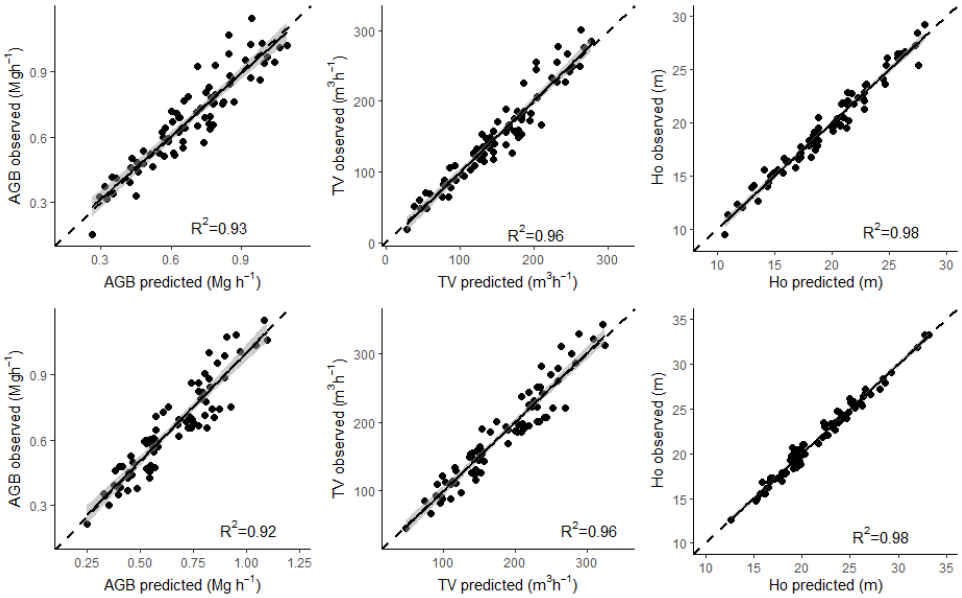

Figure 2. Relationships between observed and predicted values for total volume (TV, m^3 ha^{-1}), total above ground biomass (AGB, Mg ha^{-1}) and Assmann´s dominant height (Ho, m) of *Eucalyptus dunnii* (upper) and *E. grandis* (bottom.) in Uruguay by parametric regression. Solid line depicts

regression fit, dashed line is the 1:1 line. Correlation coefficient (R^2) value is included. Shaded areas represent 95% regression confidence intervals.

4.5.2. Imputation AGB, TV and Ho Models and Their Precision

After applying the multicollinearity analysis and the correlation test to the candidate LIDAR metrics, the remainder were not highly correlated and were used as inputs in the varSelection function. Metrics selected to be included in the imputation model as predictor variables for Ho, AGB and TV, according to generalized root mean square distance (gmsd) statistics, are shown in Table 2. The LiDAR-derived predictor metrics for AGB models in *E. dunnii* were: height percentile 75**th** (Elev.P75); all returns above mode/Total first returns * 100 (ARA2/TFR); percentage first returns above mean (PFRAM); and elevation mode (Elev.MO). For *E. grandis*, the LiDAR-derived metrics were: Elev.P75, canopy relief ratio (CRR); and Elev.MO. The LiDAR-derived metrics selected as predictors in TV models for *E. dunnii* were: Elev.P75; ARA2/TFR and Elev.MO. For *E. grandis*, the LiDAR-derived metrics were: Elev.P75, percentage first returns above mode (PFRAMO); elevation maximum (Elev.MAX) and all returns above height break (ARA2). The models fitted for Ho of *E. dunnii* included the LIDAR-derived predictor metrics Elev.P75 and ARA2; those of *E. grandis* included Elev.P75, Elev.Max and CRR.

Table 2. LiDAR-derived metrics selection according to generalized root means square distance (grmsd) as predictor variables in imputation model for total volume (TV, m^3 ha^{-1}), total above ground biomass (AGB, Mg ha^{-1}), and Assmann´s dominant height (Ho, m) of *Eucalyptus grandis* and *Eucalyptus dunnii* in Uruguay. Canopy relief ratio, CRR; elevation mode, Elev.MO; height percentile 75**th** Elev.P75; all returns above mode/total first returns * 100, ARA2/TFR; percentage first returns above mean, PFRAM; percentage first returns above mode, PFRAMO; all returns above height break, ARA2; elevation maximum, Elev.MAX; all returns above mode, ARAMO.

	E. grandis		*E. dunnii*	
	Metrics	**grmsd**	**Metrics**	**grmsd**
AGB	CRR	0.461	Elev.MO	0.466
	Elev.MO	0.479	ARA2/TFR	0.476
	Elev.P75	0.562	PFRAM	0.511
			Elev.P75	0.547
TV	Elev.P75	0.556	Elev.P75	0.394
	PFRAMO	0.567	Elev.MO	0.401
	ARA2	0.568	ARA2/TFR	0.410
	Elev.MAX	0.580		
Ho	Elev.MAX	0.303	ARAMO	0.343
	CRR	0.313	Elev.P75	0.394
	Elev.P75	0.349		

The results of imputed models are given in Table 3. We included cross-validation as accuracy estimation methods; this allowed us to analyze the predictive capacity of each model. Results show that metrics expressing middle or upper-middle percentiles of LIDAR heights (Elev.75) were included as predictors in all models for both species. All models followed a similar trend, with RMSE and nRMSE% being slightly higher compared to fitting statistics, for all variables. However, RMSE and nRMSE were lower for Ho of *E. grandis*. For Ho, TV and AGB, cross-validation of the selected models yielded average RMSE and nRMSE% values of 1.5 m and 10%; 25 m^3 ha^{-1} and 18%; and 120 Mg ha^{-1} and 17%, respectively, for both species.

Table 3. Statistics of fit and cross -validation for Assmann´s dominant height (Ho m), total volume (TV $m^3 ha^{-1}$), and above ground biomass (AGB mg ha^{-1}) of *Eucalyptus grandis* and *Eucalyptus dunnii* in Uruguay. R^2, coefficient of determination; RMSE, root mean squared error; nRMSE, normalized root mean squared.

		E. dunnii			*E. grandis*		
		RMSE	**nRMSE**	**R^2**	**RMSE**	**nRMSE**	**R^2**
Ho	Fit	1.38	7.12	0.94	1.16	5.31	0.97
	Cross Validation	2.00	10.22	0.90	1.08	4.98	0.97
TV	Fit	18.43	16.28	0.93	20.04	15.06	0.93
	Cross Validation	20.75	18.15	0.89	24.77	17.44	0.84
AGB	Fit	71.2	10.37	0.96	70.2	11.89	0.95
	Cross Validation	112.2	17.08	0.87	110	17.09	0.85

Plots of model predictions versus the observed data are shown in Figure 3. Relationships between observed and estimated AGB, TV, and Ho consistently exhibited R^2 values exceeding 0.93.

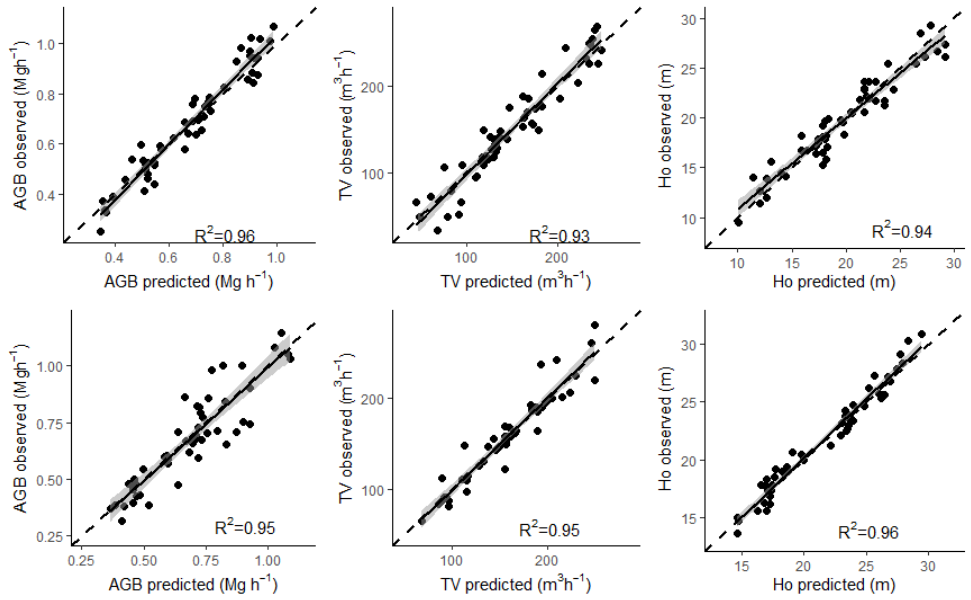

Figure 3. Relationships between observed and imputed values for total volume (TV, m^3 ha^{-1}), total above ground biomass (AGB, Mg ha^{-1}) and Assmann´s dominant height (Ho, m) of *Eucalyptus dunnii* (upper) and *E. grandis* (bottom.) in Uruguay by non-parametric method. Solid line depicts regression fit and dashed line shows the 1:1 line. Correlation coefficient (R^2) value is included. Shaded areas represent 95% regression confidence intervals.

4.5.3. Segmentation

The results of applying OTB segmentation in the delimitation of the forest stand, described by the number of segments created, varies with the combination of minimum size, range radius and spatial radius (see Tables S4 and S5, Supplementary Material). Sites B1A, B1B, B2A and B2B were established due to the distance between the original stands (see Figure 1). Table 4 shows the selected segmentation for the sites, and these values are clear in the field delineation of Figure 4.

Table 4. Selected normalized variance (wV_{nor}), normalized Moran's index (MI_{nor}), and global scores (GS) for all spatial radius, range radius, and minimum size of the region segmentations with theirs resulting number of segments and average areas. Orpheo ToolBox (OTB) mean shift segmentation approach was applied for the estimation of above ground biomass (AGB mg ha^{-1}) and total volume (TV m^3) of *Eucalyptus grandis* and *Eucalyptus dunnii* in Uruguay using LIDAR metrics.

Sites	SR	RR	Min size of region	AGB band			TV band			Ho band			Two-band average			Number segments	Area mean (ha)
				wV_{nor}	MI_{nor}	GS	wV_{nor}	MI_{nor}	GS	wV_{nor}	MI_{nor}	GS	wV_{nor}	MI_{nor}	GS		
B1A																	
	8	4	20	0.93	0.00	0.93				0.87	0.00	0.87	0.90	0.00	0.90	300	2.19
	8	4	20				0.95	0.00	0.95	0.90	0.00	0.90	0.93	0.00	0.93	287	2.28
B1B																	
	14	4	30	0.62	0.30	0.91				0.00	0.24	0.24	0.31	0.27	0.57	68	3.02
	12	4	30				0.79	0.15	0.94	0.00	0.12	0.12	0.39	0.14	0.53	61	3.36
B2A																	
	10	4	20	0.02	0.97	1.00				0.02	0.00	0.02	0.02	0.49	0.51	436	1.68
	10	4	20				0.04	0.93	0.97	0.03	0.85	0.88	0.03	0.89	0.92	449	1.63
B2B																	
	8	4	20	0.00	0.95	0.95				0.02	0.09	0.12	0.01	0.52	0.53	83	1.68
	14	4	20				0.01	0.77	0.78	0.02	0.46	0.48	0.02	0.61	0.63	77	1.81
B3																	
	8	4	40	0.50	0.02	0.53				0.38	0.02	0.40	0.44	0.02	0.46	224	3.19
	10	4	40				0.44	0.07	0.51	0.48	0.01	0.49	0.46	0.04	0.50	225	3.18

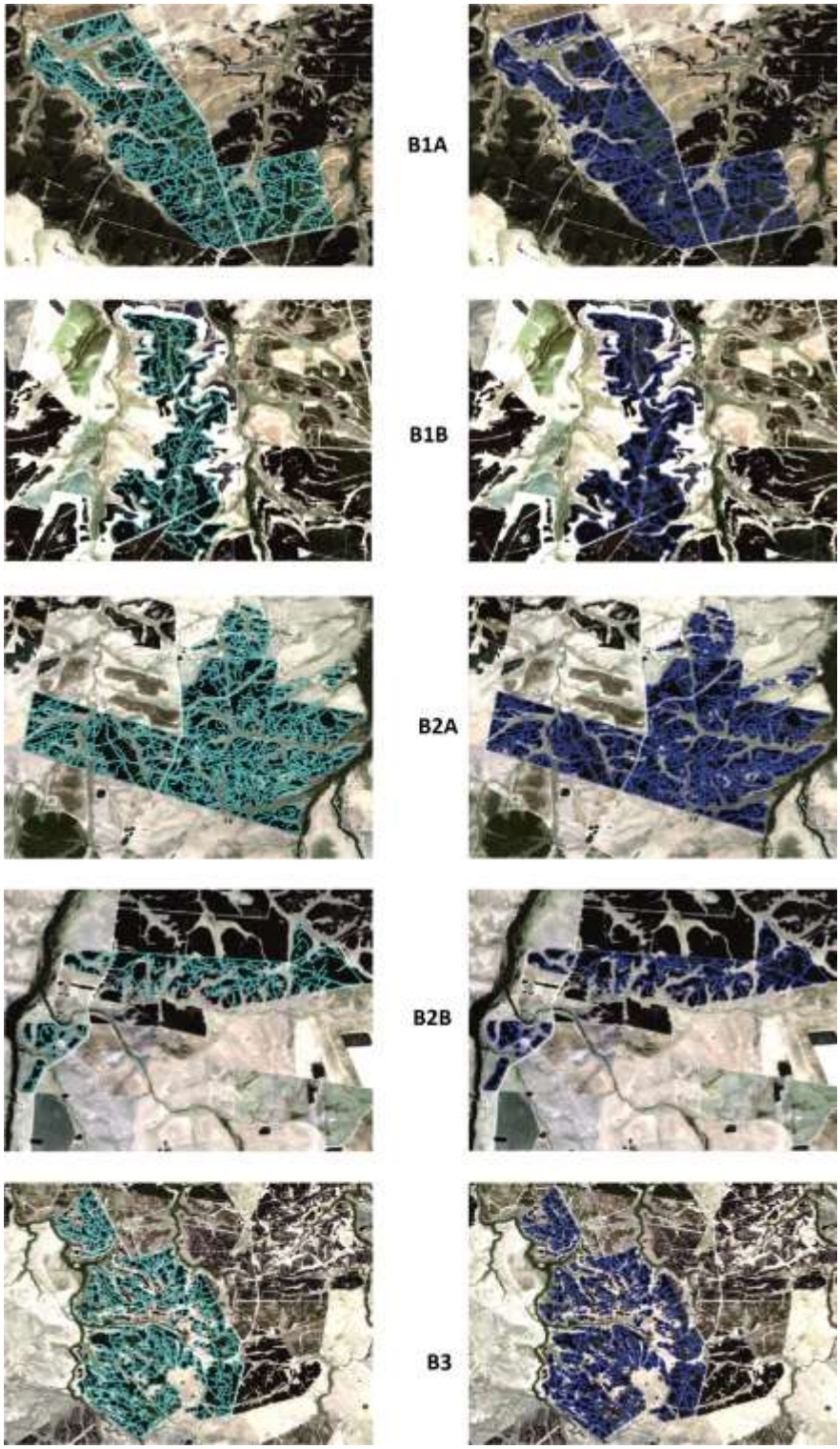

Figure 4. Stands delineated obtained using mean shift segmentation: in sky-blue: above ground biomass; in blue: total volume by sites**.**

Table 5 shows the total number of segments obtained by manual segmentation and for the Orpheo ToolBox OTB algorithm. Manual segmentation produced more segments than OTB for all sites except B2A. For site B2A, OTB by TV segmentation produced 3% more than AGB segmentation. AGB segmentation yielded more segments than TV (B1A = 3.4%, B2B = 5.9%). For B3, OTB segmentation for AGB and TV produced almost the same results in both cases, producing 25.8% fewer segments than with manual segmentation.

Table 5. Number of segments and average size of stand area, applying the Orfeo Tool Box algorithm and manual segmentation of above ground biomass (AGB) and total volume (TV), in *Eucalyptus grandis* and *Eucalyptus dunnii* plantations in Uruguay.

Block	Total block area (ha)	Segment number manual	Average Segment area (ha)	Segment number AGB	Average segment area (ha)	Segment Number TV	Average segment area (ha)
B1A	654.7	380	1.72	300	2.18	287	2.28
B1B	205.9	80	2.57	68	3.03	61	3.38
B2A	731.9	425	1.72	436	1.68	449	1.63
B2B	139.4	102	1.37	83	1.68	77	1.81
B3	716.6	302	2.37	224	3.20	225	3.18

To evaluate the effects of region size on the GS values from different combinations of range, boxplots of spatial radius versus region size were assessed (Figure 5) for AGB and TV. For small region sizes, the behavior of the GS was quite uniform either applying segmentations obtained using TV or with those obtained using AGB. Differences among sites increased as the size of the region increased. The largest difference was observed for a size of 40, in both the TV and AGB segmentations. B1B had greater variability of GS than the rest of the sites for AGB and TV, this being more pronounced for AGB. For the TV segmentations, site B2A had the highest values of GS, for all sizes, while for the AGB segmentations site B1A had the highest values of GS, for all sizes; in both cases, this was more evident in the larger regions.

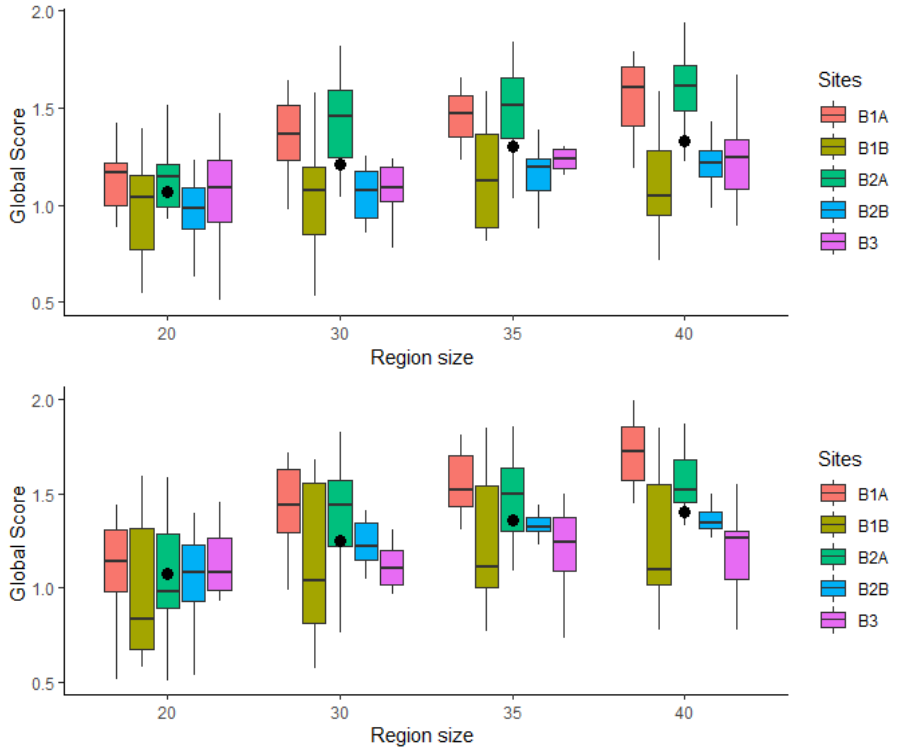

Figure 5. Global scores for total volume–dominant height (top) and **above ground biomass-**dominant height (bottom) segmentation versus minimum size. Black points are the mean value for each size.

The relationship between segment number and global score is shown in Figure 6 when the range radius was fixed at 4.

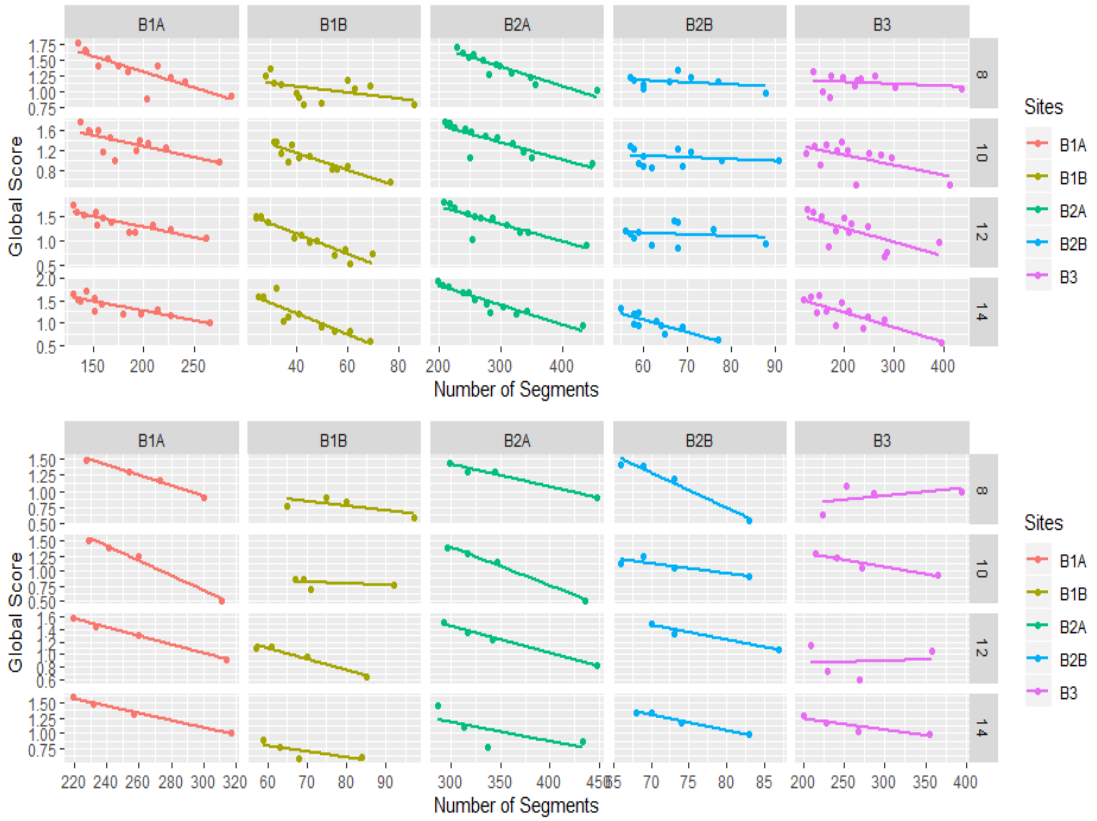

Figure 6. Trend of global score for total volume–dominant height (top) and above ground biomass-dominant height (bottom) by number of segments and **spatial radius.** Range radius was fixed in 4, continued lines are smooth (lm) trends.

4.6. DISCUSSION

Our study has compared the performance of parametric and non-parametric methods for estimating AGB, TV, and Ho, using LIDAR data at the stand level). AGB, TV and Ho are key inputs in models used to estimate the stand gross annual increment [38]. Then, we assessed the best combination of AGB-Ho and TV-Ho for stand segmentation. These results permit the generation of accurate *Eucalyptus* forest-stand segmentations using the mean shift segmentation method, which may be used to improve the programing of forestry and harvesting.

4.6.1. Assmann Dominant Height, Total Volume, and Above Ground Biomass Modeling

Ho is required for empirical models that are based on the site index (SI). The SI and height are generally used as an indicator of the quality of the forest site and for estimating the volume of standing trees [39]. ALS sensors have been widely used for the determination of forest parameters including AGB and TV [40,41], being a suitable technology for forest inventory and management [39].

In this study, we developed parametric and non-parametric models to estimate Ho, AGB and TV. Regarding LiDAR metric selection, for parametric models, the best predictors of Ho were related to the highest percentiles of the point cloud (Elev.90 and Elev.99) consistently as descriptors of dominant height. LIDAR height metrics, such as height percentiles, are frequent in studies that use LIDAR data for forest inventory [33,42]. However, using percentiles as unique independent variables will give the same result for stands with the same mean dominant height but different stand density. For volume and biomass models, the middle or upper-middle percentiles of the point cloud (Elev.70 and Elev.75) had greater importance. These upper-middle statistics of the point cloud report the tree crown properties [43,44], and have been used to explain other tree variables (e.g., stem diameter through) [45]. Hence, the 70th and 75th percentiles are expected to replace dbh in the equations developed to calculate the variables from field data (Equations (1)–(4)). Similar achievements were attained by other authors when modeling the above ground biomass in *Eucalyptus* stands [46,47].

For non-parametric models, all the k-NN models included at least one variable related to height metrics (Elev.P75, Elev.MAX, Ele.MO) and the shape of the height distribution (CRR), and most of the models included a variable related to cover metrics (PFRAM, ARMO). According to previous studies, the combination of height and density in the canopy metrics represents a description of the vertical structure of the forest stand [47]. Our k-NN models for AGB, TV, and Ho in the two *Eucalyptus* species included only one variable related to the upper-middle percentiles of the point cloud (Elev.75), as well as variables related to the density of the canopy

(ARA2/TFR, PFRM, CRR, ARMO). The results demonstrate that Elev.75 is potentially useful for improving forest models.

The percentage of returns above a certain height with respect to total returns is a metric that serves to characterize the forest cover. When modeling the dominant height (Ho), it will be more correlated with the highest percentiles of the height, since they are more related to tree height. The AGB and TV were calculated using equations including diameter (d) and height (TH) as the independent variables. Models generated on this study integrated high percentiles of forest canopy, representing tree height, and intermediate percentiles (e.g. p75 or the mode of heights) representing the diameter. Additionally, models included variables related to tree density, such as canopy relief ratio and first return above median, which could be substituted by the percentage of returns above 2 m since they belong to the same family of LiDAR metrics that provide a similar explanation for forest canopy.

The most common estimation methods of Ho, TV and AGB in forest inventories using LIDAR are ordinary simple regression methods (e.g., least squares regression) and non-parametric methods (e.g., RF, SVM and the nearest neighbor-based methods) [46]. Our results showed that both WLS and k-NN are suitable methods for predicting AGB, TV and Ho using LIDAR data. In our study, in the TV models, R^2-adj was 0.91 with Elev.70 for *E. grandis* and 0.92 with Elev.75 for *E. dunnii*, whereas the model with Elev.75 and the model with Elev.70 as the regressor took second place for *E. grandis* and *E. dunnii*, respectively. The AGB models had the same single independent variable as the TV models, for both species, but the R^2-adj values were lower: 0.86 and 0.85 for *E. grandis* and *E. dunnii*, respectively. In the Ho models, Elev.99 (R^2-adj 0.98), for *E. grandis*, and Elev.90 (R^2-adj 0.96), for *E. dunnii*, were selected as independent variables. The graphical trends of the residuals showed that the models were not affected by problems of homogeneity of variances. The accuracy of the models is confirmed by the low relative values of nRMSE, and by the values of cross-validation ($RMSE_{cv}$). Additionally, the closeness of the RMSEcv and RMSE values indicates that the models have good predictive value.

Comparison of the results of the selected parametric models with those of the non-parametric models show small differences. Our results suggest that the k-NN

(with RF distance metric) models performed better (as indicated by R^2, RMSE and RMSEcv) for TV and AGB. This has been reported also in most of the other studies that have compared parametric and non-parametric methods [47]. However, the Ho parametric model had better performance than the k-NN model, for both species, possibly explained by the strong correlation of the former with the highest percentiles. the differences between the two methods are small.

4.6.2. Segmentations

The normalized MI values, and the normalized weighted variance included in the global score of the segmentations indicate that OTB detected homogeneous stand well, in agreement with previous research [14,33,36]. The implementation of OTB for the delimitation of forest stands has proved to be simpler, more efficient and of similar precision compared to other more complex methods. Visually and quantitatively, the results show that the proposed segmentation method yielded high-quality segmentation when compared to manual segmentation. Thus, OTB segmentation could be used to automatically segment *Eucalyptus* stands, producing spatial stands that an expert could identify in a similar way to traditional photography (Figure 4). The results are consistent with other studies that use LIDAR for the automation of the delimitation of the stand applied in the field of forest inventory [11,33,39].

4.6.3. Applications in Forest Management

In this study, we have provided a framework for using LIDAR data to predict AGB, TV and Ho at the stand-level, employing parametric and non-parametric methods. We have shown that the use of regression models and non-parametric segmentation methods can provide more reliable AGB and TV distribution maps with lower error levels.

The implementation of a segmentation method such as OTB, improve time processing by increasing the area covered and maximizing the labor efficiency. The segmentation proposed on this study defines stands using TV or AGB with a similar

site index (by Ho). This allows planning activities such as road construction, localized harvests or future plantations.

Additionally, forest stand delimitation, based on these silvicultural variables and OTB method, worked well. This approach may contribute to better forest management through (i) greater success on growth and yield projections by improving the estimates of stand variables ensuring the development and implementation of growth and production models; (ii) assist the yield optimization according to the size of the stand, achieving a more efficient and homogeneous planning in terms of volume and products, (iii) the selection of stands for harvest, using a simple and inexpensive method that is regulated by the production estimates of the stands themselves, (iv) site classification is potentially improved by projecting Ho over the complete forest cover.

Having stand variables prediction models based on LiDAR metrics allows its application in large areas based on the calibration plots. Forest managers can manage more efficiently if they have wood production estimates that cover the entire area and not just those measured in traditional inventories. Forest management plans, based on prediction models, as well as stand segmentation based on these predictions, contribute to achieve coherence between inventory data and the final products harvested for the entire area covered by ALS. OTB is an economically more profitable solution than other specific forest management software, which allows forest producers to have a planning tool.

4.7. CONCLUSIONS

This study provides tools that allow the improvement of precision in two fundamental steps of forest stock quantification: stand variables modeling (above ground biomass, total volume and dominant height), using LIDAR and the delimitation of stand structure based on unsupervised evaluation. The parametric methods had better performance for Ho, and the non-parametric methods delivered better results in terms of precision and bias for TV and AGB. High-spatial-resolution maps of those variables can be created from LIDAR data once robust models have been developed which were used to stand segmentation. The segmentation

methodology proposed here provide a cost-effective and easy-to-update model for the generation of maps of AGB or TV for harvest tasks, based on rasters derived from LIDAR metrics. These tools, based on LIDAR metrics, allow forest managers to improve the decision-making process on forestry based on forest inventory, above ground biomass and total volume information for strategic management purposes (improving records of carbon sequestration rates and AGB fluxes, for example). It also exposes the need to continue advancing and promoting the application of ALS data for the inventory of forest plantations of *Eucalyptus* spp. in Uruguay.

4.8. ACKNOWLEDGMENTS

The authors thank the Instituto Nacional de Investigaciones Agropecuarias (INIA-Uruguay) for supporting our research work and for help during the fieldwork. We are particularly grateful for the support of Roberto Scoz, Demian Gomez, Zenia Barrios and Gustavo Balmelli (INIA), Mariano Blanco, Santiago Heguaburu, Carola Odone and José Carlos de Mello (FOSA). R.M.N.-C acknowledges the ISOPINE (UCO-1265298) and ESPECTRAMED (CGL2017-86161-R) projects for methodological support. We acknowledge the institutional support of the University of Cordoba-Campus de Excelencia CEIA3. We also thank the ERSAF group and, particularly. Cristina Acosta and Antonio Ariza. for their assistance during this research. We thank Dr. David Walker for his revisions of the different versions of this manuscript, and the anonymous referees for their comments and corrections.

4.9. REFERENCES

1. Hawbaker, T.J.; Gobakken, T.; Lesak, A.; Trømborg, E.; Contrucci, K.; Radeloff, V. Light detection and ranging-based measures of mixed hardwood forest structure. *For. Sci.* **2010**, *56*, 313–326.
2. Hościło, A.; Lewandowska, A. Mapping Forest Type and Tree Species on a Regional Scale Using Multi-Temporal Sentinel-2 Data. *Remote Sens.* **2019**, *11*, 929, doi:10.3390/rs11080929.

3. Naesset, E. Determination of mean tree height of forest stands using airborne laser scanner data. *ISPRS J. Photogramm. Remote Sens.* **1997**, *52*, 49–56.
4. González-Ferreiro, E.; Arellano-Pérez, S.; Castedo-Dorado, F.; Hevia, A.; Vega, J.A.; Vega-Nieva, D.; Álvarez-González, J.G.; Ruiz-González, A.D. Modelling the vertical distribution of canopy fuel load using national forest inventory and low-density airbone laser scanning data. *PLoS ONE* **2017**, *12*, e0176114, doi:10.1371/journal.pone.0176114.
5. Zhang, Z.; Cao, L.; Mulverhill, C.; Liu, H.; Pang, Y.; Li, Z. Prediction of Diameter Distributions with Multimodal Models Using LiDAR Data in Subtropical Planted Forests. *Forests* **2019**, *10*, 125, doi:10.3390/f10020125.
6. Nelson, R. How did we get here? An early history of forestry lidar1. *Can. J. Remote Sens.* **2013**, *39*, S6–S17.
7. Bouvier, M.; Durrieu, S.; Fournier, R.A.; Renaud, J.-P. Generalizing predictive models of forest inventory attributes using an area-based approach with airborne LiDAR data. *Remote Sens. Environ.* **2015**, *156*, 322–334, doi:10.1016/j.rse.2014.10.004.
8. Gregoire, T.G.; Næsset, E.; McRoberts, R.E.; Ståhl, G.; Andersen, H.-E.; Gobakken, T.; Ene, L.; Nelson, R. Statistical rigor in LiDAR-assisted estimation of aboveground forest biomass. *Remote Sens. Environ.* **2016**, *173*, 98–108.
9. Garcia-Gutierrez, J.; Gonzalez-Ferreiro, E.; Riquelme-Santos, J.C.; Miranda, D.; Dieguez-Aranda, U.; Navarro-Cerrillo, R.M. Evolutionary feature selection to estimate forest stand variables using LiDAR. *Int. J. Appl. Earth Obs. Geoinf.* **2014**, *26*, 119–131.
10. O'Hara, K.L.; Nagel, L.M. The stand: revisiting a central concept in forestry. *J. For.* **2013**, *111*, 335–340.
11. Dechesne, C.; Mallet, C.; Le Bris, A.; Gouet, V.; Hervieu, A. Forest stand segmentation using airborne lidar data and very high resolution multispectral imagery. *Int. Arch. Photogramm. Remote Sens. Spat. Inf. Sci. ISPRS Arch.* **2016**, *41*, 207–214, doi:10.5194/isprsarchives-XLI-B3-207-2016.
12. Haara, A.; Haarala, M. Tree species classification using semi-automatic delineation of trees on aerial images. *Scand. J. For. Res.* **2002**, *17*, 556–565.

13. Sanchez-Lopez, N.; Boschetti, L.; Hudak, A. Semi-Automated Delineation of Stands in an Even-Age Dominated Forest: A LiDAR-GEOBIA Two-Stage Evaluation Strategy. *Remote Sens.* **2018**, *10*, 1622, doi:10.3390/rs10101622.
14. Johnson, B.; Xie, Z. Unsupervised image segmentation evaluation and refinement using a multi-scale approach. *ISPRS J. Photogramm. Remote Sens.* **2011**, *66*, 473–483, doi:10.1016/j.isprsjprs.2011.02.006.
15. Castaño, J.P.; Giménez, A.; Ceroni, M.; Furest, J.; Aunchayna, R.; Bidegain, M. *Caracterización agroclimática del Uruguay 1980–2009*; 2011. Serie Técnica INIA 193. Montevideo, Uruguay,
16. Andrés, H.; Rafael, Na.; Jorge, F.; Maurizio, B.; Cecilia, R. *Modelling Taper, Total and Merchantable Stem Volume Considering Stand Density Effects to Eucalyptus grandis and Eucalyptus dunnii in Uruguay*; 2020.
17. McGaughey, R.J. *FUSION/LDV: Software for LiDAR Data Analysis and Visualization. February 2013–FUSION Version 3.30*; USDA Forest Service, Pacific Northwest Research Station, University of Washington Seattle, WA, USA. **2013**.
18. Silva, C.A.; Klauberg, C.; Hudak, A.T.; Vierling, L.A.; Liesenberg, V.; Bernett, L.G.; Scheraiber, C.F.; Schoeninger, E.R. Estimating Stand Height and Tree Density in Pinus taeda plantations using in-situ data, airborne LiDAR and k-Nearest Neighbor Imputation. *An. Acad. Bras. Ciênc.* **2018**, *90*, 295–309, doi:10.1590/0001-3765201820160071.
19. Lumley, T. Using Fortran Code by Alan Miller. Leaps: Regression Subset Selection. R Package Version 2.9. Available online: http://CRAN.R-project.org/package=leaps **2009** (1-8-2020).
20. *R Core Development Team A Language and Environment for Statistical Computing: Reference Index Version 3.5.1; Vienna, Austria.* 2019.
21. Mallows, C.L. Some comments on Cp. *Technometrics* **2000**, *42*, 87–94.
22. Zhao, F.; Guo, Q.; Kelly, M. Allometric equation choice impacts lidar-based forest biomass estimates: A case study from the Sierra National Forest, CA. *Agric. For. Meteorol.* **2012**, *165*, 64–72.

23. Elzhov, T. V; Mullen, K.M.; Spiess, A.-N.; Bolker, B.; Mullen, M.K.M.; Suggests, M. *Package 'minpack.lm.' Title R Interface Levenberg-Marquardt Nonlinear Least-Sq. Algorithm Found MINPACK Plus Support Bounds'* Available at: https://cran. rproject. org/web/packages/minpack. lm/minpack. lm. pdf*Pdf*; 2016.
24. Quinn, G.P.; Keough, M.J. *Experimental Design and Data Analysis for Biologists;* Cambridge, UK, Cambridge University Press. 2002; ISBN 1139432893.
25. Crookston, N.L.; Finley, A.O. YaImpute: An R Package for kNN Imputation. J. Stat. Softw. 2008, 23, 1–16..
26. Zald, H.S.J.; Wulder, M.A.; White, J.C.; Hilker, T.; Hermosilla, T.; Hobart, G.W.; Coops, N.C. Integrating Landsat pixel composites and change metrics with lidar plots to predictively map forest structure and aboveground biomass in Saskatchewan, Canada. *Remote Sens. Environ.* **2016**, *176*, 188–201, doi:10.1016/j.rse.2016.01.015.
27. Knapp, N.; Fischer, R.; Huth, A. Linking lidar and forest modeling to assess biomass estimation across scales and disturbance states. *Remote Sens. Environ.* **2017**, *205*, 199–209, doi:10.1016/j.rse.2017.11.018.
28. Kohavi, R. A Study of Cross-Validation and Bootstrap for Accuracy Estimation and Model Selection. *Int. Jt. Conf. Artif. Intell.* **1995**, *2*, 1137–1143.
29. Andersen, H.-E.; McGaughey, R.J.; Reutebuch, S.E. *Estimating Forest Canopy Fuel Parameters Using LIDAR Data*; Remote Sens. Environ. 2005, 94, 441-449 doi:l0.1016/j.rse.2004.10.0
30. Qgis, D.T. *QGIS Geographic Information System, Open Source Geospatial Foundation*; 2009.
31. Comaniciu, D.; Meer, P. Mean shift: A robust approach toward feature space analysis. *IEEE Trans. Pattern Anal. Mach. Intell.* **2002**, *24*, 603–619.
32. Wu, Z.; Heikkinen, V.; Hauta-Kasari, M.; Parkkinen, J.; Tokola, T. *Forest Stand Delineation using a Hybrid Segmentation Approach Based on Airborne Laser Scanning Data*; In: Kämäräinen, J.-K., Koskela, M. (Eds.), Image Analysis. Springer, Berlin Heidelberg,: 2013; pp. 95–106.

33. Varo-martínez, M.Á.; Navarro-cerrillo, R.M.; Hernández-clemente, R. Semi-automated stand delineation in Mediterranean Pinus sylvestris plantations through segmentation of LiDAR data : The influence of pulse density. *Int. J. Appl. Earth Obs. Geoinf.* **2017**, *56*, 54–64, doi:10.1016/j.jag.2016.12.002.
34. Grybas, H.; Melendy, L.; Congalton, R.G. A comparison of unsupervised segmentation parameter optimization approaches using moderate-and high-resolution imagery. *GIScience Remote Sens.* **2017**, *54*, 515–533.
35. Zhang, X.; Feng, X.; Xiao, P.; He, G.; Zhu, L. Segmentation quality evaluation using region-based precision and recall measures for remote sensing images. *ISPRS J. Photogramm. Remote Sens.* **2015**, *102*, 73–84.
36. Espindola, G.M.; Camara, G.; Reis, I.A.; Bins, L.S.; Monteiro, A.M. Parameter selection for region-growing image segmentation algorithms using spatial autocorrelation. *Int. J. Remote Sens.* **2006**, *27*, 3035–3040, doi:10.1080/01431160600617194.
37. Zhang, X.; Xiao, P.; Feng, X. An unsupervised evaluation method for remotely sensed imagery segmentation. *IEEE Geosci. Remote Sens. Lett.* **2011**, *9*, 156–160.
38. White, J.C.; Coops, N.C.; Wulder, M.A.; Vastaranta, M.; Hilker, T.; Tompalski, P. Remote Sensing Technologies for Enhancing Forest Inventories: A Review. *Can. J. Remote Sens.* **2016**, *42*, 619–641.
39. Mora, B.; Wulder, M.A.; White, J.C.; Hobart, G. Modeling stand height, volume, and biomass from very high spatial resolution satellite imagery and samples of airborne LIDAR. *Remote Sens.* **2013**, *5*, 2308–2326, doi:10.3390/rs5052308.
40. Böck, S.; Immitzer, M.; Atzberger, C. On the Objectivity of the Objective Function—Problems with Unsupervised Segmentation Evaluation Based on Global Score and a Possible Remedy. *Remote Sens.* **2017**, *9*, 769, doi:10.3390/rs9080769.
41. Yang, L.; Mansaray, L.R.; Huang, J.; Wang, L. Optimal segmentation scale parameter, feature subset and classification algorithm for geographic object-

based crop recognition using multisource satellite imagery. *Remote Sens.* **2019**, *11*, 514.

42. Shao, G.; Shao, G.; Gallion, J.; Saunders, M.R.; Frankenberger, J.R.; Fei, S. Improving Lidar-based aboveground biomass estimation of temperate hardwood forests with varying site productivity. *Remote Sens. Environ.* **2018**, *204*, 872–882.
43. Matasci, G.; Hermosilla, T.; Wulder, M.A.; White, J.C.; Coops, N.C.; Hobart, G.W.; Bolton, D.K.; Tompalski, P.; Bater, C.W. Three decades of forest structural dynamics over Canada's forested ecosystems using Landsat time-series and lidar plots. *Remote Sens. Environ.* **2018**, *216*, 697–714.
44. Næsset, E.; Økland, T. Estimating tree height and tree crown properties using airborne scanning laser in a boreal nature reserve. *Remote Sens. Environ.* **2002**, *79*, 105–115.
45. Lo, C.S.; Lin, C. Growth-competition-based stem diameter and volume modeling for tree-level forest inventory using airborne LiDAR data. *IEEE Trans. Geosci. Remote Sens.* **2013**, *51*, 2216–2226, doi:10.1109/TGRS.2012.2211023.
46. Guerra-Hernández, J.; Görgens, E.B.; García-Gutiérrez, J.; Rodriguez, L.C.E.; Tomé, M.; González-Ferreiro, E. Comparison of ALS based models for estimating aboveground biomass in three types of Mediterranean forest. *Eur. J. Remote Sens.* **2016**, *49*, 185–204, doi:10.5721/EuJRS20164911.
47. Jayathunga, S.; Owari, T.; Tsuyuki, S. Digital Aerial Photogrammetry for Uneven-Aged Forest Management: Assessing the Potential to Reconstruct Canopy Structure and Estimate Living Biomass. *Remote Sens.* **2019**, *11*, 338, doi:10.3390/rs11030338.

5. A MACHINE LEARNING APPROACH TO MODEL LEAF AREA INDEX IN EUCALYPTUS PLANTATIONS USING SATELLITE IMAGERY AND AIRBORNE LASER SCANNER DATA

Hirigoyen Andrés[1*], Acosta Cristina[2], Ariza Antonio[2], Varo-Martínez Mª Ángeles[2], Rachid-Casnati Cecilia[1], Franco Jorge[3], Navarro-Cerrillo Rafael[2]

Andrés Hirigoyen, ahirigoyen@inia.org.uy; *[1]National Institute of Agricultural Research (INIA) Tacuarembó. Ruta 5 km 386, Tacuarembó, Uruguay.* Corresponding author*

Cecilia Rachid, crachid@inia.org.uy; *[1]National Institute of Agricultural Research (INIA) Tacuarembó. Ruta 5 km 386, Tacuarembó, Uruguay*

Cristina Acosta, cristina.acostamunoz@gmail.com; *[2] Department of Forestry Engineering, Laboratory of Silviculture, Dendrochronology and Climate Change. DendrodatLab- ERSAF, University of Cordoba, Campus de Rabanales, Crta. IV, km 396, E-14071 Córdoba. Spain*

Antonio Ariza, antonio41993@gmail.com; *[2] Department of Forestry Engineering, Laboratory of Silviculture, Dendrochronology and Climate Change. DendrodatLab-ERSAF, University of Cordoba, Campus de Rabanales, Crta. IV, km 396, E-14071 Córdoba. Spain*

Maria Angeles Vero-Martinez, mangelesvaro@gmail.com; *[2] Department of Forestry Engineering, Laboratory of Silviculture, Dendrochronology and Climate Change. DendrodatLab- ERSAF, University of Cordoba, Campus de Rabanales, Crta IV, km. 396, E-14071 Córdoba. Spain*

Jorge Franco jfranco@fagro.edu.uy; *[3] University of the Republic, Faculty of Agronomy, Ruta 3 363 km, Paysandú, Uruguay.*

Rafael Navara-Cerrillo; rmnavarro@uco.es; *[2] Department of Forestry Engineering, Laboratory of Silviculture, Dendrochronology and Climate Change. DendrodatLab-ERSAF, University of Cordoba, Campus de Rabanales, Crta. IV, km. 396, E-14071 Córdoba. Spain*

5.1. RESUMEN

El área proyectada de hojas por unidad de superficie horizontal del suelo se define como índice de área foliar (LAI, m^2 m^{-2}), parámetro estructural forestal crucial para el manejo intensivo de las plantaciones afecta, el uso de agua y nutrientes y el balance de carbono. El objetivo de este trabajo es cuantificar LAI en rodales de *Eucalyptus dunnii* y *Eucalyptus grandis*, utilizando métricas LiDAR y métricas satelitales multiespectrales de alta resolución. Evaluamos las relaciones empíricas entre LAI y los datos de teledetección. La cobertura del dosel del bosque LiDAR, el índice de penetración del láser y la relación de relieve del dosel, de entre los datos de LiDAR, y el índice de vegetación de diferencia normalizada verde y el índice de vegetación de diferencia normalizada, de entre los datos basados en el suelo, fueron las variables seleccionadas para la estimación de LAI. Comparamos la precisión de tres algoritmos de aprendizaje automático: redes neuronales artificiales (ANN), bosque aleatorio (RF) y regresión de vectores de soporte (SVR). El coeficiente de determinación osciló entre 0,60, para ANN, y 0,84, para SVR. Los métodos de regresión SVR mostraron el mejor rendimiento en términos de precisión general del modelo y RMSE (0,60). Se presentan brevemente los algoritmos de aprendizaje automático que se utilizan para cuantificar LAI, ya sea mediante sensores ópticos remotos o métricas LiDAR. Los resultados muestran que los datos de la teledetección son una fuente de información eficaz para estimar el LAI en plantaciones de eucaliptus. La metodología propuesta es directamente aplicable para la planificación forestal operativa a nivel de paisaje. A diferencia de los métodos terrestres, la estimación remota de la estructura del dosel proporciona un avance rentable y ecológicamente significativo.

Palabras claves: IAF canopia, algoritmos de machine learning, silvicultura intensiva

5.2. ABSTRACT

The projected area of leaves per unit of horizontal soil surface is defined as leaf area index (LAI, m^2 m^{-2}). It is an important forest structural parameter, crucial for efficient intensive plantation management, and it affects the micro-meteorological conditions, water and nutrient use, and carbon balance. The current state of the art for the estimation of LAI can be by remote-sensing methods and ground-based methods. The aim of this paper is to quantify LAI in stands of *Eucalyptus dunnii* and *Eucalyptus grandis*, using LiDAR metrics and multispectral high-resolution satellite metrics. We evaluated the empirical relationships between LAI and remote-sensing data. The LiDAR forest canopy cover, laser penetration index, and canopy relief ratio - from among the LiDAR data - and the green normalized difference vegetation index and normalized difference vegetation index - from among the ground-based data - were the selected variables for LAI estimation. We compared the accuracy of three machine learning algorithms: artificial neural networks (ANN), random forest (RF) and support vector regression (SVR). The coefficient of determination ranged from 0.60, for ANN, to 0.84, for SVR. The SVR regression methods showed the best performance in terms of overall model accuracy and RMSE (0.60). Machine learning algorithms used to quantify LAI, using either optical remote sensing or LiDAR metrics, are briefly presented. The results show that the remote sensing data is an effective source of information to estimate LAI in eucalyptus plantations. The methodology proposed is directly applicable for operational forest planning at the landscape level. Unlike ground-based methods, remote estimation of canopy structure provides a cost-effective and ecologically significant advance.

Key words: LAI canopy, machine learning algorithms, intensive silviculture

5.3. INTRODUCTION

The structure of the forest canopy is generally described through variables, such as the leaf area index (LAI), crown diameter, and crown length (Weiss et al. 2004). LAI is defined as the one-sided leaf area per unit of horizontal ground surface area (Watson 1947). In commercial timber plantations, LAI plays a key role in the radiation availability and buffering of temperatures, plant water relations and fertility status, thus affecting growth and production. Therefore, LAI is one of the main variables used to evaluate many processes related to the physiological state of trees. However, LAI estimation is a complex issue, involving factors related to plant size, species composition, growth, yield, or canopy phenology. Methods of LAI estimation can be categorized as direct or indirect (Jonckheere et al. 2004). Direct methods use destructive sampling to determine the total number of leaves per tree and their area, taking into account their angles and distribution. This approach is time-consuming, labor-intensive, and costly (Jonckheere et al. 2004). In the indirect methods, LAI is inferred from observations of another variable and contact and non-contact methods are used, mostly to measure some radiative feature related to the distribution of light inside the canopy (Morsdorf et al. 2006). Indirect approaches are faster and amenable to automation, and thereby allow a larger spatial sample to be obtained (Jonckheere et al. 2004). Methods based on differences in spectral reflection between vegetation and other coverage, and using remote sensing data, have been widely applied for LAI determination in forests during recent years (Yan et al. 2019).

Spectral vegetation indices (VIs) obtained from remote sensing data are valuable for the estimation of LAI, due to their enhanced resistance to atmospheric effects. Several authors have found positive correlations between LAI and VIs derived from satellite images (Pavithra et al. 1998). The VIs used most frequently to estimate LAI are the normalized difference vegetation index (*NDVI*) and the simple

ratio (*SR*), applied in coniferous forests, grasslands, and deciduous forests (Staben et al. 2018)**,** however, these indices can saturate in dense vegetation as forest stand. Many studies report that VIs saturate at high LAI (Zhao & Popescu 2009). VIs are easily affected by atmospheric conditions and soil, VIs tend to saturate, decreasing the accuracy of prediction of forest parameters (Luo et al. 2019) and leading to underestimation of LAI. The spectral reflectance of vegetation can be similar to the background reflectance, even with the use of hyperspectral remote sensing systems that boast high spectral (Tesfamichael et al. 2018)**.**

Moreover, multispectral sensors do not have robust means of characterization of the vertically distributed forest attributes, since they provide information about plants using two dimensions; thus, they are unable to profile plants vertically (Tesfamichael et al. 2018). There are many satellite-derived LAI products, but their coarse-moderate spatial resolution (Modis 500 m, Landsat 30 m) has made it difficult to apply them at a regional scale (Zhou et al. 2020). The use of CubeSat constellations that provide frequent and high-resolution images is one way to achieve both high review frequency and high spatial resolution (Zhou et al. 2020). Planet Labs launched a constellation of CubeSats that cover the entire globe daily with a spatial resolution of 3 to 5 m **(**Planet Labs 2018**)**.

Active sensors employing light detection and range (LiDAR) technology can fill the gaps of multispectral sensors in LAI estimation by providing data on forest structural attributes, specifically canopy vertical profiles. Airborne Laser Scanner (ALS) is a LiDAR that operates from aerial platforms, while the Terrestrial Laser Scanning (TLS) uses ground platforms. It can capture more detailed information on 3-D structure, and produces data points in a three-dimensional cloud, which permits the variation of the forest canopy features distributed vertically (Peduzzi et al. 2012). Unlike traditional optical data, ALS provide a direct measurement of the vertical

structure of the forest canopy, ALS metrics has been used to predict stand variables such as volume or biomass (Jensen et al. 2008). Due to the ability to penetrate canopies and its rapid coverage of large areas, ALS has been used for LAI mapping at landscape or regional scales (Yan et al. 2019). ALS metrics (ALm) contain information on canopy structure and LAI; thus, the selection of ALm for LAI estimation modeling is a key procedure. ALS metrics (ALm) provide information on the canopy structure, the correct selection of ALm that will integrate the LAI estimation model is a key procedur (Zhao & Popescu 2009). Different ALm have been used to predict LAI in previous research, such as ALS height percentiles, laser interception index (LII) and laser penetration index (LPI) (Morsdorf et al. 2006, Peduzzi et al. 2012, Tseng et al. 2016).

The LPI is an approximation to the canopy gap fraction, it is expected to be useful for estimating the LAI. Combination ALm with hyperspectral and multispectral imagery can improve prediction accuracy of forest canopy parameters (Luo et al. 2019). Non-parametric machine learning (ML) approaches represent an alternative to overcome these limitations. ML can discover unusual non-linear relationships, as well as operate high-dimensional and collinearity problems, handle non-linearity and non-normality of data (Lary et al. 2016). Since non-parametric statistical methods do not make a priori assumptions about the data, they are more attractive to establish and describing relationships between remote sensing images and the forest variables of interest (Ingram et al. 2005). A wide range of ML algorithms have been used effectively in forest applications for both regression and classification of non-linear systems (Lary et al. 2016). ML including K-nearest neighbors, random forest (RF), tree-based models such as decision trees (DT), artificial neural networks (ANN), genetic algorithm, support vector machines (SVM), case-based reasoning (Lary et al. 2016, Jain et al. 2020).

LAI is a meaningful index for intensive plantation management, it provides information on current conditions and the possible evolution of stand growth and yield. Hence, it has been used to identify stand fertilization needs, thinning, or other management practices that improve tree growth and yield (Peduzzi et al. 2012). Thus, several studies have applied spectral vegetation indices for the easy retrieval of LAI in *Eucalyptus* plantations (le Maire et al. 2012). However, few studies have integrated vegetation indices and ALS data for the estimation of LAI in *Eucalyptus* stands (but see Tesfamichael et al., 2018).

In this study, we compared several commonly used ML algorithms in the assessment of LAI, integrating ALS metrics and vegetation indices derived from Planet imagery across stands of *Eucalyptus grandis* Hill ex Maiden and *Eucalyptus dunnii* Maiden in Uruguay. Thus, the specific objectives of the present research were: i) to evaluate the efficiency of ALS and Planet spectral data as covariates to estimate LAI; ii) to test the performance of SVM, ANN, and RF algorithms in LAI assessment; iii) to analyze the spatial consistency between products and field measurements; and iv) to assess whether Planet multispectral data can improve LAI estimates in conjunction with ALS.

The results allowed us to suggest a new approach to LAI estimation in intensive *Eucalyptus* plantations that can be applied over distinct forest test sites, selecting and applying the best features of each source of data to improve LAI estimation.

5.4. MATERIAL AND METHODS

5.4.1. Site description

The present research was established in five forest areas in Uruguay owned by Forestal Oriental SA, representing a total area of 2468 ha. We selected five areas

(Figure 1): zones b1 and b2 (43° 13′ 97” S–64° 24′ 78” W) with 861 ha; zones b3 and b4 (63° 07′ 44” S–52° 22′ 64”W) with 870.1 ha; and zone b5 (63° 44′ 33.05” S–63° 95′58”W) with 716.9 ha. The study zones have mean annual rainfall between 1300 and 1400 mm (Castaño et al. 2011). They have a temperate subtropical climate, with a mean annual temperature of 18 °C (12 °C in the coldest month, 24 °C in the warmest month). The soils of the five sites were classified as siliceous, fine-loamy, active, thermic Mollic Hapludalfs (Bentancor, 2017). All sites are planted with *E. dunnii* and *E. grandis* (Table 1).

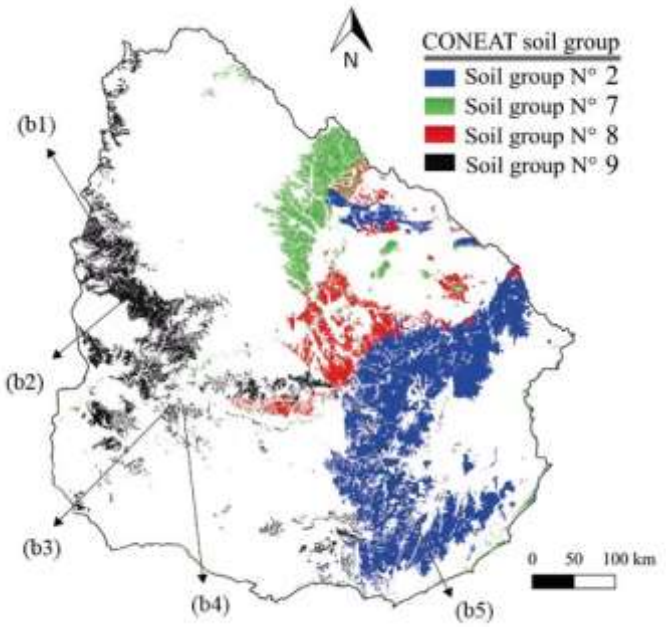

Figure 1. Location of the study sites (b1-b5) and Soils prioritized for forestry in Uruguay

Table 1. Silvicultural characteristics of *Eucalyptus grandis* and *Eucalyptus dunnii* in Uruguay. Standard deviation (stdev); minimum (min) and maximum (max) values for: stem density (N, trees ha^{-1}); diameter at breast height (Dbh, cm); total height (TH, m); leaf area index (LAI, m^2 m^{-2}) nd Age (years).

	Field Attributes	min	mean	max	stdev
E. grandis	Dbh (cm)	10.65	15.49	19.33	1.81
	TH (m)	12.57	21.69	33.3	4.46
	LAI (m^2 m^{-2})	1.2	2.95	4.78	1.05
	Age (year)	4	6	9	1.4
	N (tree ha^{-1})	634	1041	1336	144
E. dunnii	Dbh (cm)	10.83	15.27	19.38	1.53
	TH (m)	9.52	19.55	29.22	4.23
	LAI (m^2 m^{-2})	1.17	3.26	5.07	1.07
	Age (year)	4	6	8	1.1
	N (tree ha^{-1})	669	1070	1432	159

5.4.2 Field measurement of LAI

The LAI was measured in May-June 2018 in 39 of *E. dunnii* and 45 plots of *E. grandis* each with a fixed radius of 10 m (314.16 m^2), using a ceptometer (AccuPAR Model 80; Decagon Devices, Germany) (Table 1). The ceptometer was calibrated according to the instruction manual (Decagon Devices 2016). The measurements inside the plots were made by holding the instrument at a height of 1.3 m. For all plots, 6 sampling points were systematically located within the measurement area, 3 in the tree rows and 3 between rows. LAI measurement points were systematically assigned along a transect perpendicular to the two central rows of trees in each plot. In each sampling point, 4 measurements were taken (north, south, east, west), thus

giving a total of 24 values of radiation. Between plots, the incident radiation was measured on top of the canopy, in an area outside the plantation where the radiation reached the Ceptometer.

5.4.3. Planet data and spectral vegetation indices

Planet is a company that operates a constellation of more than 175 small standardized CubeSat 3U nanosatellites. Planet provides daily nadir-pointing high-resolution land surface imaging of the entire Globe (Planet Labs 2018). Planet's satellites provide multispectral high-resolution satellite images (MRS) at a spatial resolution of 3-4 m (nadir ground sampling distance) with red, green, and blue (RGB) and near-infrared (NIR) data. We using a total of 11 Planetscope Ortho Tile products (Planet Labs 2018), an orthomosaic of multiple scenes orthorectified in a single strip was merged and divided into a defined grid (25 x 25 km). The images were acquired from February to April 2018 and underwent radiometric, geometric, and sensor correction (Planet Labs 2018). The analytical format involved a 4-band, 16-bit multispectral image (RGB-NIR), having an orthorectified spatial resolution of 3.125, with daily review. Five spectral indices were calculated (Table 2). Image pre-processing and processing were performed with EVI (Exelis 2015), and post-processing with QGIS (QGIS Development Team, 2009) and R software (R Core Development Team 2015).

Table 2. Summary of vegetation indices and source used to model leaf area index (LAI) for *Eucalyptus* plantation in Uruguay**.**

Index	Formulation	Reference
Enhanced vegetation index	$EVI = 2.5\frac{\rho_{NIR} - \rho_{Red}}{1 + \rho_{NIR} + 6\rho_{Red} - 7.5\rho_{Blue}}$	(Huete & Van leeuwen 1999)
Green normalized difference vegetation index	$GNDI = \frac{\rho_{NIR} - \rho_{Green}}{\rho_{NIR} + \rho_{Green}}$	(Gitelson & Merzlyak 1998)
Normalized Difference Vegetation Index	$NDVI = \frac{\rho_{NIR} - \rho_{Red}}{\rho_{NIR} + \rho_{Red}}$	(Rouse Jr et al. 1973)
Simple Ratio	$SRI = \frac{\rho_{NIR}}{\rho_{Red}}$	(Jordan 1969)
Greenness Index	$GI = \frac{\rho_{green}}{\rho_{Red}}$	(Xue & Su 2017)

5.4.4. Acquisition and processing of ALS data

Airborne LiDAR acquisition was carried out during March 2018, using a Riegl VUX-1 laser scanner (Riegl, Germany) installed on a helicopter, with a pulse repetition rate of 550 kHz, an angular step width of 0.0687º, and a FOV of 55º, at a flight altitude of 110 m.a.s.l. The resulting point density was 20 pulses m^{-2}, geo-referenced in the WGS84 UTM 21 coordinate system. For all echoes *x* and *y* (planimetric coordinates), plus ellipsoidal height values are calculated. The FUSION software (McGaughey 2013) was used to checked and processed ALS point clouds. After the ALS data was verified and validated, a digital terrain model (DTM), a canopy height model, a digital surface model, and ALS metrics were generated. We use the *GroundFilter* function to identify and filter the returns that reach the ground. To create a DTM with a pixel size of 1 m2, the *GridSurfaceCreate* function was used

(González-Jaramillo et al. 2018). To normalize the heights, the Clipdata algorithm was applied, this tool ensures that the *z* coordinate of each point corresponds to the height above the ground. *Cover* was used to calculate the canopy cover fraction (CCF), which represents the proportion of soil that is covered by the crown vertical projection and allows the density and horizontal distribution of the vegetation to be determined. Point data stored in *las* format were converted to ASCII text format by *LDA2ASCII*. The folders obtained from these procedures included the variables x, y, and z, and intensity values for each laser pulse return (Mesas-Carrascosa et al. 2012)**.** The ALS normalized point-cloud data pre-plots were filtered according to (Peduzzi et al. 2012) and the points were categorized into three groups, depending on the height above the ground (hag): vegetation returns (Nv), ground returns (Ng), all returns (Na) , and. The ceptometer was held at approximately 1.3 m above the ground, so the vegetation returns were classified using a 1.3-m threshold (Sumnall et al. 2016b)**.** Table 3 shows the LiDAR metrics **(**ALm**).**

To record the energy of the returns reflected back to the sensor, the intensity values are stored in ALS data. This recording is a function of several variables (such as angle of incidence, reflectivity and target area, laser power, atmospheric absorption, and distance between the sensor and the target). The intensity values need to be calibrated before comparing them, this process allows to compare different flights and scans **(**Mesas-Carrascosa et al. 2012). A simple method to correct the intensity, proposed by Mesas-Carrascosa et al. (2012), if compared with a reference distance, consists of normalizing the range to a standard range established by the user, and the effect of the angle of incidence is estimated by a correction of the cosine.

$$I_{normalized} = \mathrm{I}\ \frac{\mathrm{R}^2}{(\mathrm{R}_s^2\ \cos\propto)} \qquad (1)$$

where $I_{normalized}$ is the normalized intensity, I is the raw intensity value, R is the range (sensor-target distance), R_S is the standard range, and α is the angle of incidence. As information about the flight lines was not available, we used an approximation to determine the R values, using the difference between the height of each point and the mean flight altitude (Mesas-Carrascosa et al. 2012). Due to the smooth relief of the study area, we assumed that the scan angle was the same as the angle of incidence (Mesas-Carrascosa et al. 2012).

Table 3. ALS point cloud return height and intensity distribution metrics for each plot level area. Hag= height above the ground. Subscripts were as follows: frequency (total), mean, median, minimum (min), maximum (max), standard deviation (sd), coefficient of variation (cv), skewness (sk) kurtosis (kt), and height percentiles (P10, P20, ... ,P99).

ALS metrics	Symbols
All returns (return hag > 0.2 m)	Elev.total, Elev.max, Elev.mean, Elev.median, Elev.sd, Elev.cv, Elev.sk, Elev.kt, Elev.P05 … Elev.P99
Total number and first of ground returns	Gr.total, Gr.firs
Vegetation returns (return hag > 1.3 m)	Veg.total, Veg.max, Veg.mean, Veg.median, Veg.sd, Veg.cv, Veg.sk, Veg.kt,. Veg.P5, ..., Veg.P95
Intensity value summary from vegetation returns (returns hag > 1.3 m)	Sd, Cv, Sk, Kt

5.4.4.1. ALS pseudo-waveforms construction

The waveform vertical distribution curve contains more information than the waveform-derived metrics and the returns (Zhou & Qiu 2015). We used discrete-return data to create pseudo-waveforms (PWF) as the vertical frequency distribution of the sum of the intensity, as a function of height bins (Zhou and Qiu 2015). Waveforms can be uniform Gaussian-shaped functions, asymmetric, peaked, or flattened depending on the backscattering surface material (trees, grass, ground, roofs) (Zaletnyik et al. 2010). ALS-PWF data were constructed by modifying the method proposed by (Luo et al. 2019)**.** In each plot, ALS point clouds were separated by elevation values, them they were assigned to the height bins (from hag = 0.2 m at canopy height maximum) with an interval of 0.5 m. The relative returns intensity in each height bin were calculated by dividing the sum of the intensity in each height bin by the total intensity (Peduzzi et al. 2012)**.** ALS-PWF data were obtained by connecting, with a smooth curve, the intensity corresponding to the elevation of each height bin. Each ALS-PWF series was analyzed to identify the number of peaks and its shape as a density function. To distinguish between different PWF from backscattering surface material as trees, shapes statistical measures such as skewness, kurtosis, and standard deviations can be calculated and compared (Zhou & Qiu 2015)**.** If the shape of a PWF is different from a normal distribution, the waveforms have to be separated according to the number of peaks, because skewness and kurtosis have meaning only for a normal (unimodal) distribution (Zaletnyik et al. 2010). The number of peaks in the PWF was determined with the local maximum point in a simple peak detection method by *findpeaks* function of the *pracma* package of R software. A process of Gaussian decomposition was not applied because we expected that after PWF creation, as described above, only a major peak corresponding to the tree crowns zone would be identified. The plots area did not

have undergrowth vegetation, so peaks under the crown were not expected. Figure 2 presents a visual analysis of the relationship between the shapes of the ALS-PWF and the plots from which they were obtained.

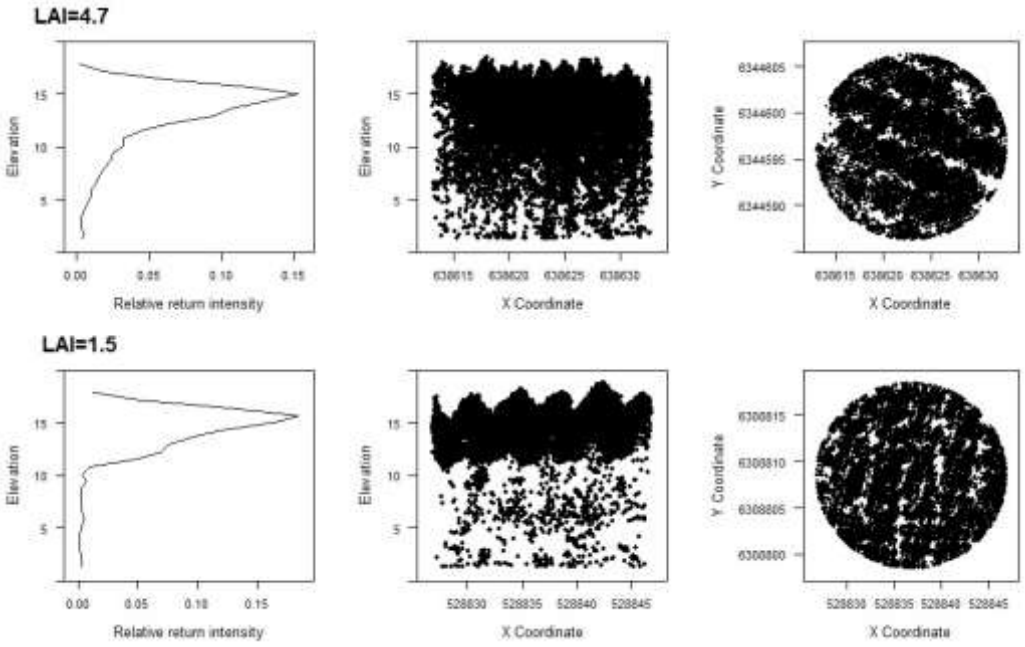

Figure 2. *Eucalyptus grandis* plots with maximum LAI (top) and minimum LAI (botton); ALS pseudo-waveform (left), sample cross section of a point cloud of a plot (middle) and sample of top view of canopy return of a plot (right).

5.4.4.2. Laser penetration index

In LPI calculation, DTM and non- ground points are taken into account. The canopy penetration and corresponding LAI can be derived from the fraction of echoes located on and below the canopy (Solberg et al. 2006)**.** LPI is based on the same principles as the instruments that measure LAI indirectly, measuring the solar light transmission or reflectance through vegetation (Peduzzi et al. 2012). The LPI can be

related to the principles used by the IAF indirect measurement instruments, these apply a vertical stratification to determine the amount of returns above or below a height threshold (Sumnall et al. 2016b)**.** We calculated five LPI (table 4) based on points data and three based on intensity information, as previously proposed (Peduzzi et al. 2012, Sumnall et al. 2016a, Tseng et al. 2016). In these works, LPI showed good correlation with the measured LAI.

Table 4. Computation of ALS penetration indices (LPI). Where: (N_g) total numbers of ground points, (N_{sg}) single-return ground points, (N_v) numbers of vegetation points (N_g), numbers of ground points, the sum of intensity of all returns (I_{all}), sum of intensity for returns below and above the ground threshold (I_g,I_v)

LPI calculation	Proposed by
$LPI_1 = \frac{N_g}{N_g+N_v}$	(Solberg et al. 2006)
$LPI_2 = \frac{N_g}{N_g+N_a}$	(Peduzzi et al. 2012)
$LPI_3 = \frac{N_g+N_{sg}}{N_g+N_a}$	(Tseng et al. 2016)
$LPI_4 = \frac{N_v}{N_g+N_a}$	(Luo et al. 2019)
$LPI_5 = \frac{I_v}{I_{all}}$	(Hopkinson & Chasmer 2009)
$LPI_6 = \frac{I_g}{I_{all}}$	(Sumnall et al. 2016a)
$LPI_7 = \frac{I_v}{I_g}$	(Sumnall et al. 2016a)

5.4.5. Variable selection

To reduce data redundancy and improve overall interpretability, a multicollinearity analysis was performed. Spearman's correlation was used to identify highly correlated ALm variables. A collinearity analysis was then performed using the Variance Inflation Factor (VIF). Independent variables were selected and collinear variables were deleted, using a VIF >10 as the critical threshold (Ariza Salamanca et al. 2019). To select the best explanatory variables from among the ALm, LPI, and VI, several authors have employed RF techniques (Luo et al. 2019)**.** The RF selection procedure uses a percentage increase in model mean square error (%MSE for regression) to select variables that explain the highest amount of variation. This variable importance score is computed as the difference in predictions on the out-of-bag observations before and after permutation in the data withheld from each tree (Pearse et al. 2017). However, importance scores computed in this way have been shown to overestimate the importance of highly correlated predictors (Pearse et al. 2017)**.**

In our study, we used permutation importance (PIMP) proposed by (Altmann et al. 2010), that reduces the bias, based on a permutation test, and returns significant p-values for each feature. PIMP is available in the *vita* package of R software (R Core Development Team 2015)**.**

5.4.6. Machine learning algorithms

Once the variables had been selected, ML was used as an empirical approach for determination of the regression between the LAI and predictors. ML methods require a training dataset and a random subset of the data for a completely independent validation. ML methods require for independent validation a random subset of the

data, and a random training data set for fit. (Lary et al. 2016)**.** We divided the dataset into two sets, one with 70% of de data: train set; and other to validate with the 30% remained: validation set. We carried out a comparison of the most well-known regressions in ML approaches (SVM, ANN, and RF) in a common framework to estimate LAI.

5.4.6.1. Support vector regression

SVM can be used for classification tasks and to solve regression problems (SVR), where a continuous prediction output is expected (Mountrakis et al. 2011; Jain et al. 2020**).** SVR is based on the principle of structural risk minimization, and looks for a hyperplane with the greatest margin to divide samples into two classes with the largest interval (Jain et al. 2020)**.** SVM operate by assuming that each set of input parameters will have a unique relationship to its response variable(Gleason & Im 2012)**.** The grouping of these predictors and their relationships are sufficient to define rules that can be applied for predicting variables (Gleason & Im 2012). This method has proven its robustness to determine dimensionality and outliers in the training data, its generalization ability, and its ability to reduce overfitting (Mountrakis et al. 2011, Gleason & Im 2012)**.** For SVR, a linear function was used as the kernel function because it showed better behavior than polynomial and sigmoidal kernel functions. To select cost and gamma parameters, we used the *svm* and *tune.svm* functions in R to find the optimal values (implemented with package e1071)

5.4.6.2. Artificial neural networks

ANN are an alternative approach for modeling non-linear and complex phenomena in forest science. ANN are typically composed of an input layer, an output layer, and one or more hidden layers (Ingram et al. 2005). Our ANN structure

included an input layer, an output layer, and five hidden layers (a ranging from 1 to 15 neurons in the hidden layers were evaluated).

5.4.6.3. Random Forest

RF has been widely used to estimate dendrometric variables. It is a bagging-based method, it creates a large group of correlated trees and then averages them. To determine how an input is related to its predictor variable, RF operated with a series of binary rule-based decisions based on classification and regression trees (Pearse et al. 2017). The samples for training each component tree were selected using bagging, RF regression output is determined by averaging the individual tree output (Jain et al. 2020). The RF algorithm has some parameters that must be configured before training the model; the number of predictors taken into account at each bifurcation of the tree (*mtry*) and the number of random trees assembled during the construction of the model (*ntree*).

5.4.7. Model assessment and validation

Set of observations for each group was separated into training (70%) and testing (30%) sets. In order to determine the goodness of fit, the determination coefficient (R^2) of the linear regression between the observed and predicted values was used during the model development stages (Fassnacht et al. 2014**).** Model performance was assessed by the root-mean-square error (RMSE) and the RMSE normalized by the mean observed values of the dependent variables (nRMSE, %). RMSE indicates the absolute value of the error, whereas nRMSE represents the relative value of the error with respect to the average plot-level. We compare the models through the R^2, RMSE, and nRMSE. According to (Fassnacht et al. 2014)**,** when describing the model performance it is necessary to report at least the RMSE and the correlation between the predictions and observations.

To achieve accurate and reasonable comparisons of different LAI estimates, all LAI values were modeled using the same input variable prediction method. Statistical analyses were carried out separately for ALS metrics with PWF, and for ALS metrics with PWF and vegetation indices together: first for each species individually (Group *E. dunnii* and Group *E. grandis*), then for both species together (Group *Eucalyptus*).

Due to the limited field data available, we used k-fold cross-validation (k-cv) with a 20-fold approach to validate the models. A model was fitted using 19 of the 20 subsets (training dataset) and then it was used to predict the remaining subset (validation dataset). This process was repeated until all subsets had been used once as the validation dataset. For k-fold cross-validation root-mean-squared (RMSEkv), determination coefficient (R^2kv) were calculated. The comparison of the results was expressed in terms of RMSE (m^2 m^{-2}), nRMSE (%), and R^2, plus the coefficients obtained in a process of k-cv RMSEkv (m^2 m^{-2}), R^2kv for each method. Higher R^2 values and lower RMSE and nRMSE values indicate higher model precision and accuracy**.**

The present study employed several data sets and required the development of remote sensing metrics and indices, as well as various data analysis procedures. A flowchart describing these steps and the relationships between each stage is provided in Figure 3.

We performed all analyses using R software (R Core Development Team 2015). The R packages used for SVM were: e1071 and *kernlab*; for ANN: *nnet*; and for RF: *randomForest* and *caret.*

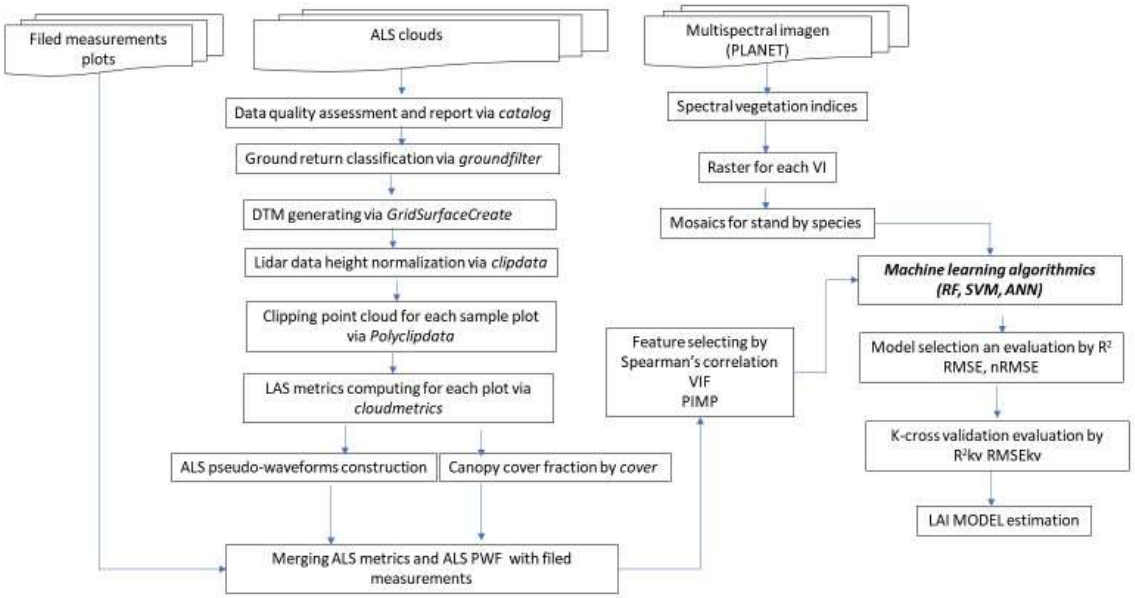

Figure 3. Flowchart describing the methodological steps used to prepare and process data and model variables and to evaluate the results. Where: root Mean Squared Error (RMSE), normalized root mean squared error (nRMSE), determination coefficient (R^2), root-mean-squared error of the k-cross-validation (RMSEkv), determination coefficient of the k-cross-validation (R^2kv), Artificial neuronal networks (ANN), SVM Support vector machine (SVM), Random forest (RF) approaches, Variance Inflation Factor (VIF) and permutation importance (PIMP).

5.5. RESULTS

5.5.1. Prediction of LAI using ALS and PWF data

After performing multicollinearity analysis and Spearman's correlation test, the remaining ALS metrics were used as input in the PIMP function. Variable importance was calculated using the corrected RF model, based on the PIMP scores of the features. In most cases, it was superior in accuracy to the conditional inference trees implemented in previous approaches. To select suitable tuning parameters for RF before it was employed in the PIMP function, the number of predictors trialled in

each split (parameter *mtry*) varied from 3 up to the maximum number of predictor variables. With *mtry* = 5, minimum MSE and stability of importance scores were achieved. Then, we varied the number of trees (*ntree*) to assess the stability of the results. An *ntree* value of 120 produced the lowest out-of-bag-error for the models and RF results. *ALSm* with a higher increase in the permutation variance import was the best variable for LAI estimation.

The four best ranked variables for estimation of the LAI of *E. grandis* were LPI 4, CCF, Elev.P40, and Cv (Figure 4 a); for *E. dunnii*, they were CCF, Elev.P99, Sk, and LPI 7 (Figure 4 b). When considering both species together, the four best ranked variables were CCF, Cv, LPI 4, and the Canopy relief ratio **(**Figure 4 c).

SVR was the model with the highest R^2 (78%) and lowest nRMSE values for estimation of LAI in *E. dunnii,* followed by RF and ANN. For *E. grandis*, SVM achieved the highest median overall accuracy (79%) and smaller RMSE and nRMSE values, followed by RF and ANN. Due to the low precision values of the *Eucalyptus* group (R^2 < 40%), each predictor variable was evaluated individually. The canopy relief ratio was eliminated because it did not improve the results. So, SVR achieved the highest overall accuracy (84%) and smaller RMSE and nRMSE values for LAI estimation in the *Eucalyptus* group, followed by RF and ANN (Table 5). The SVM and RF models explained more than 72% of the variability in LAI and ANN more than 60%.

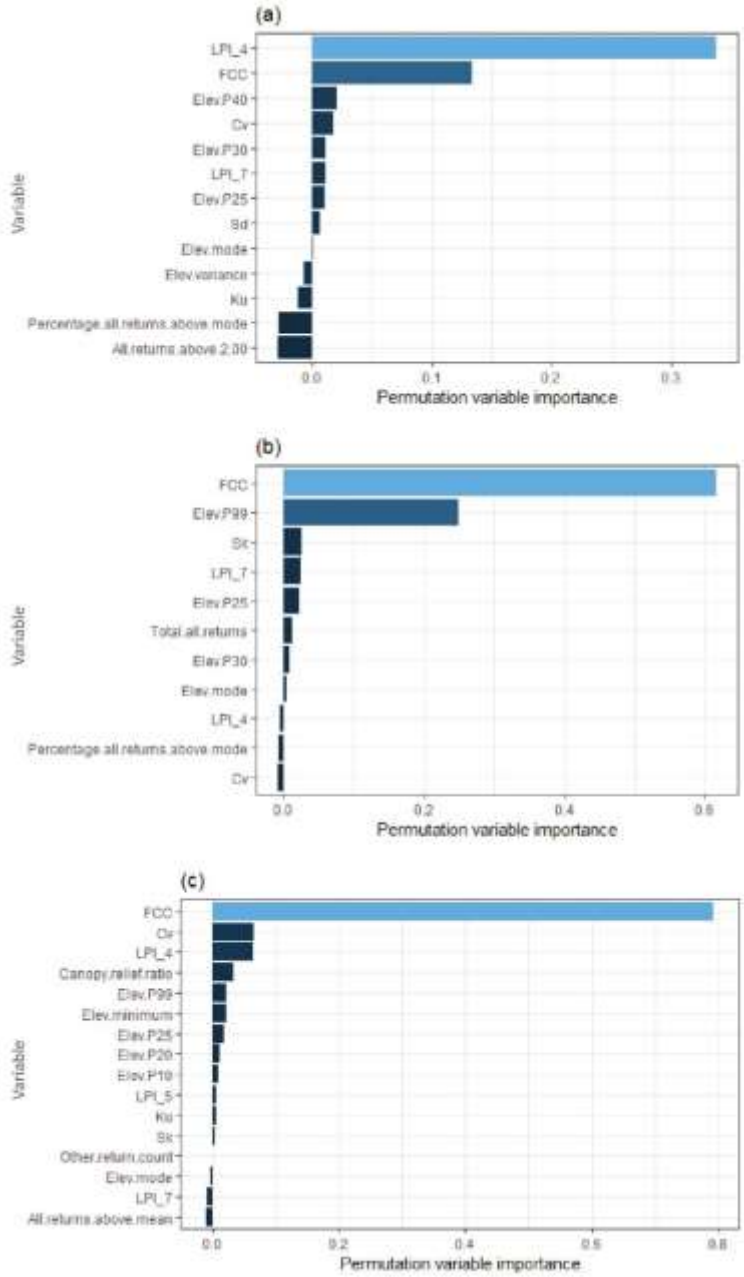

Figure 4. Conditional inference trees-derived importance ranking of the ALSm of: (a) *Eucalyptus grandis* (b) *Eucalyptus dunnii* and (c) both species. Variables (metrics) are arranged in descending order of mean importance.

By changing the training dataset, we were able to evaluate the accuracy for each ML algorithm for a mean of 20 k-fold and for each k-fold. The k-cv values in the same k-executions were recorded for the three methods, to obtain a comparable trend (Figure 5).

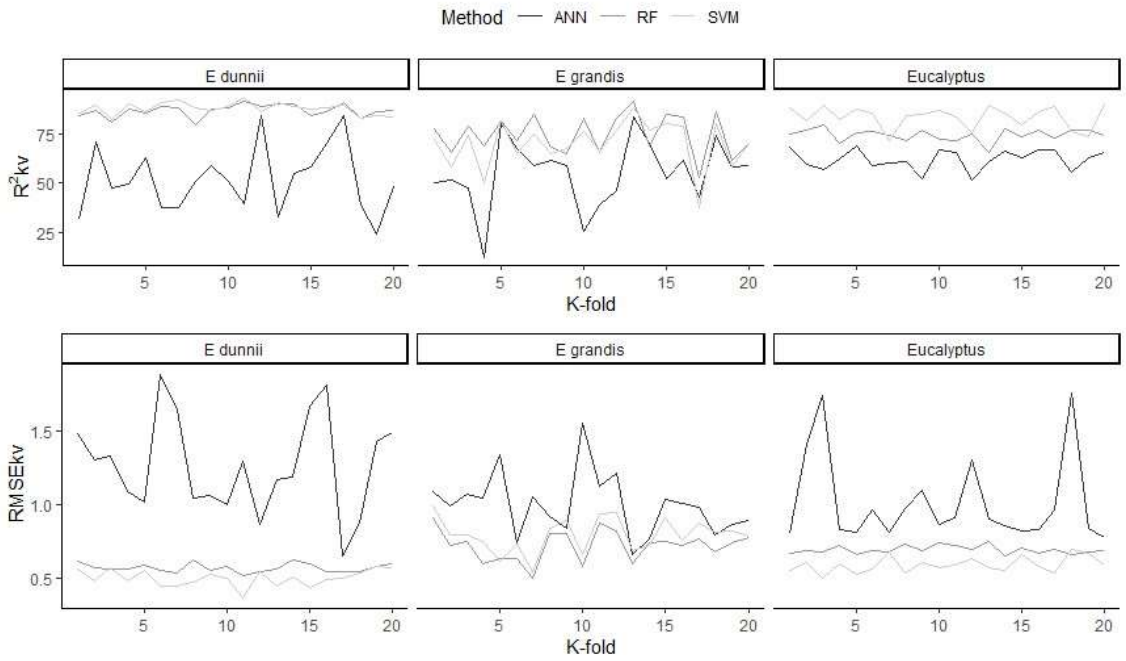

Figure 5. Trend of root-mean-square error (RMSEkv top) and determination coefficient (R^2kv bottom) of k-cross validation for *Eucalyptus dunnii. Eucalyptus grandis, and* both species (*Eucalyptus*). ANN Artificial neuronal networks (black line), SVM Support vector machine (soft grey line), RF Random forest (grey line) approaches.

ANN had the highest variability by species. ANN gave acceptable results (R^2 > 60%) in a few estimations and exhibited higher variation in R^2kv and RMSEcv terms between k-fold. These fluctuations of prediction accuracy and absolute value of error

in ANN were more pronounced than for SVR and RF (these models were more stable). Also, within the stability of the SVM and RF methods, the k-fold variations were more stable in *E. dunnii* than in the other groups.

For a single k-folder, variability of RMSEkv was observed (e.g. *E. dunnii* in k=6 had ANN=1.89, RF= 0.55, and SVR= 0.44; *E. grandis* in k=10 had ANN= 1.55, SVR=0.65, and RF= 0.58; *Eucalyptus* in k= 3 had ANN=1.7, SVR=0.77, and RF=0.67). Also, *E. dunnii* in k=19 had ANN=0.24, SVR=0.84, and RF=0.86; *E. grandis* in k=4 had ANN=0.11, SVR= 0.50, and R= 0.69; and *Eucalyptus* in k=12 had ANN=0.51, SVR=0.65, and RF=0.74.

The standard deviation of the R^2 and the RMSE of validation were calculated to represent the model stability averaged over k-iterations. Values close to 0 indicate higher model stability. The SVR method exhibited the lowest standard deviation of both the RMSE (0.056, 0.140, and 0.055 for *E. dunnii*, *E. grandis*, and *Eucalyptus*, respectively) and the validation coefficient of determination (0.031, 0.105, and 0.055 for *E. dunnii*, *E. grandis*, and *Eucalyptus*, respectively). In all cases, the R^2kv and RMSEkv indicators during validation confirmed the testing results. The SVR methods showed high precision in LAI estimation, in terms of model median overall accuracy and nRMSE, for the three groups, while ANN was the approach with the lowest precision, accuracy, and stability.

5.5.2. Prediction of LAI using combined MRS vegetation indices and ALS metrics

With the models selected in the previous section, the accuracy gain obtained by adding vegetation indices was evaluated. Due to multicollinearity between indices, each vegetation index was evaluated independently as a predictor variable. Table 5 shows the RMSE (m^2 m^{-2}), nRMSE (%), R^2, RMSEkv (m^2 m^{-2}), and R^2kv for the

models and VI. The best models for LAI were chosen based on their highest coefficient of determination (R^2) and lowest RMSE, and were corroborated using k-cross validation.

Table 5. Statistical comparison between previously selected models (with ALS metrics): using different vegetation indexes (VI) to estimate LAI in *Eucalyptus dunnii*, *Eucalyptus grandis* and *Eucalyptus* (sp) in Uruguay by Support vector regression (SVR). Where: root Mean Squared Error (RMSE), normalized root mean squared error (nRMSE), root-mean-squared error of the k-cross-validation (RMSEkv) and determination coefficient of the k-cross-validation (R^2kv). Values in bold show the best performing model per vegetation indices**.**

	Model	VI	RMSE	nRMSE	RMSEkv	R^2kv
E. dunnii	SVR	EVI	0.70	0.23	0.61	0.80
		GI	0.66	0.22	0.64	0.79
		GNDVI	0.56	0.20	0.62	0.83
		NDVI	**0.53**	**0.16**	**0.60**	**0.85**
		SRI	0.69	0.21	0.68	0.73
E. grandis	SVR	EVI	0.50	0.17	0.68	0.79
		GI	0.60	0.20	0.68	0.79
		GNVDI	**0.40**	**0.13**	**0.57**	**0.82**
		NDVI	0.43	0.14	0.59	0.80
		SRI	0.69	0.23	0.64	0.76
Eucalyptus	SVR	EVI	0.75	0.20	0.64	0.83
		GI	0.74	0.20	0.63	0.82
		GNDVI	0.78	0.20	0.61	0.82
		NDVI	**0.50**	**0.16**	**0.50**	**0.88**
		SRI	0.78	0.19	0.61	0.83

The inclusion of *SRI* gave smaller R^2 and R^2kv values in the estimation of LAI than the other VIs, whereas *NDVI* achieved the highest overall accuracy (89% in the fit and 85% in the validation) and smaller RMSE, nRMSE, and RMSEkv values (Figure

6). For *E. grandis*, *GNDVI* was incorporated as a predictor variable, exhibiting lower RMSE, nRMSE and RMSEkv values and higher R^2 and R^2kv values than the other VI. For both species together, the accuracy was higher than 90% when the best VI was incorporated (*NDVI*). The indices with the best performances were the normalized infrared differences, either with red or green. Again, spectrally, *E. grandis* behaved in a slightly different way from *E. dunnii*, although in the joint modeling (*Eucalyptus* group) it had no weight, as happened with LPI 4 and LPI 7.

Regarding the model performance assessed in terms of nRMSE, the model of LAI estimation in *E. grandis* that included *GNDVI* showed the lowest relative value error (0.13%) with respect to the average for all case (Groups and indices). The relative error values were highest for *E. dunnii*. For *E. grandis*, graphical analysis revealed an underestimation behavior for all models (Figure 6).

Overall, the LAI prediction was best for all Groups using ALSm+PWF and VI, and the LAI predictions were acceptable. Nevertheless, SRI performed relatively poorly in LAI estimation and yielded the lowest RMSE, nRMSE, and R^2 values for the *E. dunnii* and *E. grandis* groups**.** According to these results, CCF**,** Elev.P99, Sk, LPI 7, and *NDVI* (for *E. dunnii*), LPI 4, CCF, Elev.P40, Cv, and *GNDVI* (for *E. grandis*), and CCF, Cv, LPI 4, and *NDVI* (for *Eucalyptus*) were the most suitable combination indices for LAI estimation because they showed higher accuracy and precision than the other indices.

Figure 6. Observed versus predicted LAI values from models using different Vegetation indexes (Vindex)I for *Eucalyptus dunnii*, *Eucalyptus grandis* and *Eucalyptus* (sp) by Support vector regression (SVR)

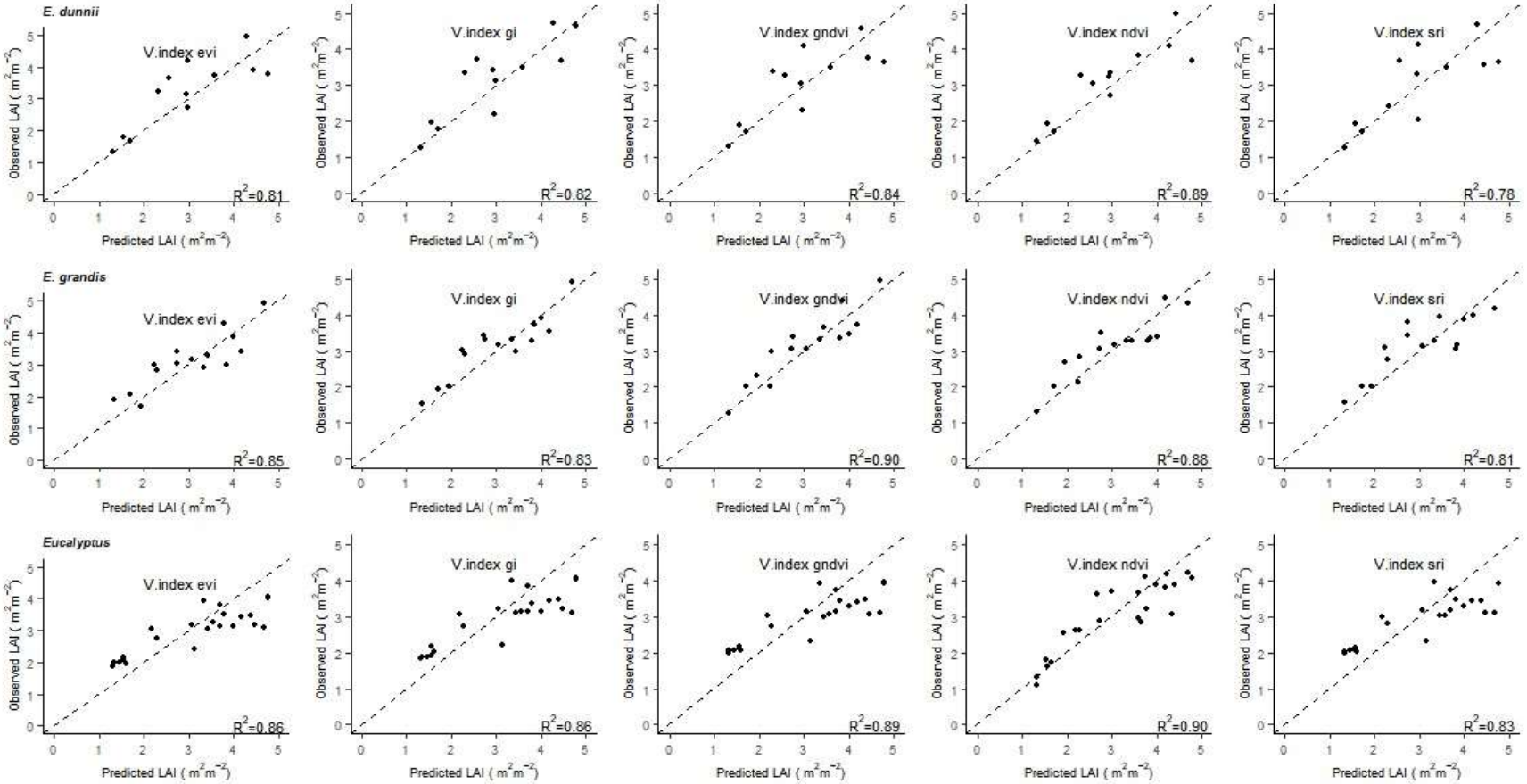

5.6. DISCUSSION

Leaf area index is one of the physiological variables that are key to the understanding of forest dynamics and growth and it has been widely used in forest models. To improve LAI estimation in intensive *Eucalyptus* plantations, we have considered an integrated two-step method, including ALS and high spatial resolution vegetation indices, based on ML algorithms. We have demonstrated the ability of this approach to estimate LAI with high accuracy and stability, which is consistent with previous research (Yuan et al. 2017). The temporal gap between the acquisition of ALS, MRS, and field data increases the uncertainty in LAI estimates (Zhao & Popescu 2009)**.** In our study, the temporal difference was less than 2 months, avoiding uncertainty.

5.6.1. LAI values and ALS variable selection

The *Eucalyptus* LAI values measured in the field varied between 1.17 and 5.07 $m^2\ m^{-2}$, with mean values of 2.95 and 3.26 $m^2\ m^{-2}$ for *E. grandis* and *E. dunnii*, respectively. Our values are within the range reported by Scurlock et al. (2001) in their review, with an LAI value for *Eucalyptus* species of 3.51 $m^2\ m^{-2}$, and by (Whitehead & Beadle 2004), who reported a value of 3.19 $m^2\ m^{-2}$. However, in Uruguay, (Alonso 2011) determined a mean LAI value of 1.82 $m^2\ m^{-2}$ in *Eucalyptus globulus* stands. This difference could be explained by differences in the species (*E. grandis* vs *E. globulus*), age (6-year-old plantations in our study vs over 10 years old for *E. globulus*), and estimation method (ceptometer vs fish-eye photography) involved, among other factors.

When ranking the importance of ALSm and PWF variables in LAI estimation, the LPI and a shape parameter were always ranked at or near the top, showing the importance of the height distribution metric. The CCF metric was the most important *ALSm* in LAI estimation, and it was included in all the LAI models selected. The CCF corresponded to the upper canopy cover, where we expected the greatest density of foliage. The number of *ALSm* selected for each model was a balance between parsimony and relevance, determined by the permutation variable importance. The difference in the branching between the two species meant that LAI

models for *E. dunnii* selected middle height percentiles (Elev.P40) while in *E. grandis* they included high height percentiles (Elev.P99).

The LPI is related to the canopy development; the closer and denser the vegetation, the fewer the laser pulses that penetrate to reach the ground (Peduzzi et al. 2012). Thus, LPI has been used to predict LAI and models including this variable were able to explain 80% or more of LAI variation (Peduzzi et al. 2012). The penetration metric selected for *E. grandis* and *Eucalyptus* was a metric of return heights (LPI 4), while for *E. dunnii* the most important penetration metric focused on intensity (LPI 7). This may be related to the characteristics of the two species; the spectral response of the leaves in *E. dunnii* was more sensitive to infrared radiation, related to a healthier status of the plantations. *Canopy relief ratio* was deleted for the *Eucalyptus* group, likely because the biological information provided by this variable was already included through the CCF.

5.6.2. LAI models

In our study, an SVM approach was chosen to predict the LAI in *E. dunnii, E. grandis*, and *Eucalyptus*. Its ability to handle non-linearity and to quantify the importance of independent variables makes SVR an effective algorithm. SVR has been implemented in a wide range of analyses with ALS and MRS in agricultural and forest investigations (Mountrakis et al. 2011). However, in our study ANN showed poor LAI prediction, which contrasts with other studies where ANN proved more efficient than RF and SVR in predicting forest structural parameters (increment in diameter, height, dbh) (Júnior et al. 2020).

The best models, with the highest R^2 (>0.78) and the lowest nRMSE (0.137 m^2 m^{-2}), included four (*E. grandis* and *E. dunnii*) or three (*Eucalyptus*) *ALSm*. These results are consistent with previous studies. Assessing *E. grandis*, (Tesfamichael et al. 2018) achieved R^2 =0.67 with two LiDAR metrics (height and standard deviation of points below the 10th height) and obtained R^2=0.83 when employing 14 metrics (with collinearity problems). Peduzzi et al. (2012) obtained models with R^2 values between 0.61 (two model inputs) and 0.83 (six model inputs). Jensen et al. (2008) reported estimated LAI R^2 values of 0.86 (RMSE = 0.76) and 0.69 (RMSE = 0.61).

Morsdorf et al. (2006) estimated returned R^2 values of 0.69 (RMSE = 0.01), but it should be noted that the LAI values in their study were within a narrower range (0–2) than ours.

We expected that ALS height metrics would be present in all the LAI models, because increases in canopy height should occur in tandem with increases in LAI, and this was observed for *E. dunnii* (Elev.99) and *E. grandis* (Elev.P40). In this study, LAI was sensitive to the inclusion of LPI, and LPI 7 and LPI 4 related the vegetation returns with the total returns and the intensity of the returns with the intensity of the ground returns. Sumnall et al. (2016a) reported an R^2 value of 0.89 when employing LPI1 in LAI estimation. We computed the vegetation return and intensity above a threshold of 1.3 m, at the same height as the LAI data (ceptometer measurements, dbh height). By implementing this minimum height threshold for the within-plot ALS, the returns and the corresponding metrics were limited to the vertical space in which the greatest amount of foliage was distributed. In addition, the link between field LAI measurement height and the threshold of what is defined as 'ground' and 'canopy' within LiDAR returns, as suggested in (Sumnall et al. 2016b), implies that estimation of the vertical distribution of LAI vertically through the canopy is possible.

5.6.3. Prediction of LAI using combined ALS and MRS variables

The integration of Planet-derived VIs markedly improved the LAI estimation with respect to the results obtained by ALSm+PWF. The integration of ALSm, PWF metrics, and VIs involved four different approaches. The use of high spatial resolution, multispectral VIs can provide continuous and detailed spectral signatures of forest biophysical attributes (Shen et al. 2018). The ANN, RF, and SVR models contained a stochastic element that resulted in a different LAI model each time they were applied to the same training data. With the addition of VIs, the improvement in the accuracy of the predictive models was significant. In general, the NIR-based VIs (i.e., *NDVI* and *GNDVI*) performed better in terms of LAI assessment than the other indices evaluated, and *NDVI* for *E. dunnii*, *GNDVI* for *E. grandis*, and *NDVI* for *Eucalyptus* were the best-fitted parameters, the improvement in nRMSE being 16%,

51%, and 39%, respectively. The gain in explained variance (R^2) was 14 % (*E. dunnii* and *E. grandis*) and 7 % (*Eucalyptus*) when using these VIs. The R^2kv and RMSEkv obtained from 20-fold cross-validation also agreed well. For a *Eucalyptus* clone (*grandis* x *urophylla*) in Brazil, R^2 values between 0.68 and 0.77 were reported when LAI was estimated with *NDVI* models, using Landsat ((De Almeida et al. 2015) and RapidEye sensors (Alvares et al. 2015).

The plots of the observed against the estimated values for the VIs (Figure 6) demonstrate that the *NDVI* showed less data dispersion with respect to the (1:1) trend line and gave lesser trends of overestimation or underestimation of LAI for the *Eucalyptus* group. *NDVI* is the most widely used vegetation index, and it is based on the red and near-infrared wavelength bands (Xue & Su 2017). On the other hand, *GNDVI* uses the green band instead of the red and can be more sensitive to chlorophyll; thus, it may be more accurate than NDVI over areas with dense vegetation cover (Gitelson & Merzlyak 1998). In Rio Grande do Sul, (De Godoy Goergen et al. 2016), using Landsat 5, found that *GNDVI*, *NDVI*, and *SRI* were correlated with the age of *E. dunnii* trees and that *GNDVI* could be used to differentiate *E. dunnii* from *E. urograndis.*

Our results demonstrate that the combination of the ALSm and PWF datasets with VIs was suitable for the estimation of LAI. Together, these variables yielded the highest prediction accuracies in the k-cross-validation, with R^2kv> 0.85 and RMSEkv <0.6 (m^2 m^{-2}). The standard deviation of RMSEcv was small for SVR, ranging from 0.05 m^2 m^{-2} (*Eucalyptus*) to 1.23 m^2 m^{-2} (*E. dunnii*). The ANN models produced substantially higher R^2kv and RMSEkv standard deviations than SVR and RF. When both species were treated as a single group (*Eucalyptus*), an increase in the accuracy (R^2kv=0.88), precision (RMSEkv=0.5 m^2 m^{-2}), and stability (standard deviations of R^2kv <0.05) was observed.

Previous studies demonstrated that the integration of these two complementary datasets can improve the prediction of forest structural parameters (Shen et al. 2018). Although multispectral data have limitations regarding the quantification of the vertical structure of forests, multispectral metrics such as VIs have the capability to improve the accuracy of the prediction of forest structural parameters. This indicates

that multispectral metrics have great potential in the prediction of forest structural parameters.

There are some potential limitations in our study. First, the temporal gap in the acquisition of the ALS, MRS, and field data may increase the uncertainty in the LAI estimates (Zhao & Popescu 2009). However, in our study, the temporal difference was less than 2 months, thus minimizing the uncertainty. Second, there was no spatial mismatch between the field measurements (plots of 314 m^2) and the CubeSat pixels (3 m resolution). This may have resulted in a homogeneous pixel covering one stand with homogeneous growth conditions. Differences among stands would have been included in the different pixels. The pixel effect can cause LAI underestimation at coarse spatial resolution because of area aggregation that produces averaged values.

5.7. CONCLUSIONS

In this study, we applied a modeling approach to estimate LAI in *Eucalyptus* plantations, integrating several remote sensing data sources. The SVM and RF models were more accurate than the ANN model. The SVM model, using ALS metrics, PWF shape parameters, and Vis from MRS, performed well for *Eucalyptus grandis*, *Eucalyptus dunnii*, and both species together. The most informative ALS metrics for LAI estimation were related to the upper and middle tree height percentiles and the canopy cover fraction. The most important pseudo-waveforms parameters shapes were the coefficient of variation (Cv, for *E. grandis* and *Eucalyptus*) and skewness (Sk, for *E. dunnii).* The NDVI and GNDVI from the Planet data were proven to be highly appropriate for the assessment and prediction of LAI in *Eucalyptus* plantations. The selected models, incorporating *ALSm*, PWF, and multispectral data, have great potential for LAI values. This study provides an important foundation for LAI estimation in intensive *Eucalyptus* plantations, which is crucial for forest management and research**.**

5.8. REFERENCES

Alonso J (2011). Modelación de procesos hidrológicos asociados a la forestación con Eucalyptus en el Uruguay. Facultad de Ingeniería, Universidad de la República.

Altmann A, Toloşi L, Sander O, Lengauer T (2010). Permutation importance: A corrected feature importance measure. Bioinformatics. 26: 1340–1347. - doi: 10.1093/bioinformatics/btq134

Alvares CA, Mattos EM de, Campoe OC, Marrichi AHC, Stape JL (2015). Uso de sensoriamento remoto na estimativa do índice de área foliar em Eucalyptus. XVII Simpósio Brasileiro de Sensoriamento Remoto. 6429–6436.

Ariza Salamanca, Navarro-Cerrillo, Bonet-García, Palazón, Polo (2019). Integration of a Landsat Time-Series of NBR and Hydrological Modeling to Assess Pinus Pinaster Aiton. Forest Defoliation in South-Eastern Spain. Remote Sensing. 11: 2291. - doi: 10.3390/rs11192291

Bentancor, L. (2017). Extracción de Nutrientes por *Eucalyptus dunnii* Maiden de 4 años con Destino a la Producción de Biomasa para Energía y Celulosa.Doctoral dissertation, Master's Thesis, Universidad de la República, Montevideo, Uruguay.

Castaño JP, Giménez A, Ceroni M, Furest J, Aunchayna R, Bidegain M (2011). Caracterización agroclimática del Uruguay 1980-2009. Montevideo. Serie Técnica INIA. 193: 33.

De Almeida AQ, Ribeiro A, Delgado RC, Rody YP, De Oliveira AS, Leite FP (2015). Índice de área foliar de eucalyptus estimado por índices de vegetação utilizando imagens TM - landsat 5. Floresta e Ambiente. 22: 368–376. - doi: 10.1590/2179-8087.103414

De Godoy Goergen LC, De Vargas Kilca R, Da Silva Narvaes I, Silva MN, Silva EA, Pereira RS, Adami M (2016). Distinção de espécies de eucaliptus de diferentes idades por meio de imagens TM/Landsat 5. Pesquisa Agropecuaria Brasileira. 51: 53–60. - doi: 10.1590/S0100-204X2016000100007

Fassnacht FE, Hartig F, Latifi H, Berger C, Hernández J, Corvalán P, Koch B (2014). Importance of sample size, data type and prediction method for remote sensing-based estimations of aboveground forest biomass. Remote Sensing of Environment. 154: 102–114. - doi: 10.1016/j.rse.2014.07.028

Gitelson AA, Merzlyak MN (1998). Remote sensing of chlorophyll concentration in higher plant leaves. Advances in Space Research. 22: 689–692. - doi: 10.1016/S0273-1177(97)01133-2

Gleason CJ, Im J (2012). Forest biomass estimation from airborne LiDAR data using machine learning approaches. Remote Sensing of Environment. 125: 80–91. - doi: 10.1016/j.rse.2012.07.006

González-Jaramillo V, Fries A, Zeilinger J, Homeier J, Paladines-Benitez J, Bendix J. (2018). Estimation of above ground biomass in a tropical mountain forest in southern Ecuador using airborne LiDAR data. Remote Sensing 10(5) 660, doi:10.3390/rs10050660.

Hopkinson C, Chasmer L (2009). Testing LiDAR models of fractional cover across multiple forest ecozones. Remote Sensing of Environment. 113: 275–288. - doi: 10.1016/j.rse.2008.09.012

Huete A, Van leeuwen W (1999). Modis Vegetation Index Algorithm Theoretical Basis. Environmental Sciences. 129.

Ingram JC, Dawson TP, Whittaker RJ (2005). Mapping tropical forest structure in southeastern Madagascar using remote sensing and artificial neural networks.

Remote Sensing of Environment. 94: 491–507. - doi: 10.1016/j.rse.2004.12.001

Jain P, Coogan SCP, Subramanian SG, Crowley M, Taylor S, Flannigan MD (2020). A review of machine learning applications in wildfire science and management. Environmental Reviews, 28(4), 478-505.

Jensen JLR, Humes KS, Vierling LA, Hudak AT (2008). Discrete return lidar-based prediction of leaf area index in two conifer forests. Remote Sensing of Environment. 112: 3947–3957. - doi: 10.1016/j.rse.2008.07.001

Jonckheere I, Fleck S, Nackaerts K, Muys B, Coppin P, Weiss M, Baret F (2004). Review of methods for in situ leaf area index determination Part I. Theories, sensors and hemispherical photography. Agricultural and Forest Meteorology. 121: 19–35. - doi: 10.1016/j.agrformet.2003.08.027

Jordan CF (1969). Derivation of leaf-area index from quality of light on the forest floor. Ecology. 50: 663–666.

Júnior IST, Torres CMME, Leite H G, de Castro NLM, Soares CPB, Castro RVO, Farias AA. (2020). Machine learning: Modeling increment in diameter of individual trees on Atlantic Forest fragments. Ecological Indicators, 117, 106685.

Lary DJ, Alavi AH, Gandomi AH, Walker AL (2016). Machine learning in geosciences and remote sensing. Geoscience Frontiers. 7: 3–10. - doi: 10.1016/j.gsf.2015.07.003

le Maire G, Marsden C, Nouvellon Y, Stape JL, Ponzoni FJ (2012). Calibration of a species-specific spectral vegetation index for leaf area index (LAI) monitoring: Example with MODIS reflectance time-series on eucalyptus Plantations. Remote Sensing. 4: 3766–3780. - doi: 10.3390/rs4123766

Luo S, Wang C, Xi X, Nie S, Fan X, Chen H, Yang X, Peng D, Lin Y, Zhou G (2019). Combining hyperspectral imagery and LiDAR pseudo-waveform for predicting crop LAI, canopy height and above-ground biomass. Ecological Indicators. 102: 801–812. - doi: 10.1016/j.ecolind.2019.03.011

Mesas-Carrascosa FJ, Castillejo-González IL, De la Orden MS, Porras AGF (2012). Combining LiDAR intensity with aerial camera data to discriminate agricultural land uses. Computers and Electronics in Agriculture. 84: 36–46. - doi: 10.1016/j.compag.2012.02.020

Morsdorf F, Kötz B, Meier E, Itten KI, Allgöwer B (2006). Estimation of LAI and fractional cover from small footprint airborne laser scanning data based on gap fraction. Remote Sensing of Environment. 104: 50–61. - doi: 10.1016/j.rse.2006.04.019

Mountrakis G, Im J, Ogole C (2011). Support vector machines in remote sensing: A review. ISPRS Journal of Photogrammetry and Remote Sensing. 66: 247–259. - doi: 10.1016/j.isprsjprs.2010.11.001

Pavithra B, Kalaivani K, Ulagapriya K (1998). Remote sensing techniques for mangrove mapping. International Journal of Engineering and Advanced Technology. 8: 27–30.

Pearse GD, Morgenroth J, Watt MS, Dash JP (2017). Optimising prediction of forest leaf area index from discrete airborne lidar. Remote Sensing of Environment. 200: 220–239. - doi: 10.1016/j.rse.2017.08.002

Peduzzi A, Wynne RH, Fox TR, Nelson RF, Thomas VA (2012). Estimating leaf area index in intensively managed pine plantations using airborne laser scanner data. Forest Ecology and Management. 270: 54–65. - doi: 10.1016/j.foreco.2011.12.048

Planet Labs (2018). Precision Ag Insights From Frequent Imaging Smarter Farming Throughout the Season. available https://www.planet.com/markets/monitoring-for-precision-agriculture/

R Core Team (2015). R: A Language and Environment for Statistical Computing, 3.2.1 ed. R Foundation for Statistical Computing, Vienna, Austria.

Rouse Jr JW, Haas RH, Schell JA, Deering DW (1973). Monitoring the vernal advancement and retrogradation (green wave effect) of natural vegetation. NASA/GSFC Type III Final Report, Greenbelt, Md, 371.

Scurlock JMO, Asner GP, Gower ST (2001). Worldwide Historical Estimates of Leaf Area Index., Vol. 27, pp. 34. - doi: 0RNL/TM-2001/268

Shen X, Cao L, Chen D, Sun Y, Wang G, Ruan H (2018). Prediction of forest structural parameters using airborne full-waveform LiDAR and hyperspectral data in subtropical forests. Remote Sensing. 10. - doi: 10.3390/rs10111729

Solberg S, Næsset E, Hanssen KH, Christiansen E (2006). Mapping defoliation during a severe insect attack on Scots pine using airborne laser scanning. Remote Sensing of Environment. 102: 364–376. - doi: 10.1016/j.rse.2006.03.001

Staben G, Lucieer A, Scarth P (2018). Modelling LiDAR derived tree canopy height from Landsat TM, ETM+ and OLI satellite imagery—A machine learning approach. International Journal of Applied Earth Observation and Geoinformation. 73: 666–681. - doi: 10.1016/j.jag.2018.08.013

Sumnall M, Peduzzi A, Fox TR, Wynne RH, Thomas VA, Cook B (2016a). Assessing the transferability of statistical predictive models for leaf area index between two airborne discrete return LiDAR sensor designs within multiple intensely managed Loblolly pine forest locations in the south-eastern USA. Remote Sensing of Environment. 176: 308–319. - doi: 10.1016/j.rse.2016.02.012

Sumnall MJ, Fox TR, Wynne RH, Blinn C, Thomas VA (2016b). Estimating leaf area index at multiple heights within the understorey component of Loblolly pine forests from airborne discrete-return lidar. International Journal of Remote Sensing. 37: 78–99. - doi: 10.1080/01431161.2015.1117683

Tesfamichael SG, van Aardt J, Roberts W, Ahmed F (2018). Retrieval of narrow-range LAI of at multiple lidar point densities: Application on *Eucalyptus grandis* plantation. International Journal of Applied Earth Observation and Geoinformation. 70: 93–104. - doi: 10.1016/j.jag.2018.04.014

Tseng YH, Lin LP, Wang CK (2016). Mapping CHM and LAI for heterogeneous forests using airborne full-waveform LiDAR data. Terrestrial, Atmospheric and Oceanic Sciences. 27: 537–548. - doi: 10.3319/TAO.2016.01.29.04(ISRS)

Watson DJ (1947). Comparative physiological studies on the growth of field crops: I. Variation in net assimilation rate and leaf area between species and varieties, and within and between years. Annals of Botany. 11: 41–76. - doi: 10.1093/oxfordjournals.aob.a083148

Weiss M, Baret F, Smith GJ, Jonckheere I, Coppin P (2004). Review of methods for in situ leaf area index (LAI) determination Part II. Estimation of LAI, errors and sampling. Agricultural and Forest Meteorology. 121: 37–53. - doi: 10.1016/j.agrformet.2003.08.001

Whitehead D, Beadle CL (2004). Physiological regulation of productivity and water use in Eucalyptus: A review. Forest Ecology and Management. 193: 113–140. - doi: 10.1016/j.foreco.2004.01.026

Xue J, Su B (2017). Significant remote sensing vegetation indices: A review of developments and applications. Journal of Sensors. 2017. - doi: 10.1155/2017/1353691

Yan G, Hu R, Luo J, Weiss M, Jiang H, Mu X, Xie D, Zhang W (2019). Review of indirect optical measurements of leaf area index: Recent advances, challenges, and perspectives. Agricultural and Forest Meteorology. 265: 390–411. - doi: 10.1016/j.agrformet.2018.11.033

Yuan H, Yang G, Li C, Wang Y, Liu J, Yu H, Feng H, Xu B, Zhao X, Yang X (2017). Retrieving soybean leaf area index from unmanned aerial vehicle hyperspectral remote sensing: Analysis of RF, ANN, and SVM regression models. Remote Sensing. 9. - doi: 10.3390/rs9040309

Zaletnyik P, Laky S, Toth C (2010). LIDAR waveform classification using self-organizing map. American Society for Photogrammetry and Remote Sensing Annual Conference 2010: Opportunities for Emerging Geospatial Technologies. 2: 1055–1066.

Zhao K, Popescu S (2009). Lidar-based mapping of leaf area index and its use for validating GLOBCARBON satellite LAI product in a temperate forest of the southern USA. Remote Sensing of Environment. 113: 1628–1645. - doi: 10.1016/J.RSE.2009.03.006

Zhou H, Wang C, Zhang G, Xue H, Wang J, Wan H (2020). Generating a Spatio-Temporal Complete 30 m Leaf Area Index from Field and Remote Sensing Data. Remote Sensing. 12: 2394. - doi: 10.3390/rs12152394

Zhou Y, Qiu F (2015). Fusion of high spatial resolution WorldView-2 imagery and LiDAR pseudo-waveform for object-based image analysis. ISPRS Journal of Photogrammetry and Remote Sensing. 101: 221–232. - doi: 10.1016/j.isprsjprs.2014.12.013

6. USE OF OPTIMIZATION MODELLING TO ASSESS THE EFFECT OF TIMBER AND CARBON PRICING ON HARVEST SCHEDULING, CARBON SEQUESTRATION, AND NET PRESENT VALUE OF *EUCALYPTUS* PLANTATIONS

Andres Hirigoyen, Mauricio Acuna, Cecilia Rachid-Casnati, Jorge Franco, Rafael Mª Navarro-Cerrillo

6.1. RESUMEN

Cuantificar el impacto del carbono (C) y los precios de la madera en la programación de la cosecha y la edad de rotación óptima es esencial para definir estrategias para el manejo sostenible de las plantaciones de rotación corta para que puedan proporcionar productos de madera y contribuir al secuestro de C. En este artículo, presentamos un modelo de programación de enteros mixtos que optimiza la edad de rotación y el cronograma de cosecha de los rodales y maximiza el Valor Actual Neto (VAN) durante un período de planificación de hasta 15 años. El modelo incluyó ingresos por la venta de madera (pulplogs) y créditos del C secuestrado durante la vida de los rodales. Además, se incluyeron en el análisis los costos de establecimiento, manejo, cosecha y transporte de la plantación. El área de estudio comprendió 88 rodales de *Eucalyptus grandis* y Eucalytus dunni ubicados en Uruguay, totalizando un área de bosque de casi 1.882 ha. El estudio investigó el impacto del C y los precios de la madera en el VAN, las edades de rotación óptimas y los programas de aprovechamiento, los flujos de madera a los clientes y el C secuestrado por período. El VAN máximo entre todos los escenarios evaluados (7,53 M $) se calculó para un precio C de 30 $ t^{-1}, una tasa de interés del 6% y un precio de la madera de 75 $ m^{-3}. Esto fue 2,14 M $ más alto que el escenario con los mismos parámetros pero que incluía solo los ingresos por madera. Los precios de C también afectaron la edad de rotación óptima de los rodales, el secuestro de C y el flujo de madera entregada a los clientes finales. En promedio, en escenarios que incluían precios de C, el flujo de

madera y el secuestro de C aumentaron en un 15,4% y 12,1%, respectivamente, cuando el precio de C pasó de 5 $ t^{-1} a 30 $ t^{-1}. Estos resultados demuestran que la programación de la cosecha, la edad de rotación óptima de los rodales y el VPN son muy sensibles a los créditos de carbono y los precios de la madera, y que los mejores beneficios económicos se obtienen cuando los rodales se manejan para maximizar la producción de madera y el secuestro de C.

6.2. ABSTRACT

Quantifying the impact of carbon (C) and timber prices on harvest scheduling and economic returns is essential to define strategies for the sustainable management of short-rotation plantations so that they can provide timber products and contribute to C sequestration. In this paper, we present a mixed-integer linear programming model that optimizes harvest scheduling at the forest level, C sequestration, and Net Present Value (NPV) over a planning period of up to 15 years. The model included revenue from the sale of timber (pulplogs) and credits from the net C sequestered during the life of the stands. In addition, plantation establishment, management, harvesting, and transportation costs were included in the analysis. The study area comprised 88 *Eucalyptus grandis* W. Hill and *Eucalyptus dunnii* Maiden stands located in Uruguay, totaling a forest area of nearly 1,882 ha. The study investigated the impact of C and timber prices on NPV, harvest schedules, stands' harvest age, timber flows to customers, and C sequestered per period. The maximum NPV among all the scenarios evaluated (USD 7.53 M) was calculated for a C price of 30 USD t^{-1}, an interest rate of 6%, and a timber price of 75 USD m^{-3}. This was USD 2.14 M higher than the scenario with the same parameters but that included only revenue from timber. C prices also impacted stands' harvest age, C sequestration, and timber flows delivered to end customers. On average, in scenarios that included C prices, timber flows and C sequestration increased by 15.4 and 12.1%, respectively, when C price increased from 5 to 30 USD t^{-1}. These results demonstrate that harvest scheduling, harvest age, and NPV are very sensitive to C and timber, and that the best economic returns are obtained when the stands are managed to maximize timber production and C sequestration.

Keywords: timber harvest scheduling; mixed-integer programming; rotation age; carbon sequestration.

6.3. INTRODUCTION

Forest ecosystems constitute the largest terrestrial carbon (C) pool in the global carbon cycle and represent one of the most significant sources to mitigate climate change effects [1]. The concentration of atmospheric carbon dioxide (CO_2) has significant effects on tree growth and carbon accumulation in forest ecosystems [2]. Whether forest ecosystems sequestrate more carbon into ecosystems (carbon sinks) or release more carbon from ecosystems (carbon sources) depends on the net ecosystem carbon exchange. Forests have a significant impact on the concentration of CO_2 in the atmosphere. As terrestrial ecosystems, forests act as C sinks, positively affecting the atmospheric CO_2 balance [2]. Carbon storage in forest ecosystems includes numerous components but particularly biomass and soil [3]. Forest ecosystems cover about 4.1 billion hectares globally, with forest vegetation and soils containing about 1.240 Pg of C [4]. This accounts for 80% of aboveground terrestrial C and 70% of all organic soil [5,6], presenting a positive net C balance [3]. The ability of forest products to store C is temporary and depends on their service life. The shelf life of products can range from weeks for biofuels to centuries for structural wood. These account for about 5% (140 M ha) of the global forest area and help mitigate the effects of climate change by sequestering C [7].

Significant C stocks are also stored in forest plantations. Optimizing harvest schedules in short-rotation plantations can increase C sequestration, which can result in increased economic returns and better adaptation of trees to climate change. Thus, C pricing can play an essential role in generating an additional revenue source and promoting adaptive silviculture [8]. C pricing in planning models may modify harvesting activities over vast geographical areas and within a very long planning horizon [9]. Harvest levels vary in response to C pricing, resulting in higher carbon sequestration than those obtained from harvest levels obtained with classic planning models that do not include C stocks as a revenue source. Considering forest C in planning models leads to increased optimal rotations and makes harvest planning

more challenging, which calls for quantitative solutions to optimize harvesting decisions [9].

Forest management involves complex decision-making with short- and long-term consequences. Forest planning at the strategical, tactical, and operational levels involves ecological, productive, and economic systems and their interaction [10,11]. This hierarchical planning approach seeks to increase the efficiency of the use, conservation, and protection of the forest resource, and ensure the sustainable and continuous supply of forest products and benefits, maintaining the economic and environmental potential of forests and their ecological functions [2]. Planning problems related to yield and distribution of timber from plantations to mills are complex to solve and are impacted by factors such as species, stand location, characteristics of the forest coupes and distances to mills, age structure, growth and yields curves, environmental conditions, and road network, among others [12,13]. This planning strategy is primarily concerned with medium-term decisions (typically 3 to 7 years in short-rotation plantations) at the tactical level (TL). Optimal resource allocation and volume of wood to harvest and deliver per period to end customers are usually determined using optimization-based commercial management systems [14]. In addition, spatial considerations such as maximum opening areas (the maximum area to be intervened during harvesting, e.g., in a clear-felling operation) and green-up constraints are also included in tactical planning models, aiming at generating feasible and sustainable solutions that cause minimum impacts on the environment [15].

Commercial forest plantations in Uruguay comprise over one million hectares; in 2018, 74,834 hectares of new Eucalyptus plantations were established, which accounted for 99% of the total planted area in that year [16]. Behind beef production, roundwood destined to kraft pulp production is the second-largest export product of Uruguay [17]. In 2018, it totaled a gross value of 2.2 billion USD, out of which forest cellulose pulp exports amounted to 1.7 billion USD [16]. In the last decade, timber production has increased substantially in Uruguay, with projections indicating that these levels will continue growing in the next decades. Dieste (2012) [18] estimated a high demand for pulpwood in the next 15 years, with an average

production of about 10 million m3 per year. In Uruguay, commercial plantations include primarily *Eucalyptus globulus* Labill, *Eucalyptus dunnii* Maiden, and *Eucalyptus grandis* W. Hill ex Maiden, with effective planted areas of 149,329, 191,035, and 235,620 ha, respectively [16]. These species have different mean annual increments (MAI), which is a consequence of the favorable site conditions and silvicultural management schemes applied to these plantations. In a previous study, Resquin et al. (2005) [19] recorded MAIs for *E. grandis* ranging between 32.8 to 55.8 m3 ha-y^{-1}, while for E. globulus and *E. dunnii*, MAI reached 18.2 and 19.6 m3 ha-y^{-1}, respectively. The roundwood harvested in *E. grandis* and *E. dunnii* stands is delivered to either pulp mills or sawmills (high-value logs), while the roundwood harvested in E. globulus stands supplies pulp mills only; in the latter case, average rotations in intensive silviculture stands occur at the age of eight years. Additionally, land price has been increasingly growing in Uruguay in the last decades, which has led forest growers to explore strategies to increase forest productivity and efficiency along the value chain (including harvesting and transport operations), and in this way, improve the competitiveness of the forest sector [20]. As part of the tactical plan and based on forest inventory data, forest companies usually prescribe short forest rotations, no longer than eight years, as a way to maximize yield per ha [12]. Traditionally, methods to determine optimal rotation or harvest ages have not been frequently employed in Eucalyptus plantations that are managed to produce roundwood for the pulp industry under operational-constrained scenarios [21]. However, this has been changing ultimately. Most forest growers are now considering determining optimal rotations for their stands to maximize economic returns and meet the growing demand for wood in the coming years.

The forest planning problem at the stand and forest level, based on both timber production and C sequestration, has been addressed previously by several authors [21–23]. C pricing can result in changes to the optimal stand rotation or harvest age, and consequently, to C stocks. This is because forest stands with longer rotation or harvest ages build up a larger volume of biomass and soil organic C than forests managed on shorter harvest cycles [24]. In Eucalyptus plantations in Australia, Enzinger and Jeffs (2000) [25] showed that the addition of C payments resulted in

longer optimal rotation ages than scenarios where stands were managed for timber production only. As indicated by Asante et al. (2011) [24], the maximization of NPV for a single harvest cycle is a standard criterion for determining the optimal stand rotation and harvest age. NPV is maximized when the capital value of standing timber (the percentage by which the value of the forest is growing) is equal to the interest rate (IR), assuming flows of revenues and costs in just one harvest cycle and not accounting for these flows in subsequent cycles [26]. From an economic point of view, the optimal rotation age (optimization at the stand level) and harvest age (optimization at the forest level) of single stands at the tactical level is the one that maximizes NPV for a flow of revenues and costs throughout the planning period, subject to supply and operational constraints. This is opposed to the biological optimal rotation that is obtained when MAI is maximized, which excludes the flow of revenues and costs involved in growing the forest stands [27].

We hypothesize that C and timber prices have an impact on harvest scheduling, C sequestration, and economic returns (NPV) in industrial Eucalyptus plantations located in Uruguay. The objectives of the study were as follows: i) formulate a mathematical model able to optimize the harvest of stands in Eucalyptus plantations, including timber (pulplogs) and C stocks as a source of revenue, ii) assess the impact of C and timber prices on harvest age at the forest level and NPV, and iii) assess the impact of C and timber prices on spatial solutions and flow of timber from stands to pulp mills. We expect that the results from this study will help forest growers in Uruguay get a better understanding of the impact of C and timber prices on harvest scheduling, orienting the management of Eucalyptus plantations in the context of a growing global demand for timber and C sequestration.

6.4. MATERIALS AND METHODS

6.4.1. Study location and characteristics

The study area comprised about 1882 ha of *Eucalyptus grandis* and *Eucalyptus dunnii* plantations owned by Forestal Oriental SA in Uruguay. Figure 1 shows the five sites included in the study: sites b1 and b2 with 861 ha (43° 13′ 97” S–64° 24′ 78” W, hereafter Guichon); sites b3 and b4 with 870 ha (63° 07′ 44” S–52° 22′

64”W, hereafter Trinidad), and site b5 with 717 ha (63° 44′ 33.05” S–63° 95′58”W, hereafter Sarandí del Yi). Climate is subtropical, with a mean annual temperature of 18 °C (12 °C in the coldest month, 24 °C in the warmest month) and a mean annual rainfall between 1300 and 1400 mm [28]. According to the National Commission for Agroeconomic Studies of the Land classification (CONEAT), the predominant soil in Guichon is planosols with a horizon A of 40–50 cm depth, characterized by low fertility, weak structure, low level of organic matter, slopes of 1–3%, sandy texture, medium to low risk of drought, imperfect drainage, moderately-slow to slow permeability, and good rooting ability. Soils in Trinidad are vertisols with a horizon A of 50–60 cm, and characterized by medium fertility, weak structure, medium level of organic matter, slopes of 2–5%, loam franc structure, low risk of drought, moderate drainage, moderately permeability, and good rooting ability. Soils in Sarandí del Yi correspond to vertisols, rupticos, and brunosols, with a horizon A of 50–60 cm depth and characterized by sandy-loam, loam franc texture, low fertility, low risk of erosion, moderate slopes (1–3%), weak structure, low organic matter, imperfect drainage, and good rooting capacity.

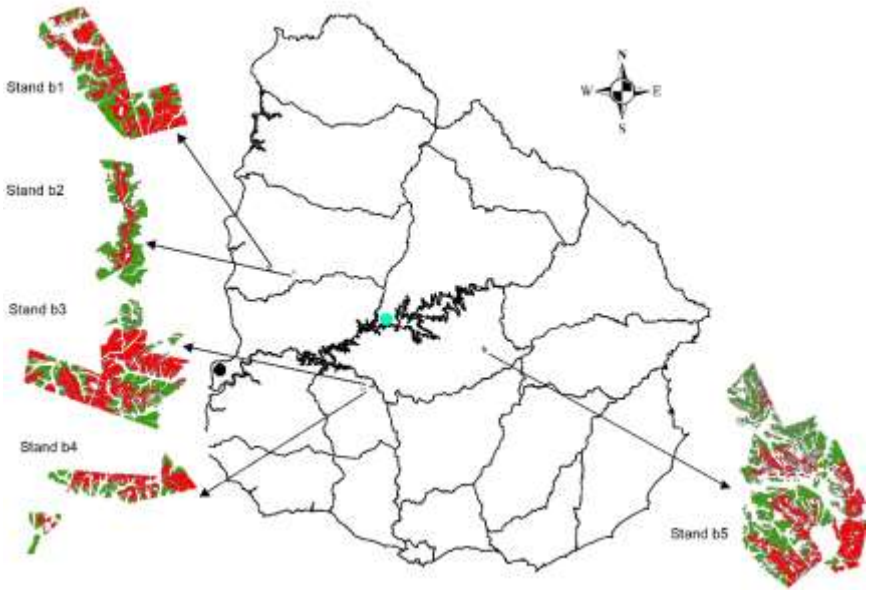

Figure 1. Location of the study sites: b1 and b2 (Guichon); b3 and b4 (Trinidad) and zone b5 (Sarandí del Yi) in Uruguay. In green *E. grandis* stands, in red *E. dunnii* stands; circle in black: Pulp mill Fray Bentos (-33.12148; -58.25455), circle in

cyan: Pulp mill Paso de Los Toros (-32.83006; -56.49728, approx. building under construction).

6.4.2. Stands information

A forest inventory including a single 10-m fixed radius (314.16 m2) plot per ha was established in the study area. In each plot, measurements included diameter at breast height (1.3 m above ground level –DBH- cm, measured with a calliper Haglöf Mantax, Långsele, Sweden), stand density (N, trees ha^{-1}), and basal area (G, m2 ha–1) of all trees with DBH ≥ 7 cm. Total height (H, m) was measured in the two central rows of the plots using a Vertex III hypsometer (Haglöf, Sweden); the height of the remaining trees was estimated using a logarithmic classic model (Table 1). As shown in the table, the stands were inventoried in real life when their ages ranged between 4.5 and 9.5. This information was used to project their growth from year 0 (plantation establishment) to year 10. For example, if a stand was inventoried in year 5, the data were used to project the state variables backward (from year 0 to year 5) and forward (from year 5 to year 10) through differential equations [29,30]. State variables projected included number of trees per hectare (N), basal area per hectare (G), quadratic mean diameter (dg), and mean arithmetic heights (Hm).

Table 1. Stand characteristics of *Eucalyptus grandis* and *Eucalyptus dunnii* in Uruguay. Variables and abbreviations: diameter at breast height (DBH, cm); total height (H, m); Above Ground Biomass (AGB, Mg C ha^{-1}), Stored Carbon (Mg ha^{-1}), Age (years), and stem density (N, trees ha^{-1}). Where: stdev=standard deviation, min= minimum, max= maximum.

	Field Attributes	min	mean	max	Stdev
E. grandis (n=43)	DBH (cm)	12.57	16.8	19.8	1.8
	H (m)	14.7	21.9	34.6	4.5
	AGB (Mg ha^{-1})	104.7	218.3	428.9	74.2
	Stored Carbon (Mg ha^{-1})	52.87	110.2	216.5	37.47
	Age (years)	4.50	6.84	9.5	1.5
	N (tree ha^{-1})	986	1051	1128	25.2
E. dunnii (n=45)	DBH (cm)	11.04	15.78	19.98	1.67
	H (m)	9.25	19.92	29.35	4.05
	AGB (Mg ha^{-1})	70.10	210.3	360.4	58.7
	Stored Carbon (Mg ha^{-1})	35.45	106.2	181.8	29.64
	Age (years)	4.5	6.28	8.4	1.20
	N (tree ha^{-1})	1028	1069	1103	16.84

6.4.3. Carbon sequestration and release assumptions

The process of photosynthesis permits green plants to uptake CO_2 from the atmosphere and convert it into organic carbon as they grow, and in turn, organic carbon is converted back to CO_2 when it is eaten or decomposed, which is known as the process of respiration [31]. In our study, the total C sequestered annually and stored in trees as organic C was computed following the procedure presented by Díaz and Rodríguez (2006) [21], and Toochi (2018) [31]. For this purpose, a basic density of 0.5 t m−3 was considered for both *E. grandis* and *E. dunnii*., as well as a C content

coefficient of 0.5 (C content equal to 50% of the tree's total weight). Thus, to calculate the C content of the species, a 0.25 conversion factor (wood density x proportion of C in the tree) was used. Only above ground carbon (AGC) was considered, assuming that in short-rotation plantations of Eucalyptus, the soil organic C does not have significant variations [30]. The aboveground biomass (AGB) required to calculate AGC was obtained using a compatible system of equations developed by Hirigoyen et al. (2020) [32] as functions of dg and Ho (Table 1). The rates of change in total AGB stocks were estimated by calculating the expected annual growth of the stand. Two cases were assessed considering the proportion of C released at harvest time and during the periods after the harvest. In the first case, it was assumed that 100% of the C stored is released at harvest time. In the second case, it was assumed that 50% of the C stored is released at harvest time, while the other 50% is stored after harvest as residues and paper products, and released linearly over the next 5 years after the final harvest [21].

6.4.4. Optimization model

6.4.4.1. Model description and mathematical formulation

To optimize harvest scheduling and stand harvest age, a mixed-integer linear programming model was developed to maximize the discounted net revenue (NPV) over a planning period of up to 15 years. Eucalyptus pulpwood stands in Uruguay are usually managed for periods of up to 10 years, with a minimum harvest age of 7 years (periods); this was taken into consideration in our study by adding a constraint to the optimization model. The objective function included revenue from timber (pulp logs) and C sequestered in the stand each year until the harvest age. It also included costs associated with plantation establishment, weed control, fertilization, and pest control, as well as timber harvest and transport to two alternative pulp mills: Paso de Los Toros (hereafter P. Toros) and Fray Bentos (hereafter F. Bentos). In each period t, the revenue generated from timber sales as well as plantation, harvest (clearfelling), and transport costs were discounted at an interest rate IR. A discount factor per period was calculated assuming the flow of revenues and costs occurred at the midpoint (t-0.5) of the period. The yearly C sequestered by each stand, from

establishment through harvest age, was accounted as a revenue source. Additionally, using similar approaches presented in previous studies [21,37], we calculated the value of the C released back to the atmosphere at harvest time and during the years after the harvest using the same C price as that used to quantify the revenue from C sequestration. Both C sequestered and released were discounted in the same way as the other revenues and costs

Sets, parameters, and variables of the optimization model are presented in Table 2. All costs, prices, and revenues in the manuscript are expressed in US dollars. The optimization, mixed-integer programming model can be expressed mathematically as follows:

Table 2. Sets, parameters, and variables of the thinning optimization model

Term	Definition
	Sets
I	Forest stands, I = {1, …, 88}
J	Destinations, J= {1, 2}
T	Planning periods, T = {1, …, 15}
$H \subset T$	Harvesting periods, H = {7, …, 10}
$P \subset T$	Periods before the minimum age for harvesting, P = {1, …, 6}
	Parameters
DPL	Delivered price of logs at pulp mill - ($ m^{-3})
CP	Carbon price - ($ t^{-1})
TC	Transport cost - ($ t-km^{-1})
DSM_{ij}	Transport distance from stand i∈ I to pulp mill j∈ J - (km)
HC_{ih}	Harvesting cost in stand i∈ I in period h ∈ H - ($)
$SPPC_i$	Site and plantation costs in stand I ∈ I - ($)
$WCFA_{it}$	Weed control, fertilization, and ant control costs in stand i∈ I in period t ∈T - ($)
$AvaPL_{ih}$	Pulp logs available in stand i ∈ I if harvested in period h ∈ H - (m^3)
$SeqC_{it}$	Carbon sequestered in stand i ∈ I in period t ∈ T - (t)
$AccC_{ih}$	Carbon accumulated in stand i ∈ I that is harvested in period h ∈ H - (t)
ir	Interest rate - (decimal)
	Decision variables
X_{ih}	Binary variable. 1, if stand i ∈ I is harvested in period h ∈ H, 0 otherwise
PLD_{ijh}	Continuous variable. Pulp logs delivered from stand i ∈ I to pulp mill j∈ J in period h ∈ H - (t)
	Accounting variables
$RevenuePLStand_i$	Revenue from the sale of pulp logs generated in stand i ∈ I - ($)
$ValueCSStand_i$	Value of carbon sequestered by stand i ∈ I - ($)
$ValueCS_{iht}$	Value of carbon sequestered by stand i ∈ I in period t ∈ T, if the stand is harvested in period h ∈ H - ($)
$ECostStand_i$	Establishment cost in stand i ∈ I - ($)
$HTCostStand_i$	Harvesting and transport cost in stand i ∈ I - ($)
$ValueCRStand_i$	Value of carbon released from stand i ∈ I - ($)
$ValueCR_{iht}$	Value of carbon released from stand i ∈ I and period t ∈ T, if the stand is harvested in period h ∈ H - ($).
$ValueCRStandA_i$	Value of carbon released from stand i ∈ I - ($) at the harvest time
$ValueCRStandB_i$	Value of carbon released from stand i ∈ I - ($) over the 5 years after the harvest

Objective function

Equation 1 was used to maximize the NPV over the planning period:

$$Max\ NPV = Revenue - Costs \quad (1)$$

where,

$$Revenue = RevenuePulpLogs + \text{Value}CarbonSequestered \quad (2)$$

$$Costs = EstablishmentCost + HarvestingTransportCosts + ValueCarbonReleased \quad (3)$$

To compute the discounted revenues and costs by period, a discount factor δ_t (Equation 4) was used:

$$\delta_t = \frac{1}{(1+ir)^{t-1/2}} \qquad \forall t \in T \quad (4)$$

Revenue and cost equations

Equations 5 and 6 were used to compute the discounted revenue from the sale of pulplogs in the stands.

$$RevenuePulpLogs = \sum_i RevenuePLStand_i \quad (5)$$

$$RevenuePLStand_i = \sum_j \sum_h PLD_{ijh} * DPL * \delta_h \qquad \forall i \in I \quad (6)$$

Equations 7-9 were used to compute the discounted revenue from the carbon sequestered in the stands.

$$ValueCS_{iht} = X_{ih} * SeqC_{it} * CP * \delta_t \qquad \forall i \in I, h \in H, t \in T \mid t \leq h \quad (7)$$

$$ValueCSStand_i = \sum_h \sum_{t \leq h} ValueCS_{iht} \qquad \forall i \in I \quad (8)$$

$$ValueCarbonSequestered = \sum_i ValueCSStand_i \quad (9)$$

Equations 10 and 11 were used to compute the discounted costs associated with plantation establishment in the stands.

$$ECostStand_i = SPPC_i + \sum_t WCFA_{it} * \delta_t \qquad \forall i \in I \quad (10)$$

$$EstablishmentCost = \sum_i ECostsStand_i \quad (11)$$

Equations 12 and 13 were used to compute the discounted harvesting and transportation costs in the stands.

$$HTCostStand_i = \sum_j \sum_h [(PLD_{ijh} * DSM_{ij} * TC) + (HC_{ih} * X_{ih})] * \delta_h \quad \forall i \in I \quad (12)$$

$$HarvestingTransportCost = \sum_i HTCostStand_i \quad (13)$$

Several equations were used to compute the value of the C released at the harvest time. Equations 14 and 15 were used for the scenario where it was assumed that 100% of the C accumulated was released at the harvest time.

$$ValueCRStand_i = \sum_h X_{ih} * AccC_{ih} * CP * \delta_h \qquad \forall i \in I \tag{14}$$

$$ValueCarbonReleased = \sum_i ValueCRStand_i \tag{15}$$

Likewise, Equations 16 to 19 were used for the scenario that assumed that 50% of the C accumulated was released at the harvest time, and the other 50% was released over the next 5 years after the harvest.

$$ValueCRStandA_i = \sum_h X_{ih} * (AccC_{ih} * 0.5) * CP * \delta_h \qquad \forall i \in I \tag{16}$$

$$ValueCR_{iht} = X_{ih} * (AccC_{it} * 0.1) * CP * \delta_t \quad \forall i \in I, h \in H, t \in T | h < t \leq h + 5 \tag{17}$$

$$ValueCRStandB_i = \sum_h \sum_{h<t\leq h+5} ValueCR_{iht} \qquad \forall \in I \tag{18}$$

$$ValueCarbonReleased = \sum_i ValueCRStandA_i + \text{Value}CRStandB_i \tag{19}$$

Constraints

In addition, three groups of constraints were included in the model to ensure that a) every stand was cut once within periods 7 to 10 (Equation (20)), b) no stand could be harvested before period 7 (minimum age to harvest a stand) [12,18] (Equation (21)), and c) the volume of timber delivered to the pulp mills did not exceed the volume available of these products in the stands (Equation (22)). A constraint in Equation (20) was included since trees harvested at an early age (≤ 6 years) produce wood with a very low pulp yield, and there is a decline in marginal growth when trees are harvested after period 10.

$$\sum_{h \in H} X_{ih} = 1 \qquad \forall i \in I \tag{20}$$

$$\sum_{p \in P} X_{ip} = 0 \qquad \forall i \in I \tag{21}$$

$$\sum_{j \in J} PLD_{ijh} = X_{ih} * AvaPL_{ih} \qquad \forall i \in I \, , h \in H \tag{22}$$

6.4.4.2. Data input

The area of the 88 forest stands used for the analysis ranged between 5.5 and 54.3 ha (average = 21.9 ha). Site and stand variables for the stands at the beginning of the planning period are presented in Table 1. Parameters associated with C stocks were calculated as per the description provided in section 2.3, while a range of C prices (from 0 to 30 USD t^{-1}) was used for the analyses. These C prices correspond to the price per ton of organic C stored in trees resulting from CO_2 sequestration. The carbon market of the European Union Emissions Trading System (https://sandbag.org.uk/carbon-price-viewe r/ (accessed on 15 December 2020) was consulted to define the C prices used in the study.

For the analysis, the base scenario included an IR of 6%, a C price of 0 USD t^{-1}, and a delivered price for pulp logs of 55 USD m^{-3}. Unit harvesting costs ranged between 17 and 21 USD m^{-3} as a function of tree volume and harvesting age (periods 7, 8, 9, or 10), assuming a typical cut-to-length (CTL) system for Eucalyptus plantations in Uruguay [33]. The CTL system comprises one or more wheeled harvesters/processors that perform tree felling and stem processing tasks, followed by forwarders that extract the processed logs to the roadside. Based on previous studies [34], a single transport cost of 0.1 USD t-km^{-1} was used. Distances from stands to pulp mills were calculated with ArcGis 10.1 (ESRI, 2011); they ranged from 152 to 337 km (average of km) to F. Bentos pulp mill, and from 107 to 191 km (average of 157 km) to P. Toros pulp mill. In Uruguay, road transport is usually performed by 6-axis trucks with a gross vehicle mass of 48 tons and an average tare of 13 tons (net payload of approximately 33 tons).

In addition to harvesting and transport costs, the NPV calculation included costs associated with site preparation and plantation (year 0 at a cost of 800 USD ha^{-1}) as

well as weed control (periods 1 to 3 at a cost of 100 USD ha^{-1}, and fertilization and ant control between periods 1 and 3 at a cost of 95 USD ha^{-1}) [33].

6.4.4.3. Model implementation

The optimization model was implemented using the IBM DocPlex library v. 2.19.202 (https://pypi.org/project/docplex/ (accessed on 15 December 2020), licensed under the Apache License v2.0 within the IBM Decision Optimization CPLEX Modeling for Python program. The model was run on a computer Dell Inspiron 5530 (Dell Inc., Texas, USA) equipped with an Intel® Core™ i7-8850H, 2.60GHz (6 cores) processing unit, and 32 Mb of RAM. The model script was coded using the PyCharm editor v.2020.3.3 (Professional Edition), and to facilitate the runs of the optimization model, a simple GUI was programmed with the PyQt5 Library (https://pypi.org/project/PyQt5/ (accessed on 15 December 2020). All the input data were imported from Excel and converted into Pandas data frames for later use in the optimization model. After each run, all the model outputs were exported back to Excel for further analysis.

6.4.4.4. Scenarios and sensitivity analysis

In total, 54 scenarios were assessed and their NVPs calculated and compared. These scenarios included the combinations of three IRs (6, 8, and 10%), three timber prices (55, 65, and 75 USD m^{-3}), and six C prices (0, 5, 10, 15, 20, and 30 USD t^{-1}), which were used to conduct the sensitivity analyses. The above scenarios were grouped into two classes to facilitate the analyses and comparisons:

1. Scenarios that included revenue only from the sale of timber (pulplogs) generated during clear-cut (SC1);
2. Scenarios that included revenue from both sources, timber generated during the clear-cut, and C sequestered over the rotation length of the stands (SC2).

Sets of outputs combining harvest periods (periods 7 to 10) and C prices included timber revenue and sequestered C and its revenue, along with harvest and transport costs to both pulp mills. The outputs also included the optimal harvest age (final cut) of each stand and the corresponding value of the objective function (NPV). All

statistical analyses and summaries were performed in Python, using the NumPy and Pandas libraries. All statistically significant differences between scenarios were computed using a paired t-test ($p \leq 0.05$). In addition, maps with the optimal spatial solutions were created using ArcGIS® software by Esri.

6.5. RESULTS

6.5.1. Effect of C and timber price, IR, and C release approach on NPV

Figure 2 shows the relationship between NPV and C price for the range of IRs, timber prices, and C release approaches (50 or 100% of C released at the harvest time) included in the study. As expected, in SC2 scenarios, NPV was sensitive to C prices and IR. There was a clear relationship between NPV and C price, with NPVs that, on average, increased at a rate of 0.55 (IR = 6%), 1.38 (IR = 8%), and 1.61 M USD (IR = 10%) for every 5 USD t^{-1} rise in C price. The maximum NPV among all the scenarios evaluated (2.52 M USD) was calculated for a C price of 30 USD t^{-1}, an IR of 6% and a timber price of 75 USD m^{-3}. In addition, there was a substantial reduction in NVP when the IR increased from 6 to 10%. For example, for a C price of 15 USD t^{-1}, a timber price of 65 USD m^{-3}, and a 100% C release approach, the NVP was 3.75, 2.73, and 1.99 M USD for an IR of 6, 8, and 10%, respectively. The differences in NPV between the three IRs were statistically significant at $p \leq 0.05$. For SC2 scenarios that included an IR of 8 and 10%, and a timber price of 55 USD t^{-1}, NPVs became positive only after a minimum C price. For an IR of 8%, this minimum C price was 5 USD m^{-3} irrespective of the C release approach being used. For an IR of 10%, the minimum price was 10 USD m^{-3} for a 50% C release approach, and 15 USD m^{-3} for a 100% C release approach.

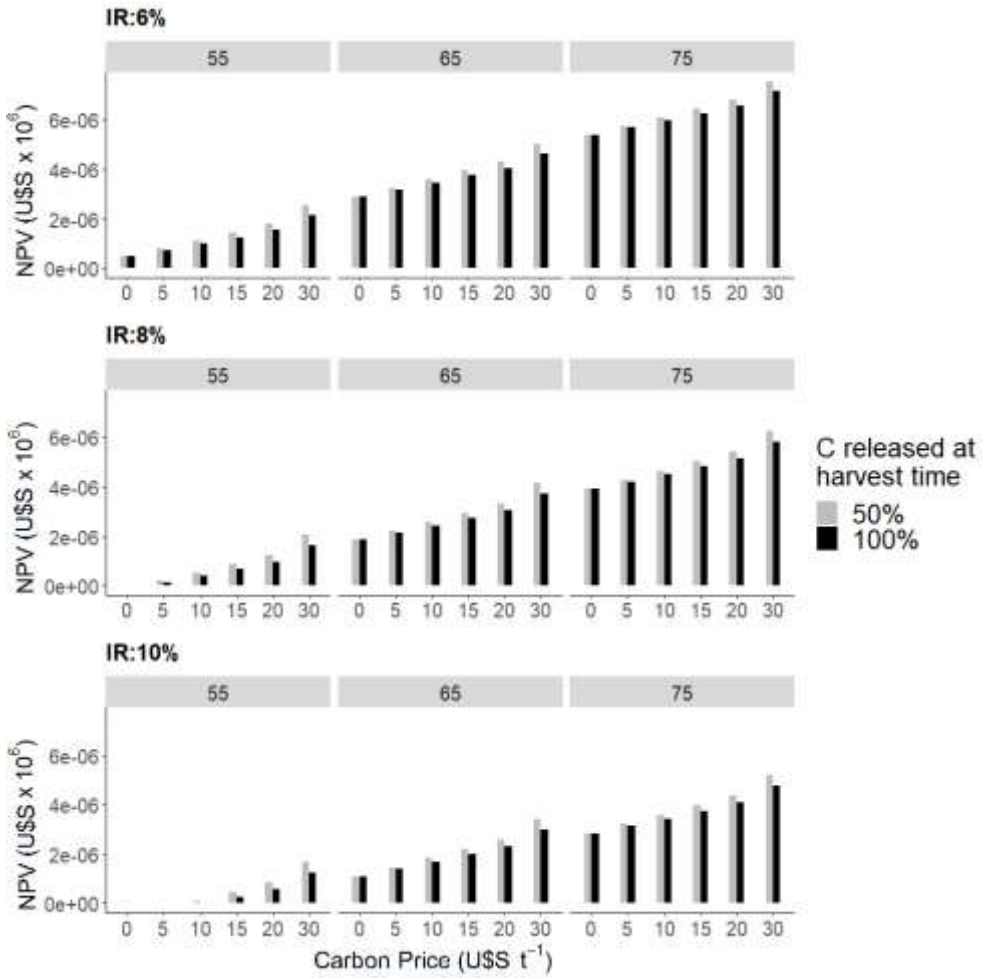

Figure 2. Net present value by C price (from 0 to 30 USD t−1) for three interest rates (IR) and timber prices (55, 65, and 75 USD t-1).

On average, using a 50% C release approach resulted in NPVs that were 8 (IR = 6%), 28 (IR = 8%), and 33% (IR = 10%) higher than using a 100% C release approach. These differences were statistically significant at $p \leq 0.05$, excepting for IR between 8 and 10%. It is worth noting that differences in NPV between the 50 and the 100% C release approaches occurred in SC2 scenarios only, since in SC1 scenarios all the revenue was obtained solely from the sale of timber. The largest difference in NPV between the two C release approaches was obtained for a C price of 30 USD t^{-1}. At this C price and a timber price of 65 USD m−3, the differences were 0.39, 0.43, and 0.43 M USD, for an IR of 6, 8, and 10%, respectively.

6.5.2. Effect of C price and timber price, IR, and C release approach on revenues

The impact of C price on revenue is presented in Table 3, considering a timber price of 65 USD m^{-3}, and a 50% C release approach. The results are broken down by IR, total revenue, revenue from C, and revenue from timber. As expected, total revenues increased with higher C prices and lower IRs. The minimum revenue (11.3 M USD) was obtained in an SC1 scenario with an IR of 10%, where 100% of the revenue resulted from the sale of timber. On the contrary, the maximum revenue (23.1 M USD) was obtained in an SC2 scenario with an IR of 6%, where 70% of the revenue resulted from the sale of timber and 30% from C credits.

Table 3: Effect of C and timber price, and IR on revenue. Values (in millions of dollars) are calculated for a timber price of 65 $ m^{-3} and considering 50% of C released at the harvest time.

C price (USD/t)	Interest rate (%)	Total Revenue (M USD)	Revenue Timber (M USD)	Revenue Carbon (M USD)
0	6	16.0	16.0 - [100%]	0.0 - [0%]
5	6	17.3	16.2 - [94%]	1.1 - [6%]
10	6	18.5	16.3 - [88%]	2.2 - [12%]
15	6	19.7	16.3 - [83%]	3.4 - [17%]
20	6	20.8	16.3 - [78%]	4.5 - [22%]
30	6	23.1	16.3 - [70%]	6.8 - [30%]
0	8	13.1	13.1 - [100%]	0 - [0%]
5	8	14.2	13.2 - [93%]	1.0 - [7%]
10	8	15.4	13.4 - [87%]	2.0 - [13%]
15	8	16.5	13.5 - [82%]	3.0 - [18%]
20	8	17.8	13.7 - [77%]	4.1 - [23%]
30	8	20.0	13.6 - [68%]	6.4 - [32%]
0	10	11.3	11.3 - [100%]	0 - [0%]
5	10	12.2	11.3 - [93%]	0.9 - [7%]
10	10	13.1	11.3 - [87%]	1.8 - [13%]
15	10	14.1	11.4 - [81%]	2.7 - [19%]
20	10	15.1	11.5 - [76%]	3.6 - [24%]
30	10	17.3	11.5 - [66%]	5.8 - [34%]

Since prices were considerably higher for timber than for C credits, regardless of C price and IR, the revenue from timber in SC2 was always higher than the revenue from C credits. The largest gap (88% difference of contribution to total revenue or 15.1 M USD) between revenue from timber and revenue from C credits was obtained for a C price of 5 USD t−1 and an IR of 6%. In contrast, the smallest gap (28% difference of contribution to total revenue or 7.7 M USD) was obtained for a C price of 30 USD t^{-1} and an IR of 10%. The highest proportional contribution to revenue from C credits was 34% for an IR of 10% and a C price of 30 USD t^{-1}, whereas the highest monetary contribution was 6.8 M USD and occurred for the same C price and an IR of 6%. Irrespective of the C price and IR, the contribution of C credits to total revenue ranged between 6–7% and 30–34%. In addition, there was a notable variation in the revenue attributed to C credits and timber. Thus, the coefficient of variation for C revenue was 74.7 (IR = 6%), 76.7 (IR = 8%), and 77.1% (IR = 10%), whereas the variation for timber revenue was only 0.5 (IR = 6%), 1.5 (IR = 8%), and 0.6% (IR = 10%), which reflects the impact of C prices on this variation.

6.5.3. Effect of C price on harvest scheduling (rotation age) and volume harvested (supplied) per period

Table 4 presents the volume harvested (m^3) by harvest age, C price, and IR. Irrespective of the IR, in SC2 scenarios, the number of stands being harvested in period 10 grew gradually as C prices passed from 5 to 30 USD t^{-1}, which resulted in higher volumes of timber being harvested and delivered to customers during this period. For example, for a C price of 30 USD t^{-1} and an IR of 6, 8, and 10%, the proportion of stands being harvested in period 10 was 100 (88 stands), 99 (87 stands), and 75% (66 stands), respectively. From Table 4, it is observed that harvest ages commenced declining when IR passed from 6 to 8 and 10%, which resulted in more stands being harvested (and a higher volume of timber delivered) in periods 7, 8, and 9. On the contrary, for a C price of 0 USD t^{-1} (SC1 scenarios) and an IR of 8 or 10%, the largest proportion of the stands were harvested in period 7 (minimum harvest age). In SC1 scenarios, due to the absence of revenue from C credits, a larger proportion of the stands was harvested in periods 7 and 8, particularly when the IR

was 8 or 10%. The most notable case was that with an IR of 10%, where 44% of the stands (39 out of 88) were harvested in period 7. Harvest ages also had an impact on the total volume being harvested across the planning periods. Thus, for example, in SC2 scenarios with a C price of 30 USD t^{-1}, a timber price of 65 USD m^{-3}, and an IR of 6, 8, and 10%, the total volume harvested in all periods was 435,830, 435,372, and 417,993 m^3, respectively. As a comparison, in SC1 scenarios (C price = 0 USD t^{-1}), the volume harvested in all periods was only 411,592, 367,740, and 356,882 m^3 for an IR of 6, 8, and 10%, respectively.

Table 4. Total volume harvested (m^3) by rotation age, C price, and IR. Numbers in parentheses represent the number of stands being harvested in each scenario. Values were calculated for a timber price of 65 \$ m^{-3} and considering 50% of C released at the harvest time.

		Harvest age				
C price (USD/t)	**IR (%)**	**Period 7**	**Period 8**	**Period 9**	**Period 10**	**Total all periods**
0	6	36,167 (11)	30,067 (4)	106,407 (17)	238,951 (56)	411,592
5	6	33,687 (9)	5449 (1)	63,306 (8)	319,907 (70)	422,349
10	6	19,218 (5)		31,062 (4)	380,126 (79)	430,406
15	6	19,218 (4)		5941 (1)	407,481 (83)	432,550
20	6	5,804 (2)			429,772 (86)	435,576
30	6				435,830 (88)	435,830
0	8	116,139 (26)	79,352 (23)	99,155 (24)	73,094 (15)	367,740
5	8	89,757 (22)	92,171 (21)	93,794 (23)	101,379 (22)	377,101
10	8	54,241 (15)	77,472 (11)	121,949 (32)	137,919 (30)	391,581
15	8	39,916 (11)	41,170 (5)	126,845 (24)	197,098 (48)	405,029
20	8	23,967 (6)	15,329 (2)	76,348 (8)	305,800 (72)	421,444
30	8			5941 (1)	429,431 (87)	435,372
0	10	150,399 (39)	76,976 (20)	74,850 (18)	54,657 (11)	356,882
5	10	129,958 (32)	82,195 (23)	84,701 (20)	65,577 (13)	362,431
10	10	129,204 (31)	79,623 (22)	87,622 (21)	66,607 (14)	363,056
15	10	110,743 (24)	72,719 (20)	91,610 (22)	96,590 (22)	371,662
20	10	76,361 (18)	86,047 (18)	92,758 (23)	128,076 (29)	383,242
30	10	13,346 (4)	28,206 (3)	89,372 (15)	287,069 (66)	417,993

The spatial distribution of the stands being harvested per period (Figure 3) was impacted by harvest age, C and timber prices, and IR. Spatially arranged harvest of stands aimed to minimize harvest and transport costs, and maximize returns from timber and C, thereby maximizing NPV. This also had an impact on the flow of timber being delivered from stands to customers (Figure 4). In the case of SC2 scenarios, the peak flow of timber from stands to P. Toros pulp mill occurred at longer harvest ages when C price increased from 5 to 30 USD t^{-1}, reaching a maximum volume (174,289 m^3) in period 10 when C price equaled 30 USD t^{-1}. On the contrary, in SC1 scenarios, the maximum flow of timber to P. Toros pulp mill occurred during periods 7 and 8, reaching a maximum of 73,807 m^3 in year 8. Regarding timber flows to F. Bentos pulp mill in SC2 scenarios, maximum volumes of 96,529, 129,289, 138,632, 186,163, and 255,142 m^3, were obtained in year 10 for C prices of 5, 10, 15, 20, and 30 USD t^{-1}, respectively. In SC1 scenarios, the maximum volume delivered to F. Bentos pulp mill (78,889 m^3) was obtained in period 9. In all scenarios that included a C price lower than or equal to 15 USD t^{-1}, there was a positive volume of timber delivered to F. Bentos pulp mill. For scenarios that included a C price of 20 USD t^{-1}, there was no timber flow to F. Bento from coupes being harvested in period 8. The same occurred in periods 7, 8, and 9 for a C price of 30 USD t^{-1}. At this C price, no timber was delivered to any pulp mills since no forest stands were harvested in these periods.

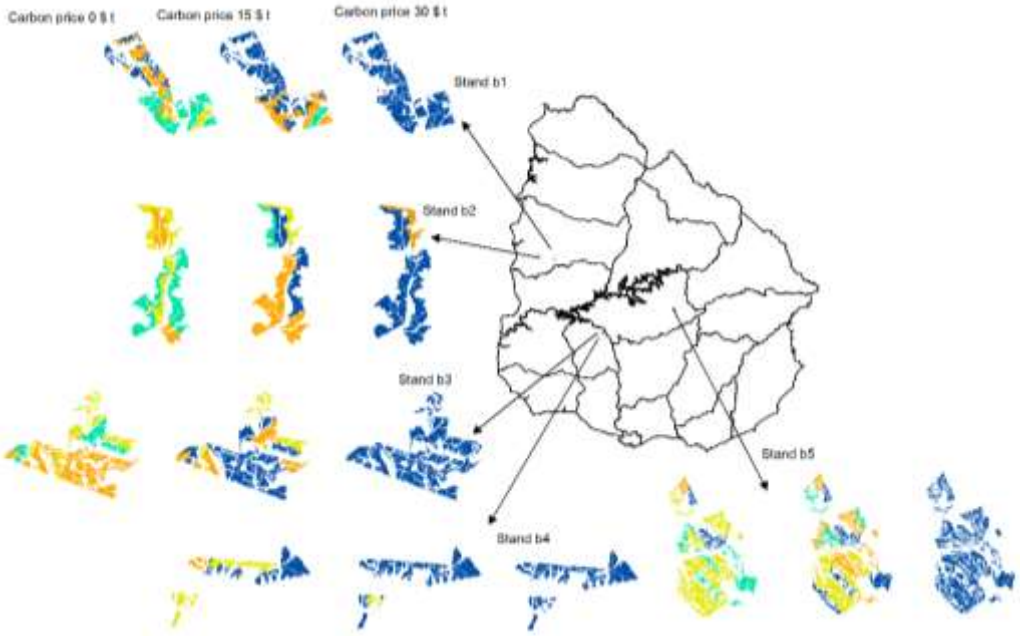

Figure 3. Rotation age and harvest spatial distribution of the stands by C price (0, 15, and 30 $ t^{-1}). The harvest age for years 7, 8, 9, and 10, are represented in yellow, green, orange and blue, respectively.

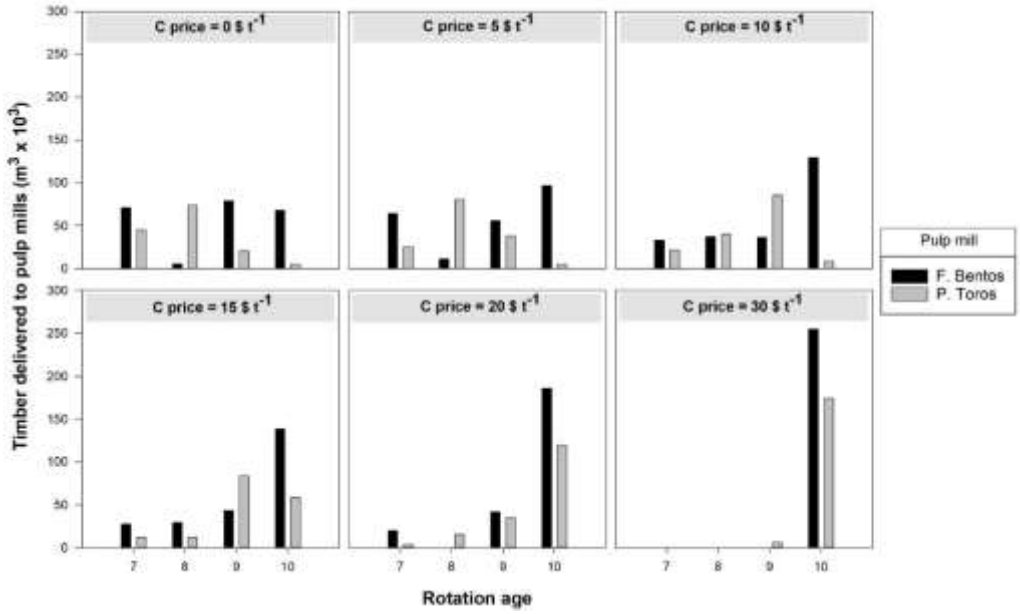

Figure 4. Timber delivered to pulp mills by C price and rotation age assuming 50% of C released at the harvest time, an IR of 8% and a timber price of 65 $ m^{-3}.

6.5.4. Effect of carbon price and IR on carbon sequestered

As observed in Figure 5, both the total and per period C sequestered were shown to be very sensitive to C prices, and highly affected by the harvest age. In all scenarios, the maximum amount of C sequestered occurred in period 10 for a C price of 30 USD t^{-1}. At this C price, most stands were harvested in period 10 to maximize revenue from C credits; amounts of C sequestered totaled 293,196 t for an IR of 6%, 289,196 t for an IR of 8%, and 203,586 t for an IR of 10%. The amount of C sequestered in period 10 declined with lower C prices, which was more evident in scenarios with an IR of 8 and 10%. In the latter case, the C sequestered dropped by 53.9% when C price was reduced from 30 to 20 USD t^{-1}. With an IR of 6%, the C sequestered declined gradually when C price was reduced from 30 to 0 USD t^{-1}. Likewise, when passing from 30 to 10 USD t^{-1}, the drop in C sequestered occurred at an average rate of 9,295 t per every 5 USD t^{-1} reduction in C price, while when

passing from 10 to 0 USD t^{-1}, the drop was about 46,145 t per every 5 USD t^{-1} reduction in C sequestered.

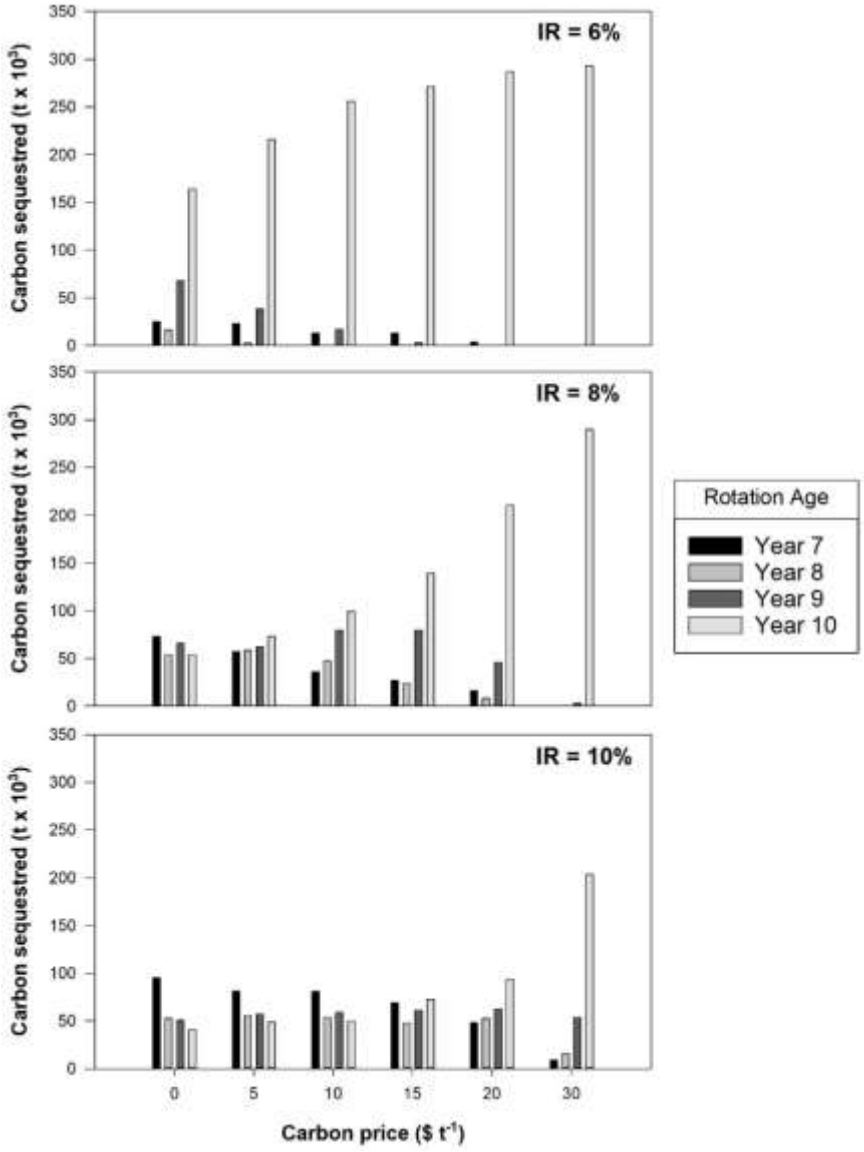

Figure 5. C sequestered and accumulated until rotation age (harvest period) by C price and interest rate (IR).

For C prices lower than 30 USD t^{-1}, the amount of C sequestered in periods 7, 8, and 9 showed a gradual increase when IR passed from 6 to 10%. Thus, for an IR of 6%, the average amount of C sequestered in periods 7, 8, and 9 was 15,590, 3,892, and 25,310 t, respectively. Likewise, for an IR of 8%, the average amount of C

sequestered in periods 7, 8, and 9 was 41,785, 38,159, and 66,703 t, respectively. Finally, for an IR of 10%, the average amount of C sequestered in periods 7, 8, and 9 was 74,909, 52,326, and 57,959 t, respectively. The above results show clearly that the optimization model aimed to maximize C sequestration at higher C prices and the production of timber at lower C prices.

6.6. DISCUSSION

The results obtained in this study show that paying for C sequestered can increase economic returns in short-rotation plantations depending on C and timber, as well as logging and market conditions. However, the implementation of forest planning that includes C sequestration as a source of revenue in Eucalyptus plantations requires regulatory changes at the international and national level [35]. Optimizing harvest schedules and harvest age of stands considering C and timber prices is key to maximize the use of the forestry resources that are subject to intensive silviculture schemes [8]. The results show that NPVs were quite sensitive to the range of C prices evaluated in the study. For any C price, adding up the revenue from C credits and the sale of timber gave the best economic returns. High C prices increased the proportional contribution of C credits to NPV and reduced the contribution of timber, as found in previous studies [8–10,36]. Growth rates were used to compute C sequestered and stored in aboveground biomass, and a sensitivity analysis was conducted to quantify the effect of IR as well as C and timber prices on NVP and optimal harvest scheduling (including stands' harvest age). Following similar approaches to those from previous studies [21,37], gross revenue in each stand was computed from the sale of timber as well as from credits associated with C sequestration due to forest growth. In addition, C released at the harvest time and costs associated with the management of the stands were used to quantify NPV. Taking all these considerations into account, our optimization modeling approach proved to be a practical and effective method to determine the impact of C and timber prices on harvest scheduling and economic returns in Eucalyptus short-rotation plantations.

The harvest schedule provided by our solution approach maximized the revenue from timber and C sequestration in each stand. This plan was generated by using a mathematical programming model that optimized harvest scheduling between periods 7 and 10, and which served as the basis to program new plantations. As confirmed in our study, optimal planning models are critical to maximize the economic and silvicultural outcomes of forest management plans [37,38]. Additionally, determining optimal harvesting scheduling and harvest age, including multiple products and services from forest ecosystems, is essential for implementing sustainable forest management strategies [39]. The production of Eucalyptus in Uruguay, however, has a clear orientation for pulp, so other products were not contemplated in our study (e.g., sawn wood), since no markets exist for these products in the country. Optimal biological rotations are dictated by the annual rate of C accumulation in tree biomass. For example, for short-rotation Eucalyptus plantations in subtropical China, Zhou et al. [44], showed that the marginal annual rate of C accumulation increased from year 4 to year 10, and sharply decreased from year 13 to year 21, suggesting optimal rotations between 12 and 15 years. However, economic and biological optimal rotations determined at the stand level usually differ from harvest ages determined at the forest level, since the former is driven by several operational constraints and affected by management costs and the prices of multiple products, such as C and timber.

Regarding economic optimal rotations, Diaz-Balteiro and Rodríguez (2006) [21], developed several models using dynamic programming to calculate the optimal rotation for intensive Eucalyptus plantations in Spain and Brazil. Their solution approach did not include operational constraints as we did in our study, but it focused primarily on determining the economic rotation age at the stand level using the Land Expectation Value. Regardless of the solution approach, when including the combined revenue from timber and C sequestration, the rotation or harvest age tends to increase when C prices are high, as reported by various authors [36–38]; this, however, will depend on the annual rate of C sequestration. In our study, the annual rate of C sequestered increased continuously until period 10, which was set as the maximum harvest age for any stand in the plantation estate. In addition to annual

rates of C sequestered, harvest ages were determined by the ratio between timber (pulplogs) and C prices. Thus, the impact of C revenue on NPV was more pronounced when C prices were high and exceeded that of pulplogs; this resulted in longer optimal harvest ages when C prices were higher and shorter optimal harvest ages when C prices were lower. IR also had an impact on the harvest age of the stands. Thus, there was a larger proportion of stands with longer harvest ages when the IR was 6% and a lower proportion when the IR was 8 or 10%. Historically, a harvest age of 8 years has been adopted by most forester growing pulp-oriented Eucalyptus plantations in Uruguay, based primarily on MAIs figures reported in previous studies [40]. The results presented in our study show that harvest ages can range between 7 and 10 years without impacting financial returns and C sequestration. However, the impact of shorter rotations (< 7 years) must be further investigated since it might have negative implications on timber supply and economic returns. Additionally, in a context where forests are one of the most important carbon sinks to mitigate climate change, a substantial reduction in the optimal harvest age may impact their C sequestration capacity [1,42]. Hence, it is essential to monitor and accurately predict and quantify changes of C stocks with the assistance of local models [43] and remote sensing technologies [38].

C pricing can be used as a political and planning tool. For example, in a study that involved forests being managed to maximize discounted revenue from both timber production and C, Pukkala (2020) [9] reported that if 100 EUR t−1 of C were paid to forest land owners every 100 years, the C sequestration of Finnish forests would increase by 70% (nearly the maximum increase obtained by subsides). Although these results are consistent with our findings, some slight differences were observed. These can be attributed to the range of forest products (multiple timber products in the case of Pukkala's study, and a single timber product in the case of our study) and C prices. In the case of our study, discounted returns obtained primarily from the sale of timber when C prices were lower than or equal to 15 USD t^{-1}, and from C sequestration when C prices were higher than 15 USD t^{-1}. The high volatility of prices in the C market might be associated with uncertain C revenues, so this

should be an important variable to be factored into the economic analysis of intensive silviculture strategies [39,44].

Our results reveal that the spatial arrangement and number of stands to be harvested in each period were sensitive to C prices. With low C prices (0 and 5 USD t^{-1}), the model aimed to maximize NPV and returns from the sale of timber, which resulted in the harvesting of a large proportion of stands in periods 7 and 8; these stands were associated with lower harvesting and transport costs due to their yield per ha and distance to the pulp mills. On the contrary, with high C prices (20 and 30 USD t^{-1}), the model aimed to maximize NPV and returns from C sequestration, which resulted in longer harvest ages (9 and 10 years) and in a large proportion of stands that reached high yields per ha in these periods.

Globally, forest planners are concerned with the sustainability of planted forests. Strategies to increase C sequestration are under consideration by many forest owners and government agencies in their forest management and logging plans [8]. Linear programming economic models of forest management that include C sequestration in intensive Eucalyptus plantations are a powerful tool to optimize their role for climate change mitigation [45]. These optimization-based solution techniques are essential to quantify the economic value and potential contribution of natural forest and plantations to climate change based on integrated returns obtained from multiple ecosystem services and forest products [46]. Silviculture geared to maximize C sequestration promotes the growth and conservation of standing biomass stocks, either by modifying the standard forest management strategies or by optimizing the rotation age [47]. In addition, these goals are achieved through the assessment and control of different silvicultural schemes, including optimal thinning and harvesting strategies, promotion of agroforestry systems, and diversification of forest uses that provide multiple ecosystems services and increase the value of the forests [48].

As far as we know, our optimal modeling proposal is the first effort in assessing the incorporation of C sequestration into forest management plans of Eucalyptus plantations in Uruguay. However, we are aware of some of the limitations of our study. Firstly, the data were collected from clonal trees in three regions in Uruguay for the two most common Eucalyptus species, plus geographical conditions,

proximity to pulp mills, harvesting technology, and market conditions may affect the impact of C prices on harvesting plans and NPV. It is expected that expanding the number of forest sites and other genetic sources might overcome these limitations. Secondly, our analysis did not include decisions on initial stocking or the possibility of thinning. Of course, these decisions can be included in future studies to be able to assess their impact on C storage strategies in low-yield plantations. Additionally, our research focused primarily on investigating how C and timber prices impact harvest scheduling (harvest age) and NPV; the assessment quantified C sequestration and storage in each period, and C released at the end of the planning period. It is worth pointing out that since there is no formal C market for plantations in Uruguay, we used a rather conservative range of C prices (from 0–30 USD t^{-1}) to analyze the potential impact that this parameter could have on the harvest age, harvest scheduling, and NPV, based on similar articles found in the literature. Additionally, due to the absence of applicable legal mechanisms for C crediting and payment in Uruguay, these models have limited use in the current scenario. On the other hand, our analysis focused more on highlighting the impact of C pricing on forestry planning (space and time) and its importance to Eucalyptus plantation afforestation rather than on comparing payment mechanisms (subsidies and taxes). The optimization model developed and presented in our study is deterministic and generates the same outcomes under a set of initial conditions and value of the parameters (e.g., timber and C prices, C accounting). We are aware of the limitations of this approach, and given the role attributed to forests in climate change policy and in view of potential future policy discussions, it is important to verify and quantify the potential of forest carbon sequestration in the presence of uncertainty [50]. Future research should test and implement alternative solution approaches (e.g., stochastic programming, robust optimization, etc.) that can deal with uncertainty in C sequestration projects, since forest management decisions under uncertainty could deviate from those made with the assistance of deterministic models. In addition, our analysis did not consider the impact of logging and transportation operations on C emissions. However, previous studies have shown that their contribution is small compared to the C contained in wood and biomass products, with ratios of about 40:1

and 45:1 for roundwood and biomass, respectively [49]. According to previous reports, other variables included in the study will also influence forest management and C storage strategies, including IRs, growth rates, and prices of sawn wood and biomass. Our analysis included a limited range of prices and costs, and their fluctuation may affect decisions related to C storage.

Management alternatives, such as silvopastoralism or forest plantations destined for solid wood, were not included. The accumulation and flux of C from these forest management alternatives may be different from those computed in our study. Biomass was not included in our analyses, since in Uruguay, a common practice is to leave the logging debris on site to mitigate the impact of the harvest equipment on the soil

6.7. CONCLUSIONS

Sustainable forest management strategies that allow the provision of multiple timber products and enhance C sequestration require the assessment of scenarios to quantify the impact of carbon (C) and timber prices on harvest scheduling and optimal harvest age. Our results show that mixed-integer linear programming is a practical and effective tool for developing optimal forest management plans in short-rotation Eucalyptus plantations. These management plans must be designed and implemented with the assistance of accurate field data, remote sensing tools (e.g., LiDAR) and growth estimation models. The results of our study in Uruguay suggest that high C prices (> 10 USD t−1) can result in longer harvest ages, as well as increased timber flows to customers, C sequestration, and economic returns in Eucalyptus stands. Our results also demonstrate that harvest scheduling, harvest age, and NPV are very sensitive to C and timber prices, and that the best economic returns are obtained when the stands are managed to maximize timber production and C sequestration.

6.8. ACKNOWLEDGMENTS

The authors thank the Instituto Nacional de Investigaciones Agropecuarias (INIA-Uruguay) for supporting our research work, for help during the fieldwork and the INIA Scholarship for PhD studies. We are particularly grateful for the support of Leonidas Carrasco Letelier, Roberto Scoz (INIA), Pablo Rodriguez, Carola Odonne, José Carlos de Mello (FOSA). We acknowledge the institutional support of the University of Cordoba-Campus de Excelencia CEIA3.

6.9. REFERENCES

1. Nunes, L.J.R.; Meireles, C.I.R.; Gomes, C.J.P.; Ribeiro, N.M.C.A. Forest management and climate change mitigation: A review on carbon cycle flow models for the sustainability of resources. *Sustainability* **2019**, *11*, 5276, doi:10.3390/su11195276.
2. Kuzminyh, Y.V.; Gryaznov, S.E.; Shaitarova, O.E.; Sukonkin, S.E.; Yu Abakulina, L. Forestry Development as An Instrument for Implementing the Climate Policy of Russia. In Proceedings of the IOP Conference Series: Earth and Environmental Science, Saint Petersburg, Russia, 16–18 June 2020; Volume 574.
3. Lal, R. Forest soils and carbon sequestration. *For. Ecol. Manag.* **2005**, *220*, 242–258, doi:10.1016/j.foreco.2005.08.015.
4. Dixon, R.K.; Wisniewski, J. Global forest systems: An uncertain response to atmospheric pollutants and global climate change? *Water Air Soil Pollut.* **1995**, *85*, 101–110, doi:10.1007/BF00483692.
5. Dixon, R.K.; Brown, S.; Houghton, R.A.; Solomon, A.M.; Trexler, M.C.; Wisniewski, J. Carbon pools and flux of global forest ecosystems. *Science* **1994**, *263*, 185–190, doi:10.1126/science.263.5144.185.
6. Hui, D.; Deng, Q.; Tian, H.; Luo, Y. Climate change and carbon sequestration in forest ecosystems. *Handb. Clim. Chang. Mitig. Adapt.* **2017**, *555*, 594.
7. Braakhekke, M.C.; Doelman, J.C.; Baas, P.; Müller, C.; Schaphoff, S.; Stehfest, E.; Van Vuuren, D.P. Modeling forest plantations for carbon uptake with the

LPJmL dynamic global vegetation model. *Earth Syst. Dyn.* **2019**, *10*, 617–630, doi:10.5194/esd-10-617-2019.

8. Acuna, M.; Ma Navarro-Cerrillo, R.; Ruiz-Gómez, F.; Lara-Gómez, M.; Pérez-Romero, J.; Varo-Martínez, M.Á.; Palacios-Rodríguez, G. How does carbon pricing impact optimal thinning schedules and net present value in Mediterranean pine plantations? *For. Ecol. Manag.* **2021**, *482*, 118847, doi:10.1016/j.foreco.2020.118847.
9. Pukkala, T. At what carbon price forest cutting should stop. *J. For. Res.* **2020**, *31*, 713–727, doi:10.1007/s11676-020-01101-1.
10. Broz, D.; Durand, G.; Rossit, D.; Tohmé, F.; Frutos, M. Strategic planning in a forest supply chain: A multigoal and multiproduct approach. *Can. J. For. Res.* **2017**, *47*, 297–307, doi:10.1139/cjfr-2016-0299.
11. Weintraub, A.; Romero, C. Operations research models and the management of agricultural and forestry resources: A review and comparison. *Interfaces* **2006**, *36*, 446–457, doi:10.1287/inte.1060.0222.
12. Viana Céspedes, V. Optimizacion en la Planificacion de Servicios de Cosecha Forestall. Tesis de maestria, Universidad de la República; Magíster en Investigación de Operaciones, Montevideo, Uruguay, 2018.
13. Acuna, M.; Sessions, J.; Zamora, R.; Boston, K.; Brown, M.; Ghaffariyan, M.R. Methods to Manage and Optimize Forest Biomass Supply Chains: A Review. *Curr. For. Rep.* **2019**, *5*, 124–141, doi:10.1007/s40725-019-00093-4.
14. Pohjanmies, T.; Eyvindson, K.; Mönkkönen, M. Forest management optimization across spatial scales to reconcile economic and conservation objectives. *PLoS ONE* **2019**, *14*, e0218213, doi:10.1371/journal.pone.0218213.
15. Shan, Y.; Bettinger, P.; Cieszewski, C.J.; Li, R.T. Trends in spatial forest planning. *Math. Comput. For. Nat.-Resour. Sci.* **2009**, *1*, 86–112.
16. MGAP (Ministerio de Ganadería Agricultura y Pesca); DIEA (Dirección de Estadísticas Agropecuarias). *Anuario estadístico agropecuario 2019*; Editorial Hemisferio Sur: Montevideo, Uruguay, 2019.
17. Instituto Uruguay XXI Informe Anual de Comercio Exterior. 2019, 10, doi:10.1017/CBO9781107415324.004.

18. Dieste, A. Programa de Promoción de Exportaciones de Productos de Madera. *DNIMIEM-CSFM*. 35p. Uruguay. **2012**
19. Resquin, F.; De Mello, J.; Fariña, I.; Mieres, J.; Assandri, L. *Caracterización de la Celulosa de Especies del Género Eucalyptus Plantadas en Uruguay*; Serie Técnica N 152; INIA*:* Montevideo, Uruguay, 2005; p. 82.
20. Andreoni, M.I.; Bussoni, A. Evaluación económica de dos programas de mejoramiento genético en *Eucalyptus grandis*/Economic Assessment of Two Breeding Programs in *Eucalyptus grandis*. *Agrocienc. Urug.* **2014**, *18*, 153.
21. Diaz-Balteiro, L.; Rodriguez, L.C.E. Optimal rotations on *Eucalyptus* plantations including carbon sequestration—A comparison of results in Brazil and Spain. *For. Ecol. Manag.* **2006**, *229*, 247–258, doi:10.1016/j.foreco.2006.04.005.
22. Raymer, A.K.; Gobakken, T.; Solberg, B. Optimal forest management with carbon benefits included. *Silva Fenn.* **2011**, *45*, 395–414, doi:10.14214/sf.109.
23. Quintero-Mendez, M.A.; Jerez-Rico, M. Heuristic forest planning model for optimizing timber production and carbon sequestration in teak plantations. *iForest* **2016**, *10*, 430–439, doi:10.3832/ifor1733-009.
24. Asante, P.; Armstrong, G.W.; Adamowicz, W.L. Carbon sequestration and the optimal forest harvest decision: A dynamic programming approach considering biomass and dead organic matter. *J. For. Econ.* **2011**, *17*, 3–17, doi:10.1016/j.jfe.2010.07.001.
25. Enzinger, S.; Jeffs, C. Economics of forests as carbon sinks: An Australian perspective. *J. For. Econ.* **2000**, *6*, 227–249.
26. Asante, P. Carbon Sequestration and the Optimal Economic Harvest Decision by Patrick Asante A thesis submitted to the Faculty of Graduate Studies and Research in partial fulfillment of the requirements for the degree of Doctor of Philosophy in Forest Biology and Man. Ph.D. Thesis, University of Alberta, Edmonton, AB, Canada, 2011.
27. Loza-Balbuena, I. Impacto del Mercado del Carbono en la Performance Económica de Proyectos Forestales. Estudio de Caso para Uruguay. In *Simposio*

Internacional Medición y Monitoreo de la Captura de Carbono en Ecosistemas Forestales; Valdivia, Chile, 2001; pp. 145–249.

28. Castaño, J.P.; Giménez, A.; Ceroni, M.; Furest, J.; Aunchayna, R.; Bidegain, M. *Caracterización Agroclimática del Uruguay 1980–2009*; INIA: Montevideo, Uruguay, 2011.
29. Methol, R. *SAG Eucalyptus: Sistema de Apoyo A la Gestión de Plantaciones Orientadas A la Producción de Celulosa En Uruguay*; INIA*:* Montevideo, Uruguay, 2008.
30. Methol, R. *SAG Grandis Sistema de Apoyo A la Gestión de Plantaciones de Eucalyptus grandis*; Serie Técnica 131; INIA: Montevideo, Uruguay, 2003.
31. Toochi, E.C. Carbon sequestration: How much can forestry sequester CO_2? *For. Res. Eng.* **2018**, *2*, 148.
32. Hirigoyen, A.; Varo-Martinez, M.A.; Rachid-Casnati, C.; Franco, J.; Navarro-Cerrillo, R.M. Stand Characterization of *Eucalyptus* spp. Plantations in Uruguay Using Airborne Lidar Scanner Technology. *Remote Sens.* **2020**, *12*, 3947, doi:10.3390/RS12233947.
33. Panorama Forestal Nro 34. Available online: http://tardaguila.com.uy/web/forestal?start=16 (accessed on 26 December 2020).
34. Acuna, M.; Strandgard, M.; Wiedemann, J.; Mitchell, R. Impacts of early thinning of a *Eucalyptus* globulus labill. Pulplog plantation in Western Australia on economic profitability and harvester productivity. *Forests* **2017**, *8*, 415, doi:10.3390/f8110415.
35. Yan, Y. Integrate carbon dynamic models in analyzing carbon sequestration impact of forest biomass harvest. *Sci. Total Environ.* **2018**, *615*, 581–587.
36. Bourque, C.P.A.; Neilson, E.T.; Gruenwald, C.; Perrin, S.F.; Hiltz, J.C.; Blin, Y.A.; Horsman, G.V.; Parker, M.S.; Thorburn, C.B.; Corey, M.M.; et al. Optimizing carbon sequestration in commercial forests by integrating carbon management objectives in wood supply modeling. *Mitig. Adapt. Strateg. Glob. Chang.* **2007**, *12*, 1253–1275, doi:10.1007/s11027-006-9072-3.

37. Quintero-Méndez, M.A.; Jerez-Rico, M. Optimizing thinnings for timber production and carbon sequestration in planted teak (Tectona grandis L.f.) stands. *For. Syst.* **2019**, *28*, 1, doi:10.5424/fs/2019283-14649.
38. Rubilar, R.A.; Allen, H.L.; Fox, T.R.; Cook, R.L.; Albaugh, T.J.; Campoe, O.C. Advances in silviculture of intensively managed plantations. *Curr. For. Rep.* **2018**, *4*, 23–34.
39. Keleş, S. Edades óptimas de corte en bosques de álamos híbridos incluyendo captación de carbono: Un estudio de caso en Turquía. *Rev. Chapingo Ser. Cienc. For. Ambiente* **2016**, *22*, 339–349, doi:10.5154/r.rchscfa.2015.12.053.
40. Binkley, D.; Campoe, O.C.; Alvares, C.; Carneiro, R.L.; Cegatta, Í.; Stape, J.L. The interactions of climate, spacing and genetics on clonal *Eucalyptus* plantations across Brazil and Uruguay. Forest *Ecol. Manag.* **2017**, *405*, 271–283 doi:10.1016/j.foreco.2017.09.050.
41. Zhou, W.; Gao, L. The impact of carbon trade on the management of short-rotation forest plantations. *For. Policy Econ.* **2016**, *62*, 30–35, doi:10.1016/j.forpol.2015.10.008.
42. Wang, G.B.; Deng, F.F.; Xu, W.H.; Chen, H.Y.H.; Ruan, H.H. Poplar plantations in coastal China: Towards the identification of the best rotation age for optimal soil carbon sequestration. *Soil Use Manag.* **2016**, *32*, 303–310, doi:10.1111/sum.12284.
43. Resquin, F.; Navarro-Cerrillo, R.M.; Carrasco-Letelier, L.; Casnati, C.R. Influence of contrasting stocking densities on the dynamics of above-ground biomass and wood density of *Eucalyptus benthamii*, *Eucalyptus dunnii*, and *Eucalyptus grandis* for bioenergy in Uruguay. *For. Ecol. Manag.* **2019**, *438*, 63–74, doi:10.1016/j.foreco.2019.02.007.
44. Olschewski, R.; Benítez, P.C. Optimizing joint production of timber and carbon sequestration of afforestation projects. *J. For. Econ.* **2010**, *16*, 1–10, doi:10.1016/j.jfe.2009.03.002.
45. Ruíz-Peinado Gertrudix, R. Modelos para la estimación del carbono en la biomasa de los sistemas forestales. Influencia de la selvicultura en los stocks de carbono. *Cuad. Soc. Esp. Cienc. For.* **2013**, 231, doi:10.35376/10324/4437.

46. Callaghan, D.W.; Khanal, P.N.; Straka, T.J.; Hagan, D.L. Influence of forestry practices cost on financial performance of forestry investments. *Resources* **2019**, *8*, 28, doi:10.3390/RESOURCES8010028.
47. Loisel, P. Under the risk of destructive event, are there differences between timber income based and carbon sequestration based silviculture? *For. Policy Econ.* **2020**, *120*, 102269, doi:10.1016/j.forpol.2020.102269.
48. Romero, C.; Putz, F.E. Financial viability and carbon payment potential of large-scale silvicultural intensification in logged dipterocarp forests in Indonesia. *For. Policy Econ.* **2017**, *85*, 95–102, doi:10.1016/j.forpol.2017.09.005.
49. Blouin, M.; Cormier, D. Carbon and greenhouse gas accounting of forest operations in FPInterface. *Int. J. For. Eng.* **2012**, *23*, 64–69.
50. Dumortier, J. The effects of uncertainty under a cap-and-trade policy on afforestation in the United States. Environ. *Res. Lett*. **2013**, ***8***, 11.

7. DISCUSIÓN GENERAL

Un manejo forestal sostenible incluye la administración de los recursos forestales, así como actividades de recolectar, analizar e interpretar los diferentes parámetros dendrométricos, ecológicos, económicos y sociales; estableciendo metas y programando acciones para lograr los resultados esperados (Silva de Carvalho, 2016). Se generan así, información y estadísticas que se emplean, por ejemplo, para planificar programas forestales (a nivel empresa o regionales), evaluar la sostenibilidad de los recursos forestales, calcular inversiones forestales, evaluar el impacto ambiental, planificar a nivel estratégico y presentar informes a entidades internaciones o nacionales (Kangas et al., 2018). En esta visión, el inventario forestal tiene un papel clave ya que debe brindar el apoyo técnico y científico necesario para que se logren los objetivos propuestos. El uso de nuevas técnicas y métodos estadísticos, combinados con el uso de datos de teledetección, representa una gran oportunidad para cuantificar y estimar los rendimientos, la capacidad productiva, mejorar la gestión de los montes, aumentando la cantidad y calidad de la información generada en los inventarios forestales. Esta tesis proporciona herramientas que permiten mejorar la precisión en cuatro aspectos fundamentales para la cuantificación y manejo del stock forestal: i) el uso de modelos compatibles y aditivos; ii) el modelado de las variables del rodal a gran escala empleando datos de teledetección; iii) la delimitación de zonas homogéneas dentro del rodal basada en una evaluación no supervisada; y iv) un método de optimación de los planes de cosecha basado en la disponibilidad de madera, los precios del carbono y la edad de corta.

La modelación forestal es clave para contar con datos completos e informativos de las actividades silvícolas (Pretzsch y Rais, 2016). Las mediciones realizadas en parcelas y el uso de modelos de predicción son la base de todo inventario forestal. Muchas veces estos modelos no están validados o calibrados para las zonas en las que se emplean, brindando información sesgada o poco precisa (Scolforo et al., 2019). El ajuste de modelos de estimación para las variables productivas forestales mediante procesos que aseguren la aditividad y la

compatibilidad, empleando datos de la misma zona, de la misma especie y en el rango de edades derivados del inventario, aseguran resultados adecuados y coherente a lo largo de todo el proceso de gestión.

El inventario tradicional en las parcelas de calibración es clave para asegurar el correcto flujo de información. El tipo de parcela a emplear dependerá de la estructura y de la homogeneidad del rodal. La forma y el tamaño de la parcela tiene un efecto menor sobre la precisión de los resultados, siendo la fuente principal de incertidumbre la falta de coincidencia espacial entre los datos de teledetección y de las parcelas, generando errores de ubicación que se propagan a los modelos (Kangas et al., 2018). Se debe planificar la cantidad y la distribución de las parcelas para fines de modelado desde el análisis previo de los datos de teledetección, los cuales exhibirán las características biofísicas del área. Para fines de modelado, es aconsejable datos con la mayor variación posible en las variables explicativas (Kangas et al., 2018). La información precisa reduciría la necesidad de inventarios previos a la cosecha y luego posiblemente introducirá importantes ahorros de costos. Además de los mapas de recursos forestales, la planificación operativa se beneficiaría de mapas sobre la accesibilidad del terreno (por ejemplo, Ågren et al., 2014).

La teledetección se ha empleado para la producción y la generación de mapas más que para la estimación de parámetros regionales (Kangas et al., 2018). Los avances en los sensores de teledetección y en las tecnologías de toma y procesamiento de datos, han creado varias posibilidades para la producción rentable de conjuntos de datos forestales sobre grandes superficies. Sin duda, esto repercute también en la forma en que se planifican y realizan los inventarios forestales, lo que ocurre actualmente en varios países, que se mapean los recursos forestales utilizado el escaneo LiDAR aerotransportado (ALS) en lugar de la fotointerpretación clásica (Kangas et al., 2018). En esta tesis, se ha proporcionado un marco teórico-práctico para el uso de datos LiDAR y multiespectrales en modelos predictivos para el índice de área foliar (IAF), la biomasa área total (BMT), el volumen total (VT) y la altura media dominante (Ho) a nivel de rodal, empleando métodos paramétricos y no

paramétricos (Figura 2). Así como, métodos de segmentación no paramétrica para la obtención de rasters de distribución de BMT y VT con niveles de error bajos y relacionados con la calidad del sitio (inferida a través de la Ho). El interés en la predicción del IAF radica en que constituye una de las variables fisiológicas clave para comprender la dinámica y el crecimiento de los bosques y se ha utilizado ampliamente en modelos forestales. En este estudio, se aplicó un enfoque de modelado para estimar IAF que integra fuentes de datos de teledetección.

En la construcción de mapas, con las variables forestales de interés medidas a partir de las parcelas de campo, se predice su valor en las celdas de la cuadrícula sin mediciones, según las características establecidas para el tamaño de pixel de los productos LiDAR. El uso de técnicas no paramétrica, como la imputación k-NN, permiten que todas las características se pueden estimar al mismo tiempo, utilizando el mismo enfoque (Zianis y Mencuccini, 2003). Al usar este tipo de estimaciones, se flexibilizan los supuestos de la regresión clásica la cual también se utiliza a menudo con fines de mapeo. El empleado de datos de teledetección (LiDAR e imágenes multiespectrales) presenta una alternativa para realizar relevamientos a gran escala y con mayor velocidad que los inventarios tradicionales. Los relevamientos con teledetección tienen bajo coste por unidad de superficie en la realización de cartografía e inventarios.

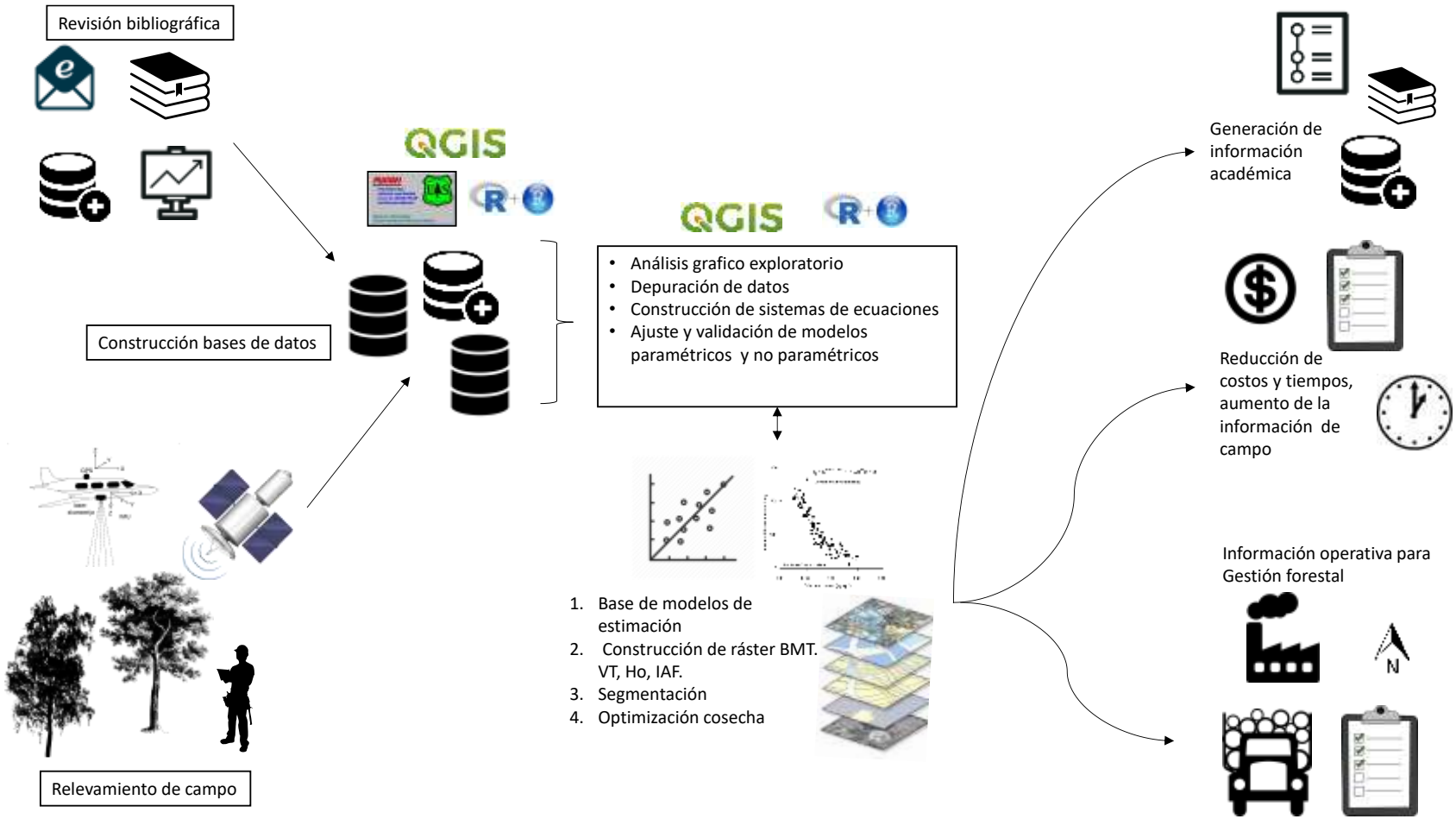

Figura 2: Flujo e integración de procesos y metodologías incluidas en el estudio.

Los datos de teledetección aportan información sobre las características estructurales del bosque, poseen un gran potencial para realizar mediciones directas y estimaciones de variables dendrométricas. Además, brindan información tridimensional geográficamente extensa, continua y de alta precisión, lo que supone contar con un gran volumen de información sobre la estructura del bosque. Por otro lado, además de las métricas utilizadas en la modelación, se obtienen Modelos Digitales del Terreno, de Superficie y de Vegetación que permiten el estudio del medio físico, la ordenación de un determinado territorio o evaluación de otros parámetros ambientales (Dong y Chen, 2017). Trabajar con grandes cantidades de datos requiere de algoritmos cada vez más sofisticados, capaces de manejar y detectar relaciones poco claras. En este sentido, se ha desarrollado una amplia gama de algoritmos de aprendizaje automático, tanto para resolver problemas de clasificación, como de regresión. El presente trabajo permitió evaluar la capacidad de la información generada en el procesado de datos LiDAR e imágenes multiespectrales, combinado con diferentes metodologías estadísticas para la estimación de variables de interés en la gestión forestal (Figura 2). Si bien este estudio se centró en inventarios de rodales dedicados a la producción de pulpa, las metodologías derivadas del mismo son trasladables a rodales con otros destinos (biomasa o madera sólida) u otras especies (por ejemplo, en bosque nativo). Las empresas forestales y el pequeño productor pueden utilizar estos modelos en la optimización del trozado de los troncos, en la planificación de la adquisición de madera o biomasa, en la logística del movimiento de madera y las cosechas en función de la demanda actual o la selección del uso óptimo para cada rodal.

7.1. MODELOS Y SILVICULTURA

En este estudio, para mejorar la estimación de la biomasa total área y sus componentes, se propuso un sistema aditivo que asegura que las funciones de estimación de los componentes sean compatibles con la biomasa total estimada. Las estadísticas de validación y el ajuste del modelo indican que los sistemas de ecuaciones desarrollados en este estudio contribuirán a la estimación precisa de la

biomasa total. Los métodos de ajuste aditivo no pretenden mejorar la precisión de las estimaciones de BMT, sino más bien conciliar las estimaciones de la biomasa total y la suma de las fracciones de biomasa (Coutinho et al., 2018). El enfoque de ajuste individual clásico, para ecuaciones de biomasa ignora la correlación inherente entre los componentes de biomasa medidos en los mismos árboles y en la misma parcela. Tener en cuenta esta correlación en el desarrollo de un sistema de ecuaciones de biomasa aditiva produce una mayor eficiencia estadística (Parresol, 2001). Algunos autores (Parresol, 2001, Carvalho y Parresol, 2003) han comparado diferentes métodos para lograr la aditividad, concluyendo que NSUR logra estimaciones más eficientes y debería ser la opción para la aditividad. En el presente trabajo, una vez ajustado individualmente cada componente de la biomasa, los modelos seleccionados se ajustaron simultáneamente utilizando la metodología NSUR. Los sistemas simultáneos obtenidos tendieron a sesgar ligeramente las estimaciones de BMT, en un 0,25%, 0,42% para *E. dunnii* y *E. grandis* respectivamente. En nuestro estudio, para ambas especies, la estimación por NSUR tuvo un sesgo menor que los otros métodos, oscilando entre -7,9 y 7,7 y entre -11,8 y 24,7 para *E. dunnii* y *E. grandis*, respectivamente. Esto representa una mejora con respecto al enfoque individual tradicional, que dio valores que van desde -18,3 a 13,7 para *E. dunnii* y de -13,2 a 48,5 para *E. grandis*, y el enfoque de suma WLS, con rangos de -18,3 a 21,9 y -16,7 a 35,2 para *E. dunnii* y *E. grandis*, respectivamente. En general, la mayor sobreestimación obtenida por los enfoques WLS en comparación con NSUR refleja la ganancia en la calidad de predicción obtenida al aplicar este último. Según Scolforo et al. (2019), al comparar el ajuste individual y NSUR, se puede ver que ambos enfoques tienen estadísticas de precisión similares. La inclusión de las correlaciones contemporáneas, entre la biomasa de los componentes y la biomasa total en el ajuste de los sistemas de ecuaciones a través de NSUR resultó en una ganancia de eficiencia, al reducir los intervalos de confianza y predicción de las estimaciones de biomasa (Parresol, 1999).

Los resultados de las ecuaciones de ahusamiento, de volúmenes totales y comerciales, ajustadas para ambas especies indicaron que el modelo propuesto por Fang et al. (2000) fue el más preciso y el menos sesgado. Para asegurar la

consistencia numérica se utilizó un procedimiento de ajuste simultáneo basado en el método de estimación FIML. Este método se ha utilizado con éxito en varios estudios porque optimiza los parámetros de ahusamiento y de volumen comercial, al tiempo que minimiza y homogeneiza la desviación estándar. Investigaciones anteriores encontraron que la modificación del modelo de exponente variable de Muhairwe era el mejor modelo para describir la forma del fuste de *E. grandis* (Gomat et al,. 2011). Por otro lado, Methol (2008) ajustó el modelo segmentado de Max y Burkhart (1976) para ambas especies, modelo que ocupó el segundo lugar en nuestro estudio. El sistema de Fang et al. (2000) se usa ampliamente para la descripción de la forma de los fustes y el volumen, su implementación ha sido reportada en sistemas biométricos para una amplia gama de especies y países (Tang et al., 2016, Diéguez-Aranda et al., 2006). Este modelo tiene el mérito de ser muy flexible y analíticamente integrable en un sistema que proporciona estimaciones muy precisas del volumen del fuste para cualquier segmento del mismo. Rachid- Casnati et al. (2014) han ajustado para *E. grandis* el modelo explícito para volumen total de Schumacher-Hall, este modelo se ha integrado al modelo ajustado en este estudio. La calidad de ajuste en términos de eficiencia del modelo fue similar en ambos estudios, el RSME fue levemente menor en Rachid-Casnati et al. (2014), y los valores de los parámetros fueron similares, con pequeñas diferencias atribuibles al ajuste simultáneo aplicado en este estudio (Liu et al., 2020, Sharma y Parton, 2009). Las funciones de volumen tradicionales no consideran la dependencia del volumen de la competencia o la forma del fuste, generalmente involucran Dap y Ht como variable de predicción (Spurr, 1954). Incluyendo la edad y la densidad de los árboles, se tiene en cuenta parte de la variabilidad del sitio que afecta las condiciones de crecimiento de cada árbol individual. Con esto se logra mejorar las predicciones de la conicidad (Liu et al., 2020). En este estudio, la densidad del rodal tuvo una influencia estadísticamente significativa en la estimación del volumen para *E. grandis*, mientras que para *E. dunnii* el rango limitado de densidad del rodal en comparación con *E. grandis* podría ser demasiado estrecho para explorar adecuadamente los efectos sobre el volumen. Los resultados no mostraron diferencias en la forma del fuste por rango de densidad, Ahnlund et al., (2014) encontraron resultados similares con *Pinus*

sylvestris, donde no hubo diferencias significativas en la forma del fuste para árboles con Dap> 5 cm entre tratamientos de densidad. A diferencia de lo informado por Jacobs et al., (2020) sobre la existencia de efectos de la densidad en la forma del fuste, los troncos de árboles del mismo tamaño disminuyeron en ahusamiento debido al aumento de la competencia. Los resultados mostraron que la densidad del rodal tuvo un efecto sobre los parámetros de volumen para *E. grandis*.

7.2. SENSORAMIENTO REMOTO E INVENTARIO FORESTAL

El LiDAR ha sido la principal fuente de datos para el inventario y para la delimitación de los rodales tanto en Finlandia como en Noruega desde 2010; en estos países los inventarios se llevan a cabo con datos de ALS y parcelas de campo para la calibración de modelos (Kangas et al., 2018). Los métodos de estimación de Ho, VT y BMT que utilizan métricas LiDAR son métodos de regresión simple, mínimos cuadrados ordinarios (OLS) o ponderados (WLS), y métodos no paramétricos: *Random Forest* (RF), *Support vector machine* (SVM) o métodos basados en el vecino más cercano (k-NN) (Guerra-Hernández et al., 2016). En este trabajo se ha comparado el rendimiento de estos métodos paramétricos y no paramétricos para estimar BMT, VT y Ho, utilizando datos LIDAR a nivel del rodal.

Los sensores ALS se han utilizado ampliamente para la determinación de parámetros vegetales, incluidos AGB y VT (Yang et al., 2019), siendo una tecnología adecuada para el inventario y la ordenación forestal. Con respecto a la selección de métricas LiDAR, para los modelos paramétricos, los mejores predictores de Ho se relacionaron con los percentiles más altos de la nube de puntos (Percentiles 90 y 99). Las métricas de altura LIDAR, como los percentiles de altura, son frecuentes en estudios de inventarios forestales. Para los modelos de volumen y biomasa, los percentiles medio o medio-alto de la nube de puntos (Percentiles 70 y 75) tuvieron mayor importancia. Estas estadísticas medias-altas de la nube de puntos informan sobre las propiedades de la copa de los árboles (Matasci et al., 2018) y se han utilizado para explicar otras variables del árbol (por ejemplo, el diámetro del fuste). Por lo tanto, se espera que los percentiles 70 y 75 reemplacen el Dap en las ecuaciones desarrolladas para calcular las variables a partir de datos de campo. Para

los modelos no paramétricos, todos los modelos k-NN incluyeron al menos una variable relacionada con las métricas de altura y la forma de la distribución de altura y la mayoría de los modelos incluyó una variable relacionada con métricas de cobertura. Según estudios previos, la combinación de la altura y la densidad en las métricas del dosel representan una descripción de la estructura vertical de la masa forestal (Jayathunga et al., 2019). Los modelos k-NN para BTM, VT y Ho obtenidos para las dos especies de *Eucalyptus* incluyeron sólo una variable relacionada con los percentiles medio-altos de la nube de puntos, así como variables relacionadas con la densidad del dosel. Los resultados demuestran que Percentil 75 es potencialmente útil para mejorar los modelos forestales.

Nuestros resultados mostraron que tanto WLS como k-NN son métodos adecuados para predecir BMT, VT y Ho utilizando datos LIDAR. En nuestro estudio, en los modelos de VT, el R^2-adj fue de 0,91 para *E. grandis* y 0,92 para *E. dunnii*. Los modelos para BMT tenían la misma variable independiente que los modelos VT, para ambas especies, pero los valores R^2-adj fueron de 0,86 y 0,85 para *E. grandis* y *E. dunnii*, respectivamente. En los modelos de Ho se obtuvieron un R^2-adj de 0,98; para *E. grandis*, y R^2-adj de 0,96 para *E. dunnii*. La comparación de los resultados de los modelos paramétricos seleccionados con los modelos no paramétricos muestra pequeñas diferencias.

Los valores de IAF de eucaliptus medidos en campo variaron entre 1,17 y 5,07 $m^2\ m^{-2}$, con valores medios de 2,95 y 3,26 $m^2\ m^{-2}$ para *E. grandis* y *E. dunnii*, respectivamente. Estos valores están dentro del rango reportado por Scurlock et al. (2001) en su revisión, con un valor IAF para especies de *Eucalyptus* de 3,51 $m^2\ m^{-2}$, y por Whitehead y Beadle (2004) quienes reportaron un valor de 3,19 $m^2\ m^{-2}$. Nuestros resultados demuestran que la combinación de los conjuntos de datos LiDAR: métricas clásicas (ALSm), parámetros estructurales de la pseudo forma onda (PFO) e índices laser de penetración (LPI), junto con datos multiespectrales fue adecuada para la estimación de IAF. Al seleccionar variables LiDAR según su importancia en la estimación de IAF, una métrica de cobertura del dosel, una métrica de altura, un índice de penetración laser y un parámetro de forma de onda siempre

resultaron seleccionados. La fracción de cabida cubierta (FCC) fue seleccionada en todos los modelos de estimación. La FCC corresponde a la cobertura del dosel superior, donde se esperaba la mayor densidad de follaje. La diferencia en la ramificación entre las dos especies significó que los modelos IAF para *E. dunnii* seleccionaron percentiles de altura media (Percentil 40) mientras que en *E. grandis* incluyeron percentiles de altura alta (Percentil 99). El índice de penetración laser está relacionado con el desarrollo del dosel; cuanto más cercana y densa es la vegetación, menos pulsos de láser penetran para llegar al suelo (Peduzzi et al., 2012). Por lo tanto, el LPI se ha utilizado para predecir el IAF y los modelos que incluyen esta variable pudieron explicar el 80% o más de la variación del IAF (Peduzzi et al., 2012). El LPI seleccionada para *E. grandis* y *Eucalyptus* fue una métrica de alturas de retorno (LPI 4), mientras que para *E. dunnii* el LPI más importante se centró en la intensidad (LPI 7). Esto puede estar relacionado con las características de las dos especies; la respuesta espectral de las hojas en *E. dunnii* fue más sensible a la radiación infrarroja, relacionada con un estado más saludable de las plantaciones. La curva de distribución vertical de la onda LiDAR contiene información que puede complementar la que aportan las métricas derivadas de los retornos (Zhou y Qiu, 2015). En este trabajo utilizamos los datos de retorno discreto para crear pseudo formas de onda (PFO) como la distribución de frecuencia vertical de la suma de la intensidad, en función de los intervalos de altura (Zhou y Qiu, 2015). Las PFO se construyeron modificando el método propuesto por Luo et al., (2019). En cada parcela, las nubes de puntos ALS fueron separadas por valores de elevación, los cuales fueron asignados a los rangos de altura con un intervalo de 0,5 m. La intensidad de retorno relativa en cada intervalo de altura se calculó dividiendo la suma de la intensidad en cada intervalo de altura por la intensidad total (Peduzzi et al., 2012). Los datos de PFO se obtuvieron conectando con una línea curva la intensidad correspondiente a la elevación de cada intervalo de altura. Cada serie PFO se analizó para identificar el número de picos y su forma como una función de densidad. Para distinguir y comparar entre diferentes PFO, se registraron las medidas estadísticas como asimetría, curtosis, desviaciones estándar y coeficiente de variación (Zhou y Qiu, 2015).

En nuestro estudio, se eligió un enfoque basado en SVM para predecir el IAF en *E. dunnii*, *E. grandis* y *Eucalyptus* (sin diferenciar especies). Su capacidad para manejar la no linealidad y cuantificar la importancia de las variables independientes hace que SVM sea un algoritmo eficaz. ANN se ha implementado en una amplia gama de análisis con ALS y datos multiespectrales en investigaciones agrícolas y forestales (Mountrakis et al., 2011). Sin embargo, en nuestro estudio, ANN mostró una pobre predicción de IAF, lo que contrasta con otros estudios donde ANN resultó más eficiente que RF y SVM para predecir los parámetros estructurales del bosque (incremento de diámetro, altura, Dap) (Júnior et al., 2020). Los mejores modelos, con el R^2 más alto (> 0,78) y el nRMSE más bajo (0,137 m^2 m^{-2}), incluyeron cuatro (*E. grandis* y *E. dunnii*) o tres (*Eucalyptus*) ALSm. Estos resultados son consistentes con estudios previos. Al evaluar *E. grandis*, Tesfamichael et al., (2018) logró R^2 = 0.67 con dos métricas LiDAR (altura y desviación estándar de puntos por debajo de la décima altura) y obtuvo R^2 = 0.83 al emplear 14 métricas (con problemas de colinealidad). Peduzzi et al., (2012) obtuvieron modelos con valores de R^2 entre 0,61 (dos variables) y 0,83 (seis variables); Jensen et al., (2008) informaron valores estimados de IAF con R^2 de 0,86 (RMSE = 0,76) y 0,69 (RMSE = 0,61).

La integración de los índices de vegetación (IV) derivados de imágenes Planet mejoró notablemente la estimación de IAF con respecto a los resultados obtenidos por ALSm y PFO. El uso de IV multiespectrales de alta resolución espacial puede proporcionar firmas espectrales continuas y detalladas de los atributos biofísicos del bosque (Shen et al., 2018). Con la adición de IV, la mejora en la precisión de los modelos predictivos fue significativa. En general, los IV basados en NIR (es decir, NDVI y GNDVI) se desempeñaron mejor en términos de evaluación de IAF que los otros índices evaluados. Se seleccionaron el NDVI para *E. dunnii*, el GNDVI para *E. grandis* y el NDVI para *Eucalyptus*, siendo la mejora en nRMSE del 16%, 51% y 39%, respectivamente. La ganancia en la varianza explicada (R^2) fue del 14% (*E. dunnii* y *E. grandis*) y del 7% (*Eucalyptus*) al usar estos IV.

7.3. RODALIZACIÓN A PARTIR DE DATOS DE INVENTARIO

Los mapas de existencias, en volumen y en biomasa, pueden ser rodalizados (segmentados) en regiones más pequeñas y homogéneas. La segmentación junto con las estimaciones de BMT, VT y Ho se pueden utilizar para la planificación del manejo forestal. Los valores del índice de Moran normalizados y la varianza ponderada normalizada incluida en la Puntuación Global de las segmentaciones, indican que la segmentación usando Orpheo ToolBox (OTB), detectó segmentos homogéneos de forma correcta, de acuerdo con investigaciones anteriores (Varo-Martínez et al., 2017). La implementación de OTB para la delimitación de masas forestales ha demostrado ser más simple, más eficiente y de similar precisión en comparación con otros métodos más complejos. Visual y cuantitativamente, los resultados muestran que el método de segmentación propuesto produjo una segmentación de alta calidad en comparación con la segmentación manual. Por lo tanto, la segmentación OTB podría utilizarse para segmentar automáticamente masas de eucaliptus, produciendo rodales que un experto podría identificar de manera similar con fotografía tradicional (Ahmad et al., 2018). Los resultados son consistentes con otros estudios que utilizan LiDAR para la automatización de la delimitación del rodal aplicada en el campo del inventario forestal. La implementación de un método de segmentación como OTB, mejora el tiempo de procesamiento aumentando el área cubierta y maximizando la eficiencia laboral. La segmentación propuesta en este estudio define rodales basados en VT o BMT con un índice de sitio similar (por Ho).

7.4. OPTIMIZACIÓN DE COSECHA

Cuantificar el impacto del carbono (C) y los precios de la madera en el retorno económico de las plantaciones de rotación corta es fundamental para definir estrategias de manejo sostenible para que puedan proporcionar productos maderables y contribuir al secuestro de C. En este estudio se trabajó con un modelo de programación que optimiza la edad de rotación y el cronograma de cosecha de los rodales y maximiza el Valor Actual Neto (VAN) durante un período de planificación

de hasta 15 años. El modelo incluyó ingresos por la venta de madera y créditos del C secuestrado durante la vida de los rodales. Además, se incluyeron en el análisis los costos de establecimiento, manejo, cosecha y transporte de la plantación. Se trabajó con dos escenarios, uno que incluye ingresos solo por la venta de madera generada durante la corta final (ES1), y otro incluyendo los ingresos de la madera generada durante la cosecha y del C secuestrado durante la rotación de los rodales (ES2).

Los resultados obtenidos en este estudio han demostrado que pagar por el secuestro de C puede incrementar los retornos económicos en plantaciones de rotación corta dependiendo de las condiciones del mercado. Optimizar los cronogramas de cosecha y la edad de rotación de los rodales considerando C y los precios de la madera es clave para maximizar el uso de los recursos forestales bajo esquemas de silvicultura intensiva (Acuna et al., 2021). Los resultados mostraron que el VAN fue bastante sensible a los precios C evaluados. Para cualquier precio de C, la suma de los ingresos de los créditos C y los de la venta de madera dieron los mejores rendimientos económicos. Los precios altos de C aumentaron la contribución proporcional de los créditos de C al VAN y redujeron la de la venta de madera de celulosa, lo que confirmó los hallazgos mostrados en estudios previos (Bourque et al., 2007; Pukkala, 2020, Acuna et al., 2021). Se utilizaron tasas de crecimiento para calcular las existencias de C en la biomasa aérea y se realizó un análisis de sensibilidad para cuantificar el efecto de la tasa de interés (TI), así como los precios del C y de la madera sobre el VAN y las rotaciones óptimas de los rodales. Siguiendo enfoques similares a los de estudios previos (Díaz-Balteiro y Rodríguez 2006), los ingresos brutos en cada rodal se computaron por la venta de madera, así como por los créditos asociados con el secuestro de C debido al crecimiento forestal. Además, las emisiones de C en el momento de la cosecha y los costos asociados con el manejo de los rodales se utilizaron para cuantificar los ingresos netos y el VAN. Teniendo en cuenta todas estas consideraciones, nuestro enfoque de modelado de optimización demostró ser un método práctico y eficaz para determinar cómo el C y los precios de la madera afectan la programación de la cosecha y los retornos económicos en las plantaciones de eucaliptus de rotación corta.

El cronograma de cosecha proporcionado por nuestro enfoque de solución maximizó los ingresos de la captura de madera y C en cada rodal. Este plan se generó mediante un modelo de programación matemática que optimizó la edad de rotación de los rodales, y que sirvió de base para programar nuevas plantaciones. Como se confirma en nuestro estudio, la integración de datos de campo y de sensores remotos (por ejemplo, LiDAR) y los modelos de planificación óptimos son fundamentales para maximizar los resultados económicos y silvícolas de los planes de manejo forestal (Rubilar et al., 2018; Hirigoyen et al., 2020). Además, determinar la edad de rotación óptima que incluya múltiples productos y servicios de los ecosistemas forestales es esencial para implementar estrategias de manejo forestal sostenible (Keleş, 2016). Las rotaciones biológicas óptimas vienen dictadas por la tasa anual de acumulación de C en la biomasa de los árboles. Por ejemplo, para las plantaciones de eucaliptus de rotación corta en China subtropical, Zhou et al., (2007), mostraron que la tasa marginal anual de acumulación de C aumentó del año 4 al año 10, y disminuyó drásticamente del año 13 al año 21, lo que sugiere un óptimo rotaciones entre 12 y 15 años. Sin embargo, las rotaciones óptimas económicas y biológicas suelen diferir ya que la primera se determina al incluir restricciones operativas además de los costos de gestión y los precios de múltiples productos, como la madera y el C, como hicimos en nuestro estudio.

En cuanto a las rotaciones económicas óptimas, Díaz-Balteiro y Rodríguez (2006) desarrollaron varios modelos utilizando programación dinámica para calcular la rotación óptima para plantaciones intensivas de eucaliptus en España y Brasil. Su enfoque de solución no incluyó restricciones operativas como en nuestro estudio, pero se centró en determinar la edad de rotación económica utilizando el valor esperado de la tierra. Independientemente del enfoque de la solución, cuando se incluyen los ingresos combinados de la madera y el secuestro de C, la edad de rotación óptima tiende a aumentar cuando los precios del C son altos, según lo informado por varios autores (Diaz-Balteiro et al., 2009, 2014; Keleş, 2016), sin embargo, esto dependerá de la tasa anual de secuestro de C. En nuestro estudio, la tasa anual de C secuestrado aumentó continuamente hasta el año 10, que fue establecido por el productor forestal como la duración máxima de rotación para

cualquier rodal en la finca de la plantación. Además de las tasas anuales de captura de C, la duración de la rotación se determinó mediante la relación entre la madera (trozas) y los precios del C.

Por lo tanto, el impacto de los ingresos por C sobre el VAN fue más pronunciado cuando los precios del C eran altos y excedían a los de las trozas; esto resultó en las rotaciones óptimas de los rodales eran más largas cuando los precios de C eran más altos y más cortas cuando los precios de C eran más bajos. La proporción de rodales con mayores edades de rotación fue mayor cuando TI fue del 6% y menor cuando fue del 8% o 10%. Una rotación óptima de 8 años se ha vuelto muy popular en las plantaciones de eucaliptus orientadas a la pulpa en Uruguay, basándose principalmente en las cifras de IMA de estudios anteriores (Binkley et al., 2017). Los resultados reportados en nuestro estudio muestran que las rotaciones óptimas pueden oscilar entre 7 y 10 años sin afectar los retornos financieros y el secuestro de C. Sin embargo, los impactos de rotaciones más cortas (<7 años) deben investigarse más a fondo, ya que esta estrategia podría tener implicaciones negativas en el suministro de madera y los beneficios económicos. Es fundamental monitorear y cuantificar las existencias de C utilizando modelos locales (Resquin et al., 2019) y datos de inventario recolectados con tecnologías de teledetección (Hirigoyen et al., 2020).

En el caso de nuestro estudio, los rendimientos descontados provienen principalmente de la venta de madera cuando los precios de C eran menores o iguales a 15 $ t^{-1}, y del secuestro de C cuando los precios de C eran mayores de 15 $ $t^{-1.}$ La alta volatilidad de los precios en el mercado de C podría estar asociado con una incertidumbre significativa en los ingresos de C y debería ser un factor importante a considerar en el análisis económico de la silvicultura intensiva (Olschewski y Benítez, 2010; Keleş, 2016).

Nuestros resultados también mostraron que la disposición espacial de los rodales cosechados por período es sensible a los precios del C. Los resultados revelaron que la disposición espacial, así como el número de rodales a recolectar en cada período, eran sensibles a los precios del C. Con precios bajos del carbono (0 y 5 $ t^{-1}), el modelo apuntó a maximizar el VAN y los retornos de la venta de madera, lo que resultó en la recolección de una gran proporción de rodales en los años 7 y 8;

estos rodales se asociaron con menores costos de cosecha y transporte debido a su rendimiento por hectárea y la distancia a las plantas de celulosa. Por el contrario, con precios altos de C (20 y 30 $ t^{-1}), el modelo tenía como objetivo maximizar el VAN y los retornos del secuestro de C, lo que resultó en edades de rotación óptimas más largas (9 y 10 años). Esto resultó en la cosecha de una gran proporción de rodales de altas tasas de crecimiento que alcanzaron altos rendimientos por hectárea en los años 9 y 10.

A nivel mundial, los planificadores forestales están preocupados por la sostenibilidad del uso de los bosques, y muchos propietarios de bosques y agencias gubernamentales han comenzado a considerar estrategias para aumentar la captura de C en sus planes de manejo forestal y tala (Acuna et al.2021). Los modelos económicos de programación lineal de manejo forestal que incluyen el secuestro de C en plantaciones intensivas de eucaliptus son una herramienta poderosa para optimizar su papel en la mitigación del cambio climático (Ruiz-Peinado et al., 2017). Estas técnicas de solución basadas en la optimización son esenciales para cuantificar el valor económico y la contribución potencial de los bosques naturales y las plantaciones al cambio climático con base en los retornos integrados obtenidos de múltiples servicios ecosistémicos y productos forestales (Callaghan et al., 2019). La silvicultura realizada con el objetivo de maximizar el C promueve el crecimiento y la conservación de las existencias de biomasa en pie, ya sea modificando las estrategias estándar de manejo forestal u optimizando la edad de rotación (Loisel, 2020).

8. CONCLUSIONES Y PERSPECTIVAS

8.1. CONCLUSIONES GENERALES

Se presentan a continuación las conclusiones específicas que se derivan de los diferentes trabajos abordados para alcanzar los objetivos propuestos

- La aplicación de herramientas de geomática forestal en el sector forestal supone cambios en las prácticas de inventarios, desde su planificación, ejecución y resolución, así como la capacidad de generar modelos predictivos de variables dasométricas y algoritmos de rodalización con una precisión mayor a las obtenidas con inventarios de campo.
- Se estimó la biomasa total aérea de *E. grandis* y *E. dunnii* utilizando un enfoque NSUR. Representando el primer intento de cuantificar la biomasa total de árboles con un sistema de ecuaciones no lineales ponderadas, ajustadas simultáneamente para plantaciones en Uruguay.
- Los modelos alométricos ajustados utilizando la metodología NSUR proporcionaron estimaciones de biomasa total y de sus fracciones, precisas y que garantizan la aditividad entre componentes para *E. grandis* y *E. dunnii* en Uruguay.
- El sistema de ahusamiento-volumen compatible de Fang et al. (2000) se propone como el más adecuado para describir el perfil del fuste y predecir el volumen total y comercial de *E. dunnii* y *E. grandis*.
- Para *E. grandis*, el ajuste del sistema y su rendimiento de predicción, mejoraron al incluir la densidad del rodal dentro de la ecuación de volumen. Para *E. dunnii* no se observó ninguna mejora probablemente debido a un rango de población estrecho en el conjunto de datos.
- En el ajuste de modelos de estimación basados en métricas LiDAR, los métodos paramétricos tuvieron un mejor desempeño para la altura dominante (Ho), y los métodos no paramétricos entregaron mejores resultados en términos de precisión y sesgo para el volumen (VT) y la biomasa (BMT).
- Se lograron mapas de alta resolución espacial para Ho, VT, y BMT a partir de los datos LIDAR que se han empleado para la segmentación a escala de

rodal. Los métodos paramétricos tuvieron un mejor desempeño para Ho, y los métodos no paramétricos entregaron mejores resultados en términos de precisión y sesgo para el VT y la BMT.

- La metodología de rodalización (segmentación) propuesta proporciona un modelo rentable y fácil de actualizar para la generación de mapas de BMT o VT para tareas de cosecha, basado en rasters derivados de métricas LIDAR.
- La rodalización obtenida brinda herramientas que permiten mejorar la precisión en dos pasos fundamentales en la cuantificación del stock forestal: el modelado de las variables del rodal (biomasa aérea, volumen total y altura dominante), utilizando LiDAR, y la delimitación de la estructura del rodal basada en una evaluación no supervisada. La metodología de segmentación propuesta permite generar y actualizar de manera sencilla rasters de BMT o VT para tareas de cosecha y ordenamiento forestal.
- Para la estimación de IAF los modelos SVM y RF fueron más precisos que el modelo ANN para *Eucalyptus grandis*, *E. dunnii* y ambas especies juntas. Los modelos seleccionados incorporan métricas LiDAR (percentiles de altura del árbol superior o medio y la fracción de cobertura del dosel), parámetros de pseudo-formas de onda (coeficiente de variación y asimetría) e índices de vegetación (NDVI y GNDVI).
- El uso de datos procedentes de diferentes sensores y plataformas incrementa las posibilidades de automatización de inventarios forestales, y del análisis de los mismos mediante la integración de basas de datos e información complementaria (sensores pasivos y activos), aumentando la resolución espacial y temporal de la cartografía forestal.
- La optimización mediante técnicas de programación lineal es una herramienta básica para el manejo forestal óptimo de las plantaciones de eucaliptus en Uruguay.
- Los planes de manejo deben basarse en un modelo de programación matemática para formular la organización espacial y económica, mediante la integración de datos de campo, herramientas de teledetección (por ejemplo, LiDAR) y modelos de estimación de crecimiento.

- La integración de los ingresos de la madera y el secuestro de C aumentó las edades óptimas de rotación y aumentó los ingresos económicos en los rodales de eucaliptus. La edad de rotación óptima fue de 7 años (dependiendo de las tasas de interés) para precios de C por debajo de 5 $ US, y cuando los precios de C aumentaron, las edades de rotación óptimas se alargaron a 9 y 10 años.

8.2. PERSPECTIVAS

El desarrollo de esta Tesis ha permitido configurar nuevas líneas de investigación en el ámbito de los inventarios forestales basados en el uso de nuevas herramientas de geomática forestal. Alguna de estas líneas son las siguientes:

1) Aplicación de la metodología de inventario integrando datos de campo y sensores remotos a otras especies y objetivos de planificación forestal: los trabajos desarrollados aportan herramientas automáticas de segmentación y optimización que mejoran la planificación y la gestión de los recursos forestales, principalmente relacionados con plantaciones intensivas, colaborado así con los sistemas de toma de decisiones independiente de la especie y del destino de producción.

2) Perfeccionamiento y uso de técnicas no paramétricas: los algoritmos utilizados de *machine learning*: Random Forest; Support Vector Machine y Artificial Neural Networks, han sido capaces de estimar diversas variables de rodal (IAF, Ho, BMT y VT) con muy buena precisión. Sin embargo, su uso en el sector forestal nacional es escaso, debido a los requerimientos estadísticos y a la dominancia de modelos paramétricos sin garantía de que cumplan las condiciones adecuadas para su empleo.

3) Uso de técnicas no paramétricas para la identificación de especies sobre la base de vuelos LiDAR, en rodales vecinos o con posible mezcla de especies.

4) Generalización del uso de datos procedentes de sensores sobre diferentes plataformas tripuladas y no tripuladas. La disponibilidad de datos recogidos por sensores remotos permite modelar procesos que ocurren en grandes áreas. Siendo necesario considerar la resolución espacial, espectral y temporal, así como el costo económico de la obtención y gestión de dichos datos. Si bien

existe información de libre acceso esta suele ser de resoluciones medias y bajas, si se necesita información a muy alta resolución espacial su disponibilidad es menor y a un costo mayor.

5) Planificar el uso de modelos a nivel de árbol individual para su posible seguimiento y monitoreo de hábitat derivados de los MDT, MDV de los datos LiDAR

6) Diseño y realización de inventario forestal nacional sobre la base de su uso y explotación a partir de información procedente de sensores remotos y modelos de volumen y de crecimiento más precisos (por ej. localización submétrica de las parcelas de inventario).

7) Planificar inventarios estratificados e integración de esos inventarios en bases de datos masivos, a partir de los datos de sensores remotos en zonas de alto interés forestal.

8) Incluir en el análisis económico las alternativas de manejo como raleo, silvopastoreo o plantaciones forestales destinadas a madera maciza. La acumulación y el flujo de C de estas alternativas de manejo forestal pueden ser diferentes a los propuestos en este estudio.

9. BIBLIOGRAFÍA

Acuna M, Navarro-Cerrillo R, Ruiz-Gómez F, Lara-Gómez M, Pérez-Romero J, Varo-Martínez MÁ, Palacios-Rodríguez G. 2021. How does carbon pricing impact optimal thinning schedules and net present value in Mediterranean pine plantations? Forest Ecology Management, 482, 118847, doi:10.1016/j.foreco.2020.118847.

Ågren AM, Lidberg W, Strömgren M, Ogilvie J, Arp PA. 2014. Evaluating digital terrain indices for soil wetness mapping–a Swedish case study. Hydrology and Earth System Sciences, 18(9), 3623-3634.

Aguirre-Salado C, Treviño-Garza E, Aguirre-Calderón O, Jiménez-Pérez J, González-Tagle M, Valdéz-Lazalde J, Sánchez-Díaz G, Haapanen R ,Aguirre-Salado A, Miranda-Aragón L. 2014 Mapping aboveground biomass by integrating geospatial and forest inventory data through a k-nearest neighbor strategy in North Central Mexico. Journal of Arid Land, 6(1), 80–96.

Ahmad F, Uddin M, Goparaju L. 2018. 3D Mapping by Photogrammetry and LiDAR in Forest Studies, 95(3), 224–234.

Ahnlund Ulvcrona K, Ulvcrona T, Nilsson U, Lundmark T. 2014. Stand density and fertilization effects on aboveground allocation patterns and stem form of Pinus sylvestris in young stands. Scandinavian Journal of Forest Research, 29(3), 197–209. https://doi.org/10.1080/02827581.2014.906648

Arias-Rodil M, Diéguez-Aranda U, Álvarez-González JG., Pérez-Cruzado C, Castedo-Dorado F, González-Ferreiro E. 2018. Modeling diameter distributions in radiata pine plantations in Spain with existing countrywide LiDAR data. Annals of Forest Science, 75(2), 36. https://doi.org/10.1007/s13595-018-0712-z

Asante P. 2011. Carbon Sequestration and the Optimal Economic Harvest Decision. Thesis Doctor of Philosophy in Forest Biology and Management. Canadá. University of Alberta. 200 p

Binkley D, Campoe OC, Alvares C, Carneiro RL, Cegatta Í, Stape JL. 2017. The interactions of climate, spacing and genetics on clonal *Eucalyptus* plantations across Brazil and Uruguay. Forest Ecology and Management, 405, 271-283 doi:10.1016/j.foreco.2017.09.050.

Blázquez-Casado Á. 2019. Aplicación de imágenes de satélites y datos LiDAR en la modelización de recursos forestales. Tesis doctoral. Programa de doctorado en conservación y uso sostenible de sistemas forestales. España. Universidad de Valladolid. 138 p

Bourque CPA, Neilson ET, Gruenwald C, Perrin SF, Hiltz JC, Blin YA, Horsman GV, Parker MS, Thorburn CB, Corey MM. 2007. Optimizing carbon sequestration in commercial forests by integrating carbon management objectives in wood supply modeling. Mitigation and Adaptation Strategies for *Global Change*, 12, 1253–1275, doi:10.1007/s11027-006-9072-3.

Broz D, Durand G, Rossit D, Tohmé F, Frutos M. 2017. Strategic planning in a forest supply chain: A multigoal and multiproduct approach. Canadian Journal of Forest Research, 47(3), 297–307. https://doi.org/10.1139/cjfr-2016-0299

Callaghan DW, Khanal PN, Straka TJ, Hagan DL. 2019. Influence of forestry practices cost on financial performance of forestry investments. Resources, 8, doi:10.3390/RESOURCES8010028.

Carus M. 2017. Biobased economy and climate change—important links, pitfalls, and opportunities. Industrial Biotechnology, 13(2), 41–51.

Carvalho JP, Parresol BR. 2003. Additivity in tree biomass components of Pyrenean oak (Quercus pyrenaica Willd.). Forest Ecology and Management, 179(1–3), 269–276. https://doi.org/10.1016/S0378-1127(02)00549-2

Chuvieco-Salinero E. 1996. Fundamentos de teledetección espacial. Madrid, Rialp.

Coutinho VM, Sanquetta CR, Bittencourt PA, Silva S, Proceke KH, Delarrmelina WM, Moreau J. 2018.Simultaneous Equations to Estimate Aboveground Biomass of Pinus caribaea var . hondurensis. Floresta e Ambiente, 25(3).

https://doi.org/10.1590/2179-8087.045216

Crespo P, Ruiz L, Balaguer Á y Estornell J. 2015. Análisis temporal de la estructura forestal mediante métricas derivadas de LiDAR full-waveform.Teledetección: Humedales y Espacios Protegidos. XVI Congreso de la Asociación Española de Teledetección. Sevilla, España

Cruz-Leyva IA, Valdez-Lazalde JR, Ángeles-Pérez G, de los Santos-Posadas HM. 2010. Modelación espacial de área basal y volumen de madera en bosques manejados de Pinus patula y P. teocote en el ejido Atopixco, Hidalgo. Madera Bosques, 16(3), 75–97. https://doi.org/10.21829/myb.2010.1631168

Deo RK, Russell MB, Domke GM, Woodall CW, Falkowski MJ, Cohen WB. 2017. Using Landsat Time-Series and LiDAR to Inform Aboveground Forest Biomass Baselines in Northern Minnesota, USA. Canadian Journal of Remote Sensing, 43(1), 28–47. https://doi.org/10.1080/07038992.2017.1259556

Díaz-Balteiro L, Rodriguez LCE. 2006. Optimal rotations on Eucalyptus plantations including carbon sequestration-A comparison of results in Brazil and Spain. Forest Ecology and Management, 229(1–3), 247–258. https://doi.org/10.1016/j.foreco.2006.04.005

Diéguez-Aranda U, Castedo-Dorado F, Álvarez-González JG, Rojo A. 2006. Compatible taper function for Scots pine plantations in northwestern Spain. Canadian Journal of Forest Research, 36(5), 1190–1205. https://doi.org/10.1139/x06-008

Dieste A. 2012. Programa de promoción de exportaciones de productos de madera. Uruguay DNIMIEM-CSFM. 35p.

Dong P, Chen Q. 2017. LiDAR remote sensing and applications. CRC Press.

Fankhauser KE, Strigul NS, Gatziolis D. 2018. Augmentation of traditional forest inventory and Airborne laser scanning with unmanned aerial systems and photogrammetry for forest monitoring. Remote Sensing, 10(10), 1–17. https://doi.org/10.3390/rs10101562

Franklin S. 2001. Remote Sensing for Sustainable Forest Management. Boca Raton. Lewis Publishers, CRC press.

García D, De Miguel S, Gutierrez F, García D. 2010. Estimación de variables de interés forestal basada en datos lidar en el monte número 117 del CUP Término municipal de Cuenca. España. Escuela Universitaria de Ingeniería Técnica Forestal-Universidad politécnica de Madrid. 194 p.

Gomat H, Saya A, Gomat H, Gomat H, Deleporte P, Moukini R, Mialounguila G. 2011. What factors influence the stem taper of Eucalyptus : growth , environmental conditions , or genetics ? Annals of Forest Science, Springer Verlag/EDP Sciences, 2011, 68 (1), pp.109-120. 10.1007/s13595-011-0012-3 .

González-Ferreiro E, Diéguez-Aranda U, Miranda D. 2012. Estimation of stand variables in Pinus radiata D. Don plantations using different LiDAR pulse densities. Forestry, 85(2), 281–292. https://doi.org/10.1093/forestry/cps002

Gregoire TG, Næsset E, McRoberts RE, Ståhl G, Andersen HE, Gobakken T, … Nelson R. 2016. Statistical rigor in LiDAR-assisted estimation of aboveground forest biomass. Remote Sensing of Environment, 173, 98–108. https://doi.org/10.1016/j.rse.2015.11.012

Guerra-Hernández J, Tomé M, González-Ferreiro E. 2016. Cartografía de variables dasométricas en bosques Mediterráneos mediante análisis de los umbrales de altura e inventario a nivel de masa con datos LiDAR de baja resolución. Revista de Teledetección, 0(46), 103–117. https://doi.org/10.4995/raet.2016.3980

Gujarati D, 1999. Econometría Segunda Parte. Estados Unidos. 120 p.

Hausman J. 1975. An instrumental variable approach to full- information estimators for linear and certain nonlinear econometric models. Econometrica, 43, 727–738

Hawbaker TJ, Gobakken T, Lesak A, Trømborg E, Contrucci K, Radeloff V. 2010. Light detection and ranging-based measures of mixed hardwood forest structure. Forest Science, 56(3), 313–326.

Hirigoyen A, Varo-Martinez M, Rachid-Casnati C, Franco J, Navarro-Cerrillo R. 2020. Stand Characterization of Eucalyptus spp. Plantations in Uruguay Using Airborne Lidar Scanner Technology. Remote Sensing. 12(23):3947. https://doi.org/10.3390/rs12233947

Instituto Uruguay XXI. 2019. Informe Anual de Comercio Exterior, 10. https://doi.org/10.1017/CBO9781107415324.004. [Em líena] 1julio 2021. https://www.uruguayxxi.gub.uy/es/centro-informacion/informes-de-comercio-exterior/

Jacobs M, Rais A, Pretzsch H. 2020. Analysis of stand density effects on the stem form of Norway spruce trees and volume miscalculation by traditional form factor equations using terrestrial laser scanning (TLS). Canadian Journal of Forest Research, 50(1), 51–64. https://doi.org/10.1139/cjfr-2019-0121

Jayathunga S, Owari T, Tsuyuki S. 2019. Digital Aerial Photogrammetry for Uneven-Aged Forest Management: Assessing the Potential to Reconstruct Canopy Structure and Estimate Living Biomass. Remote Sensing, 11(3), 338. https://doi.org/10.3390/rs11030338

Júnior IDST, Torres CMME, Leite HG, de Castro NLM, Soares CPB, Castro RVO, Farias AA 2020. Machine learning: Modeling increment in diameter of individual trees on Atlantic Forest fragments. Ecological Indicators, 117(2), 106685. https://doi.org/10.1016/j.ecolind.2020.106685

Juntheikki J. 2014. Estimation of eucalyptus forest plantations carbon sequestration potential in Uruguay with the CO2fix model. Tesis master. Finland.University of Helsinki, Faculty of Agriculture and Forestry, Department of Forest Sciences. Helsingfors universitet. 106 p.

Kangas A, Astrup R, Breidenbach J, Fridman J, Gobakken T, Korhonen KT, … Olsson H. 2018. Remote sensing and forest inventories in Nordic countries–roadmap for the future. Scandinavian Journal of Forest Research, 33(4), 397–412. https://doi.org/10.1080/02827581.2017.1416666

Keleş, S. 2016. Edades óptimas de corte en bosques de álamos híbridos incluyendo captación de carbono: Un estudio de caso en Turquía. Revista Chapingo, Serie Ciencias Forestales y del Ambiente 22, 339–349, doi:10.5154/r.rchscfa.2015.12.053.

Kozak A. 1969. Methods for Ensuring Additivity of Biomass Components by Regression Analysis. The Forestry Chronicle, 46(5), 402–405. https://doi.org/10.5558/tfc46402-5

Kuzminyh YV, Gryaznov SE, Shaitarova OE, Sukonkin SE, Yu Abakulina L. 2020. Forestry development as an instrument for implementing the climate policy of Russia. In Proceedings of the IOP Conference Series: Earth and Environmental Science. 574(1) p 012044.

Lal R. 2005. Forest soils and carbon sequestration. Forest Ecology and Management,

Liu Y, Yue C, Wei X, Blanco JA, Trancoso R. 2020. Tree profile equations are significantly improved when adding tree age and stocking degree: an example for Larix gmelinii in the Greater Khingan Mountains of Inner Mongolia, northeast China. European Journal of Forest Research, 139(3), 443–458. https://doi.org/10.1007/s10342-020-01261-z

Loisel, P. 2020. Under the risk of destructive event, are there differences between timber income based and carbon sequestration based silviculture? Forest Policy and Economics 120, 102269, doi:10.1016/j.forpol.2020.102269.

Loza-Balbuena I. 2001. Impacto del Mercado del Carbono en la Performance Económica de Proyectos Forestales. Estudio de Caso para Pinus taeda en Uruguay. In Simposio Internacional Medición y Monitoreo de la Captura de Carbono en Ecosistemas Forestales. Valdivia, Chile. Citeseer.

Luo S, Wang C, Xi X, Nie S, Fan X, Chen H., … Zhou G. 2019. Combining hyperspectral imagery and LiDAR pseudo-waveform for predicting crop LAI, canopy height and above-ground biomass. Ecological Indicators, 102(1), 801–812. https://doi.org/10.1016/j.ecolind.2019.03.011

Matasci G, Hermosilla T, Wulder MA, White JC, Coops NC, Hobart GW., … Bater CW. 2018. Three decades of forest structural dynamics over Canada's forested ecosystems using Landsat time-series and lidar plots. Remote Sensing of Environment, 216, 697–714. https://doi.org/10.1016/j.rse.2018.07.024

Max T, Burkhart HE. 1976. Segmented polynomial regression applied to taper equations. Forest Science. 22: 283–289.

Methol R. 2008. SAG Eucalyptus: Sistema de apoyo a la gestión de plantaciones orientadas a la producción de celulosa en Uruguay. Montevideo. Serie Técnica INIA 173.

MGAP-DIEA (Ministerio de Ganadería Agricultura y Pesca, Dirección de Estadísticas Agropecuarias, Uruguay). 2019. Anuario estadístico agropecuario 2019. Montevideo, Uruguay. Editorial Hemisferio Sur.

MGAP-OPYPA (Ministerio de Ganadería Agricultura y Pesca, Oficina de Programación y Política Agropecuaria, Uruguay). 2019. Montevideo, Uruguay. Editorial Hemisferio Sur.

Mora B, Wulder MA, White JC, Hobart G. 2013. Modeling stand height, volume, and biomass from very high spatial resolution satellite imagery and samples of airborne LIDAR. Remote Sensing, 5(5), 2308–2326. https://doi.org/10.3390/rs5052308

Mountrakis G, Im J, Ogole C. 2011. Support vector machines in remote sensing: A review. ISPRS Journal of Photogrammetry and Remote Sensing, 66(3), 247–259. https://doi.org/10.1016/j.isprsjprs.2010.11.001

Noordermeer L, Bollandsås OM, Ørka HO, Næsset E, Gobakken T. 2019. Comparing the accuracies of forest attributes predicted from airborne laser scanning and digital aerial photogrammetry in operational forest inventories. Remote Sensing of Environment, 26–37. https://doi.org/10.1016/j.rse.2019.03.027

Olschewski R, Benítez PC. 2010. Optimizing joint production of timber and carbon

sequestration of afforestation projects. Journal of Forest Economics 16, 1–10, doi:10.1016/j.jfe.2009.03.002.

Parker GG, Lowman MD, Nadkarni NM. 1995. Structure and Microclimate of Forest Canopies. Forest Canopies, 73–106.

Parresol BR. 2001. Additivity of nonlinear biomass equations. Canadian Journal of Forest Research, 31(5), 865–878. https://doi.org/10.1139/x00-202

Parresol BR. 1999. Assessing tree and stand biomass: a review with examples and critical comparisons. Forest Science, 45(4), 573–593.

Peduzzi A, Wynne RH, Fox TR, Nelson RF, Thomas VA. 2012. Estimating leaf area index in intensively managed pine plantations using airborne laser scanner data. Forest Ecology and Management, 270, 54–65. https://doi.org/10.1016/j.foreco.2011.12.048

Pettorelli N. 2019. Satellite remote sensing and the management of natural resources. Oxford University Press.

Poder Legislativo. 1987. Ley N° 15.939. Ley Forestal [En línea]. Consultado 1 diciembre 2020. Disponible en: http://www.parlamento.gub.uy

Pretzsch H, Rais A. 2016. Wood quality in complex forests versus even-aged monocultures: review and perspectives. Wood Science and Technology, 50(4), 845–880. https://doi.org/10.1007/s00226-016-0827-z

Pukkala T. 2020. At what carbon price forest cutting should stop. Journal of Forestry Research, 31(3), 713–727. https://doi.org/10.1007/s11676-020-01101-1

Rachid-Casnati C, Euan M, Richard W, Resquin F. 2014. Volume and Taper Equations for P. taeda (L.) and *E. grandis* (Hill ex. Maiden). Agrociencia Uruguay, 18(2), 47–60. https://doi.org/10.2477/vol18iss2pp47-60

Resquin F. 2019. Producción de biomasa en plantaciones intensivas de Eucalyptus spp. en Uruguay. Tesis doctoral. España. Departamento de Ingeniería Forestal, Universidad de Cordóba. 260 p.

Resquin F, De Mello J, Fariña I, Mieres J, Assandri L. 2005. Caracterización de la celulosa de especies del género Eucalyptus plantadas en Uruguay. Montevideo: Serie Técnica INIA 152, 82.

Rubilar RA, Allen HL, Fox T, Cook RL, Albaugh TJ, Campoe OC. 2018. Advances in silviculture of intensively managed plantations. Current Forestry Reports, 4, 23–34.

Ruiz-Peinado R, Oviedo J, Senespleda E, Oviedo F, del Río Gaztelurrutia M. 2017. Forest management and carbon sequestration in the Mediterranean region: A review. Forest Systems, 26(2), 10

.Sanquetta, CR, Behling A, Dalla Corte AP, Arlindo Simon A, Lourenco Rodrigues A, Camacho Cadori G, Costa Junior S. 2015. Modelling crown volume in Acacia mearnsii stands. African Journal of Agricultural Research, 10(28), 2756–2762. https://doi.org/10.5897/ajar2015.9778

Scolforo HF, McTague JP, Burkhart H, Roise J, Campoe O, Stape JL. 2019. Eucalyptus growth and yield system: Linking individual-tree and stand-level growth models in clonal Eucalypt plantations in Brazil. Forest Ecology and Management, 432, 1–16. https://doi.org/10.1016/j.foreco.2018.08.045

Scurlock JM, Asner GP, Gower ST. 2001. Worldwide Historical Estimates of Leaf Area Index (Vol. 27). https://doi.org/0RNL/TM-2001/268

Sharma M, Parton J. 2009. Modeling stand density effects on taper for jack pine and black spruce plantations using dimensional analysis. Forest Science, 55(3), 268–282.

Shen X, Cao L, Chen D, Sun Y, Wang G, Ruan H. 2018. Prediction of forest structural parameters using airborne full-waveform LiDAR and hyperspectral data in subtropical forests. Remote Sensing, 10(11). https://doi.org/10.3390/rs10111729

Sileshi GW. 2014. A critical review of forest biomass estimation models, common mistakes and corrective measures. Forest Ecology and Management, 329, 237–

254. https://doi.org/10.1016/j.foreco.2014.06.026

Silva CA, Klauberg C, Hudak AT, Vierling LA, Liesenberg V, Carvalho SPC, Rodriguez LCE. 2016. A principal component approach for predicting the stem volume in Eucalyptus plantations in Brazil using airborne LiDAR data. Forestry, 89(4), 422–433. https://doi.org/10.1093/forestry/cpw016

Silva de Carvalho M. 2016. Comparação da estimativa de parâmetros estruturais e de mapas de predição de biomassa produzidos por meio de simulações de métodos de amostragem e dados LIDAR na reserva florestal da Embrapa Acre. Brasil . Universidade Federal do Acre Programa de pós-graduação em Ciência, Inovação e Tecnologia para a Amazônia.71 p.

Somers G, Farrar R. 1991. Biomathematical growth equations for natural longleaf pine stands. Forest Science. 18, 76-86

Spurr S. 1954. Simplified Computation of Volume and Growth. Journal of Forestry. 52: 914–922. doi: 10.1093/jof/52.12.914

Staben G, Lucieer A, Scarth P. 2018. Modelling LiDAR derived tree canopy height from Landsat TM, ETM+ and OLI satellite imagery. A machine learning approach. International Journal of Applied Earth Observation and Geoinformation. 73: 666–681. - doi: 10.1016/j.jag.2018.08.013

Stereńczak K, Lisańczuk M, Erfanifard Y. 2018. Delineation of homogeneous forest patches using combination of field measurements and LiDAR point clouds as a reliable reference for evaluation of low resolution global satellite data. Forest Ecosystems, 5(1), 1–12. https://doi.org/10.1186/s40663-017-0128-5

Sullivan FB, Ducey MJ, Orwig DA, Cook B, Palace MW. 2017. Comparison of lidar- and allometry-derived canopy height models in an eastern deciduous forest. Forest Ecology and Management, 406(10), 83–94. https://doi.org/10.1016/j.foreco.2017.10.005

Tang X, Pérez-Cruzado C, Fehrmann L, Álvarez-González, JG. 2016. Development of a Compatible Taper Function and Stand-Level Merchantable Volume Model

for Chinese Fir Plantations, M, 1–16. https://doi.org/10.1371/journal.pone.0147610

Tesfamichael SG, van Aardt J, Roberts W, Ahmed F. 2018. Retrieval of narrow-range LAI of at multiple lidar point densities: Application on *Eucalyptus grandis* plantation. International Journal of Applied Earth Observation and Geoinformation, 70(4), 93–104. https://doi.org/10.1016/j.jag.2018.04.014

Tinkham WT, Mahoney PR, Hudak AT, Domke GM, Falkowski MJ, Woodall CW, Smith A. M. S. 2018. Applications of the United States forest inventory and analysis dataset: A review and future directions. Canadian Journal of Forest Research, 48(11), 1251–1268. https://doi.org/10.1139/cjfr-2018-0196

Vanclay J. 1994. Modelling forest growth and yield application to mixed tropical forests. CAB International, Wallingford

Varo-Martínez MÁ, Navarro-Cerrillo RM, Hernández-Clemente R. 2017. Semi-automated stand delineation in Mediterranean Pinus sylvestris plantations through segmentation of LiDAR data : The influence of pulse density. International Journal of Applied Earth Observations and Geoinformation, 56, 54–64. https://doi.org/10.1016/j.jag.2016.12.002

Viana Céspedes V. 2018. Optimizacion en la planificacion de servicios de cosecha forestal. Tesis de maestria. Uruguay. Magíster en Investigación de Operaciones. Universidad de la República, Facultad de Ingeniería. Uruguay. 97 p.

Vo AV, Laefer DF, Bertolotto M. 2016. Airborne laser scanning data storage and indexing: state-of-the-art review. International Journal of Remote Sensing, 37(24), 6187–6204. https://doi.org/10.1080/01431161.2016.1256511

White JC, Coops NC, Wulder MA, Vastaranta M, Hilker T, Tompalski P. 2016. Remote Sensing Technologies for Enhancing Forest Inventories: A Review. Canadian Journal of Remote Sensing. https://doi.org/10.1080/07038992.2016.1207484

Whitehead D, Beadle CL. 2004. Physiological regulation of productivity and water

use in Eucalyptus: A review. Forest Ecology and Management, 193(1–2), 113–140. https://doi.org/10.1016/j.foreco.2004.01.026

Wong J, Prokofieva I. 2014. Report presenting synthesis of regional sectoral reviews to describe the State of the European NWFP. Project Deliverable D, 1.

Woodcock, C, Allen, R, Anderson M, Belward A, Bindschadler R, Cohen W, Gao F, Goward, S, Helder D, Helmer E, Nemani R, Oreopoulos L, Schott J, Thenkabail P, Vermote E, Vogelmann J, Wulder M, Wynne R. 2008. Free access to Landsat imagery. Science 320(5879): 1011-1013

Yang L, Mansaray LR, Huang J, Wang L. 2019. Optimal segmentation scale parameter, feature subset and classification algorithm for geographic object-based crop recognition using multisource satellite imagery. Remote Sensing, 11(5). https://doi.org/10.3390/rs11050514

Zellner A. Theil H. 1962.Three stage least squares: Simultaneous estimation of simultaneous equations. Econometrica, 30.

Zhao K, Popescu S. 2009. Lidar-based mapping of leaf area index and its use for validating GLOBCARBON satellite LAI product in a temperate forest of the southern USA. Remote Sensing of Environment, 113(8), 1628–1645. https://doi.org/10.1016/J.RSE.2009.03.006

Zhou Y, Qiu F. 2015. Fusion of high spatial resolution WorldView-2 imagery and LiDAR pseudo-waveform for object-based image analysis. ISPRS Journal of Photogrammetry and Remote Sensing, 101, 221–232. https://doi.org/10.1016/j.isprsjprs.2014.12.013

Zianis D, Mencuccini M. 2003. Aboveground biomass relationships for beech (Fagus moesiaca Cz.) trees in Vermio Mountain, Northern Greece, and generalised equations for Fagus sp. Annals Forest Science. 60, 439–448. https://doi.org/10.1051/forest:2003036